Characterisation and optimisation of biosorption of metals by dealginated seaweed.

ROMERO GONZALEZ, Maria Elena.

REFERENCE

Characterisation and Optimisation of the Biosorption of Metals by Dealginated Seaweed

María Elena Romero González

A thesis submitted in partial fulfilment of the requirements of
Sheffield Hallam University
for the degree of Doctor of Philosophy

October 2001

DX233694

Declaration

The work described in this thesis was carried out by the author at the School of Science and Mathematics, between November 1997 and October 2001. The author declares that this work has not been submitted for any other degree. The work is original except where acknowledged by reference.

María Elena Romero González

Acknowledgments

First, I would like to express my gratitude to God Almighty, the strength of my life.

I would also like to express my appreciation to the following people for their contribution to this project:

- Consejo Nacional de Investigaciones Cientificas y Tecnologicas (CONICIT) and La Universidad del Zulia (LUZ), Venezuela for their financial support.
- My supervisors Dr. Philip Gardiner and Dr. Ceri Williams, for their guidance and advice throughout this work, their friendship and unconditional support over the past years.
- Dr. Steve Gurman for his contribution to the EXAFS study, his help with the calculations and the discussion on this part of the project.
- Dr. Stephen Habesh, for his help and feedback during the ESEM study.
- Dr. Peter Drew, for his useful discussions, feedback and his unlimited supplies of bibliographic material.
- The technical staff at the School of Science & Mathematics, Materials Research Institute and School of Chemical and Process Engineering of The University of Sheffield for their help and advice during the experimental part of this work. Also to the personnel of the Environmental Process Engineering Group for sharing time in the lab, help and support.
- To all my friends, here, there and everywhere, for providing good times and for support during bad times without whom none of this would have been possible.
- To Prof. Hilda Ledo, for encouraging me to explore, seek and research into the deepest of chemistry and beauty of life.
- A special thank you goes to Rachel, Mary, John, Peter, Felipe and Edward, for helping to keep my mental health.
- To Mami, Papi and the rest of my family, for their unlimited encouragement, support and love throughout my life.

Abstract

The ability of dealginated seaweed a waste material derived from the commercial processing of seaweed for alginate production, to remove cadmium, lead, nickel, copper, chromium, silver, aluminium and gold from solution was determined. Metal sorption was found to be rapid (90% removal within 5 minutes), achieving a residual concentration of 0.9 mg L^{-1} after 1 h contact time from an initial solution concentration of 10 mg L^{-1}. The binding of metal by dealginate was found to be pH dependent, optimal sorption occurring at around pH 6-8 for cadmium, lead, nickel, copper and chromium and pH 3-4 for aluminium and gold respectively, suggesting an ion exchange mechanism. Determination of a molar ratio in the displacement of calcium by cadmium on dealginate supported the presence of an ion-exchange relationship, since the displacement of approximately 1 mol of calcium by 1 mol of cadmium was observed.

The sorption data was best fitted in the ion exchange approximation as opposed to the Langmuir model. The binding capacities were found to be 1.2, 0.5, 1.6, 0.8, 1.2, 0.4, 0.9 and 0.4 mmol g^{-1} for cadmium, lead, nickel, copper, chromium, silver, aluminium and gold respectively. The ion exchange constants were calculated to be 3.3×10^{-6}, 4.1×10^{-6}, 6.2×10^{-6}, 1.8×10^{-6}, 2.3×10^{-6}, 2.4×10^{-7},8×10^{-10} for cadmium, lead, nickel, copper, chromium, silver and aluminium. The values of the capacities and ion exchange constants showed affinity of the biosorbent to specific metals. The identification of the binding sites on the surface of dealginated seaweed was investigated by a number of techniques. Potentiometric titration revealed three distinct pKa values, the first having a similar value to carboxyl groups, the second being comparable with that of saturated thiols and amines and the third similar to sulphonate groups. Esterification of the dealginate resulted in the subsequent reduction in metal sorption, indicating that carboxyl groups are largely responsible for sorption except in the case of aluminium and gold, where 40-60% of the metal remained in solution after modification of the surface. Evidence of the FT-IR spectra confirmed the presence of carboxyl groups in untreated dealginate, while the number of carboxyl groups was markedly reduced in the esterified sample.

The occurrence of other mechanisms apart from ion exchange was suggested by the FT-IR spectrum for aluminium and gold. ESEM images of the surface of dealginated seaweed showed the algae cell structure still present in large areas. X-ray maps revealed the presence of silver, aluminium and gold associated with sulphur atoms on the dealginate surface. EXAFS results showed that cadmium, lead, copper and silver were bound to the dealginate through oxygen atoms, possibly from carboxylate groups. Evidence of gold reduction from Au (III) to Au(I) and Au(O) was also confirmed by the bond distance calculated for this metal.

Methods for the on-line preconcentration of cadmium, chromium, copper and lead and chemical speciation of Cr^{3+} and CrO_4^{2-} using a microcolumn packed with dealginated seaweed were developed. Effective column capacities were 4.0, 8.7, 9.4 and 8.5 μmol L^{-1} for cadmium, chromium, copper and lead, respectively. The application of the method was extended to the determination of zinc, cobalt, mercury, scandium, strontium, vanadium, arsenic, selenium, manganese and antimony. The analytical procedures developed for metal preconcentration and chromium speciation were validated by analyses of two Lake Ontario reference materials, TMDA 51.2 and TMDA 54.2 and a synthetic seawater sample. The findings of this study demonstrated that the sorption of metal by dealginate is mainly due to an ion-exchange mechanism. The binding capacities of the biosorbent for the elements studied were adequate for trace analysis and the use of dealginate was shown to be a cheaper alternative to synthetic resins.

Table of Contents

General Introduction

Chapter 1

Introduction

Section 1.1

During the last few decades, increasing attention has been focused on pollution of the natural environment. Heavy metals pose a serious threat of pollution to the biosphere. Due to their importance in industry, metals have become a major source of pollution in the environment. The mining, mineral processing and metallurgical industries are known to generate billions of tons of wastes (1). In most cases, it is possible to reduce the level of pollutants through the use of conventional technologies. However, the costs of technologies for the removal of heavy metal ions are often high and the efficiency of the treatment is inefficient due to the non-degradable nature of these elements.

To improve the current cleaning processes and satisfy environmental regulations, new supplementary methods must be developed. Biologically-induced metal removal has been perceived as a promising technique in the last decade (2). Natural materials that are available in large quantities or certain waste products from industrial operations have shown potential as inexpensive sorbents (3). The removal of metals from solution can be achieved using actively living cells via the process of bioaccumulation, or passively at the surface of both living and dead cells, in which case the process is referred to as biosorption (2).

The use of dead biomass is of particular interest, because the biosorbents can be employed in the same way as synthetic adsorbents. As such, regeneration is possible and the use of a dead biomass eliminates the problems of waste toxicity and nutrient requirements.

A wide range of dead biomasses have been studied as potential biosorbents for the removal of metal ions from aqueous solution (2, 4-8). Of the bacteria, fungi, yeast and algae studied, dead marine macroalgae have shown the highest capacity for the removal of heavy metals with almost unlimited availability. Furthermore, the microalgal product obtained from the production of biomaterial has become a cheap source of biosorbents (9).

The production of polysaccharides from marine macroalgae or seaweeds is an economically important global industry. The extraction of agars, agaroses, algins and carrageenans for use in the food and pharmaceutical industries produces residues that could be used as cheap biosorbents (10).

Alginate is a polysaccharide-based biosorbent formed from algin by replacing protons in the carboxylic groups with metal ions such as Na, Ca and Mg to make commercial alginate products. It has been reported (11) that the ability of alginate to exchange heavy metal ions is an adsorption process.

Dealginate is a residue produced from the alginate extraction process from brown seaweed. This product has no marketable use and is dewatered after the extraction process for disposal. Since alginate has biosorptive properties, the waste dealginate product may also be a potential biosorbent for the removal of heavy metals from solution. The use of this waste material to remove and recover metal ions from aqueous effluents would be both environmentally and energetically satisfying.

This study aims to unravel the mechanisms of the binding of metal ions to dealginated seaweed waste material through a detailed understanding of the behaviour of those ions and their interaction with the surrounding environment. The specific aims of this study were:

- To characterise the uptake of Cd, Pb, Ni, Cu, Cr, Ag, Al and Au by dealginated seaweed.
- To elucidate the sorption mechanism involved in the uptake of the metal ions studied.
- To model the sorption process using different mathematical approaches.
- To identify the functional groups responsible for the sorption process.
- To optimise and improve the sorption process.

- To develop a suitable method for the simultaneous removal of the aforementioned metal ions from aqueous solutions, and to use this as an application for a wide range of metals.

In order to achieve these aims a variety of analytical methods and techniques were used to provide the necessary data.

The dealginated seaweed characterisation was performed using batch and continuous methods. Parameters such as the amount of biomass, volume of effluent, pH and contact time were optimised using these methods. The identification of the functional groups on the dealginated seaweed surface was achieved by titration of the biosorbent surface. The presence of the functional groups was evaluated using Fourier transform infrared spectroscopy, environmental scanning electron microscopy and extended X-ray fluorescence analyses. A continuous flow system was developed for the application of dealginated seaweed for the removal of metal ions from aqueous solutions.

Literature Review

Section 1.2

1.2.1. The sorption process

Diverse chemical, physical and biological processes occur at the boundaries of two phases. Variation in the concentration of a substance at the interface is referred to as adsorption (12). Adsorption is a concept that was developed for the gas-solid interface, involving the equilibrium of the gas with the bulk phase and the interfacial layer. The term adsorption denotes the process of molecules accumulating in the interfacial layer, while desorption deals with the converse process (13). A typical sorption process involves different phenomena that can alter the distribution of contaminants between and among the constituent phases and interfaces of the system. Sorption interactions generally operate in all phases present in any system and at the interfaces between these phases (14).

In adsorption, solute accumulation is generally restricted to a surface or interface between the solution and the adsorbent. In contrast absorption is a process in which solute transferred from one phase to another penetrates the sorbent phase. An additional variation of the process occurs if a sufficiently high accumulation of solute occurs at the interface to form a precipitate or some other type of molecular solute-solute association. When it is unclear whether the process is either adsorption or absorption, or the retention mechanism is unknown the word sorption is used.

Sorption arises as a result of a variety of different types of attractive forces between solute molecules, solvent molecules and the molecules of a sorbent. Such forces usually act together, but one or the other is usually more significant in a particular situation. Absorption processes involve exchanges in the molecular environment. In such case the energy of an individual molecule is altered by its interactions with the solution and sorbent phases. Adsorption entails intermolecular forces, but it is molecules at the surface of the sorbent rather than the molecules in the bulk phase that are involved, and the former typically manifest a broader range of interactions (15).

Accordingly, three loosely defined categories of adsorption, namely physical, chemical and electrostatic, are traditionally distinguished, according to the class of attractive force that predominates (15). Figure 1 summarises some significant features of these different interactions and categories of adsorption.

Figure 1 Characteristic interactions associated with categories of adsorption after Weber (15)

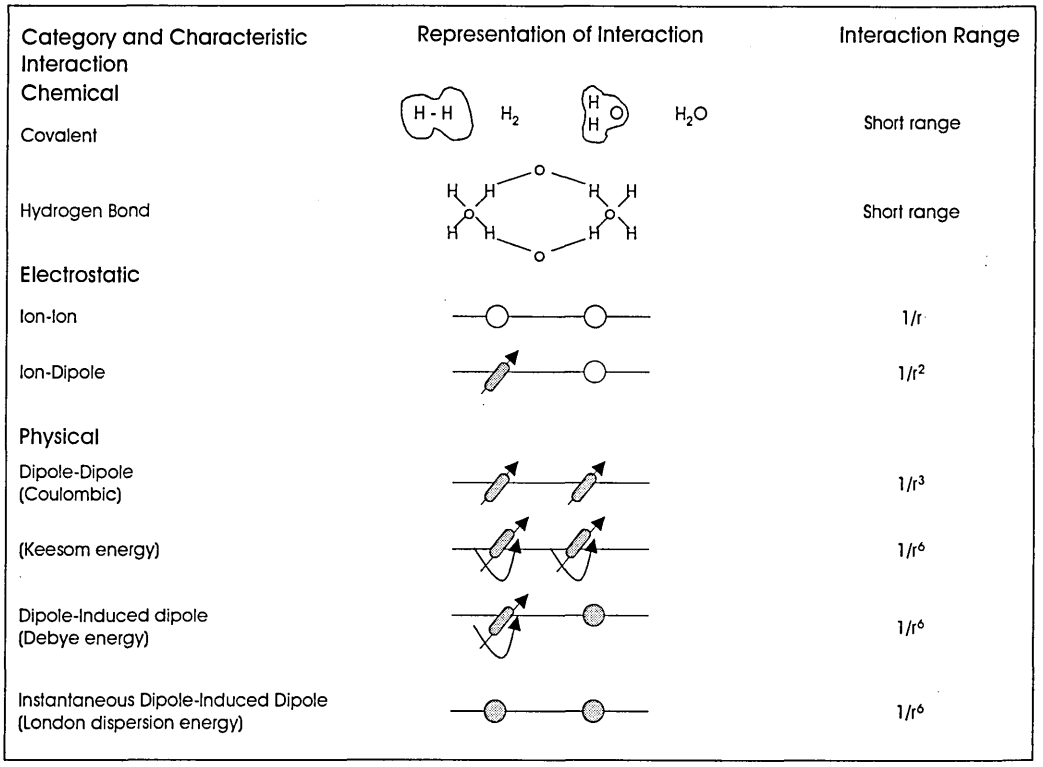

Firstly, there are those that are purely electrostatic in origin arising from the Coulomb force between charges. The interactions between charges, permanent dipoles and quadrupoles fall into this category. Secondly, there are polarisation forces that arise from the dipole moments induced in atoms and molecules by the electric fields of nearby charges and permanent dipoles. Thirdly, there are forces that are quantum mechanical in nature. Such forces give rise to covalent or chemical bonding and to the repulsive steric or exchange interactions that balance the attractive forces at very short distances.

Forces associated with interactions between the dipole moments of sorbate and sorbent molecules commonly underlie physical sorption processes. Forces attributable to rapidly fluctuating or instantaneous dipole moments resulting from the motions of electrons in their orbitals are the so-called London dispersion forces. Forces of greater intensity and longer range exist between discretely charged entities. These forces derive from specific electrostatic interactions between localised charges and exhibit much higher energy of sorption than those associated with physical sorption. Electrostatic forces extend over long distances, varying inversely with the square of the distance between molecules and directly with the product of the charges. These forces can be attractive in the case of oppositely charged species or repulsive between species having like charges. The final category of sorption defined according to predominant surface-solute interaction is chemical sorption or chemisorption. The bonds that form between solute molecules and specific surface chemical groups in this type of sorption have all of the characteristics of true chemical bonds and are characterised by relatively large energy of sorption. The reactions may involve substantial activation energies and be favoured by high temperatures (16).

1.2.2. Adsorption Processes

Adsorption may be defined as the accumulation of matter at the solid-water interface and is the basis of most surface-chemical processes. It influences the distribution of substances between the aqueous phase and particulate matter. Adsorption affects the electrostatic properties of suspended particles and colloids, that, in turn, influences their tendency to aggregate and attach and influences the reactivity of the surfaces (15).

Adsorption reactions are considered to be intermolecular interactions between the solute and the solid phases. This includes surface complexation reactions such as surface hydrolysis, the formation of dative bonds between metals and ligands, electrostatic interactions at surfaces,

extending over longer distances than chemical forces; hydrophobic expulsion, adsorption of surfactants and adsorption of polymers and polyelectrolytes (14).

1.2.2.1. Equilibrium Models

Models for characterising the equilibrium distribution of a solute among the phases and interfaces of a system typically relate the amount of solute, *q*, sorbed per unit of sorbing phase or interface to the amount of solute, *C*, retained in the solvent phase. A plot of *q* versus Ce at a given temperature is termed a sorption isotherm. The general types of behaviour are shown in Figure 2.

Figure 2 General types of sorption isotherms

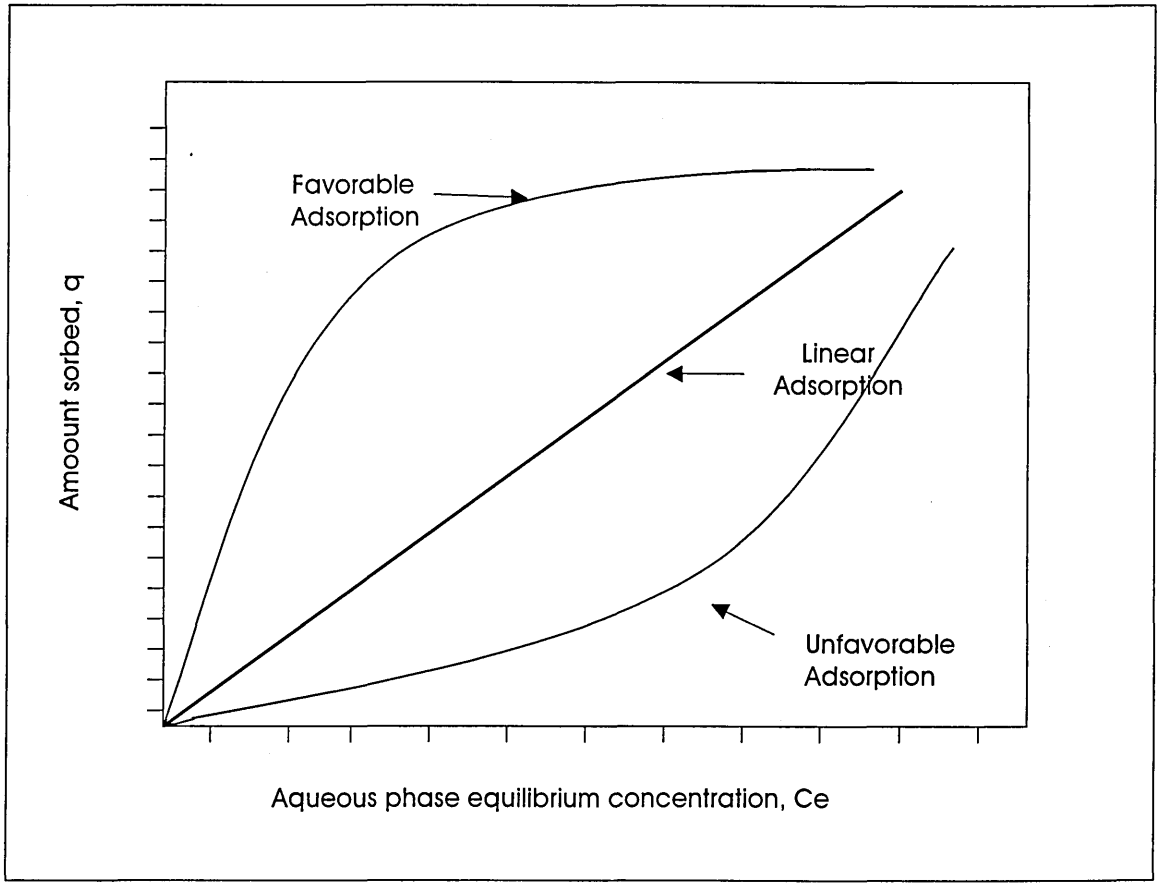

1.2.2.1.1. Linear isotherm

The linear model describes the situation in which the accumulation of solute by the sorbent is directly proportional to the solution phase concentration:

$$q = K \cdot C_e \qquad (1)$$

The constant of proportionality or distribution coefficient, K, is often referred to as a partition coefficient. C_e and q are typically expressed in terms of mass per unit volume and mass per unit mass respectively, and K has the unit of volume per mass (15).

The linear isotherm accurately describes adsorption and desorption in certain instances, most commonly at very low solute concentrations and for solids of low sorption potential. Linear approximations are appropriate for modelling contaminant fate and transport, but even when a particular set of data are reasonably well described by a linear model, caution should be exercised in the application of the model because it may not be valid over wide concentration ranges.

1.2.2.1.2. Langmuir Isotherm

In the Langmuir model it is assumed that the adsorption sites, S, on the surface of the adsorbent become occupied by adsorbate, A, from the solution. The energy of sorption for each molecule is the same and independent of surface coverage, and that adsorption occurs only in localised sites and involves no interactions between sorbed molecules.

The Langmuir isotherm can be derived by treating the adsorption process as an equilibrium process - except in this case the equilibrium is between the liquid phase molecules *A*, together with vacant surface sites, and the species adsorbed on the surface. Thus, for a non-dissociative (molecular) adsorption process, the adsorption is represented by the following chemical equation (14, 15):

$$S + A \rightleftharpoons S\text{-}A \qquad (2)$$

Langmuir derived a relationship for q and C based on some certain assumptions: a uniform surface, a single layer of adsorbed material and a constant temperature. The rate of attachment to the surface is proportional to the activity multiplied by area. The activity is proportional to the concentration in the liquid phase and the area is the amount of available surface. If the fraction of covered surface is ϕ, the rate of sorption per unit of surface is:

$$\textit{rate of adsorption} = k_1 C (1-\phi) \qquad (3)$$

The evaporation from the surface is proportional to the amount of surface covered:

$$\textit{rate of desorption} = k_2 \phi \qquad (4)$$

Where: k_1 and k_2 are rate constants

C = concentration in the fluid

ϕ = fraction of the surface covered

At equilibrium, the two rates are equal, hence:

$$\phi = \frac{k_1 C}{k_2 + k_1 C} \qquad (5)$$

By dividing the numerator and denominator by k_1

$$\phi = \frac{C}{(k_2/k_1 + k_1 C)} \quad (6)$$

Since q will be proportional to ϕ, the useful form of the equation is:

$$q = \frac{q_m K_0 C}{1 + K_0 C} \quad (7)$$

Where $q_m = q$ for a completely covered monolayer

K_o = a constant

Taking reciprocals and rearranging:

$$\frac{1}{q} = \frac{1}{q_m} + \frac{1}{K_0 q_m C} \quad (8)$$

A plot of $\frac{1}{q}$ versus $\frac{1}{C}$ should be a straight line with a slope of $\frac{1}{K_0 q_m}$ and an intercept of $\frac{1}{q_m}$.

1.2.2.1.3. Ion Exchange

The adsorption of ions from solution can occur onto oppositely charged surface sites. This is known as ion exchange (16). Some materials typically contain a variety of surfaces that exhibit electrical charge characteristics, which in turn can exert a strong influence on the sorption of ionic and polar species. Surface charges can arise in two ways:

- By ionisation or dissociation of surface groups such as the dissociation of protons from surface carboxylic groups, which leaves behind a negatively charged surface and

- By the adsorption of ions from solution onto a previously uncharged surface, for example, the binding of Ca^{2+} onto the zwitterionic groups of lipid bilayer surfaces results in a positive surface charge.

Irrespective of the origin an equal but oppositely charged region of counter-ions balances the final surface charge. The counter-ions may be bound, usually transiently, to the surface within the so-called Stern or Helmholtz layer, or may form a surrounding layer of ions on rapid thermal motion close to the surface, known as the diffuse electric double layer (Figure 3) (14).

Figure 3 Schematic representation of an electrical double layer

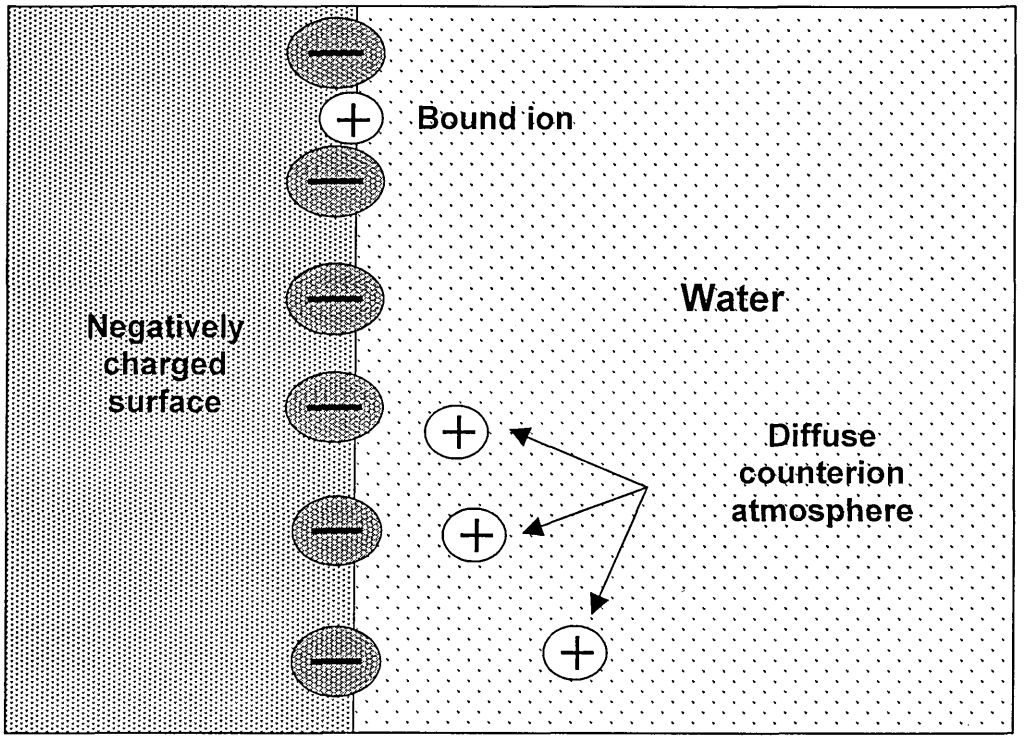

This double layer consists of the charged surface sites and an equivalent aqueous-phase excess of ions of opposite charge (counter-ions), which accumulate in the solution near the surface of the particle. The counter-ions are attracted electrostatically to the interfacial region, giving rise to a concentration gradient, which in turn sets up a potential for random diffusion of ions away from the surface. The competing processes of electrostatic attraction and counter-diffusion spread the charge over a diffuse layer in which the excess concentration of counter-ions is highest immediately adjacent to the surface of the particle and decreases gradually with increasing distance from the solid-water interface (15).

A number of relationships have been developed to describe the ion-exchange equilibria. The exchange of a cation A^{n+} of charge n, dissolved in solution, for a monovalent cation B^+, associated with an adsorbent surface, can be written in terms of simple stoichiometry for a fixed charged site, S^-, as:

$$A^{n+} + n(S^-)B^+ \rightleftharpoons (S^-)_nA^{n+} + nB^+ \quad (11)$$

A parameter corresponding in form to the mass law equilibrium constant but more correctly referred to as a selectivity coefficient can be defined in terms of the chemical activities of the species involved as:

$$K^A_B = \frac{(a_{SnA})\ (a_B)^n}{(a_A)\ (S_{SB})^n} \quad (12)$$

The selectivity coefficients of the mass law approach are related to ion size and ion charge (15).

1.2.2.2. Biosorption

Gadd (1990) defined biosorption as the removal of metal or metalloid species, compounds and particulates from solution by biological material (7). The term biosorption can also mean uptake by living or dead biomass via physico-chemical mechanisms such as adsorption or ion exchange although, in living biomass, metabolic processes may also influence and contribute to the process (17). Biosorption involves the passive sorption and complexation of metals by biomass or material derived from that biomass. Bioaccumulation includes all processes responsible for the uptake of metals by living cells, and thus includes biosorptive mechanisms, together with intracellular accumulation and bioprecipitation mechanisms (18). There are a variety of mechanisms by which biological cells can remove metals from solution. Metabolism-independent binding or biosorption of metals to cell walls, extracellular polysaccharides, pigments or other materials can occur in living or dead cells and may be rapid (7, 19).

The complexity of the biomass structure implies that there are many ways for the metal to be captured by the surface. Biosorption mechanisms are therefore various and in some cases, they are still not very well understood. Biosorption mechanisms can be divided into:

- metabolism dependent, and
- non-metabolism dependent

Depending on the location where the metal removed from the solution is found, biosorption may be classified as:

- extracellular accumulation/precipitation
- cell surface sorption/precipitation
- intracellular accumulation

Cell walls of microbial biomass which are mainly comprised of polysaccharides, proteins and lipids, offer particularly abundant metal-binding functional groups, such as carboxylate, hydroxyl, sulphate, phosphate and amino groups. Metal sorption to these sites is reversible and rapid (20). In this case, the biomass behaves like a synthetic resin. Precipitation of the metal may take place both in solution and on the cell surface (21).

The use of living organisms for metal removal and recovery is not generally feasible due to certain inherent difficulties. Wastewater usually contains high concentrations of toxic metals and pH fluctuations are not favourable conditions under which living micro-organism thrive. Dead microbial biomasses are therefore preferred (22).

1.2.2.3. Choice of metals

The increase in industrial activities has intensified environmental pollution and the deterioration of some ecosystems. As such growing attention has been given to the potential health hazard presented by heavy metals in the environment. Metals are among the most commonly encountered and difficult to treat environmental pollutants. Mining, metallurgical waste waters, refining of ores, combustion of fossil fuels, industrial processes and the disposal of industrial and domestic wastes are considered to be the major sources of heavy metal contamination (21, 23). The recognition of toxic effects from low concentrations of some heavy metals has resulted in regulations to reduce their presence in the environment. Precipitation, ion exchange and electrochemical processes have been commonly used to treat metal-containing solutions. Biosorption based on the metal binding capacities of various biological materials such as algae, bacteria, fungi, yeast and plant residues has emerged as an alternative process for the remediation of metal laden wastewaters (18 - 20, 22, 24, 25).

Metal ions can be classified using the hard and soft acids and bases approach. Pearson (1963) classified a number of Lewis acids as "hard" or "soft" in terms of equilibria data. Those metals that bind strongly to bases or nonpolarisable bases are denoted as hard and those that bind strongly to highly polarisable or unsaturated bases are named soft. Based on metal behaviour with respect to various degrees of ionic and covalent binding, electron correlation phenomena and solvatation effects the characteristics of the two classes of Lewis acids are easily discernible (26). Elements in class "hard" are small in size and have high positive oxidation state while elements in class "soft" are associated with a low or zero oxidation state and are large in size. Although elements can fit this classification, there are those whose behaviour is not in either class. These are considered borderline elements.

The essential metal ions such as Na^+, K^+, Ca^{2+} and Mg^{2+} are class "hard" cations. These metals are involved in nerve transmission, homeostasis and enzymatic reactions and they are not toxic except at high doses. Aluminium forms part of this group and is often referred to as the new toxic element, since its large use and exploitation has increased its presence in the environment. High levels of aluminium have been mobilised in the environment due to the phenomenon of acid rain, with devastating effects on plants and animals (27).

The group of intermediate metal ions includes the first row transition series metals. From a biological point of view, nickel, chromium and vanadium are considered as beneficial and manganese, iron copper, cobalt and molybdenum are considered as being essential. Tolerance levels for living organisms with respect to these metals are high if they are in the appropriate oxidation state. In the case of chromium, Cr^{3+} is thought to be involved in glucose metabolism in humans, while Cr^{6+}, as chromate is extremely toxic and carcinogenic. Chromates are widely used in the metallurgy industry and as pigments. Copper and zinc are essential trace elements to life and found as components of several metalloenzymes, but they are also toxic to many microorganisms at high levels.

The class 'soft' metal ions include the most common toxic elements cadmium, lead and mercury. Their wide use in industrial processes has increased their concentrations in the environment. These metals have no beneficial function in a normal healthy organism and their toxicity may be attributed to their ability to attack the active site such as sulphur of enzymes, competing with an essential element. Precious metals such as gold and silver are prime targets for study since an effective recovery method could use sorption processes in concentrating the metallic species of interest from dilute solutions. Apart from the toxicological criteria, the interest in studying the biosorption of specific metals may be based on their behaviour, their solution chemistry and their industrial use (14, 23, 27 - 29).

1.2.2.4. Biosorption by Algae Materials

Many biological materials bind heavy metals, but only those with sufficiently high metal-binding capacity and selectivity are suitable for use in a biosorption process (30). Seaweeds collected from the ocean have shown a capacity for biosorption of metals. Brown algae in particular are suited for binding metallic ions (31). Macroalgae have been used for analytical purposes to recover quantitatively metal ions from natural water samples at very low concentrations (32 - 34). Crist *et al* (1988) described the biosorption of heavy metals in two phases: a fast (<4 s) surface reaction attributed to surface adsorption based on anion exchange and a much slower second phase (2 h) where the metal uptake takes place via diffusion of ions into the cell structures (35). Although there is controversy about the different mechanisms of biosorption, the extensive range of biomasses studied have demonstrated that the removal of heavy metal by algae material is possible.

Crist *et al* (1981) demonstrated that the alga *Vaucheria s.* was able to adsorb Cu^{2+}, Na^{+}, Sr^{2+}, Zn^{2+} and Mg^{2+} while displacing H^{+}. The process was pH dependent and an ion exchange mechanism was proposed with the following binding strength: $Cu^{2+}>Sr^{2+}>Zn^{2+}>Mg^{2+}>Na^{+}$ that suggested a trend from probable covalent to electrostatic bonding. Functional groups amino, carboxyl and sulphates have been proposed as being responsible for the metal

binding on the algae cell wall (4). The algae *Chlorella vulgaris* was found to exhibit a capacity for binding metal ions such as Au^{3+}, Ag^{+}, Hg^{2+}, Cr^{3+}, Co^{2+}, Ni^{2+}, Cu^{2+}, Zn^{2+}, Pb^{2+}, Sn^{2+}, U^{6+} (as UO_2^{2+}), Fe^{3+} Be^{2+} and Al^{3+} between pH 5 and 7 (36). All these metal ions except Au^{3+}, Ag^{+} and Hg^{2+} are weakly bound at lower pH, while the latter were tightly bound at pH 2. The binding of the metals may be reversed by lowering the pH, thus enabling selective recovery. The interaction of gold complexes with *Chlorella vulgaris* was demonstrated to be nearly independent of pH from 1 to 8 suggesting that the sorption of tetrachloroaurate (III) and gold (I) by *C. vulgaris* may be covalent in nature (37). Further modifications of the algae surface indicated that the amine group plays an important role in the binding of gold to *C. vulgaris*.

Non-living *Sargassum natans* and *Ascophyllum nodosum* showed extraordinary uptake capacity for gold and cobalt was possible via ion exchange mechanism (20). The electrostatic interactions between cationic species and the negatively charged cell surfaces may be responsible for the metal binding. The solution pH influenced the uptake capacity whereas the equilibrium biosorption isotherms were independent of the initial concentration of the metal in solution. Comparisons between living and non-living biosorbents showed that dead biomass tends to sequester and effectively retain the metal ions due to the absence of active ion transport mechanisms. Desorption of the metal ions from the biomass was also demonstrated.

Adsorption of Na^{+}, K^{+}, Li^{+}, Cs^{2+}, Mg^{2+}, Ca^{2+}, Ba^{2+} and Sr^{2+} on *Vaucheria*, *Spirogyra* and *Oedogonium* was quantitatively represented by the Langmuir adsorption isotherm (35). The number and nature of surface sites were quantified by a pH titration technique. The maximum amount of metal adsorbed, y_m and the equilibrium constant K, were determined for each metal ion. Variations in the adsorption parameters with pH and type of metal indicated that metal ions adsorb to algal surfaces by electrostatic attraction to negative sites, such as carboxylate anions.

The abilities of *Ecklonia maxima*, *Lessonia flavicans* and *Durvillea potatorum* and two seaweeds derivatives, alginate fibres and dealginated seaweed waste to remove Cu^{2+}, Ni^{2+}, Zn^{2+}, Pb^{2+} and Cd^{2+} from solution have been investigated (38). All the biomasses were found to efficiently remove (up to 0.98 mg/g) the metal ions studied. Although all the seaweeds and derived materials exhibited a relatively good ability to remove heavy metal ions, the seaweed-derived materials showed better overall performance. Selectivity in the adsorption process and recovery of the metal ions by the biomasses was also demonstrated. Further studies (39) demonstrated a molar relationship between nickel uptake and calcium release for *Ecklonia maxima*, dealginated seaweed waste and alginate fibre. The rate of uptake of nickel and the extent of ion exchange involved in the metal ion adsorption may vary for the different biomasses studied.

Another study performed using the blue-green algae *Entromorpha*, *Cladophora* and *Bryposis* described the ability of these biomaterials to bind Cu^{2+}, Au^{3+} and Al^{3+} (40). The results showed increased metal binding with pH. A significant decrease in the measured pH of the supernatant was observed for those biomaterials, which demonstrated greater metal binding, suggesting an ion-exchange type mechanism due to the release of protons. The different metal binding profiles and capacities exhibited for the studied algae may enable the selective recovery of metals from solution by the manipulation of the solution pH. Studies indicated that gold could be sequestered from dilute or concentrated acidic solutions by dead *Sargassum natans* biomass (41, 42). The biosorptive gold sequestering mechanism may be based on adsorption in combination with a gold reduction process. The biomass was identified as a potent biosorbent material that can release the metal in a subsequent elution regenerative cycle.

The binding of Cu (II) to *Chlamydomonas rehinhardii* algae and exudates from the biomass was studied by a combination of several analytical techniques (43). The metal ion solution was used to titrate the biomass surface and the concentrations of Cu (II) species were determined

by ion selective electrode, differential pulse polarography and acid treatment. The results were evaluated in terms of conditional equilibrium constants at pH 6.5. The information was used to simulate the binding of copper species to the biomass. Under the conditions studied, the binding of Cu (II) to algal exudates had a more significant dependency on copper speciation than the binding to the algal surfaces.

Biomass of non-living, dried brown marine algae *Ascophyllum nodosum*, *Fucus vesiculosus* and *Sargassum natans* demonstrated high equilibrium uptake of cadmium from aqueous solutions (44). A Langmuir sorption model served to estimate the maximum metal uptake values. Results showed that *A. nodosum* uptake exceeded the commercial ion exchange resin DUOLITE GT-73 with the highest amount of cadmium accumulated by the biomass exceeding 100 mg g^{-1}. There was no damage to the biosorbent appearance and performance in repeated metal uptake/elution cycles employing 0.1-0.5 M HCl. The same group of brown algae mentioned above revealed a high biosorptive uptake of lead and nickel (45). Langmuir approximations were used to evaluate the sorption process. Metal uptake performance was demonstrated to be pH dependent. The sorption capacity and physical properties were reinforced by crosslinking the biomass with formaldehyde, bis(ethenyl)sulfone and 1-chloro-2,3-epoxypropane, resulting in a slight increase in the uptake performance of the biomass.

The effect of temperature, initial pH and initial metal ion concentration on the adsorption of chromium (VI) ions to *Chlorella vulgaris* and *Clodophara crispata* was investigated (46). The results were evaluated using the Freundlich adsorption model and the Freundlich constants were reported for both biomasses. Maximum adsorption rates were found at pH 1–2 and high adsorption capacities were observed at low concentrations of metal ions.

Experimental studies have shown that brown marine algae *Ecklonia radiata*, can be used for the removal of heavy metal ions from wastewater (47). An uptake capacity of 1.36 mM g^{-1} for

lead was reported within a pH range of 4.5 to 5.5. The equilibrium data fitted well to the Langmuir model. The presence of metal ions such as sodium, calcium, magnesium and potassium in solution did not significantly affect lead adsorption (<10%) in contrast to commercial ion exchange resins.

The removal of heavy metals from an effluent from a Brazilian zinc-producing industry by *Sargassum sp.* showed efficiencies close to 100% in the biosorption of Zn^{2+}, Cd^{2+}, Cu^{2+}, Al^{3+} and Mn^{2+} in the presence of high concentrations of Ca^{2+}, Na^{+}, Mg^{2+} and K^{+} (48). Batch experiments indicated no absorption of the alkaline-earth metal ions by the biomass but an influence on the uptake performance was observed suggesting an ion-exchange mechanism. The continuous system gave comparable treatment efficiency, with a high operational stability, suggesting the viability of recycling the recovered metals.

The biosorption process using a *Sargassum* biosorbent to remove and recover copper from ferruginous water has been demonstrated (49). The algal biomass binds approximately 2.3 meq g^{-1} of metal cations from water by ion exchange. The values of ion exchange equilibrium constants showed that the affinities of metals towards the biosorbent decreased in the following order Cu>Ca>Fe. Results showed that the biosorbent saturated with Cu could be regenerated with HCl. In an attempt to improve the performance of this seaweed biosorbent, protonated and Ca-forms were prepared, by washing the biomass with H_2SO_4 or with $Ca(OH)_2$ (50). The biosorbent bound up to 40 mg^{-1} of Cr (III) at pH 4. An ion-exchange model which assumed that the only species taken up by the biomass were $Cr(OH)^{2+}$ successfully fitted the experimental biosorption data for Cr (III). Cr (VI) was efficiently removed by this biosorbent in the vicinity of pH 2. The existence of the optimum pH for the removal of Cr (VI) may be explained by the desorption of Cr (III) from the biomass at low pH and the effect of pH on the reduction potential of Cr (VI) in aqueous solutions. Subsequently, it was demonstrated that protonated, non-living biomass of *Sargassum fluitans* effectively sequestered uranyl ions from aqueous solution (51), with the maximum uranium sorption capacity exceeding 560 mg g^{-1}. Isotherms

were interpreted in terms of the Langmuir model at various pH levels. The biosorption was demonstrated to be an ion exchange process between the uranium ions and protons introduced to the biomass binding sites during the acid pre-treatment.

Another study indicated that *Durvilliea potatorum*; *Ecklonia radiata* and *Laminaria japonica* have high adsorption capacities and binding affinities for Pb^{2+}, Cu^{2+} and Cd^{2+} (52), showing adsorption capacities comparable to those of commercial ion exchange resins and higher than other types of biomass that have been previously studied. The results generally fitted the Langmuir equation and showed low interference effects from other metal ions.

The biosorption characteristics of the brown algae *Macrocystis pyrifera*, *Kjellmaniella crassiforia* and *Undaria pinnatifida* for Cd^{2+} and Pb^{2+} ions have been investigated (53). The number of surface sites and the acid dissociation constants were determined by potentiometric titration, revealing the presence of carboxylic groups on alginic acid. The results showed that the biosorption of bivalent metal ions to the biomass studied was due to bivalent binding to the carboxylic groups on alginic acid present in the brown algae. A metal complexation model was applied to evaluate the results and the model gave good results for the description of the binding data.

The simultaneous biosorption of Cr (VI) and Fe (III) ions together on the biosorption of Cr (VI) and Fe (III) ions by *Chlorella vulgaris* was investigated in terms of initial rates of biosorption and equilibrium isotherms (54). Since initial biosorption rates and equilibrium metal removal decreased with increasing concentrations of the other metal ion, the combined action of Cr (VI) and Fe (III) ions on C. *vulgaris* was generally found to be antagonistic. The competitive Freundlich model for binary metal mixtures was suitable for most adsorption equilibrium data of Cr (VI) and Fe (III) ions on the biomass.

The sorption and desorption of Cu and Cd by two brown algae *Laminaria japonica* and *Sagassum kjellmanianum* and five species of microalgae *Spirulina patensis, Nanochloropsis oculata, Phaeodactylum tricornutum, Platymonas cordifolia* and *Chaetoceros minutissimus* were studied (55). The macroalgae exhibited high capacities at pHs between 4 and 5 while for the microalgae the optimum pH value was at 6.7. Results evaluated using the Freundlich model suggested a multiplicity of mechanisms and sorption sites. The reversibility of metal sorption was achieved employing HCl and EDTA. The presence of other cations impaired the sorption process.

Calcium saturated *Durvillaea potatorum* and *Ecklonia radiata* were used as biosorbents for the removal of Pb^{2+} and Cu^{2+} from aqueous solutions (56). The biomasses showed adsorption capacities comparable with those of commercial ion-exchange resins. Optimum pH value for the process was 4.5. Both biosorbents were effective in removing lead and copper in the presence of chelating agents and other light metal ions in the wastewater.

The Freundlich and Langmuir adsorption models were used for the mathematical description of the biosorption of Cu^{2+}, Ni^{2+} and Cr^{6+} to dried *C. vulgaris, S. obliquus* and *Shynechocystis* sp. (5). The results showed that the adsorption equilibrium data fitted very well to both models. Optimum pH values were determined as 5, 4.5 and 2 for all three algae respectively. The results demonstrated that variations in algal concentration affect the biosorption process.

Another brown marine algae *Pilayella littoralis* was evaluated as a potential biosorbent for Al (III), Cd (II) Co (II), Cr (VI), Cu (II), Fe (III), Ni (II) and Zn (II) (57). High binding capacities between 430 and 2000 $\mu mol\ g^{-1}$ of dried biomass were reported for the metals studied. Fast rate of uptake and pH dependence in metal ions binding was found for the biosorption process. Metal ions were efficiently desorbed using 0.12 M HCl.

Rapid kinetics for the removal of Ni^{2+} by *Chlorella miniata* were found (58). Langmuir parameters and an adsorption capacity value of 2985 $\mu g\ g^{-1}$ were reported. The algae showed better sorption for Ni^{2+} compared with *C. vulgaris* under the same conditions.

It is evident that extensive laboratory studies have been carried out to study the biosorption of a range of metal ions by many different biomasses. However, the optimum process conditions largely depend on the type of biosorbent used, the nature of the metal studied and the mathematical approach used to describe the data.

1.2.2.4.1. Biosorption Columns

The metal binding capacity exhibited by biosorbents makes them suitable for remediation of metal-bearing industrial effluents. The fixed-bed and the continuous flow stirred tank reactor are two systems that could be used for the evaluation of these biosorbents on an industrial scale. The continuous flow fixed-bed reactor is now commonly used, despite the limited availability of granulated biosorbents (2). The advantages of using columns are that a steady state separation is achieved and parameters such as pH and solution concentration can be controlled. Column experiments are useful for the determination of biosorbent capacities, effective binding capacities, breakthrough curves and ion exchange capacities. Parameters such as flow rate, particle size and solution conditions evaluated using a bench scale experiment can be successfully applied to production scale prototypes (6).

The performance of columns is related to the length and shape of the ion exchange zone developed during the sorption and regeneration process. This zone is formed between the part of the column that is saturated with the adsorbed metals and the section that still contains unsaturated biosorbent. The zone moves along the column as the loading or regeneration of the biosorbent progresses. Once the sorbent saturation zone approaches the end of the column, the metal concentration in the outlet stream increases sharply, this is known as the breakthrough point (59).

Biosorption can be exploited for the preconcentration of metals from dilute solutions (32, 60). A large volume of the dilute metal solution is passed through the column, and the sorbed metal is stripped from the column by lowering the pH using a much smaller volume of acid (61). Algal material has been used to preconcentrate specific analytes before quantitative determination by spectrometric techniques. Early attempts at using algae to preconcentrate metals did not employ column type systems. A strain of *Stichococcus bacillaris* was used to preconcentrate Cd ions from a solution of 270 $\mu g\ L^{-1}$ cadmium in a batch type experiment (62). Cd uptake was affected by the analyte concentration, volume of solution and pH. Evaluation of the effectiveness of Cd biosorption and preconcentration from riverine and marine reference materials was later found to be unsuccessful because of the high salinity of the solutions. It was possible to analyse a sample in 4 min using this approach (33).

Copper preconcentration from seawater and riverine water samples by *Chlorella* and determination by slurry graphite furnace atomic absorption spectrometry has been described (34). The adsorption of Cu was improved by washing the algae with HCl and concentration factors between 5 and 100 were found. The seawater matrix showed no effect on the biosorption process. Similar preconcentration factors were found for nickel and cobalt (63). In this study, sampling volume, matrix effects and pH were evaluated and the results showed no influence from these parameters. Acid washing improved the biosorbent performance.

In a further development, an on-line system employing a column packed with silica-immobilised *Chlorella pyrenidosa* for the separation and detection of Pb^{2+} and Cu^{2+} by anodic stripping voltammetry was described (64). The data indicated that algae-silica preparations were durable under continuous flow conditions. Diluted acid was used as a regenerant and the column was continuously used for up to 100 Anodic Stripping Voltammetry cycles. The results confirmed the feasibility of using algae-silica column in an on-line configuration. The high binding capacity of algal biomass combined with the structural features of porous silica made the biosorbent suitable for column use.

A biosorbent material derived from brown marine alga *Ascophyllum nodosum* has been examined in a packed-bed flow through sorption column for the removal Cd^{2+} (65). The algae were previously crosslinked with formaldehyde and the dry granules of this material were used to pack the column. The breakthrough times for the columns were determined for different flow rates and bed depths at pH 5.5. The Bohart and Adams theoretical approximation was used to evaluate the column performance. The results showed a 99% reduction in the concentration of Cd^{2+} from solution in a continuous flow operation. The high performance of the column, short contact time, short critical bed depth and the high adsorptive capacity for the biosorbent were demonstrated.

Continuous flow experiments were carried out using *Ecklonia radiata* in a packed column (47). The chromatographic columns (1 cm diameter) were loaded with algal granules and Pb^{2+}, Cd^{2+} and Cu^{2+} solutions were injected at a flow rate of 1.5 ml min^{-1}. The sorption capacities of the column were reported to be between 1.25 and 1.35 mM g^{-1}. The capacities found were comparable to the capacities determined in a batch experiment. It was demonstrated that metals in solution at the parts per billion levels could be removed by the biosorbent column.

Polysilicate immobilised *Medicago sativa* has been used to show that up to 600 mg L^{-1} of copper ions in solution could be removed under flowing conditions (66). Diluted acid was employed to desorb the copper bound at a flow rate of 2 ml min^{-1}. Using this experimental set up, 97% of copper ions in solution were efficiently removed and the column remained relatively stable after 10 binding/recovery cycles of 120 bed volumes per cycle using 5 mgL^{-1} copper solution.

Cell fragments of *Datura innoxia* immobilised on a polysilicate matrix were used for the removal of Ag^{+}, Cu^{2+}, Cd^{2+} and Ca^{2+} (40). The biomass column was coupled on-line to form a frontal affinity chromatography type set up and furnace atomic absorption spectrometry was used for the determination of the elements. The metal binding affinity order at solution pH

3 – 5 was determined to be $Cu^{2+} > Cd^{2+} \approx Ag^{+} > Ca^{2+}$. The application of a regularised least-squares method indicated the existence of two classes of sites on this biosorbent involved in the binding of Ag^{+}.

A continuous metal biosorption system was conducted using a laboratory acrylic column packed with *Sargassum sp.* (48). Concentration factors of 514, 224 and 96 for cadmium, zinc and manganese respectively were reported. Experiments conducted in the absence of alkaline and alkaline-earth elements in solution produced much higher efficiency values, demonstrating the influence of these elements in the biosorption process.

An ion exchange type of mechanism was proposed to explain the biosorption of Cu^{2+} by *Sargassum fluitanis* biomass protonated by acidic wash or loaded with Ca^{2+} (67). Binary biosorption systems (Cu/H, Cu/Ca, Ca/H) were studied with the pre-treated biomass at controlled pH. Calcium bound biomass offered the advantage of longer column lifetime for sorption, but did not allow the effective recovery of Cu. Furthermore, the $CaCl_2$ pre-treated biomass was prone to leaching leading to reduced Cu column capacity. The protonated biomass offered the advantage of efficient Cu recovery, but the sorption capacity was less than that for the calcium biomass. The Ca/H system had a longer column life, excellent Cu recovery but was time-consuming to prepare. Cu removal and recovery from the biosorption column was predicted by numerically solving the equations of a proposed ion-exchange model.

Macroalgae *S. kjellmanianum* packed into glass column and saturated with Cu was studied for its adsorption/desorption performance (55). EDTA and HCl were evaluated as desorption solutions. HCl was more effective than EDTA for the desorption of Cu from the macroalgae column (99.5%).

Effective copper removal/recovery from ferruginous wastewater using a *Sargassum* biosorbent packed column has been described (49). The chromatographic behaviour could be described using an ion-exchange model. It was demonstrated that the column removed Cu^{2+} by biosorption and Fe (III) by precipitation. Desorption of the Cu and Fe was achieved by lowering the pH of the feed solution.

A laboratory strain of *S. cerevisiae* immobilised on sepiolite was successfully used to preconcentrate Fe and Ni in brass (NBS SRM 37e) demonstrating the capacity of the method for the determination of trace metals in metal alloys (68). A column packed with either *D. potatorum* and *E. radiata* could be used to remove lead ions from a 2 mM solution so that only parts per billion levels could be detected in the effluent (56). The total adsorption capacities for both biosorbents were reported to be 1.6 and 1.3 mmol g^{-1} respectively.

The recovery of the metal from the biomasses was achieved using nitric acid. The authors also demonstrated that *D. potatorum* could be used as an efficient biosorbent for the treatment of cadmium bearing waste streams (69). Pre-treatment of the native biomass with calcium chloride and subsequent thermal treatment considerably improved the swelling properties and physical stability of the biomass granules. Packed bed studies showed that the biosorbent column could purify (below 0.1 mg L^{-1}) 500 bed volumes of 0.5mM $Cd(NO_3)_2$ solution.

Immobilised alfalfa biomass (*Medicago sativa*) on silica has been employed as column packing for the biosorption studies of a mixture of cadmium, copper, lead, chromium, nickel and zinc ions in solution (70). The order of metal adsorption was found to be: Cu(II) > Pb(II) ≈ Cr(III) > Zn(II) > Cd(II) ≈ Ni(II). Metal leaching with HCl resulted in recoveries greater than 90% except for Cr for which 44% was recovered.

Dry potassium pre-treated *Sargassum* algal biosorbent was used in the biosorption of Cu, Cd and Zn from multi-component mixtures in a column-type system (71). In a mixed solution

containing Zn and Cd, the retention of Zn was reduced, because of the higher affinity of packing material for cadmium. The process was computationally simulated using the IMPACT programme.

A similar set up using Ca-*Sargassum* biomass was employed to evaluate the sorption process for Cu, Cd and Zn (72). The results showed similar behaviour for Zn and Cu as described above. An ion exchange equilibrium model (ECM) was used to predict the metal displacement from the column. The ECM model successfully predicted the occurrence and the magnitude of the displacement. The column lifetime was predicted by combining the ECM with a mass transfer column model (MTCM).

The silica-immobilised cationic polyelectrolyte, [poly (N-xylene-N,N' dicyclohexyl ethylenediamine dibromide)], capable of electrostatic binding with the biofilm of a natural alga *Spirogyras* sp. was used in a column separation for the enrichment of trace analytes (73). The biosorbent AlgaSORB-sp could be used to selectively separate and preconcentrate Cu^{2+} ions from the mixture of multi-element samples at pH 6.9. Co-sorption of Cd^{2+} and Pb^{2+} ions was not observed at the studied pH despite the fact that individual metal solution experiments demonstrated that approximately 100% of metal was sorbed by AlgaSORB-sp. A total Cu^{2+} sorption capacity of 1.23 $\mu mol\ g^{-1}$ was reported. The kinetics of the sorption phenomena were expressed using the Langmuir equation. Recoveries between 92 and 100% for Cu^{2+} were achieved when HCl was used as a stripping agent. The preconcentration factor of AlgaSORB-sp was 175-fold for Cu^{2+} ions. The results of the evaluation of three water samples containing Cu^{2+}, Pb^{2+}, Fe^{3+}, Fe^{2+}, Zn^{2+}, Cd^{2+} and Co^{2+} demonstrated that AlgaSORB-sp selectively sorbed Cu^{2+} without interference from other ions. The study demonstrated that the biosorbent could be used under continuous flow conditions for over 100 cycles.

Some other biological substrates apart from algae have been used for the adsorption and preconcentration of metals in continuous flow systems. Columns packed with *Escherichia coli* and *Pseudomonas putida* immobilised on silica were used to retain and preconcentrate gold

from solution (74). The results showed that the optimum pH values of 9 and 11 for *P. putida* and *E. coli*, respectively. Preconcentration factors between 2.5 and 25 were found for both bacteria, with a gold recovery of approximately 97% and 87% for *E. coli* and *P. putida*, respectively.

The adsorption of Be (II), Cd (II), Se (IV) and Hg (I) by immobilised *E. coli* and *P. putida* was also studied (8). Metal sample solutions, real samples and standard reference materials, Water SRM 1643c, Water SRM 1641b and Coal Fly Ash SRM 1633a were analysed as received. Metals were eluted using HNO_3 and the fractions were analysed by ETAAS. Breakthrough capacities and recoveries between 98 and 101% were reported for each metal studied. The method was demonstrated to have applicability across a wide pH range. The detection limits were better than others reported previously and it was free from interference. The packing showed acceptable flow rates and no detectable signs of swelling.

The separation and speciation of Cr (III) and Cr (VI) with *Saccharomyces cerevisiae* immobilised on sepiolite has also been described (75). Samples of both chromium species at pH 2 were flushed through a glass column filled with the immobilised biomass and HCl was used to elute the retained Cr(III). Total Cr was determined after the reduction of Cr(VI) to Cr (III) in the eluted sample by the addition of concentrated H_2SO_4 and ethanol. The recovery of the analyte was >95% and the column was relatively stable for up to 20 runs. A breakthrough capacity of 228 $\mu mol\ g^{-1}$ for Cr (III) was reported. The presence of other metal ions such as Zn^{2+}, Cu^{2+}, Cd^{2+}, Ca^{2+}, Mg^{2+} and Na^{+} did not significantly affect the retention of chromium. The proposed method was successfully applied to the separation, preconcentration and speciation of Cr (III) from Cr (VI) in spiked sample solutions and Kizilirmak river water samples.

A column containing *Escherichia coli* immobilised on sepiolite was used for the preconcentration of Cu, Zn, Fe, Ni and Cd (76). Different pH values, bed height, type and volume of elution solutions and flow rates were evaluated. Breakthrough capacities

determined from breakthrough curve plots were reported for each metal studied. The determination of Cu, Zn, Fe and Ni using the biosorbent column was performed for Standard Reference Material (NBS SRM 85b). Results in good agreement with the reported values were found. The column was found to be relatively stable for up to 20 runs.

1.2.2.4.2. Modification of the Biosorbents

Chemical modification techniques have been used to explore the chemistry involved in metal ion adsorption by biomasses. Several chemical treatments have been employed to modify the functional groups such as carboxyl, amino and phosphate, that are considered to be the principal functional groups responsible for the adsorption process.

A decreasing in the sulphydryl groups available in algal cell walls of *Chlorella vulgaris* determined by polarographic titration with *p*-(hydroxymercuri)phenylsulfonate was shown when the algae was treated with tetrachloroaurate (III) (37). Other cell-wall modification experiments indicated that treatment of *C. vulgaris* with succinic anhydride lead to blockage of the amine group that resulted in a decrease in the binding capacity for Au (III).

Modification of carboxyl groups present in *Cyanidium caldarium, Eisenia bicyclis, Laminaria japonica, Spirulina platensis* and *Chlorella pyrenoidosa* was performed using acidic methanol (77). The degree of modification was monitored by base hydrolysis of the modified biomass and subsequent analysis of the released methanol by gas chromatography. All esterified biomasses showed a dramatic decrease in Cu^{2+} and Al^{3+} sorption capacities along with an enhancement of Au^{3+}capacity, although the degree of reduction varied with the algal species. Hydrolysis of the biomass showed that during the first 12 h of esterification 90% of the carboxyl groups were modified and the remaining 10% were esterified in the subsequent 24 to 48 h. These results indicate that carboxyl groups on algal cells were responsible for a great portion of Cu^{2+} and Al^{3+} binding and play an inhibitory role in Au^{3+} binding.

Humic substances extracted from Sphagnum peat moss were esterified using acidic methanol and trimethoxymethane (78). The esterified carboxyl groups were hydrolysed by pH adjustment with sodium hydroxide. The binding of copper ions to both modified biomasses was studied. The Cu (II) binding ability decreased in the esterified biomass from 100% to 80% at pH 5, implying that although carboxyl groups are involved in the adsorption process, other groups such as phenol or hydroxyl groups may also bind Cu. After base hydrolysis the Cu (II) binding ability was completely restored.

The esterification of carboxylate groups present in the cell walls of *Datura innoxia* led to a decrease in metal uptake by as much as 40% for Cd^{2+}, 21% for Cu^{2+} and 18% for Sr^{2+} at pH 5 (61). Experiments performed at pH 2 showed no change in the metal uptake ability of this modified material, supporting the assumption that other groups participated in the adsorption process. Base hydrolysis demonstrated the reversibility of the process. The results showed that the material retains a great portion of its binding capability even after being subjected to adverse conditions.

The role played by carboxylate groups was confirmed using the *D. innoxia* biomass for the binding of Pb^{2+} and Al^{3+} and monitoring the impact of the modification by FTIR and solid state-NMR (30, 79). In the same context, the X-ray absorption techniques, XANES and EXAFS were used to verify the possible mechanism of Cr (III) and Ni (II) binding by alfalfa biomass (80). The esterified biomass sample exhibited less binding capacity due to the reduction of the carboxylate groups on the surface, and the EXAFS results showed that the binding mostly occured through coordination with oxygen ligands. Esterification using propylene oxide in water was found to be faster and more selective than esterification using acidic methanol. The acidic methanol method was found to cause desulphonation reactions making it impossible to independently distinguish their effect on metal complexation (81). The use of these two techniques allowed distinction between the carboxylate contribution (methanol esterification) and the sulphonates contribution (propylene oxide esterification).

It was found that lead was more efficiently bound to a modified sample of *S. fluitanis* with higher sulphonates content, while the cadmium binding capacity remained similar for both modified samples (82). Further modification of the biomass, using acetone/water as an extracting agent for hydrolysable polyphenols showed no reduction in cadmium or lead uptake.

The chemical modification of different biomasses such as hetrotrophs, methanothrophs, algae, sulphate reducers and exopoly-saccharide-producing cultures was performed using a variety of methods including encapsulation in polysulphone resin, acid, alkali, carbon disulphide, phosphorus oxychloride, anhydrous formamide, sodium thiosulphate, sodium chloroacetic acid and phenylsulphonate treatments (83). Treatments with sodium chloroacetic acid, carbon disulfide, phosphorus oxychloride and sodium thiosulfate resulted in significant enhancements in metal cation-binding capacity, however chemically modified biosorbents do not appear to be very stable with repeated use. Some chemical treatments such as phosphorus oxychloride produced biosorbents capable of binding anions. Selective elution of metals bound to biosorbents demonstrated that a purification of mixtures of metals could be achieved.

Esterification of carboxylate groups and methylation of amino groups were performed on portions of raw *Aspergillus niger* biomass, in order to study the role played by these functional groups in the biosorption of copper, lead and cadmium (84). It was found that modification of the functional groups significantly reduced the biosorption of the studied metals. Lead biosorption was observed to be more sensitive to modifications of the carboxyl group than of the amine group, while cadmium and copper binding was found to be more sensitive to modifications of the amino group than the carboxyl group. Release of Ca, Mg and K ions was observed during the biosorption by raw biomass suggesting an ion-exchange mechanism.

The surface of non-living biomass of *Pycnoporus sanguineus* was chemically modified for lipid extraction by a methanol-chloroform mixture and proteins were extracted using sodium hydroxide in order to study their role in lead, copper and cadmium biosorption (85). Methylation of the amino groups and esterification of the carboxylate groups was also performed. Results showed a reduction in the metal uptake from the solution. The use of scanning electron microscopy indicated that the structure of biomass had changed due to the adsorption of the metals onto the cell walls. EDAX analysis showed release of calcium during the sorption process indicating the occurrence of an ion-exchange mechanism.

1.2.2.5. Modelling the biosorption process

Biosorption typically involves a combination of active and passive transport mechanisms starting with the diffusion of the metal ion to the surface of the biomass cell. Once the metal ion has diffused to the cell surface, it will bind to sites on the cell surface, which exhibit some chemical affinity for the metal. This step includes a number of passive accumulation processes and may include adsorption, ion exchange, coordination, complexation, chelation and microprecipitation. Generally, such metal ion adsorption is fast, reversible and not a limiting factor in bioremoval kinetics when dealing with dispersed cells. Biosorption is often followed by a slower metal ion binding process in which additional metal ions are bound, often irreversibly. This slow phase of metal uptake can be due to a number of mechanisms, including covalent bonding, surface precipitation, redox reactions, crystallisation on the cell surface or diffusion into the cell interior and binding to proteins and other intracellular sites (5).

The occurrence of a diversity of different processes opens the possibility to model the biosorption process using different approaches. Adsorption isotherms and ion exchange models are the most commonly employed mathematical approximations used to simulate the biosorption process. A number of approximations and mathematical programmes have been developed based mainly on these two approaches.

The application of an ion-exchange model to illustrate the adsorption of Cu^{2+}, Sr^{2+}, Zn^{2+}, Mg^{2+} and Na^{+} by *Vaucheria s.* has been described (4). The approach to determine the ion-exchange constants was based on measuring the amounts of all species, sorbed as well as in solution. The molar ratios of H^{+} displaced to mol of M^{2+} adsorbed for Cu^{2+}, Zn^{2+}, Mg^{2+} and Sr^{2+} were 1.2, 0.66, 0.59 and 0.30 respectively, with Na^{+} showing no affinity. Experiments conducted displacing Na^{+} and Sr^{2+} resulted in ion-exchange constants giving the strength of adsorption of metal ions to algae as Cu>Sr>Zn>Mg (by displacement of Na^{+}) and Cu>Zn>Mg (by displacement of Sr^{2+}). The constants by displacement of Na^{+} were found to be 2.6×10^{-3}, 3.7×10^{-3}, 7.7×10^{-3} and 8.1×10^{-3} for Cu, Sr, Zn and Mg, respectively. Ease of displacement was reflected by larger constants.

Further studies on *Vaucheria sp.*, *Rhizoclonium sp.* and *Tribonema sp.* demonstrated that the overall stoichiometry of proton uptake was that 1 divalent metal (Ca or Mg) was released when 2 protons were adsorbed (86). The stoichiometry of Sr adsorption by *Vaucheria* with an equivalent amount of Ca, Mg released identified the adsorption phenomena as an ion-exchange process. Sorption of amines on *Vaucheria* has also been studied using the approximation described above (87). Results showed the adsorption to be essentially an ion exchange process. The stoichiometry resulted in a displacement of equivalent amounts of Ca and Mg when the algae sorbed protonated ethylenediamine and ethyl glycinate. An unusually high sorption for ethylenediamine occurred at pH 10.5 indicating the possibility of other types of interaction, more probably including hydrogen bonding, since the amine is in a neutral form at this pH value.

Ion exchange constants for Mg, Mn, Ca, Ni Zn, Cd, Cu and Pb displacing calcium on Peat moss using the same approach have also been determined (88). A model in which two ion exchange sites are used has been compared to the experimental data for the sorption of Cd, Cu and Zn by protonated *Sargassum fluitans* in systems containing two metal ions and protons at pH values of 2.5, 3 and 4.5. Equilibrium constants were determined using MATLAB 4.0. The

experimental data and the model showed that the binding is independent of the metal concentration, indicating metal competition for the same limited number of binding sites. In order to apply the model, only two equilibrium constants were necessary and the results showed that it was possible to predict the behaviour of a two-metal system using data from a single metal system, considerably reducing the amount of experimental work. The model was able to simulate the relative binding of the metals to the biomass. From the results, it was concluded that both electrostatic attraction and covalent bonds may contribute to biosorption.

The behaviour of a Cu-Zn system varying pH values for a constant total concentration of each metal showed that Zn is weakly bound to the biomass compared to Cu (89). The system was successfully modelled using the chemical equilibrium programs MINEQL+, demonstrating the predictive power of the model and the description of metal ion binding at different pH values can be achieved. The model employed as described above has also been used along with a fix-bed model to describe Cu^{2+} removal and recovery in a biosorption column packed using *Sargassum fluitans* seaweed biomass (67). Ion-exchange isotherms described the biosorption equilibrium for Ca-biomass and H-biomass as being "favourable" leading to a self-sharp dynamic exchange zone in the fixed-bed system, as was shown by the breakthrough results. The good agreement between the theoretical and experimental results revealed that the model could be used as a mathematical representation for the first biosorption cycle in the fixed-bed system. However, the use of the model is limited since it does not take into account variations in the values of the overall mass-transfer coefficients of the sorbing species with time.

A model combining an isotherm model and the Donnan model has been developed to predict the equilibrium of protons, Cd^{2+} and Ca^{2+} ions binding by the brown alga *Sargassum* (90). The effects of metal ion concentration, pH and ionic strength were established. The model showed that the Na^{+} concentration has no influence on Cd binding if the ionic strength was very high or if the Na concentration was very low. The model predicted a 50% reduction in

Cd binding when the Ca^{2+} concentration was between 2 and 100 times higher than that of Cd^{2+}. The model demonstrated that divalent ions had a greater effect on the Cd binding due to its higher electrostatic accumulation and because it partially binds co-ordinately.

The biosorption of Cu and Ni at different ionic strengths by *Sargassum*, *Colpomenia*, *Petalonia* and *Ulva* have been illustrated by a modified version of the model described above (91, 92). The pH effect on metal binding and the change in proton binding were predicted by the model and stoichiometries for the studied metal were proposed.

The equilibrium column model (ECM) for fixed-bed columns was introduced along with the ion-exchange model for the evaluation of Cu biosorption from ferruginous wastewater by *Sargassum* algal biomass (49). The ECM has been developed to describe the competitive ion exchange in a column and has proved to be useful for assessing the technical and economical feasibility of an ion exchange process. It is based on the assumptions that the composition of the feed solution is constant; that no neutralisation, complex formation or precipitation in the exchanger bed occur, the pre-saturation of the biosorbent is homogeneous and the mass transfer resistance for ions diffusing from the bulk of the feed solution into the biosorbent particle is negligible. The model predicted the chromatographic effect in the column performance due to the differences in sorption affinities of Fe and Cu. The Fe and Cu breakthrough curves could be predicted, however the assumption of negligible mass transfer resistance resulted in a steeper breakthrough curve than the one obtained, showing the limitation of the model.

A mathematical model to describe the uranium equilibrium binding to a nonliving protonated *Sargassum* biomass has been proposed (93). The hydrolysed ion exchange model (HIEM) was based on the assumptions that in the range of acidic to neutral pH values the uranium cation $UO_2^{2+}$is hydrolysed in an aqueous solution and the presence of hydrolysed uranium species depends on the solution pH and on the total uranium concentration in the solution. The ion

exchange reaction takes place between various hydrolysed uranium ions and protons in the biomass binding sites; the total uranium uptake consists of the binding of all forms of hydrolysed uranium ions by biomass and all types of possible biomass binding sites have the same affinity to uranium cations. The other parameters required for the application of the model such as equilibrium constants for hydrolysed species, protons and uranium ions could be regressed from the isotherm experimental data at various pH values. The total binding capacity of biomass could be determined by acid-base titration for the protonated biomass. A nonlinear square method developed in MATLAB was employed to find the optimal combination of the parameter sets. The regressed model curves at pH 2.4, 3, 3.5 and 4 corresponded very well with the experimental points obtained. The model demonstrated that the monovalent behaviour of the hydrolysed uranyl ion enhances the overall uranium uptake. The acidic elution of the uranium bound to the biomass was successfully modelled. No significant error was found due to the heterogeneous nature of the binding sites, although the use of a multiple site model would be more appropriate. The model could predict the equilibrium status from the initial conditions for both uranium biosorption and acid desorption.

The multi-component Langmuir model, the ion exchange model and isotherms developed and described above were applied to evaluate the biosorption of Cd by brown seaweeds *Durvillaea*, *Laminaria*, *Ecklonia* and *Horosira* pre-saturated with Ca, Mg or K (31). The ion exchange model fitted very well at low concentrations, and it was postulated that the Langmuir model was applicable at higher metal concentrations, where binding of the displaced ion is low. Application of the model allowed establishment of the biosorption metal affinity sequences for the materials studied. The calculated parameters could be used in the derivation of dimensionless ion-exchange isotherms for the prediction of the behaviour of the biosorbents in dynamic flow-through biosorption systems.

The IMPACT computer programme has been used to model the column performance in the biosorption of Cu, Cd and Zn from multi-component mixtures by potassium-saturated

Sargassum biosorbent (71). The IMPACT code and the associated modelling methodology were adapted for describing the transport of chemicals for various flow patterns, assuming mass transfer kinetic limitations, steady flow, constant temperature, pressure and pore geometry. IMPACT accounts for the flow structure in the sorption bed by assuming a series of ideal mixing cells of uniform composition. The user has to define the parameters of the series, such as number and volume of cells, flow rate, chemical interactions and elementary reactions, including name of species, their stoichiometric coefficients and the equilibrium constants. The programme performed the simulations for three experimental column system and provided the concentration breakthrough profiles for the ionic species chosen. IMPACT could reasonably simulate the complex column biosorption performance, however the predictions for breakthrough times for zinc and cadmium were shifted ahead by 20% and copper simulation was not successfully completed.

The Equilibrium Column Model (ECM), described previously and the Mass Transfer Column Model (MTCM) have been applied in modelling the occurrence and magnitude of overshoots of toxic heavy metals sorbed by *Sargassum* algal biomass (72). An efficient and accurate numerical method previously developed (94) has been adapted for solving model equations, which consider different rate control mechanisms formulated for fixed bed multi-component ion exchange processes. The algorithms were applicable to both ion exchange and liquid adsorption and showed to be extendable to a general form of isotherms. The model enabled testing the approach for the case of biosorption while reducing the number of equations to a minimum. The elution order of the sorbed metals, the existence and the extent of the metal overshoots and the column lifetime were predicted by combining the two methods.

A titration model and the Langmuir isotherm sorption model have been applied to describe copper, cadmium and iron biosorption by a culture of *Arthrobacter sp.* (95). The results suggested the possible existence of two weakly acidic sites, demonstrated by the titration model. The chemical model was able to predict copper biosorption data between pH 3 and

5, iron and cadmium modelling were not taken into consideration. The application of the model is limited since the occurrence of ion exchange and complexation could not be confirmed as unique mechanisms in the pH range studied.

The non-ideal competitive adsorption model (NICA) developed and applied to model metal ion binding to humic substances (96 - 99) has been used to describe the biosorption of protons, calcium, cadmium, zinc and lead ions by two bacteria strains. The proposed model assumes that two site types are involved in metal ion binding and the biosorption of bivalent metal ions is due to monodentate binding to all sites, resulting in a maximum adsorption for protons and for bivalent cations equal to the number of available binding sites. The model gave good results for the description of metal ion binding to whole cell bodies of the bacteria (53, 100).

The competitive adsorption Langmuir and Freundlich models have been used to describe and compare the competitive biosorption of Cr (VI) and Fe (III) ions to *C. vulgaris* and *R. arrhizus* (37). An interaction term η_i, which is a characteristic of each species and depends on the concentrations of the other components, has been added to the competitive Langmuir model. The data fitted both the non-competitive Langmuir and Freundlich models. The modified Langmuir model successfully characterised the competitive adsorption of Cr (VI) and Fe (III) ions from two components system by *R. arrhizus*, while the Freundlich model was satisfactory for most adsorption data of these ions on *C. vulgaris*. Because of the previous results on *C. vulgaris*, the Freundlich model has been applied for the simulation of the biosorption of copper (II) and chromium (VI) in a single-staged batch reactor (101). The residual concentration and equilibrium isotherms for one metal ion depending on a second metal ion were estimated at equilibrium.

Alternatively, Freundlich and Langmuir models have been applied to a multistage purification process employing *Schizomeris leibleinii* and *Rhizopus arrhizus* as biosorbents (102, 103). The

adsorption of iron (III), lead (II) and cadmium (II) was modelled and the isotherm constants were calculated for both processes. The data fitted both Langmuir and Freundlich models and was useful for the estimation of residual metal concentrations at equilibrium at each stage. The calculated constants could be used to predict the parameter values in different purification systems serving different wastewater compositions.

1.2.3. Spectroscopic Techniques

1.2.3.1. Inductively Coupled Plasma Optical Emission Spectrometry (ICP-OES)

A variety of metals can be determined using inductively coupled plasma atomic spectrometry in a wide range of concentrations. This method has shown high sensitivity in the analysis of water, soil and biological samples, making it suitable for the determination of metals present in different matrices.

In principle, ICP can be used for the determination of all elements other than argon. The sample is nebulised and introduced in the flow of plasma support gas, which is typically Ar, where the atoms of the elements present are ionised, excited and quantified using a detector (Figure 4).

An inductively coupled plasma (ICP) is a very high temperature (7000-8000K) excitation source that efficiently desolvates, vaporises, excite, and ionises atoms. Molecular interferences are greatly reduced with this excitation source but are not eliminated. ICP sources are used to excite atoms for atomic-emission spectroscopy and to ionise atoms for mass spectrometry.

The plasma torch (Figure 5) consists of concentric quartz tubes. The inner tube contains the sample aerosol and Ar support gas and the outer tube contains flowing gas to keep the tubes cool. A radio frequency (RF) generator (typically 1-5 kW at 27 MHz) produces an oscillating current in an induction coil that wraps around the tubes. The induction coil creates an

oscillating magnetic field. The magnetic field generated induces a current in the ionised Ar gas stream and a plasma is formed almost instantaneously when the Ar gas is seeded with energetic electrons. These electrons are produced either by a high voltage Tesla discharge, or a solid-state piezoelectric transducer. The atoms and ions contained in the plasma vapour are excited into a state of radiated light (photon) emission. The radiation emitted can be passed to the spectrometer optics via an optical fibre, where it is dispersed into its spectral components.

Figure 4 Schematic representation of an ICP-OES

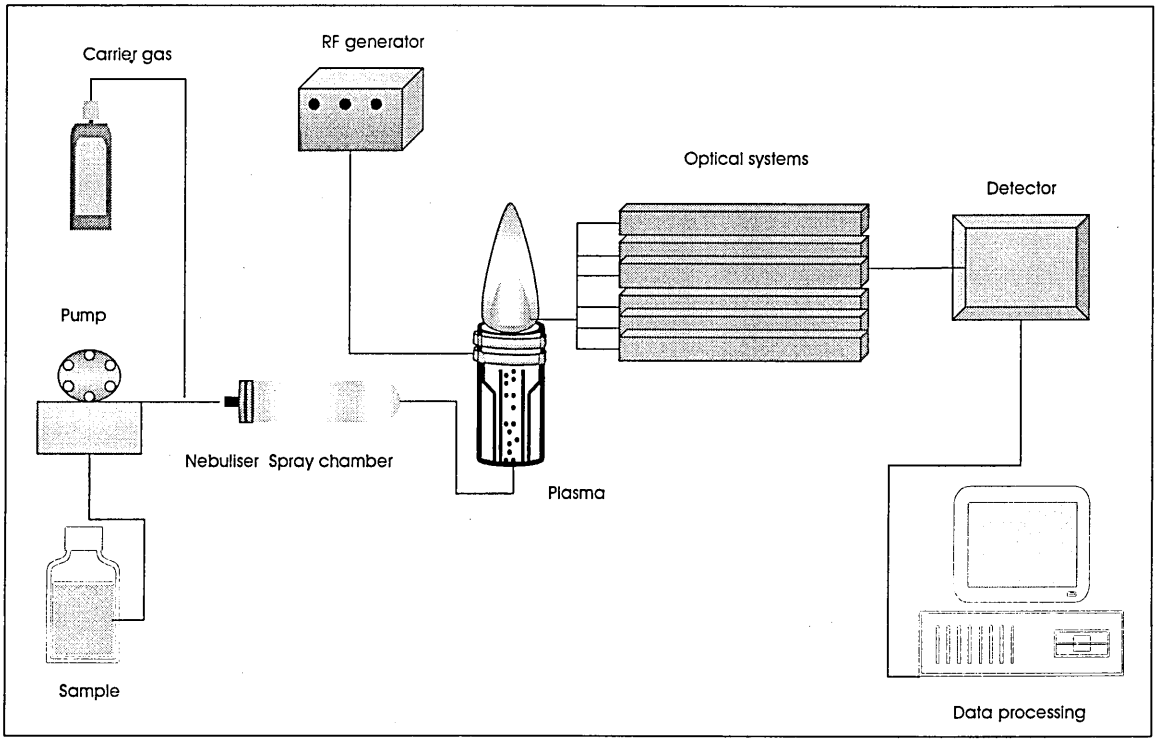

Figure 5 Simplified model of the plasma

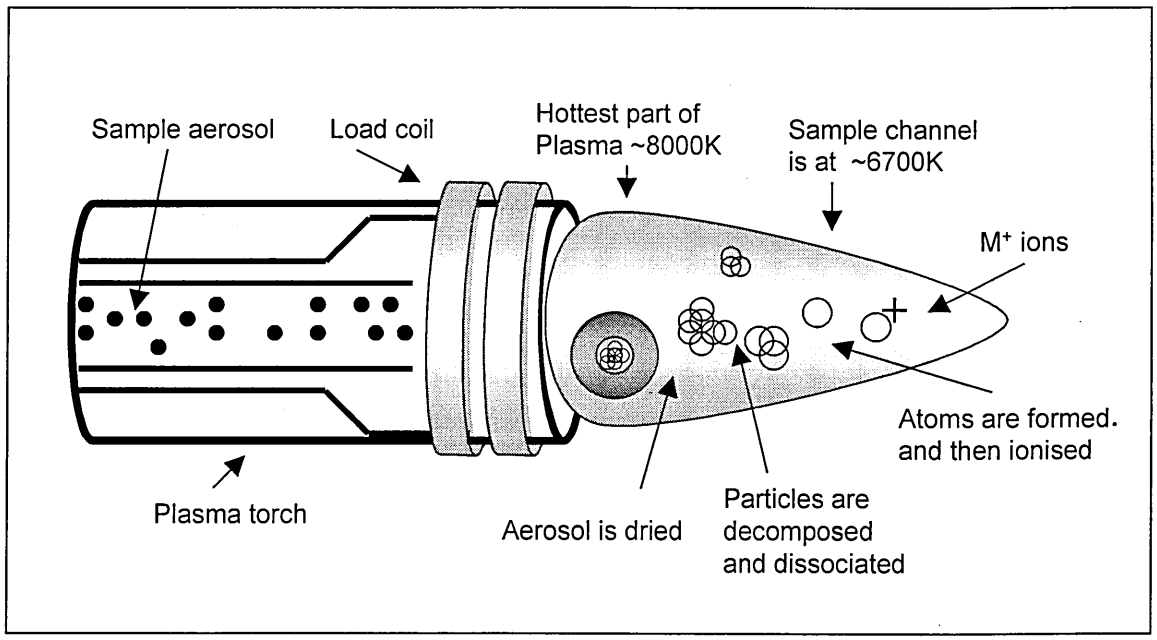

From the specific wavelengths emitted by each element, the most suitable line for the application is measured by means of a PMT (photomultiplier tube) or a CCD (charge coupled device). The radiation intensity, which is proportional to the concentration of the element in the sample, is recalculated internally from a stored set of calibration curves and can be shown directly as percent or measured concentration (104, 105).

1.2.3.2. Inductively Coupled Plasma Mass Spectrometry (ICP-MS)

Inductively coupled plasma-mass spectrometry has become one of the most important techniques for elemental analysis because of its low detection limits for most elements, its high degree of selectivity and its good precision and accuracy. Ions produced in a conventional ICP torch are sampled through a differentially pumped interface linked to a quadrupole mass spectrometer, resulting in an optical spectrum consisting of a simple series of isotope peaks for each element studied. An important part of the ICP-MS instrumentation is the interface that

couples the ICP torch, which operates at atmospheric pressure with the mass spectrometer, which requires pressure levels of less than 10^{-4} torr (106).

The sampling cone consists of a water-cooled nickel cone with a small orifice at its centre, which serves as a passage for the hot plasma gas that is pumped through this orifice into a region that is maintained at a pressure of about 1 torr. In this region, the gas is expanded and cooled. A fraction of the gas then passes through a small hole in a second cone called a skimmer and into a chamber maintained at the pressure of the mass spectrometer. In the chamber the positive ions that are separated from electrons and molecular species by a negative potential, are accelerated, and are focused by a magnetic ion lens onto the quadrupole mass analyser. ICP-MS instrument can determine elements in the mass range 3 to 300, to resolve ions differing in *m/z* by 1, detect up to 90% of the elements in the periodic table with a measurement times of 10 s per element with detection limits in the 0.1 to 10 $\mu g\ L^{-1}$ range for most elements (106).

1.2.3.3. Infrared Spectrometry

Infrared (IR) spectroscopy measures the absorption of infrared radiation by chemical bonds. Infrared radiation is defined as electromagnetic radiation with frequencies between 14300 and 20 cm^{-1}. When a normal molecular motion such as vibration, rotation, rotation/vibration or overtone of these normal vibrations results in a change in the molecule's dipole moment, a molecule absorbs infrared radiation. Chemical structural fragments of molecules, known as functional groups tends to absorb IR radiation in the same frequency range regardless of the structure of the rest of the molecule that the functional group is in. This correlation between the structure of a molecule and the frequencies at which it absorbs IR radiation allows the structure of unknown molecules to be identified (107).

Fourier transform infrared spectrometry (FT-IR) has been developed in order to measure all the infrared frequencies simultaneously. This is accomplished using an interferometer, which produces a unique type of signal that has all of the infrared frequencies encoded into it. The signal can be measured very quickly, usually in one second or so, reducing the time of analysis per sample. The interferometer uses a beamsplitter which takes the incoming infrared beam and divides it into two optical beams, one beam reflects off of a flat mirror which is fixed in place and the other beam reflects off of a flat movable mirror. The two beams are recombined when they meet back at the beamsplitter at different lengths interfering with each other, resulting in an interferogram. The measured interferogram signal is decoded using Fourier transformation performed by a computer, which then presents the analyst with the desired spectral information for analysis. The major advantages of FT-IR are fast analysis because all of the frequencies are measured simultaneously in seconds; it is a very sensitive technique, the fast scans enable the addition of several scans in order to reduce the random measurement noise to a desired level, and the instruments are self calibrating employing a HeNe laser as an internal wavelength calibration standard (106).

Infrared spectrometry has been used to elucidate the biosorbent composition and mechanism of metal biosorption by different biomasses. The infrared spectroscopy of gold-laden *S. natans* revealed that the polysaccharidic carbonyl groups of the biomass were mainly responsible for binding gold with amino groups playing perhaps a minor role (108).

Infrared spectra of protonated *Sargassum* biomass showed the characteristic bands corresponding to free carbonyl double bonds from the carboxyl functional group, which correlated with the spectrum for alginic acid spectra (82). Cadmium loaded alginic acid and *Sargassum* biomass infrared spectra showed a clear shift of the carbonyl-stretching band, typical of the complexation of the carbonyl group by dative coordination with cadmium. These results provided evidence for the ion exchange by complexation.

Infrared analysis has been performed on esterified and unesterified biomass of Sphagnum peat moss (78). Results confirmed the presence of carboxyl groups on the unesterified samples. The esterification of these groups was also demonstrated. Modified and native *D. innoxia* biomasses contacted with Cd^{2+}, Sr^{2+} and Cu^{2+} have been analysed using FT-IR. The spectra obtained for native cell fragments contacted with metal ions were the same as the blank samples, although the presence of carboxylate groups was elucidated (30, 61). Differences between the untreated, esterified and saponified samples demonstrated the presence of carboxyl groups and confirmed the modification of these groups by the chemical modification procedures employed.

The surfaces of *Cyclotella cruptica* and *Chlamydomonas reinhardtii* have been characterised using chemical and spectroscopic methods that included FT-IR (109). Results showed spectra comparable to those obtained for *D. innoxia* and seaweed, and indicated a wide variety of functional groups, of which some, like the –OH groups of carbohydrates, are not relevant for proton and metal binding. The importance of N-containing groups has also been indicated.

Infrared spectra of raw and chemically modified *Aspergillus niger* have been obtained to evaluate the effects of chemical treatment on the functional groups involved in the biosorption of lead, cadmium and copper (84). The spectra showed the presence of carboxylate and amino groups. The results from biosorption studies using chemically modified biomass suggested that both groups play an important role in the biosorption of the metal studied.

Chemically modified *Pycnoporus sanguineus* has been analysed using FT-IR (85). Modifications included methylation of the amino groups and esterification of the carboxylic acids. IR spectra of raw biomass showed the presence of amino groups, possibly from protein, and no carbonyl groups were observed in the range expected although some differences were observed in comparison with the spectra from the esterified samples. The spectra for the NaOH treated

biomass was significantly reduced in intensity because of the amino-acid modification. Results from the biosorption studies were correlated to the functional groups described.

The infrared spectra of pure *Spirogyra* and prepared AlgaSORB have been used to monitor the immobilisation of the raw biomass on silica (73). Vibrations corresponding to terminal secondary amine groups were present in the native biomass spectrum but not in the polymer spectrum. The occurrence of C-N and C-Br vibrations in the polymer spectrum supported the immobilisation of the matrix onto silica gel. The presence of carboxylate anions was observed as well as prominent peaks for phosphate and sulphydryl groups.

FT-IR has been used to elucidate the main chemical groups present on the cell membrane of *Arthrobacter sp* (95). The IR spectrum obtained revealed the existence of amino, hydroxyl, amide, acidic and phosphate groups, suggesting a polysaccharide structure of the biomass.

1.2.3.4. Scanning Electron Microscopy

The Scanning Electron Microscope (SEM) is one of the most versatile and widely used tools of modern science as it allows the study of both morphology and composition of biological and physical materials.

High-resolution images of the morphology or topography of a specimen, with great depth of field, at very low or very high magnifications can be obtained by scanning an electron probe across a specimen. Compositional analysis of a material may also be obtained by monitoring secondary X-rays produced by the specimen-electron beam interaction. Detailed maps of elemental distribution can be produced from multi-phase materials or complex, bioactive materials. Characterisation of fine particulate matter in terms of size, shape and distribution as well as statistical analyses of these parameters, may be performed (110, 111).

The SEM consist basically of an illuminating/imaging system, which produces the electron beam and directs it onto the sample; an information system that collects the data released by the sample during electron bombardment; a detector which discriminates amongst and analyses these information signals; a display system consisting of one or two cathode tubes for observing and photographing the surface of interest and the vacuum system for the removal of gases from the microscope column, which would otherwise interfere with high-resolution imaging (112).

One of the most important developments of the SEM technique is the Environmental Scanning Electron Microscope (ESEM). In essence, conventional SEM samples would normally have to be clean, dry, vacuum compatible and electrically conductive in order to produce useable and easily obtained results. A number of SEM preparation techniques promoted the introduction of artefacts to a number of different types of materials. The use of ESEM makes possible wetting, drying, absorption, melting, corrosion, crystallisation allowing one to monitor and record dynamic processes as they happen, with virtually no sample preparation. The advantages of ESEM includes secondary electron imaging in dry gas or water vapour at full SEM resolution, up to 2 nm with FEG system; imaging of wet samples with no dehydration and observation of the sample in its natural environment. No sample preparation is required even for insulating samples, X-ray analysis of non-conductive samples and observation of dynamic experiments at high temperatures in a gas environment can also be achieved (113, 114).

Scanning electron microscopy has been employed mainly for the study of the morphology of several biological materials. Previous micrographs of *Stichococcus bacillaris* used for the preconcentration of cadmium and lead have been reported (33, 115). The micrographs showed the morphology of the colony and an average radius of 1.54 μm was determined. The electron micrograph of the immobilised algae on silica showed an incomplete total surface coverage. The overlapping of the cell walls and the large surface contact area

between the silica and the algae surface observed suggested a loss of the metal sorption sites.

Both scanning and transmission electron microscopy were used to examine the possible morphological effects of exposure to high and trace concentrations of copper on *M. rouxii* (116). Electron micrographs of inactivated cells grown at higher copper concentration showed abnormal development in contrast to the filamentous hyphae which resulted when the same strain was grown at trace copper concentrations.

SEM has been used to evaluate the morphological changes in the drying of *P. littoralis* used for the biosorption of Al (III), Cd (II), Co (II) Cr (VI), Cu (II), Fe (III), Ni (II) and Zn(II) (57). The electron micrographs of the freeze-dried and oven-dried material showed that the freeze-drying procedure was a gentler method of preservation, since the original plant's tissue microstructure was still present on the sample. Salt crystals could be observed on the algal fragments. No significant differences were reported when the metal binding efficiency of the two samples was evaluated.

The microstructures of different forms of dry samples of the biomass of marine macro alga *D. potatorum* have been obtained using SEM (117). The micrographs showed a structure of cylinder or fibre-like shaped sizes between 3 to 5 μm and a uniform distribution of copper and cadmium ions on the biomass structure however, speciation of the ions could not be identified. The methods of drying and pre-treatment seemed to affect the internal structure of the biosorbent.

Electron micrographs of different biomasses have been recorded on a Transmission Electron Microscope (20, 23, 118). The results revealed that the cell wall of *S. natans* was responsible for sequestering gold and cobalt from solution; cadmium was accumulated within large vacuoles

of *S. cerevisiae* and iron was distributed on the cell wall as well as in the cytoplasmic and nuclear materials of *S. fluitans*.

1.2.3.5. Extended X-ray Absorption Fine Structure

X-ray absorption spectrometry (XAS) using synchrotron radiation is based on the irradiation of a sample with a monochromatic X-ray microbeam of tunable energy. By scanning the energy over an absorption edge of an element of interest in fractional steps and recording either the absorption of the beam (absorption XAS), the fluorescence radiation produced (fluorescence XAS) or another shell dependent phenomenon, the fine structure of the edge is measured. The edge location and the shape provide information on the chemical environment, as the energy necessary to excite the bound electron shifts slightly with changes in the chemical environment of the chemical species involved. Two energy regions around the edge may be exploited and provide different structural information, the near edge region (XANES) and the extended region. The extended X-ray absorption fine structure, EXAFS, provides information on the number, the atomic number and the distance of neighbouring atoms (119).

EXAFS does not occur for isolated atoms but only appears when atoms are in a condensed state. The absorption edge corresponds to an X-ray photon having enough energy to just free a bound electron in the atom. When the electrons are in the most tightly bound n = 1 shell the edge is called the K-edge. For the next most tightly bound shell of atoms, the n = 2 shell, the corresponding edges are called the L=edges. Atoms in molecules can absorb X-rays. Generally, the proportion of X-rays absorbed (the absorption coefficient) will decrease as their energy increases, but at certain values of energy, specific to each element, a sudden increase in the amount of energy absorbed is observed. These energies are known as absorption edges.

The energies correspond to the ejection of an electron from the atom in question (*i.e.*, ionisation). The ejected electron can be considered as a wave, travelling outwards from the

central absorbing atom. The increase in absorption at the edge occurs when the energy of the incident X-rays is equal to the threshold energy necessary to eject an electron. Simple models of X-ray absorption predict a gradual monotonic decrease in the absorption coefficient with increasing energy away from the absorption edge. Such behaviour is observed in the spectra of isolated atoms such as Xe and Kr, but for atoms either in a molecule or a condensed phase, the presence of other atoms around the absorber causes oscillations in the absorption coefficient near the edge. These oscillations in the post edge region arise from the backscattering of the emitted electron wave of neighbouring atoms and so the structure of the post edge region of the X-ray absorption spectrum is related to the radial distribution of atoms in the sample (Figure 5) (119).

Figure 6 Illustration of the EXAFS process

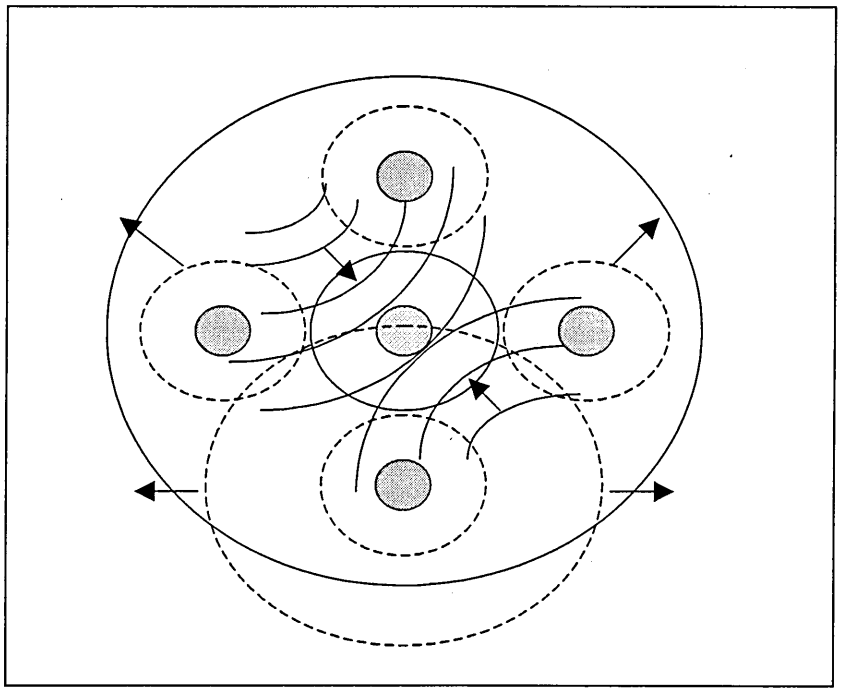

The solid lines represent the energy of the X-ray absorbed by the central atom and the dashed lines indicate the outgoing scattered wave backscattered off from the surrounding atoms. How the oscillation varies with the wavelength of the photoelectron depends on the distance

between the centre atom and backscattering atom. The variation of the backscattering strength as a function of the energy of the photoelectron depends on the type of atom doing the backscattering. Thus, by analysing the structure, the frequency and amplitude of the oscillations, information about the local environment of the absorbing element can be derived (120).

EXAFS has been used for the characterisation of Cr (III) and Ni (II) binding with alfalfa biomass (80). For nickel, good fits were obtained for six oxygens and six nitrogens and the distances were calculated. No reasonable fits were found using only sulphur or a mixture of sulphur and oxygen or nitrogen. Results for $Cr(NO_3)_2$ standard and Cr biomass showed a good fit for six oxygens, suggesting that Cr binds to the biomass by oxygen ligands.

EXAFS results for the uptake and biotransformation of Cu (II) in *Larrea tidentata* have shown that a Cu(II)-O interaction occurs in the roots, stems and leaves (121). The presence of a strong Cu-S interaction in the roots, stems and leaves has also been observed with relative coordination numbers of 2, 2 and 4 respectively.

EXAFS and XANES experiments have been carried out to study the effect of oxidation state on iron binding by *Medicago sativa* (122). The data for iron (II) and iron (III) biomass indicated similar metal coordination environments and good fits for Fe-O were obtained in both cases. Monodentate carboxylate coordination was found to be more likely to occur than bidentate. The XAS data indicate that both iron (II) and iron (III) uptake proceeds without a redox change via carboxylate ligation.

Further EXAFS studies have been carried out to characterise the binding of Cr (VI) and Cr (III) by *Avena monida* biomass (123). The results demonstrated a reduction of Cr (VI) to Cr (III) by the biomass and the reduced Cr (III) was bound to oxygen containing ligands (possibly carboxyl groups) similar to a weak cation-exchange resin.

The reduction and accumulation of gold by *Medicago sativa* has been studied using X-ray absorption spectroscopy (124). XANES results revealed that Au (III) is reduced to Au(0) and there was no evidence for either Au (III) or Ai (I) bound to the biomass. Analysis of the isolated first shell EXAFS oscillation was used to determine the size of the Au (0) particles.

EXFAS and XANES have been used for the determination of gold binding to *Chlorella vulgaris*(105). The oxidation state of the algae-bound gold was determined to be Au (I) and Au (III) and no Au (0) state was observed. Strong evidence was presented for ligand-exchange reactions leading to the formation of bonds between Au (I) and sulphur or nitrogen contained in the algae. The mode of binding appears to be different for the samples derived from the Au (I) complexes than for those derived from $Au(III)Cl_4^-$.

Materials and Methods

Chapter 2

2.1. Materials

2.1.1. Reagents

All reagents were Aristar grade and supplied by BDH, Poole, U.K. Deionised Millipore, (Milli-Q RG) water was used throughout. 10 mg L^{-1} single metal solutions of cadmium, copper, chromium, lead, nickel, silver, gold and aluminium ions were prepared by dissolving cadmium nitrate, copper nitrate, chromium nitrate, lead nitrate, nickel nitrate, silver nitrate, gold chloride and aluminium nitrate salts in distilled water. In the case of the column experiments, a multielement stock solution containing 10 mg L^{-1} of Cu, Cd, Cr and Pb was prepared from individual 1000 mg L^{-1} Spectrosol solutions. Working standard solutions for ICP-AES and ICP-MS analysis were prepared by dilution of the 10 mg L^{-1} stock solution. The unbuffered standard solutions were kept in the pH range 5.5 – 6.5 by the addition of either 1.0 M HCl or NaOH solutions. Buffered solutions were prepared in 0.05 M ammonium acetate except for copper and silver, which were prepared in 0.1 M potassium dihydrogen phosphate. For the preconcentration experiments a multielement stock solution containing 10 mg L^{-1} of antimony, arsenic, cadmium, chromium, cobalt, copper, gold, lead, manganese, mercury, nickel, palladium, scandium, selenium, silver, strontium, tellurium, vanadium and zinc was prepared from individual 1000 mg L^{-1} Spectrosol solutions. Methanol was used for the esterification of the biomass. A NaOH 0.1 M solution was employed for the hydrolysation experiments. The potentiometric determination of Cd and Pb was performed using standard solutions prepared from cadmium nitrate and lead perchlorate. A 5 M $NaNO_3$ (Orion ISA 940011, Beverly, USA) solution was used as an ionic strength adjustor. All glassware was cleaned and stored in a 1% v/v HNO_3 solution until required. Each item of glassware was then thoroughly rinsed with deionised water before use.

2.1.2. Source of the Biomass

The dealginated seaweed waste was supplied courtesy of FMCc Biopolymers, Haugesund, Norway. This material is the residue after the commercial extraction of alginates and carageenans for the food and pharmaceutical industries. The material has undergone a number of processing steps in the extraction of alginates before being finally dewatered by calcium precipitation prior to disposal. This material has a moisture content of 66%. The fresh product was stored in the frozen state in order to prevent microbiological spoilage and alterations in the biosorption performance of the material.

2.1.3. Apparatus

An orbital shaker (Gallenkamp) was used to agitate the samples during the batch uptake experiments. A pH electrode (Gelplas, BDH) connected to a pH meter (Orion model 740A) was used for pH measurements. A cadmium ion selective electrode (Orion Sure Flow combination cadmium electrode model 9648, Beverly, USA) was used for the determination of Cd ions. Lead ion measurements were carried out using a Pb ion selective electrode (Orion Ionplus series model 9682, Beverly, U.S.A.). A centrifuge RC5C Sorval Instruments (Du Pont, U.S.A) was used to centrifuge the samples. After the esterification and hydrolysis process, an Edwards freeze dryer, cold trap 1000 (S.B. Freeze Driers, Kent, U.K.) was employed to dry the samples. UV/Vis UV2 spectrometer (Unicam Instruments, Cambridge, U.K.) was used for Cr determination.

2.1.4. Inductively Coupled Plasma Spectrometers

An ICP-AES (Spectro Instruments, Kleve, Germany) or an ICP-MS HP 4500 (Hewlett Packard, Yokogawa Corporation, Japan) was used to determine the metal concentrations. The instrument conditions are shown in Table 1.

Table 1 ICP operation conditions

ICP and sample introduction	ICP – MS	ICP - AES
Power	1200 W	1200 W
Column to spray chamber distance	70 mm	70 mm
Torch	Fassel Torch	Three piece torch
Spray chamber	Cyclonic	Cyclonic
Nebuliser	Babington	Cross flow
Sample introduction	Peristaltic Pump	Peristaltic Pump
Solution uptake rate	0.8 ml min^{-1}	0.8 ml min^{-1}
Coolant gas flow rate	16 L min^{-1}	16 L min^{-1}
Nebuliser gas flow rate	1.28 L min^{-1}	1.0 L min^{-1}
Nebuliser gas pressure	590 kPa	234 kPa
No of sweeps per replicate	1	1
No of replicates	3	3
Masses / Wavelength (nm)	^{27}Al	
	^{45}Sc	
	^{51}V	
	^{53}Cr	Cr 267.716
	^{55}Mn	Mn 257.610
	^{58}Ni	Ni 231.603
	^{59}Co	Co 238.892
	^{63}Cu	Cu 324.754
	^{64}Zn	Zn 213.856
	^{75}As	As 228.812
	^{80}Se	Se 196.026
	^{88}Sr	Sr 407.771
	^{107}Ag	Ag 328.068
	^{111}Cd	Cd 226.502
	^{121}Sb	Sb 252.852
	^{197}Au	Au 267.595
	^{202}Hg	Hg 253.852
	^{208}Pb	Pb 220.351
Measurement mode	Time resolved analysis	
Integration time	2 sec	2 sec
Measurement time	800 sec	800 sec
Detector mode	Dual mode	

2.1.5. Titration Experiment

Dealginated seaweed samples were titrated potentiometrically using an automatic titrator Metrohm 678 EP/KF processor (Herisau, Switzerland) with a combined pH glass electrode (Model 6.0202) and a 665 Dosimat automatic burette.

2.1.6. Elemental Analysis

A Perkin Elmer 2400 CHN Elemental Analyser (Llantrisant, U.K.) was used for CHN determination.

2.1.7. Infrared Studies

Infrared measurements were performed using a Nicolet 860 E.S.P Magna infrared spectrometer (Nicolet, Wisconsin, U.S.A) employing a Nicolet Smart Golden Gate Single Reflection Diamond ATR accessory (Specac, Nicolet, Wisconsin, U.S.A) featuring a type IIa diamond with up to 250 pounds of pressure available to keep the sample in optical contact with the diamond.

2.1.8. Environmental Scanning Electron Microscope

The Environmental Scanning Electron Microscope used in this study was a FEI-Philips, XL30-ESEM-FEG (FEI company, Eindhoven, The Netherlands). The instrument was operated in ESEM mode using water vapour as the deionising gas. An acceleration voltage between 15-30 Kev and a beam current of 2-8 nA was used for the imaging and X-ray surface analysis. The X-ray analyser employed was an ISIS/300 EDS Analyser (Oxford Instruments, Hygh Wycombe, U.K.) using a Pentajet SATW detector.

2.1.9. X-ray Absorption Fine Structure Spectroscopic Studies

The X-ray absorption spectra were measured at room temperature at the Synchrotron Radiation Source at CLRC Daresbury Laboratory, U.K. For the X-ray measurements, the synchrotron was running at energy of 2 Gev and beam currents of 100 – 200 mA during all

experiments. Station 9.2 was used to measure Au, Ag, Cu and Pb. This station has a water-cooled, harmonic-rejecting double crystal Si (220) monochromator. Data were obtained in fluorescence mode using a Canberra 13 element solid state detector filled with a 32 channel scale to allow a maximum count rate of 85 KHz per channel. A monitor foil placed in front of a third ion chamber was used to determine the edge energy with precision. Ni was measured in Station 8.1, which has a water-cooled focussing double crystal Si (III) monochromator and a toroidal focussing mirror. A Canberra 13 element 550 detector with a maximum count of 17 kHz per channel was employed.

2.2. Methods

2.2.1. Optimisation of the mass to volume ratio

In order to investigate the optimal quantity of biomass required to effectively sequester heavy metal ions from solution, experiments were conducted with known weight of biomass. 50 ml of 10 mg L^{-1} cadmium ion solution was contacted with 0.1, 0.2, 0.5, 1, 1.5, 2.5 and 5.0 g of biomass dry weight. The samples were agitated in an orbital shaker for 2 h since previous studies showed that 2h was sufficient to achieve equilibrium. After the contact time, the samples were filtered through a Whatman No 1 filter paper, and analysed for cadmium content by Inductively Coupled Plasma Atomic Emission Spectrometry (ICP-AES). The concentration of cadmium in solution showed no differences in cadmium uptake between 0.2 and 2.5 g. There was a reduction in cadmium uptake using 0.1g, and the increase in cadmium uptake using 5 g was not high enough to justify the use of such an amount of biomass. Therefore, a mass to volume ratio of 1:100, or 10 g L^{-1}, was chosen for all the experiments.

2.2.2. Pretreatment of the Dealginated Seaweed

The dealginated seaweed used in early stages was as supplied. In order to optimise the biosorption process, the biomass was washed with deionised water several times. This process efficiently removed any precipitated salt on the surface of the biomass, but left bound cations. Cations such as calcium, sodium, potassium and magnesium were washed out using dilute hydrochloric acid. Hydrochloric acid was chosen in order to avoid the use of oxidising acids. Studies were carried out using 0.01, 0.1, 0.5, 1.0, 2.5 and 5.0 M HCl keeping a mass to volume ratio of 1:100. The biomass was stirred for 1, 2, 3, 4, 5, 6 and 24 h and filtered through a Whatman No 1 filter paper. The biomass was washed with deionised water three times and then was left to air dry. The pH of the water fraction was recorded. After this process the biomass was ready for use. The filtrate and the water fraction were analysed for calcium, sodium, potassium and magnesium content by ICP-AES. For silver the biomass was washed using phosphoric acid, since excess of chloride ions in the matrix led to silver chloride precipitation.

2.2.3. Batch Laboratory Experiments

2.2.3.1. pH Studies

The influence of the pH on the biosorption process was carried out using buffered and non-buffered solutions. 10 g of dealginate was placed in contact with 1 L of 10 mg L^{-1} of metal solution with the pH adjusted to 2.0, 3.0, 4.0, 5.0, 6.0, 7.0, 8.0 and 10.0. The pH was continuously monitored using an immersed pH electrode connected to a pH meter. The pH was adjusted when necessary using either 0.1 M NaOH or HCl. Five millilitre aliquots were taken at set times up to a period of 24 hrs. The liquid was filtered as described above and the pH was recorded. The concentration of metal ions in the filtrate was determined by ICP-AES. For the non-buffered solutions, the pH of the sample was adjusted using either 0.1 M NaOH or HCl, except for Ag experiments where 0.1 M solutions of either H_3PO_4 or KOH were employed. In the case of the buffered solutions, the Au, Al, Cd, Cr, Cu, Ni and Pb metal ion solutions were

prepared in 0.05 M ammonium acetate buffer and the pH was adjusted using 0.1 M solutions of acetic acid or ammonium hydroxide. The solutions for Cu and Ag were prepared in 0.05 M potassium phosphate and the pH was adjusted using 0.1 M solutions of phosphoric acid or potassium hydroxide.

2.2.3.2. Kinetics Studies

The rate of adsorption of metal ions by dealginate was determined for Ag, Al, Au, Cu Cd, Cr, Ni and Pb. A 10 mg L^{-1} solution of each metal ions was prepared by dissolving the metal nitrate salt in distilled water. The pH of the solutions was adjusted to 6 using 0.1 M NaOH and 0.1 M HCl except for Al and Au where the pH working ranges were 4 for Al and 3 for Au because above this pH values Al and Au hydroxides may precipitate. 10 g of biomass was added to 1 L of the 10 mg L^{-1} metal solution in a 2 L beaker. The mixture was agitated on a magnetic stirrer. Five millilitres aliquots were taken at set times up to a period 24 h and the liquid was filtered through a Whatman Number 1 filter paper. The concentration of metal ions in the filtrate was determined by ICP-AES. All experiments were conducted in triplicate at room temperature. Control experiments without dealginate were carried out in order to determine the degree of removal of metal ions from solution by the glassware and filter papers.

The kinetics of the sorption process was also determined using a batch procedure as follows: 0.5 g of dry biomass was added to 50 ml of the 10 mg L^{-1} metal solution in a 150 mL glass flask. The biomass and metal solution was contacted by agitation on an orbital shaker for periods ranging between 5 minutes and a maximum period of contact of 24 hours. After the appropriate period had elapsed, the liquid was separated from the biomass by filtration through a Whatman Number 1 filter paper. The concentration of metal ions in the filtrate was determined by ICP-AES. All experiments were conducted at room temperature and triplicates of each experiment were carried out in order to ascertain the degree of variation in the experimental procedure.

2.2.3.3. Equilibrium Experiments

Standard adsorption experiments were conducted according to the batch method except that the initial solution pH was maintained at pH 6 for Cu, Cd, Cr, Ni, Pb and Ag, 3 and 4 for Au and Al respectively. The period of biomass and solution contact was fixed at two hours. The initial concentration of metal in solution was varied between 1 and 750 mg L^{-1}. Metal concentrations in these experiments were determined by ICP-AES.

2.2.3.4. Saturation Experiments

The saturation capacity of dealginate to adsorb metals was studied in the batch mode. 5 g of washed dry dealginate was suspended in 500 mL of 500 mg L^{-1} single metal ion solution at the desired pH for two hours. After the appropriate contact time, the sample was filtered and the filtrate was kept for ICP-AES analysis. The biomass was then returned to the beaker and a fresh 500 mL aliquot of the 500 mg L^{-1} metal ion solution was added to the beaker. The previously described methodology was repeated at this stage so that the beaker containing the biomass and the single metal ion solution was agitated for another two hours. These cycles were carried out using the same sample of biomass until the metal concentration in the filtrate did not change. Portions of these samples of biomass were kept for Infrared, Scanning Electron Microscopic and Extended X-ray Absorption Fine Structure spectroscopic analysis.

2.2.3.5. Titration of Dealginated Seaweed

Dealginated seaweed was titrated potentiometrically using the following procedure: 2.0 g of dry sample was suspended in a reaction vessel containing 50 mL of 0.1 M $NaClO_4$, which was used as an inert electrolyte maintained the ionic strength in the solution. The sample was stirred and continuously purged using nitrogen. The titration was performed by adding standardised 0.1 M HCl or NaOH to the sample every 30 seconds. The pH was recorded throughout the process. The software package Microcal Origin 5.0 (Microcal Software Inc, Northampton, USA) was used to calculate the first derivative of the titration curve.

2.2.3.6. Esterification of Dealginated Seaweed

Modification of the carboxyl groups on dealginate using acidic methanol was performed as follows: 9 g of dry washed dealginate was suspended in 633 mL of 99.9% methanol to which 5.4 mL of concentrated hydrochloric acid was added (0.1 M HCl final concentration). The solution was continuously stirred and heated to 60°C for 48 h. The biomass was then washed three times with cold deionised water in order to quench the esterification reaction, and then centrifuged to remove excess water. The esterified sample was lyophilised and used in metal binding experiments (77).

2.2.3.7. Hydrolysation of Dealginated Seaweed

Hydrolysation was performed as follows. 9 g of dry dealginate was reacted with 100 mL of 0.1 M NaOH. The biomass was washed three times with deionised water and lyophilised for use in further metal binding experiments (77).

2.2.4. Column System Development

2.2.4.1. Preparation of Dealginated Seaweed Microcolumn

A sample of dealginate was oven dried at 105°C overnight, allowed to cool and gently separated with a spatula. The sample was ground using a pestle and mortar and sieved. Particles retained in an 85-mesh screen (mean particle size approximately 120 μm) were used to pack the column. The column (50 mm x 7 mm i.d. MF-plus, Alltech Associates, Carnforth, UK) fitted with an acid resistant plastic PEEK frit was packed with a known weight of dry biomass (ca. 0.34 g) that had been slightly moistened to aid packing. The biomass was held in place by another frit fitted at the top of the column. The column was then connected to the inductively coupled plasma atomic emission spectrometer. The diagram of the on line system for the preconcentration, speciation and determination of the metals is shown in Figure 1.

Figure 7 Schematic diagram of the on-line system

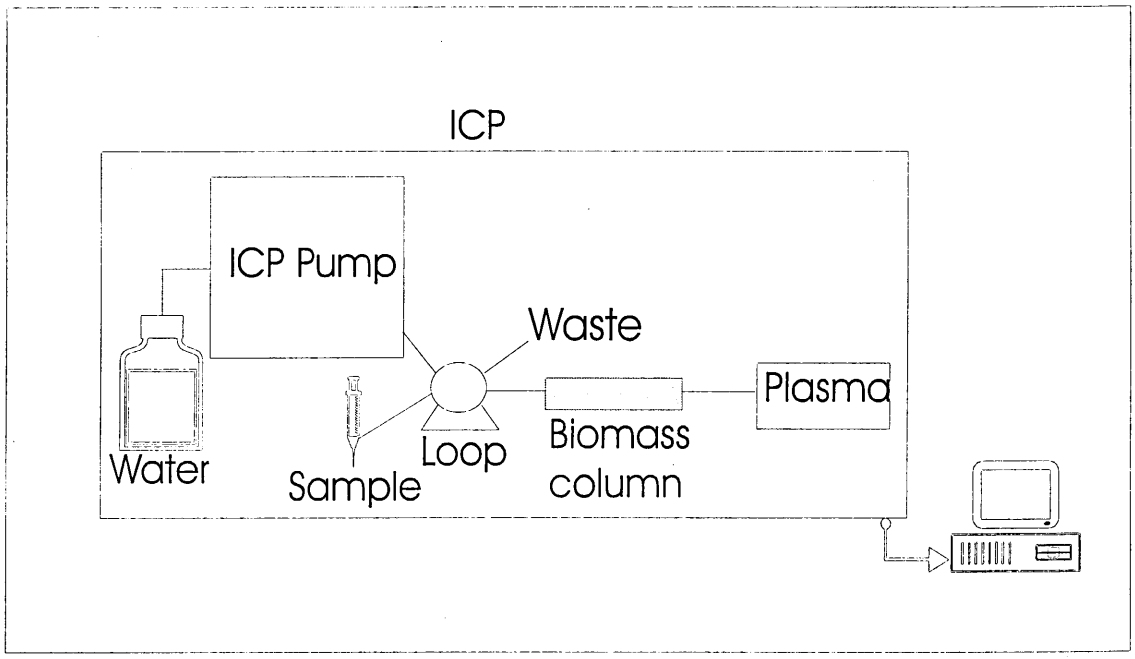

2.2.4.2. Operation of the Dealginated Seaweed Microcolumn using ICP-AES and ICP-MS Detection

The standard procedure adapted for metal preconcentration in the biomass column is described as follows. Deionised water followed by 1 M HCl was pumped through the column using the pump on the instrument at a flow rate of 0.8 mL min^{-1} for 10 min, respectively. In use the column was connected on-line to either of the spectrometers using a 1.42 mm internal diameter tube (Altec Products Limited, Alton, U.K.) with the tube length (70 mm) kept short to minimise dead volume in operation. Deionised water was used as the carrier solution and pumped continuously through the column at a flow rate of 0.8 mL min^{-1}. For metal preconcentration, 1 mL of either a single metal ion solution, the multielement standard solutions at metal concentrations of 0.1, 0.25, 0.5 and 1.0 mg L^{-1} or samples were loaded into the injection valve by syringe and then injected into the carrier stream onto the column. The preconcentrated metals were stripped off by manually injecting 500 μL, 1.0 M HCl, into the 1 mL sample loop on the column and detected by ICP-AES. Calibration graphs were

constructed from the integrated area under each metal peak using the software package Microcal Origin 5.0 (Microcal Software Inc, Northampton, USA). Water and 1.0 M HCl blanks were run previous to any measurement.

The biomass microcolumn was then connected to the ICP-MS instrument, and used to preconcentrate metals in a low range of concentration employing the procedure described above.

Calibration curves were constructed at metal concentrations of 1.0, 5.0, 25.0 and 50.0 $\mu g\ L^{-1}$. Multielement standard solutions of 0.01 $\mu g\ L^{-1}$ of antimony, arsenic, cadmium, chromium, cobalt, copper, gold, lead, manganese, mercury, nickel, palladium, scandium, selenium, silver, strontium, tellurium, vanadium and zinc at pH 4 were analysed using the procedure described above. Detection limits for the studied elements were calculated from 10 replicates of the signal intensity obtained for deionised water using the system.

The effect of sample volume, acid concentration, acid volume and flow rate on the performance of the biomass microcolumn was studied by varying these parameters. Sample loops of 0.5, 1 and 5 mL were employed for this study. HCl solutions of 0.1, 0.5, 1.0, 2.5, 5 and 6 M were evaluated for the desorption experiments. The influent flow rates examined were 0.5, 0.8, 0.9, 1.0, 1.2, 1.5, and 2.0 ml min^{-1}. When not in use the column and contents were stored at 4 °C in order to prevent bacterial and fungal growth.

2.2.4.3. Breakthrough Experiments

Breakthrough experiments were carried out by pumping either individual or multielement standard solutions through the column at a flow rate of 0.8 mL min^{-1} until a constant signal intensity was obtained by the ICP-MS detection system. The column was conditioned with deionised water and individual 500 $\mu g\ L^{-1}$ single metal solutions of cadmium, copper,

chromium, lead, nickel, silver, zinc, mercury, and antimony ions at pH 6, gold solution at pH 3 and aluminium solution at pH 4 were pumped through the column while the signal intensity was continuously monitored. Multielement standard solutions of 100 $\mu g\ L^{-1}$ of antimony, arsenic, cadmium, chromium, cobalt, copper, gold, lead, manganese, mercury, nickel, palladium, scandium, selenium, silver, strontium, tellurium, vanadium and zinc at pH 4 were also analysed.

2.2.4.4. Determination of binding capacity

The capacity of dealginated seaweed to adsorb the studied metals was determined at the saturation point from the breakthrough curves obtained. Once the intensity signal had reached a constant value suggesting that the effluent concentration had reached the influent concentration, the sample flow was stopped. Water was then passed through the lines for 10 s to remove metal-containing solution from the column dead volume and line tubing. The column was disconnected from the ICP-MS instrument, and the metal adsorbed into the biomass was stripped out from the column using 5 ml of 0.5 M HCl. The fractions were collected and the metal content was determined by ICP-AES. Acidified standards, which were not retained by the column, were pumped through the system after stripping. The signals from these standards were used to construct a calibration curve.

2.2.4.5. Analyses of Water Reference Materials

Two Lake Ontario water reference materials (National Water Research Institute, Canada) TMDA 51.2 and TMDA 54.2 and synthetic seawater (Sea water corrosion test mixture to DEF 1053/B.S. 3900/ B.S 2011, BDH, Poole, U.K.) were analysed in order to test the suitability of the procedure for the determination of the elements in real samples. 1 mL of the samples were injected onto the column and 0.5 mL of 1.0 M HCl was used for desorption. For these determinations, the pH of the Lake Ontario water reference materials were adjusted to 7.0 before metal preconcentration in the column.

2.2.4.6. Chromium Speciation

2.2.4.6.1. Separation of Cr (III) and Cr (VI) by the Dealginated Seaweed Microcolumn

The same system configuration was used to study the distribution of chromium species but here ICP-MS was used for the Cr detection. As with metal preconcentration, 1 mL of a mixed chromium standard or sample was loaded onto the column via the injection valve. Unretained Cr (VI) was eluted almost immediately and detected. Adsorbed Cr (III) was stripped off using 500 μL, 1.0 M HCl as described for metal preconcentration. Calibration curves in the range 10 - 250 μg L^{-1} were prepared from mixed Cr (III) and Cr (VI) standards.

2.2.4.6.2. Determination of Chromium (VI) by the 1,5 diphenylcarbohydrazide Method

Independent confirmation of the Cr (III):Cr (VI) ratio was obtained by using the 1,5 diphenylcarbohydrazide method based on UV/Visible detection (125). This procedure measures only Cr (VI), therefore to determine total Cr the sample was treated with permanganate in order to oxidise the other chromium species. The oxidation of Cr (III) was carried out by adding to 10 mL of sample an excess of 1:1 H_2SO_4:H_2O solution until the volume was adjusted to 40 mL. The mixture was then boiled on a hot plate, to which 2 drops of $KMnO_4$ solution. After 2 min, 1mL NaN_3 solution was added and gentle boiling was continued and then the solution was cooled. 0.25 mL of concentrated H_3PO_4 was added to the solution. Measurements of Cr (VI) in all samples were carried out as follows. An appropriate sample portion was diluted to 100 mL, adjusted to pH 1 using 0.2 N H_2SO_4 and 2 mL diphenylcarbohydrazide solution was added. The solution was mixed and left to stand for 5 to 10 minutes for full colour development. A portion was transferred to a 1 cm absorption cell and its absorbance was determined at 540 nm. Calibration curves were prepared in the range of 10 to 100 μg L^{-1}.

2.2.5. Calcium Displacement Experiments

An investigation of the effect of the presence of adsorbed calcium ions on the uptake of cadmium from solution by dealginate was undertaken. 0.2 g of dealginate (dry weight) was added to 10 ml of deionised water that was spiked with a solution of calcium to provide a final calcium concentration of 30 mg L^{-1}. Lithium hydroxide (0.01 M) was added to the solution to keep the pH constant at a value of 6. The biomass was left to adsorb calcium ions for 2 hours. At this point varying concentrations of cadmium in solution (50, 100, 225 and 450 mg L^{-1}) were added to each flask for a period of 2 hours. The biomass was removed by filtration (Whatman number 1 filter paper) and the concentrations of cadmium and calcium ions in the solutions were determined by ICP-AES.

2.2.6. The speciation of cadmium, lead and silver ions in the adsorption process using ion selective electrode

The speciation of cadmium ions in the samples prepared for the standard equilibrium experiments was determined by the use of a cadmium ion selective electrode. The electrode response and the calibration curve were determined using standard solutions of cadmium, prepared from cadmium nitrate at concentrations ranging from 0.01 to 1000 mg L^{-1}. Samples at a high solution pH were neutralised at pH 7 prior to measurement. A 5 M $NaNO_3$ solution was used in order to adjust the ionic strength of the samples and standards. An aliquot of 10 mL of standard or sample was placed in a beaker and 200 µL of ISA solution was added. The sample was stirred using a magnetic stirrer and direct measurements were taken by placing the electrode into the beaker. When a stable reading is displayed, the mV value was recorded.

The speciation of lead ions was carried out using the procedure described above. An ion selective electrode for lead and lead perchlorate solution was employed to construct calibration curves. A methanol-formaldehyde solution was added in a ratio 1:1 to samples

and standards to decrease solubility and retard oxidation of the pellet. The ionic strength adjustor used was a 5 M $NaClO_4$ solution.

2.2.7. Elemental Composition of Dealginated Seaweed

Elemental Analysis of carbon, hydrogen and nitrogen was performed to characterise the elemental composition of dealginate. The sample was left to stand in a desiccator for 24 h. After this time, the sample was ground to a fine powder using an agate mortar and pestle. 3 mg of sample was weighed for analysis and a stable six decimal place weight recording was attained. The tin capsule enclosing the sample was placed in the Perkin Elmer 2400 CHN Elemental Analyser auto sampler for analysis. The gases eluting from the column were measured as a function of thermal conductivity. This measurement was carried out at the Department of Chemistry of The University of Sheffield.

2.2.8. Infrared Studies

Infrared spectra were obtained for dealginated seaweed untreated biomass, washed biomass, esterified biomass and metal-saturated biomass for the following metal ions: Ca, Mg, Cu, Cd, Cr, Ni, Pb and Ag at pH 2 and 6, Au samples at pH 3 and Al samples at pH 4. An aliquot of the dry sample was placed in the Golden Gate Single Reflection Diamond accessory in the infrared spectrometer and the infrared spectra was taken in the transmission mode. Five scans were carried out for each sample.

2.2.9. Environmental Scanning Electron Microscopic Studies

The surface of dealginated seaweed was examined under both fully hydrated chamber conditions and at intermediate relative humidity conditions using a Peltier stage. Microphotography was obtained for dealginated seaweed untreated biomass, washed biomass, esterified biomass and metal- saturated biomass for Cu, Pb and Ag at pH levels of 2 and 6, Au samples at pH 3 and Al samples at pH 4. A small amount of dry sample was

mounted in the stage. Samples were analysed in hydrated conditions at 5°C and 5 Torr H_2O vapour pressure. Similarly, for dehydration, conditions were 16°C and < 2 Torr H_2O vapour pressure. In each case, elemental X-ray mapping and spot analysis identified metal concentrations on the seaweed surface.

2.2.10. X-ray Absorption Fine Structure Spectroscopic Studies

X-ray spectra of untreated dealginated seaweed biomass, esterified biomass and metal-saturated biomass for Cu, Cd, Ni, Pb and Ag at pH 2 and 6, and Au samples at pH 3 were taken. The samples were lightly pressed into thin (approximately 0.5 mm) cardboard sample holders with sellotape windows. Solution standards were held in perspex sample holders of approximately 0.5 mm in thickness filled with Mylar windows. Metal standards were measured as an aqueous solution in transmission mode. Nitrate salts of Cu, Cd, Ni, Pb and Ag and $HAuCl_4$ were measured as solids on the tape in transmission mode. All of the metal biomass samples were run as solid powders on tape in fluorescence mode. The absolute energy positions were calibrated with metal foils, except for Pb measurements where lead acetate salt was used. The EXAFS data obtained were calibrated, background subtracted and analysed using the standard Daresbury packages EXCALIB, EXBACK and EXCURVE98 respectively.

Characteristics of Metal Biosorption by Dealginated Seaweed

Chapter 3

3.1. Introduction

The uptake of Cd, Pb, Ni, Cu, Cr, Ag, Al and Au by dealginated seaweed was characterised using batch methods. Parameters such as the amount of biosorbent, the solution volume, contact time and pH were optimised. The optimum conditions were used to simulate the adsorption process. The titration method was used to characterise the functional groups on the surface of dealginated seaweed. Modification of the surface of the biosorbent was also carried out. The results obtained are described and discussed in the following sections.

3.2. Batch Laboratory Experiments

3.2.1. Optimisation of the mass to volume ratio

In order to optimse the amount of metal adsorbed per unit of biosorbent different dealginated mass to solution volume ratio were studied. Table 2 shows the percentage of cadmium removed using the different ratios investigated. The results are comparable at mass-to-volume ratios of 10, 16 and 20, the bulk of dealginate is considerable at 20. As a result, 10 was chosen as the mass to volume ratio for subsequent experiments.

Table 2 The effect of varying the Mass of Dealginate on Cadmium removal

Mass of dry dealginate (g)	Concentration (g L^{-1})	Cadmium removed (%)
0.1	2	92
0.2	4	95
0.3	6	97
0.5	10	99
0.8	16	99
1.0	20	99
1.5	30	95
2.0	40	96

3.2.2. Elemental Composition of Dealginated Seaweed

The elemental analysis of dealginate revealed the following weight composition: C 30.0%, H 4.5%, N 1.8% and S 1.3%. Carbon was the major component found on the sample as was expected in a seaweed derived material. The presence of nitrogen and sulphur was identified although their percentage concentrations were not very high compared with C and H. Previous energy dispersive X-ray spectroscopy (EDAX) analysis (126) showed no significant quantity of metal ions except calcium, on the surface of the material prior to use. Acidic digestion showed Ca, Na, Mg and K concentrations of up to 0.3, 0.3, 0.2 and 0.01 mmol g^{-1}, respectively.

3.2.3. The effect of pH on metal biosorption

Figure 8 shows the removal of cadmium from 10 mg L^{-1} solution over 24 h contact time at solution pHs of 2, 3, 4, 6, 7, 8 and 10. The error bars on the figures were omitted for visualisation purposes. Data points were plotted from average of 5 replicates. The precision was within 5% error for all samples analysed. Results show that variations in pH influence the sorption of cadmium by dealginate. It has been shown that $Cd(OH)_2$ precipitates after pH 9 (14). At pH values of 2, 3 and 4 cadmium is retained, but a considerable amount of Cd ions still remain in solution. Cd is effectively removed by dealginate at pH between 5 and 8, with the best performance at a pH 6 and 7.

There were little variations in the sorption of Cd after 1 h at the pH values studied. Therefore, 1h was chosen as the equilibrium contact time for subsequent studies. Figure 8 shows that the kinetics of the sorption process are affected by solution pH. Figures 9 - 13 showed a similar pattern for Pb, Cu, Cr, Ni and Ag, respectively. Approximately 90% of the metal ions were removed between pH 6 and 7. The least metal ions were removed when the solution pH was maintained at 2 or at pH 10.

Figure 8 Effect of pH on Cd sorption throughout 24 h contact time

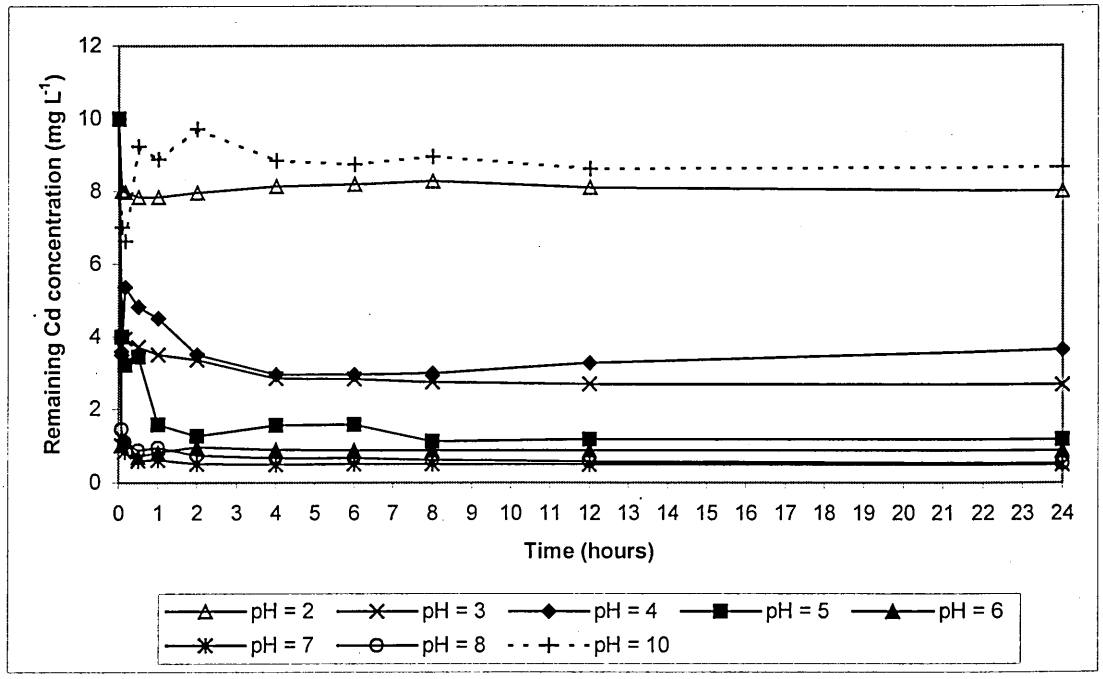

Figure 9 Effect of pH on Pb sorption throughout 24 h contact time

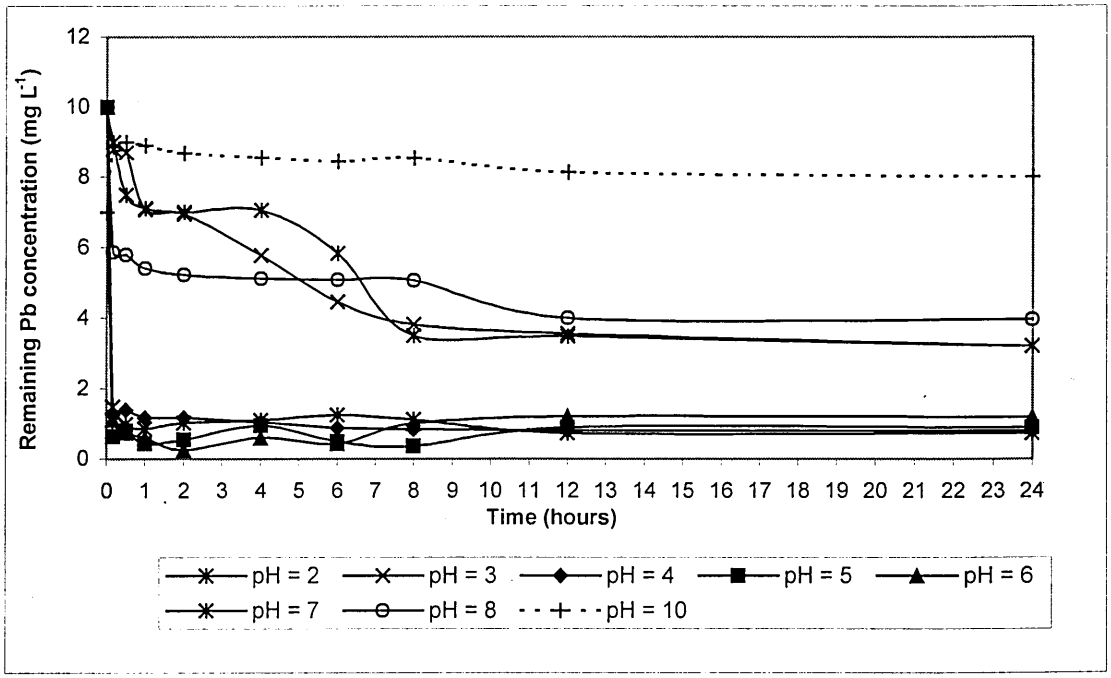

Figure 10 Effect of pH on Cu sorption throughout 24 h contact time

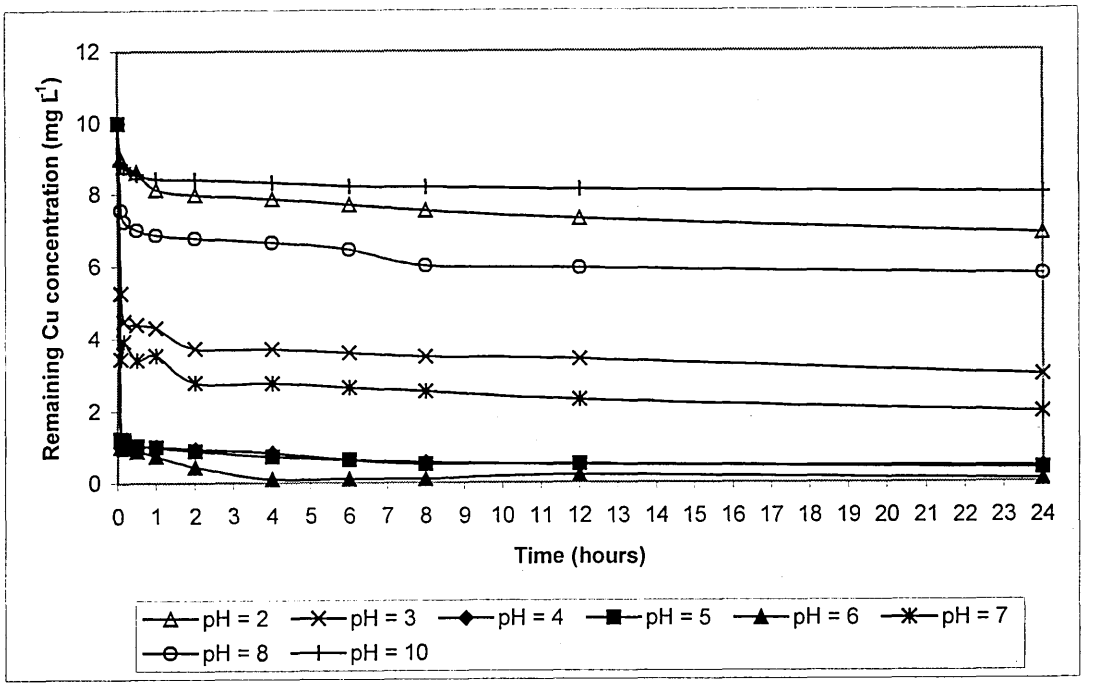

Figure 11 Effect of pH on Cr sorption throughout 24 h contact time

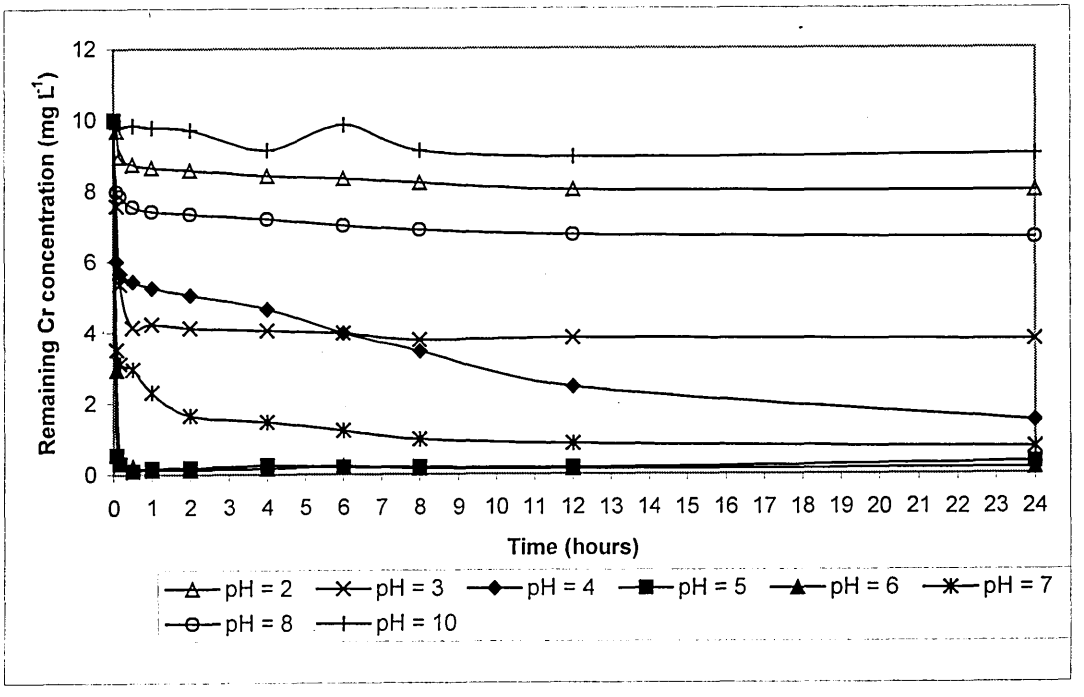

Figure 12 Effect of pH on Ni sorption throughout 24 h contact time

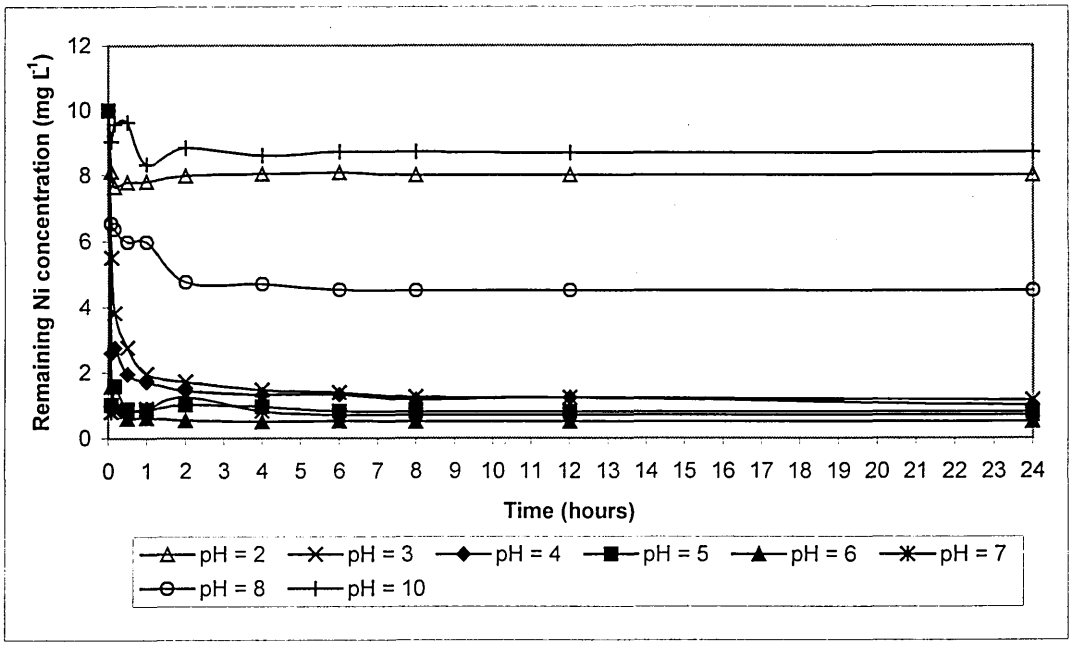

Figure 13 Effect of pH on Ag sorption throughout 24 h contact time

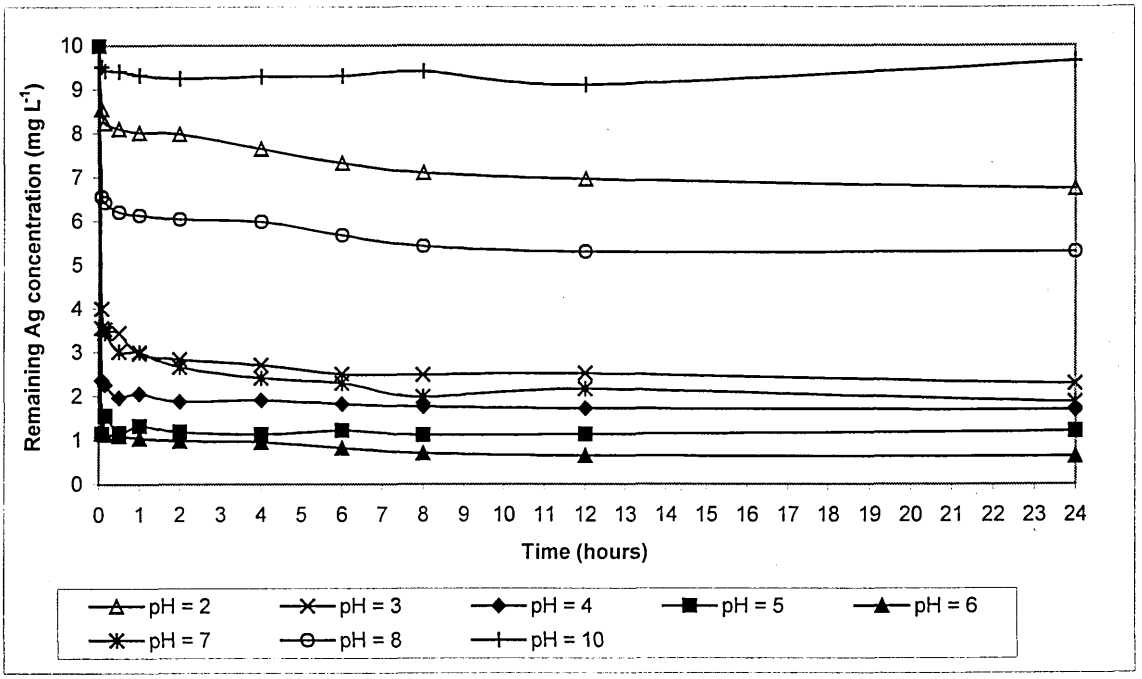

In the case of Al, hydroxide complexes precipitate at pH 5.5 (127). Optimum removal was found at pH 4 (Figure 14). Figure 15 shows the pH influence on Au sorption by dealginated seaweed. Results were obtained for the pH range 2 – 6, since the chemical behaviour of Au was markedly affected at higher solution pH. Colloidal gold aggregates are formed at pH values higher than 4.5 (128). At pH values lower than 2, Au^{+} and Au^{3+} are in solution as metal ions, but little removal of gold from the solution was observed. When the solution pH was adjusted to higher than 5.0, the solution was observed to change colour, from transparent to red, which is characteristic of the presence of colloidal gold complexes. Because of the formation of colloidal complexes the pH study was terminated at pH 6 for the 24 h experiment. However, data was obtained for 1 h contact time for the complete range of pH in order to compare with the data for other metals.

The overall effect of pH on metal ion sorption by dealginated seaweed is shown in Figures 16 and 17. A similar pattern was found for Cd, Pb, Ni (Figure 16) Cu, Cr and Ag (Figure 17), while Al and Au showed marked differences in sorption behaviour across the pH range (Figure 18). Au and Al sorption were found to be highly pH dependent.

Figure 14 Effect of pH on Al sorption throughout 24 h contact time

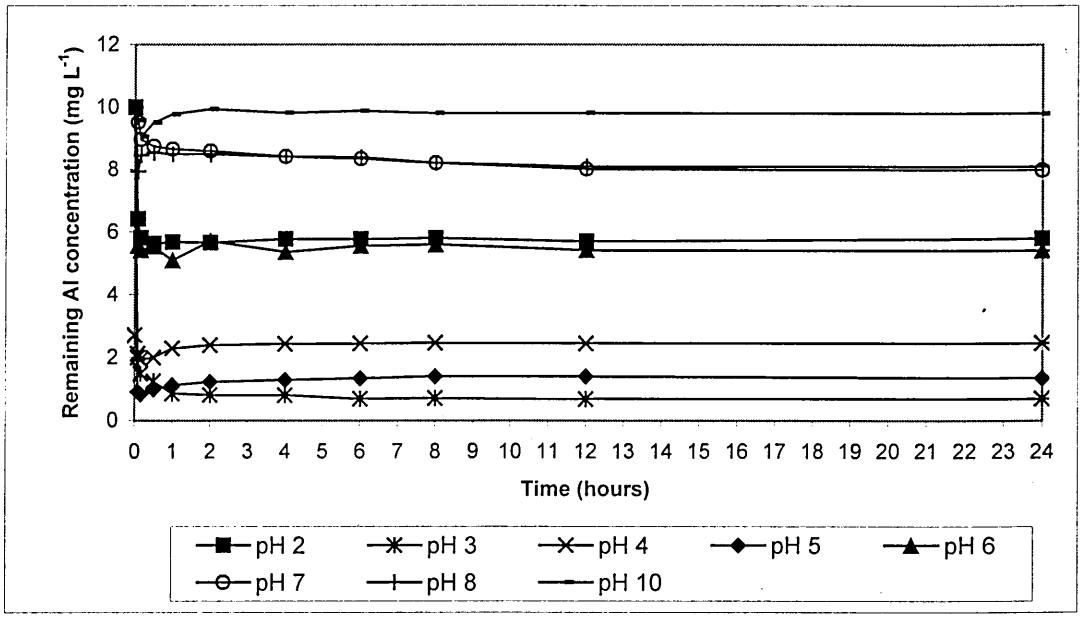

Figure 15 Effect of pH on Au sorption throughout 24 h contact time

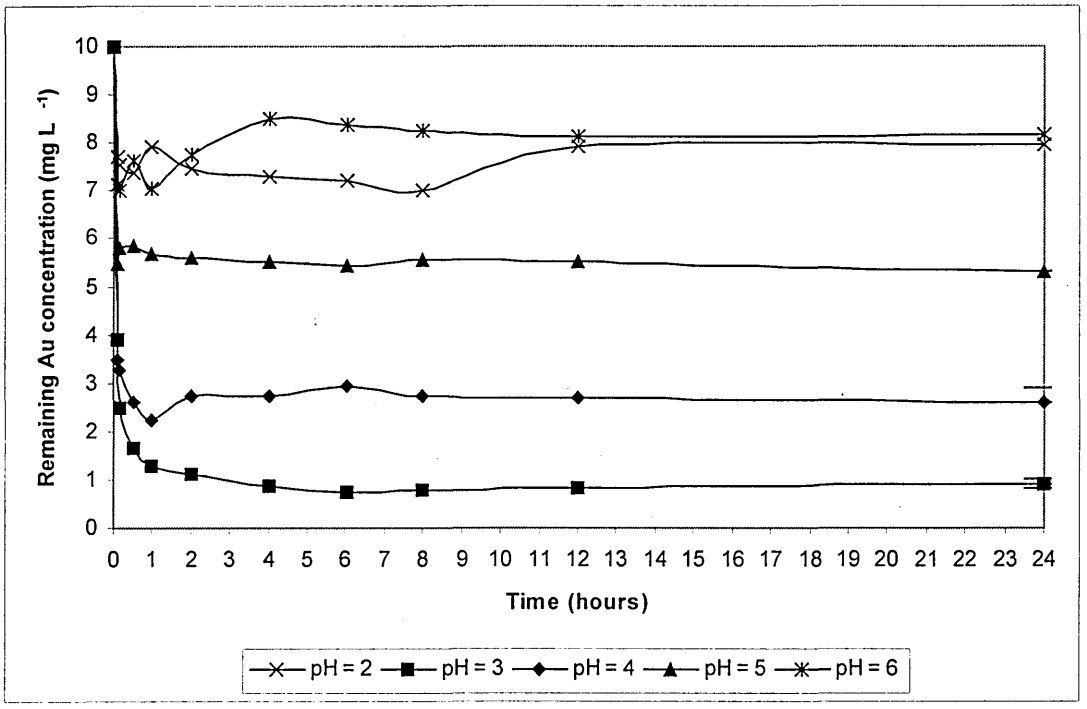

Figure 16 Effect of pH on Cd, Pb and Ni sorption

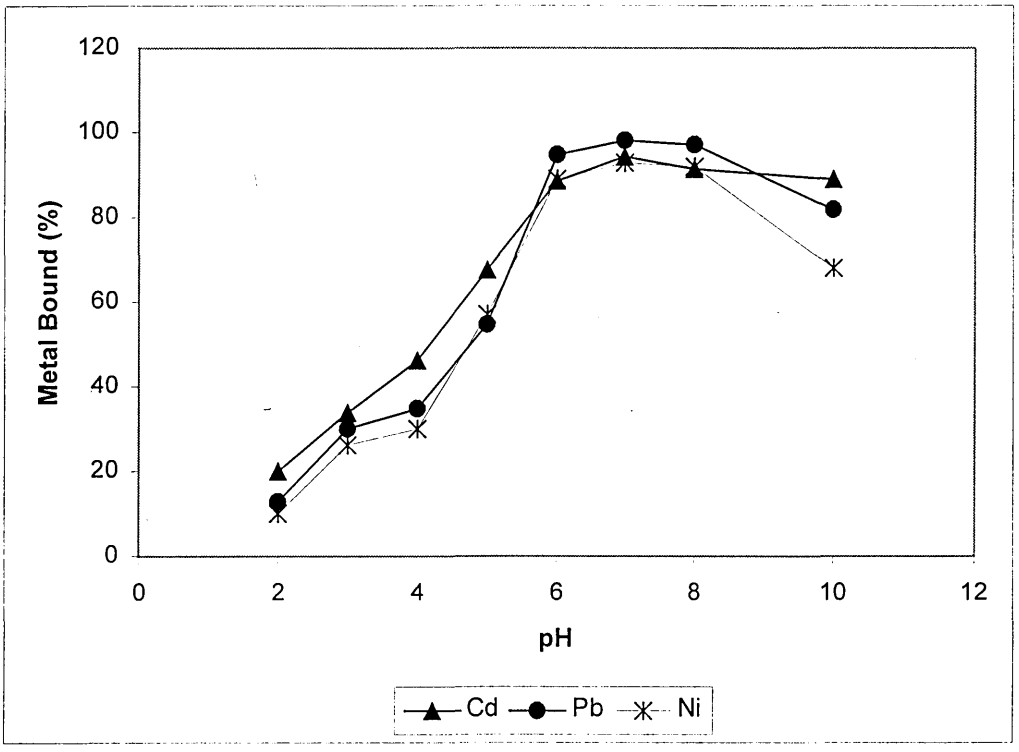

Figure 17 Effect of pH on Cu, Cr and Ag sorption

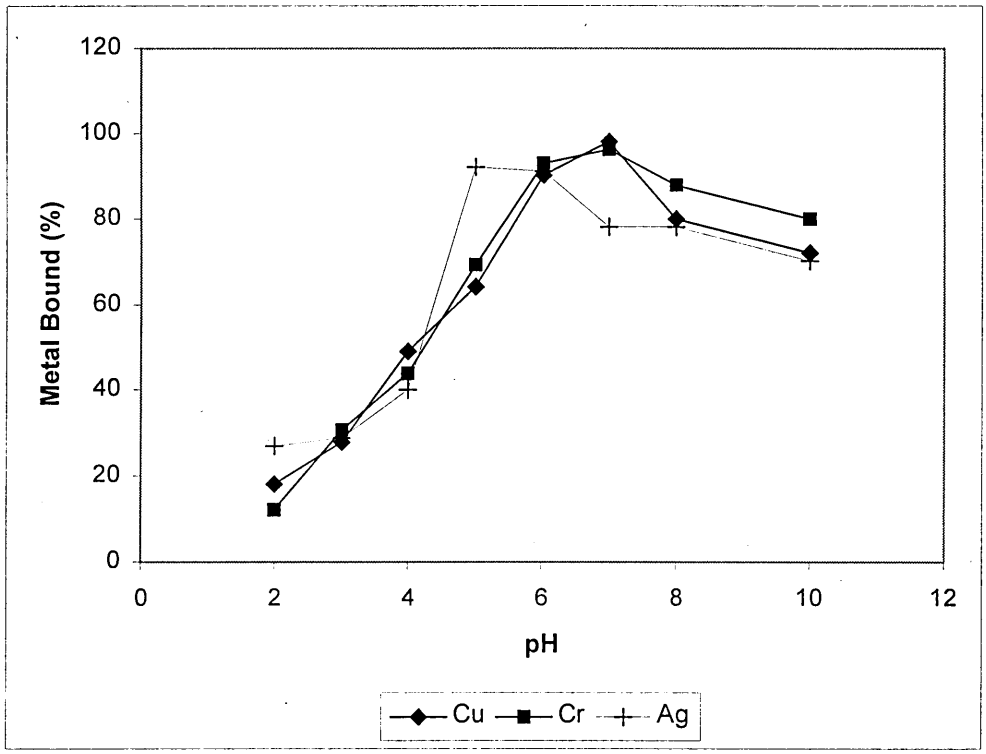

Figure 18 Effect of pH on Aluminium and Gold sorption

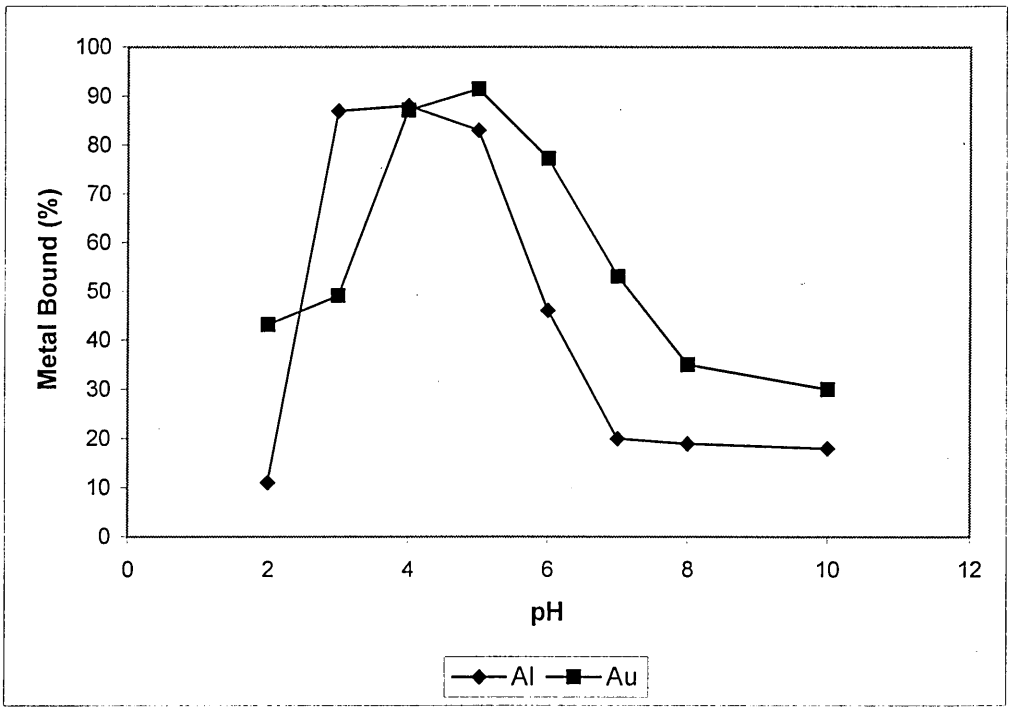

These results demonstrate the importance of pH monitoring and control throughout any metal ion removal process that uses dealginated seaweed as a biosorbent.

In order to complete the pH study, buffered metal solutions were prepared using the procedure described in Chapter 2 section 2.3.1. In the experiments using unbuffered solutions, the difference in pH before and after contact with the biomass was less than 0.1 pH units. Results obtained using both buffered and unbuffered solutions were similar. The findings showed that the sorption process was not affected by the presence of buffer solution in the system.

Schnitzer and Skinner (129) studied metal-fulvic acid interactions and concluded that two types of reactions can occur: (1) a major mechanism involving the simultaneous presence of both acidic and phenolic OH groups, and (2) of minor importance the weakly acidic carboxylic groups. At the high pH, strong acid groups are ionised while weak acids are still protonated.

Since Cd, Pb, Ni, Cr, Cu and Ag are not hydrolysed at pH $\leq$ 6.0, the observed influence of pH on their binding by dealginated seaweed is an indication of the interaction of the biosorbent active sites with hydrogen ions. Metal ions therefore compete for the same binding sites, with more sites being available for metal ion sorption at higher pH values. Crist *et al.* (86) recognised that the main effect of pH on metal ion binding consisted of a reduction in the number of binding sites available with decreasing pH. Similar results were found for *Chlorella vulgaris*, *Sargassum fluitans*, *Pilayella litorallis* and *Medicago sativa* (24,31, 70, 75, 124).

A net negative charge on the surface of dealginate at pH values greater than the isoelectric point would be expected to lower any electrostatic energy barrier for the cations to bind to the negatively charged material. This might explain the increased metal ion removal at pH greater than 5. Gardea Torresdey *et al.* (130) found that this kind of behaviour suggests that carboxyl groups may play a major role in metal binding by the biomasses since the acid dissociation

constants (pKa) for various carboxyl groups are reported to be around 3-4. At low pH values, the carboxyl groups are protonated thus reducing the available sites for metal binding. When the pH is higher than 4 the carboxyl groups are deprotonated, therefore negatively charged and able to bind positively charged metal ions. It is likely that the metal ions are bound to the biomass through the carboxyl groups in an ion-exchange type mechanism. Similar results were found for the sorption of Cd, Cu and Pb on *Vaucheria* (131), and for the binding of Cu, Pb and Zn on Peat Moss (132).

3.3. Titration of dealginated seaweed

A sample of dealginate was titrated with acid or alkali in order to identify possible metal binding sites. The titration data obtained is shown in Figure 19. Two end points were clearly discernible in the plot of the cadmium concentration against pH. Figure 19b shows a plot of buffer capacity against the pH. The buffer capacity was defined as the inverse of the slope of the titration curve:

$$\beta = -\frac{dC}{dpH} \quad (13)$$

This approach was used to calculate the acidity constants (pKa) since the maximum buffer capacity occurs when:

$$[HA] = [A^-] \quad (14)$$

Therefore,

$$pH = pK \quad (15)$$

The two pKa values found were pKa_1 = 3.63 and pKa_2 = 9.09, respectively. The pKa_1 is comparable to the values reported for carboxylic acids (77). The pKa_2 value is similar to the reported for phenolic groups (9.5). (14). These groups are likely to be responsible for metal ion sorption. Crist *et al.* (131) reported a pK value between 5 and 7 for the carboxyl groups of marine algae. The pK value of the carboxylic groups in pure alginic acid is lower, 3.38 for

polymannuronic acid and 3.65 for polyguluronic acid, respectively (133). This difference in pKs highlights the effect of molecular environments on the values measured.

Figure 19 (a) Titration data for dealginate. (b) Plot of buffer capacity β against pH

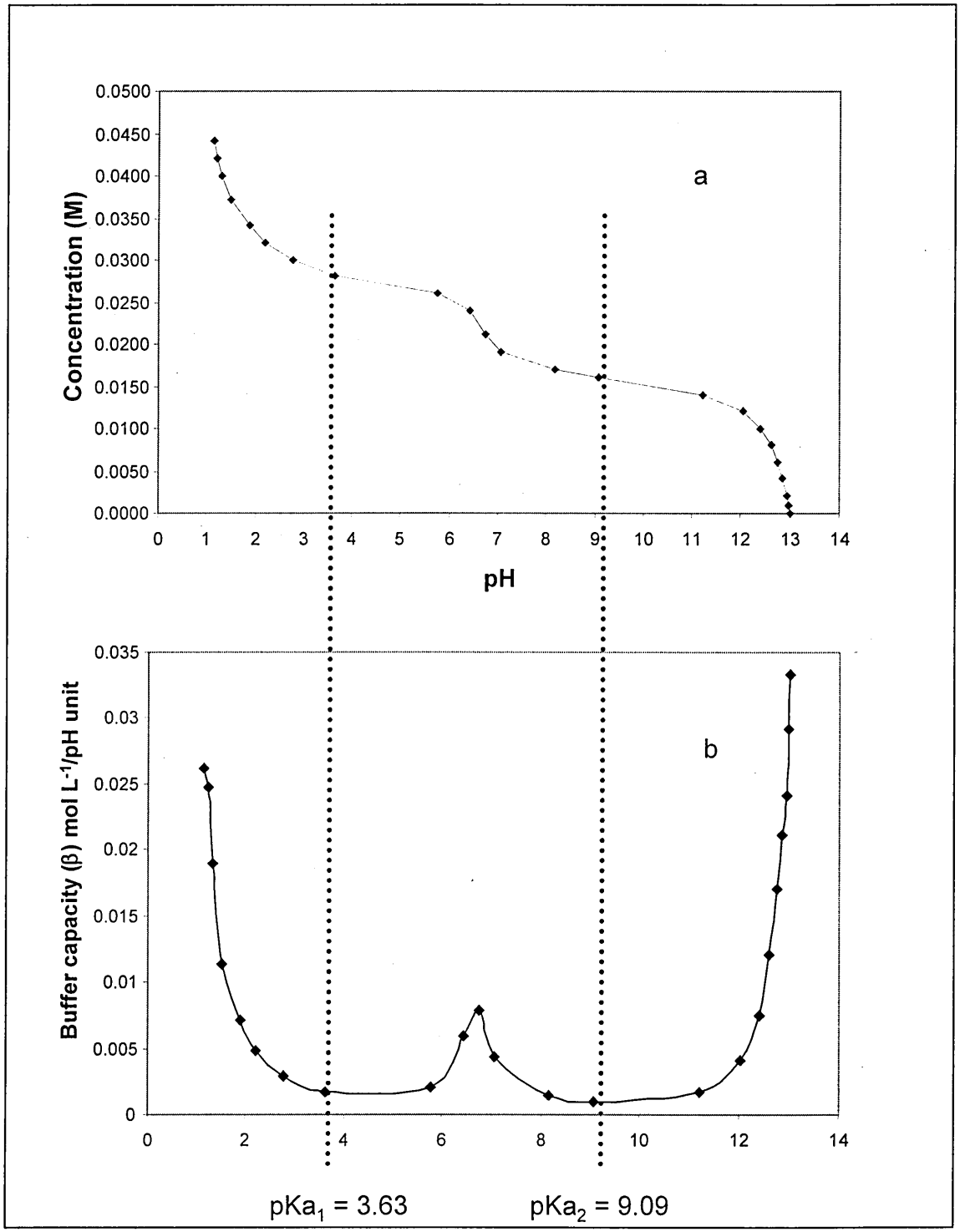

From the inflection points on the titration curve the total concentration of binding sites was determined to be 1.5 ± 0.04 mmol g^{-1} and 0.81 ± 0.06 mmol g^{-1} for pKa 3.63 and 9.09, respectively. The former value is comparable to those reported for the green alga *Ulva fascia*, and the brown seaweeds *Sargassum, Colpomenia* and *Petalonia* were reported to be 1.1, 2.6, 1.5 and 2.9 mmol g^{-1}, respectively (92).

The concentration of the binding sites at a particular pKa may not be assumed to be the total amount of binding sites for a determined biosorbent, since the titration did not approach zero at the endpoint of the titration of the weakly acidic groups. This means that no more protons are bound to the titrated weakly acidic carboxyl groups. Other binding sites with higher pKa values may still be protonated. These binding sites should therefore be taken into account in calculating the total amount of binding sites.

The titration plot clearly shows a steep increase in pH at the beginning of the titration, characteristic of the presence of strongly acidic groups, which are probably most sulphonates (82).

To estimate the amount of remaining binding sites, the titration was started by adding a known amount of HCl to the solution prior to the titration. The intersection between the linearly decreasing portion and the linear slowly increasing branch, corresponding to the titration of the weak acidic groups, yielded a quantitative estimation of the strong acidic groups in dealginate. This corresponds to the first equivalence point of the potentiometric titration curve. The amount of sulphate groups for dealginate was estimated to be 0.29 ± 0.06 mmol g^{-1} and the pKa was 1.8. This result is similar to those reported by Fourest *et al.* (82) and Schiewer *et al.* (90) for *Sargassum fluitans*, where the amount of sulphonate sites was estimated to be 0.25 mmol g^{-1} at pK 2. Crist *et al.* (131) reported the pK of biomass sulphate groups to be 1 and 2.5.

The isoelectric point calculated from the relationship:

$$PZC = 0.5 (pK_1 + pK_2) \quad (16)$$

was 2.8. Thus, at low pHs below 2.8, the biomass has a net positive charge resulting in low metal sorption. Maximum sorption is likely to occur at pH values greater than 2.8 when the biomass has a net negative charge.

3.4. Kinetic studies

Experiments which studied the rate of metal sorption were carried out using metal solutions in contact with dealginate for varying lengths of time. These showed that sorption was rapid, 90% of the metal ions in solution were taken up by dealginate in the first 5 min, with equilibrium being attained after 2 h. A 5% increase in the metal bound to dealginate after 24 h was observed for Pb, Cu and Au (Figure 20 and 21). The fast kinetics observed in the first stage of the process indicates the occurrence of an ion-exchange type mechanism. However, other mechanisms may be involved subsequently. Results obtained using both batch and continuous methods were similar.

3.5. Equilibrium Experiments

Figure 22 shows the representation of the metal sorption isotherm, the capacity (q) of dealginate in mmol g^{-1} against the equilibrium concentration at pH 6. All the isotherms show steep initial slopes, indicative of high adsorption affinities for the metal ions studied. The Cd, Pb and Cu isotherms show a significant upward slope at higher concentrations and saturation was not achieved in the range studied. This behaviour was markedly observed for Cd isotherm. The same result was found for 9 different species of marine macro algae (134), and it was suggested that the difference in behaviour could be related to the different algal composition and uptake mechanism.

Figure 20 Kinetics of metal sorption by dealginate

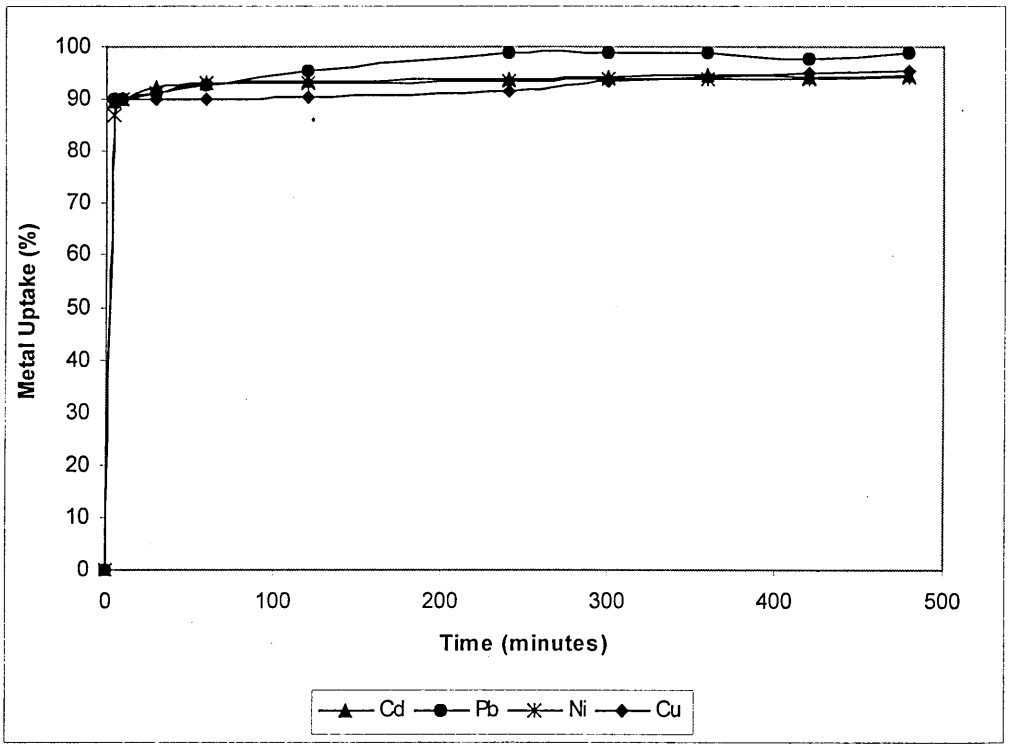

Figure 21 Kinetics of metal sorption by dealginate.

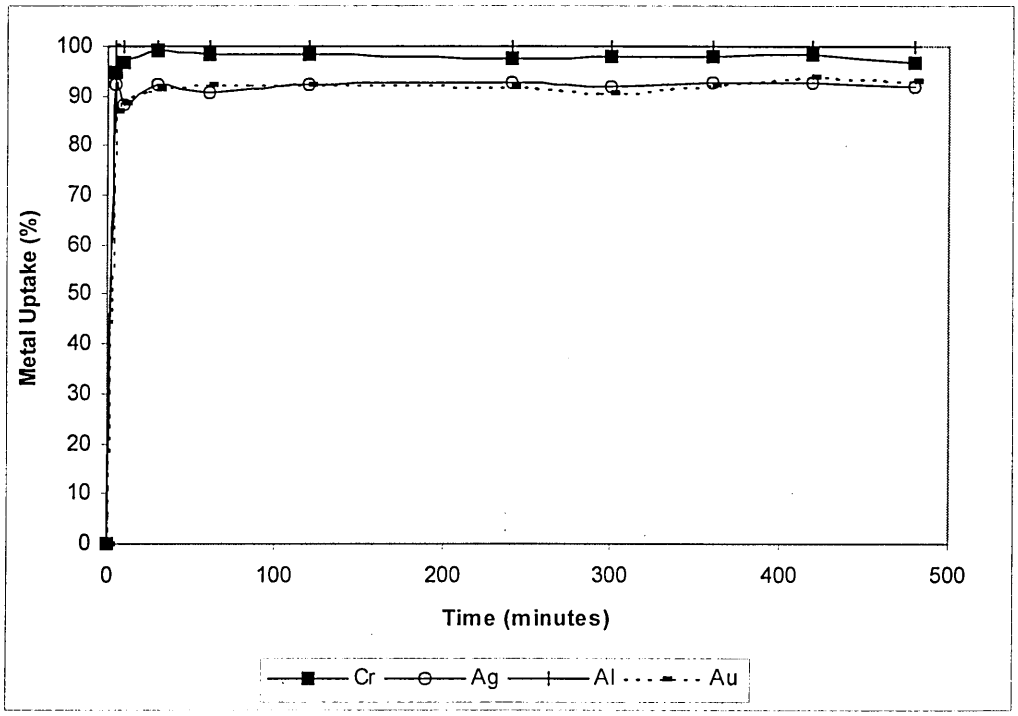

Figure 22 The isotherm for the sorption of Cd, Pb, Cu, Ni, Cr and Ag by dealginate at pH 6

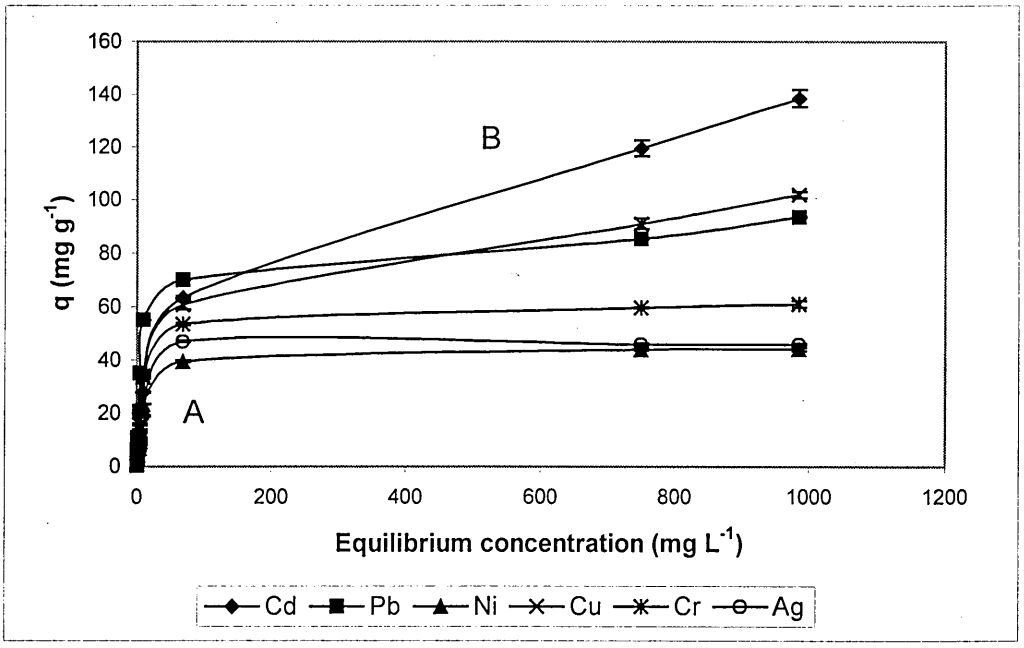

In the case of the isotherm for Cd the shape of the curve can be divided into two regions, A and B. The shape of the curve would seem to indicate that there are two types of metal binding sites. As the readily available sites in region A become saturated, the excess cadmium is bound to another type of site with reduced affinity for the metal as shown by the slope of the graph in region B. A similar behaviour was observed for Cu and Pb to some extent; however, Ni, Cr and Ag showed a levelling off at high concentration values.

The shape of the Ni, Cr and Ag isotherms indicate a different sorption process. For these elements the Langmuir isotherm describes their behaviour. Langmuir behaviour is observed when the energy of sorption for each molecule is the same and independent of surface coverage, and that sorption occurs only in specific sites involving no interactions between sorbed molecules.

All sets of equilibrium sorption data were found to fit the linear model at concentrations between 0 and 250 mg L^{-1}. Results fit the linear model, since linear isotherms prevail at low

solute concentrations (15). Sorption isotherm parameters for linear model are show in Table 3. The K_{ads} values obtained for Pb and Cd suggests that the distribution of these ions in the sorbent phase is better, resulting in a higher affinity for dealginate to sorb these ions, giving higher values. The general affinity sequence for dealginated seaweed was $Pb^{2+} > Cd^{2+} > Cu^{2+} > Cr^{3+} > Ni^{2+} > Ag^{+} > Au^{3+}$.

Table 3 The sorption isotherm parameters for the Linear model

Element	q_{max} (mmol g^{-1})	K_{ads} (L $mmol^{-1}$)	R^2
Cd	1.24	4.47	0.999
Pb	0.45	6.05	0.997
Cu	1.59	3.49	0.997
Ni	0.75	2.34	0.943
Cr	1.18	3.27	0.976
Ag	0.43	1.95	0.961
Au	0.40	0.10	0.991

The maximum capacity of dealginated seaweed to sorb the studied ions may be considered high compared to other biomasses (135, 136). The uptake capacity for Cd, Cu and Cr cations was higher than those for Pb, Ni, Ag or Au. Yu *et al.* (134) reported the metal uptake capacity for a wide range of biomasses including *Ascophyllum nodosum*, *Durvillaea potatorum*, *Ecklonia radiata* and *Ecklonia maxima*. The capacities for Pb (II), Cu (II) and Cd (II) were in the range of 1.0-1.6, 1.0-1.2 and 0.8-1.2 mmol g^{-1} dry biomass, respectively, for all species of algal biomass. These capacities are comparable to those found in this study. These results can also be compared to the capacities of ion exchange resins, which are typically in the range of 1 to 2 mmol g^{-1} (137).

The binding capacities exhibited by dealginated seaweed for the elements studied are adequate for metal removal across a wide range of concentration. The main advantage

compared to synthetic resins and living materials is that the biomass is a much cheaper alternative, since it has no commercial use and requires minimum preparation and maintenance.

The levelling off of the isotherm for Ni, Cr and Ag at high concentrations suggested the occurrence of a different binding mechanism. Modelling of the data obtained for Ni, Cr and Ag using the Langmuir equation at high concentrations showed a straight line, demonstrating that the equilibrium sorption data fits the Langmuir model much better than the linear model. Langmuir parameters were calculated and are shown in Table 4. The Langmuir model fit was poor for the other metals studied. Although the b values were lower than the K_{ads} values calculated from the linear fitting of these metals, the non-linear behaviour was demonstrated when individual K_{ads} values were observed. For example, individual K_{ads} values for Ni ranged from 0.4 L g^{-1} to 7.5 L g^{-1}, indicating non-linear sorption, since K_{ads} depends on the concentration studied.

The calculated capacity, q_{max}, for Ni using the Langmuir model was similar to that obtained using the linear model, but lower for Cr and higher for Ag, respectively. The higher value for Ag could be explained since a higher range of concentration was used to calculate the Langmuir model, thus yielding a higher capacity value.

Table 4 Langmuir Parameters for Ni, Cr, Ag and Al

Element	q_{max} (mmol L^{-1})	b (L $mmol^{-1}$)	R^2
Ni	1.35	1.42	0.997
Cr	0.96	5.67	0.995
Ag	1.14	6.93	0.994
Al	0.94	0.91	0.957

The isotherm for Al at pH 4 showed a shape indicative of a favourable sorption process (Figure 23) but it was not possible to apply the model. The Langmuir parameters for Al sorption are shown in Table 4. The K_{ads} and b values obtained for Au and Al (Tables 3 and 4 respectively) suggest that dealginate has a low capacity to sorb these metals, and in the case of Al, the degree of fit of the model was the poorest observed. A similar fitting for aluminium sorption by *Sargassum fluitans* has been reported at Ph 4.5 (138), however the maximum capacity was higher (8.70 mequiv g^{-1}) compared to the results found in this study.

Figure 23 Aluminium isotherm at pH 4

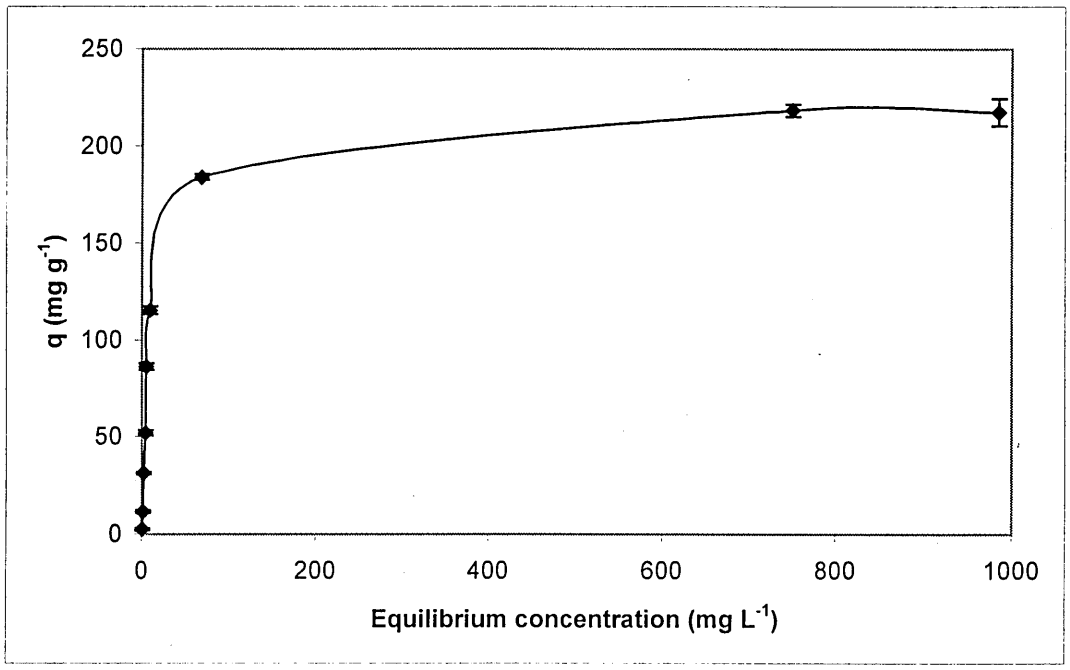

The behaviour of gold was different to that of the other metals studied. Gold (III) may exist in natural waters as a complex anion $AuCl_4^-$. Figure 24 shows the gold isotherm at pH 3, which was chosen since retention of Au is strongly pH dependent, as shown previously in Figure 18. Although the shape of the isotherm is different from the other cations studied, the data fitted the linear model between 0 and 250 mg L^{-1}. The parameters calculated for low concentrations are reported in Table 3.

The dealginate sorption capacity for Au is the lowest in comparison with the other metals studied because $AuCl_4^-$ is the predominant species at this pH. Any sorption occurring must be due to the presence of positively charged sites on the dealginate surface. However, Greene *et al.* (37) reported that gold (I) and (III) sorption by *Chlorella vulgaris* was nearly independent of pH from 1.0 to 8.0 and suggested covalent interactions between the gold complexes and the algae. The possibility of the occurrence of covalent bonding in Au(III) sorption by dealginated seaweed was demonstrated by the presence of a purple colour in the algae, which remained permanently. The colour is associated with the "Purple of Cassius", the colour exhibited by certain colloidal gold suspensions (124, 128, 139).

The reduction of Au(III) to Au(0) by the algal biomass also has been proposed as a possible mechanism, along with photochemical reduction (70, 124). Hosea *et al.* (140) suggested that at least three classes of gold binding sites were present in *Chlorella vulgaris*;

- A class composed of weak binding sites, which provides a suitable environment for the reduction of bound Au (I) to Au (0).

- A stronger second class which do not permit the reduction and

- A class of intermediate strength. An apparent enhancement in the binding of gold was reported as an effect of the presence of Au(0) on the biomass.

A possible explanation was that the gold could migrate from the binding site to a growing gold crystal during or after reduction, thus freeing the binding site for additional binding. It was also suggested that gold atoms deposited on the algal cell during reduction of bound Au^+ serve as nucleation sites, and additional gold is deposited directly into a growing crystal without first binding to the algae.

Figure 24 Gold isotherm at pH 3

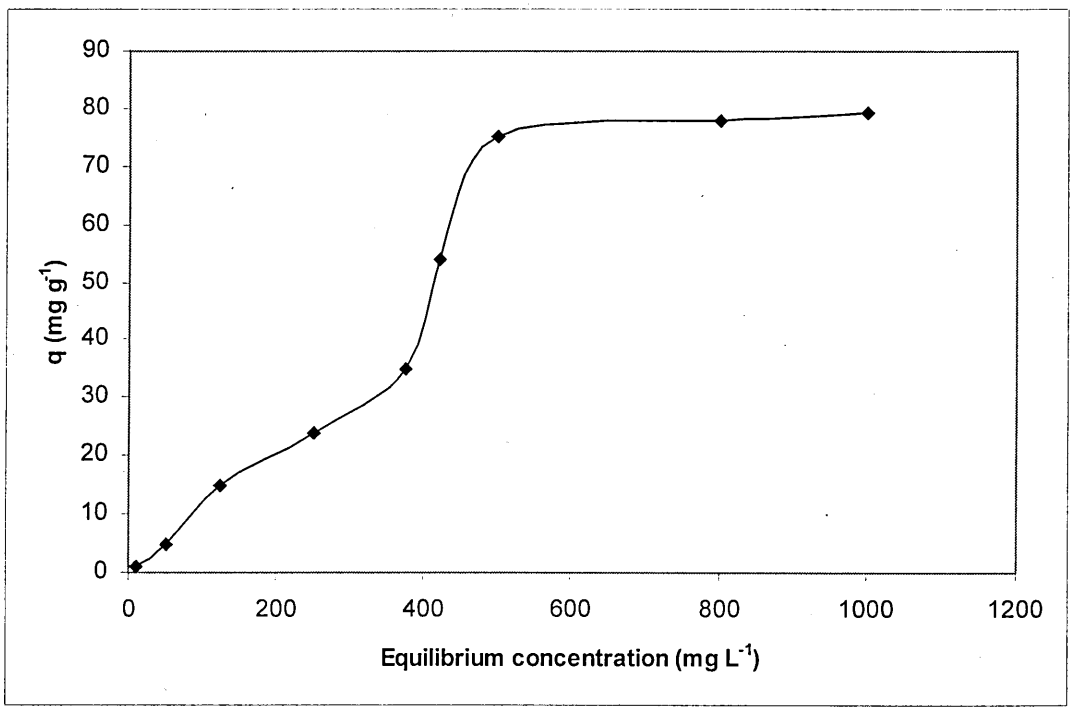

The results suggest that the sorption mechanism may occur in two stages. The first, where ion-exchange between the cations in solution and the hydrogen bound on the surface, filling the ready available sites. Once these sites are filled, a second mechanism takes place, where the remaining cations in solution start slowly filling a homogeneous type-site until the dealginate surface is saturated.

According to phase partitioning theory, dealginated seaweed exhibits an essentially linear isotherm for Cd, Pb, Cu, Ni, Cr, Ag and Au at low concentrations. The values of the distribution coefficient of the linear model, K_{ads}, were independent of the initial equilibrium concentration, when calculated from individual measured values. Therefore, the linear model is appropriate to describe the sorption data obtained for these metals.

Although current literature reports the occurrence of different *K* values, a direct comparison was not possible in most cases since the results were obtained by applying a variety of models from different sources.

It is clear from inspection of the data that the Langmuir treatment is not appropriate for the experimental data at low solute concentrations, and may not be suitable in general to explain the mechanism of sorption by dealginated seaweed. One main disadvantage of this model is that the slope and intercept change with concentration because the reverse reaction with protons or other cations present in solution is not considered.

3.6. Non-linear regression fit and Scatchard Plots

Non-linear regression models have also been used to interpret the sorption data. A plot of 'free' ligand vs. 'bound' ligand gives a curve that is known as a rectangular hyperbola, binding isotherm, or saturation binding curve. *Y* is zero initially, and increases to a maximum plateau value named *Bmax*, expressed by:

$$Y = \frac{(B_{\max} \cdot X)}{K_D \cdot X} \quad (17)$$

This equation describes the equilibrium binding of a ligand to a receptor as a function of increasing ligand concentration, assuming one-site binding. *X* is the concentration of the ligand, and *Y* is the specific binding. B_{max} is the maximum number of binding sites, expressed in the same units as the Y-axis (usually mol of metal per g of biosorbent). K_D is the equilibrium dissociation constant, expressed in the same units as the X-axis (concentration). When the metal concentration equals *Kd*, half the binding sites are occupied at equilibrium.

Non-linear regression data is often displayed as a Scatchard plot. Although *Bmax* and K_D values can be calculated from Scatchard plots, the transformation distorts the experimental error and thus violates several assumptions of linear regression, giving erroneous results. This is the reason why the Scatchard plots are only used to display the non-linear regression results. In this plot, the X-axis is specific binding and the Y-axis is specific binding divided by free metal concentration.

A non-linear regression model, based on the one-site binding assumption and subsequent Scatchard plots were used to model the sorption data obtained for Cd, Cu, Cr, Ni, Pb, Ag, Au and Al and dealginated seaweed. The test was performed using GraphPad Prism, Version 3.0 for Windows, (GraphPad Software, San Diego California, U.S.A, www.graphpad.com). Figures 25 to 28 show the results obtained for Cd, Pb, Cu and Ag.

The data fits the model well for Cd, Pb, Cu and Ag. *Bmax* and K_D values were calculated from the non-linear regression model and the results are shown in Table 5. From a Scatchard plot, a linear regression would be expected, with slope of $-K_D$ and an intercept of $(K_D)(sorbed\ amount)_{max}$. A curved plot which appears linear at low and high sorbate concentrations would normally be interpreted as adsorption on a material with two types of sites having different K_D and $(sorbed\ amount)_{max}$ because of the different slopes and intercepts.

Table 5 Adsorption parameters from the non-linear regression model

Metal	B_{max} mmol g-1	K_D L mmol^{-1}	R^2
Cd	1.21	0.85	0.983
Pb	0.40	0.08	0.987
Cu	1.48	0.23	0.989
Ag	0.45	0.71	0.985

Figure 25 Cd sorption data fitted into a non-linear regression model and Scatchard plot

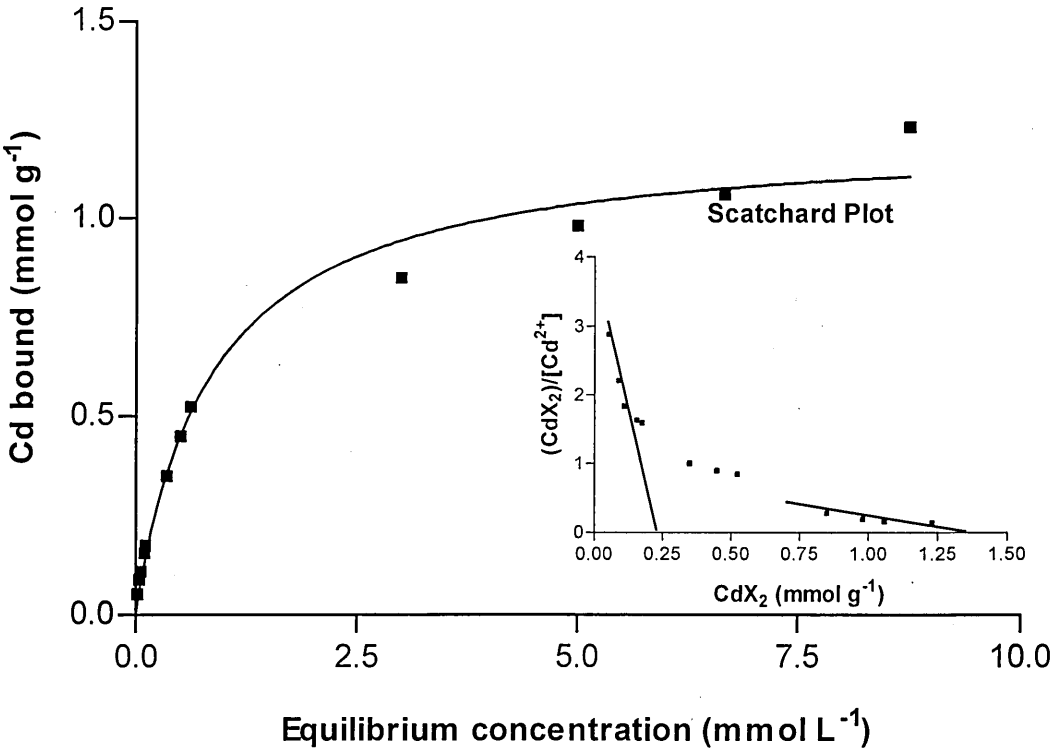

Figure 26 Pb data fitted into a non-linear model and Scatchard plot

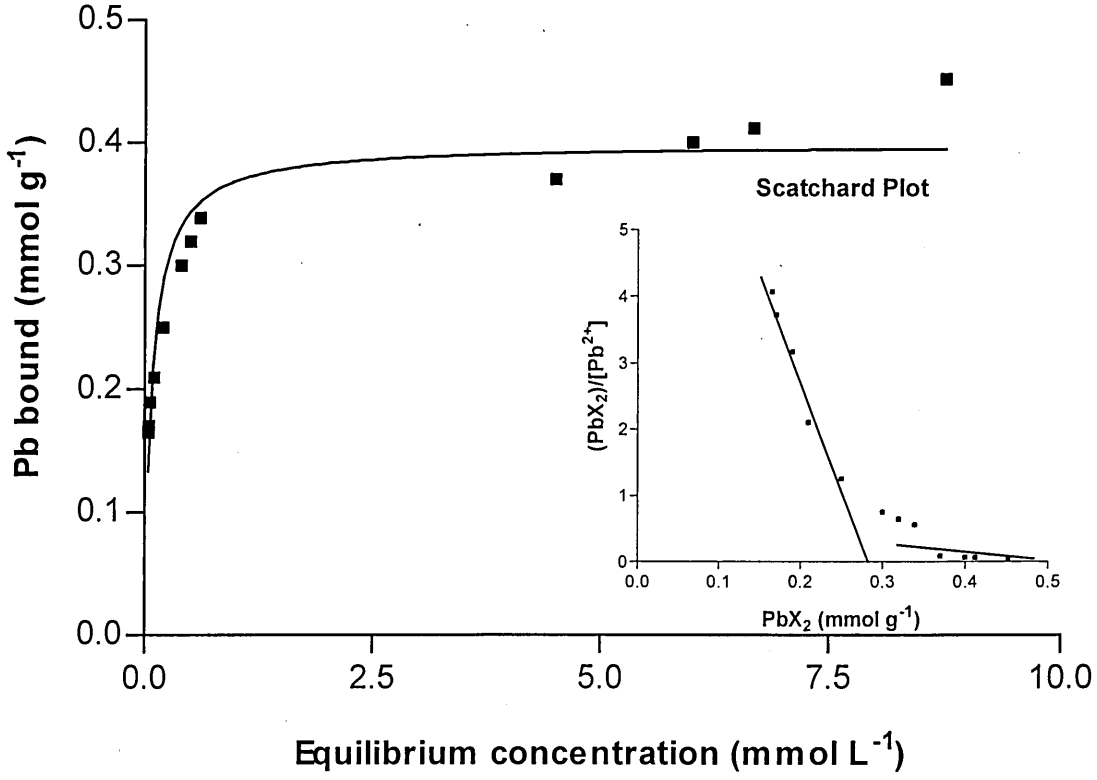

Figure 27 Cu data fitted into a non-linear model and Scatchard plot

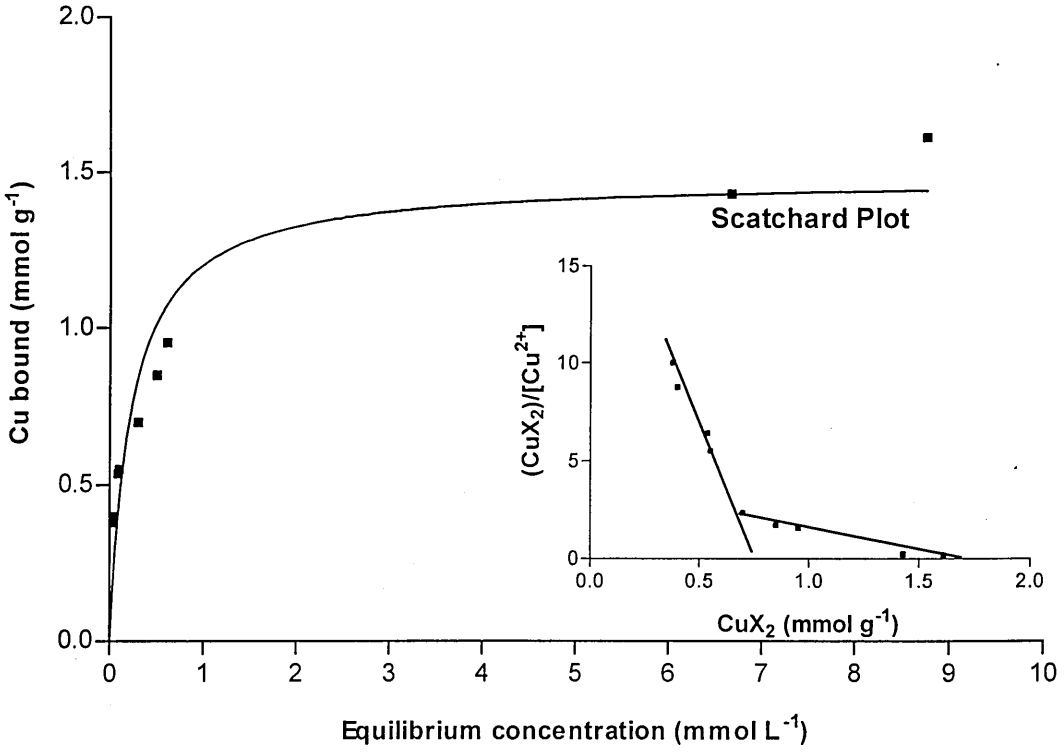

Figure 28 Ag data fitted into a non-linear model and Scatchard plot

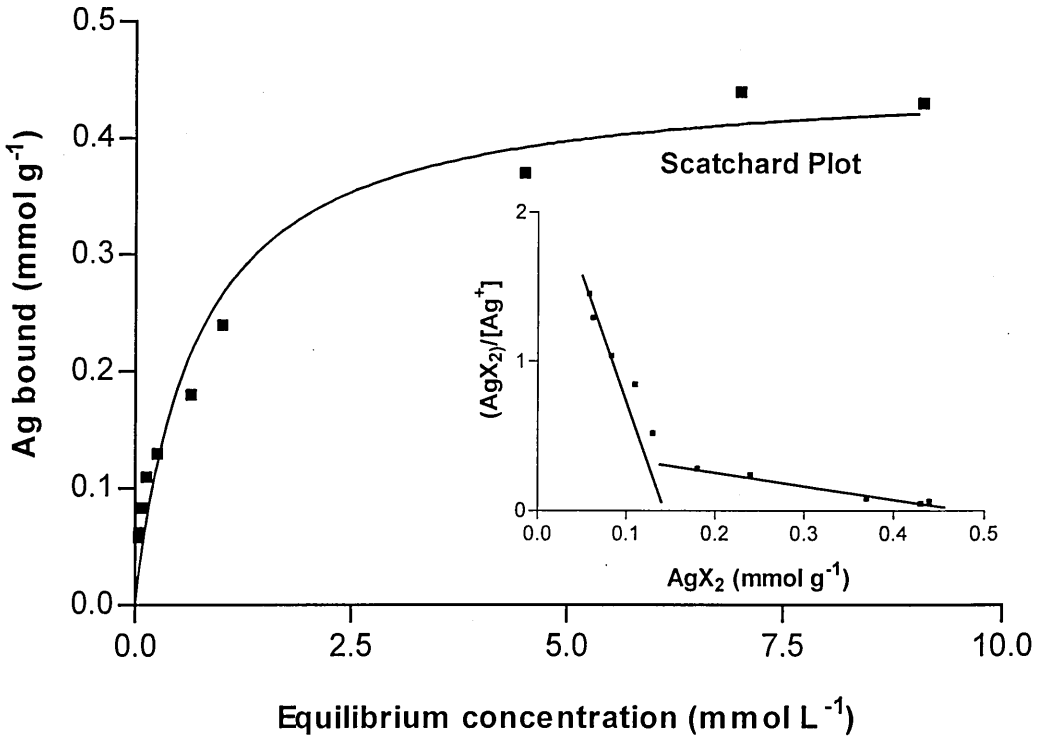

The Scatchard plots of the data modelled using the non-linear regression model showed two limiting regions corresponding to high and low concentrations of sorbing material. Surprisingly the data for Ag, which seems to fit the Langmuir model at high concentrations gave very different results from that obtained previously using the Langmuir equation. The data generated using one type of site with a given K_{ex} and $(sorbed\ amount)_{max}$ generated results analogous to the two-site binding. Crist *et al.* (86) reported similar results for the biosorption of Zn on *Vaucheria* and stated that curved Scatchard plots prepared in biosorption studies, therefore should be viewed with caution, since it may indicate that the chemical process is one of ion exchange and not simple adsorption.

The approach used demonstrated that although it is useful to fit the sorption data for Cd, Pb, Cu and Ag using the Scatchard plots, the interpretation is not exactly what one might expect for a one-site binding model.

Figures 29 - 31 show the fitting of the sorption data of Ni, Cr and Al by dealginated seaweed using the non-linear regression model and the respective Scatchard plot. In the case of Ni, Cr and Al the Scatchard plot showed a linear relationship. Ni and Cr showed this behaviour on the application of the Langmuir model at high concentrations. The fact that the results from both models are comparable may suggest that Ni and Cr binding could be to a very specific site on the surface of dealginated seaweed. The Al data fitted this model much better than was the case for the linear or Langmuir models.

The data for Au is not shown because it did not fit the model. Parameters calculated from this model for Ni, Cr and Al are shown in Table 6.

Figure 29 Ni data fitted into a non-linear model and Scatchard plot

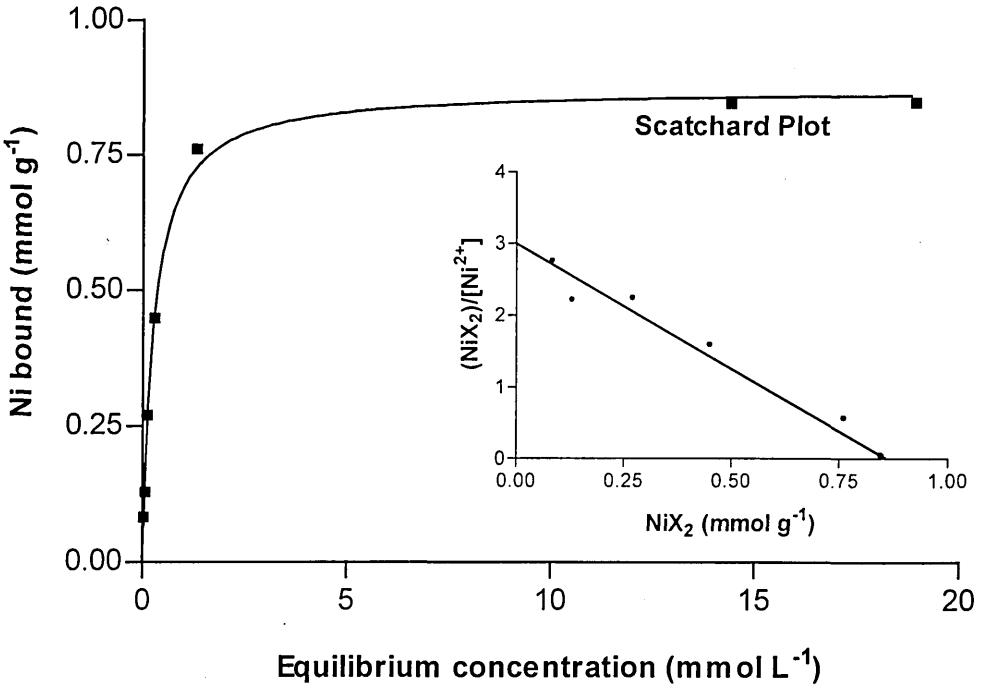

Figure 30 Cr data fitted into a non-linear model and Scatchard plot

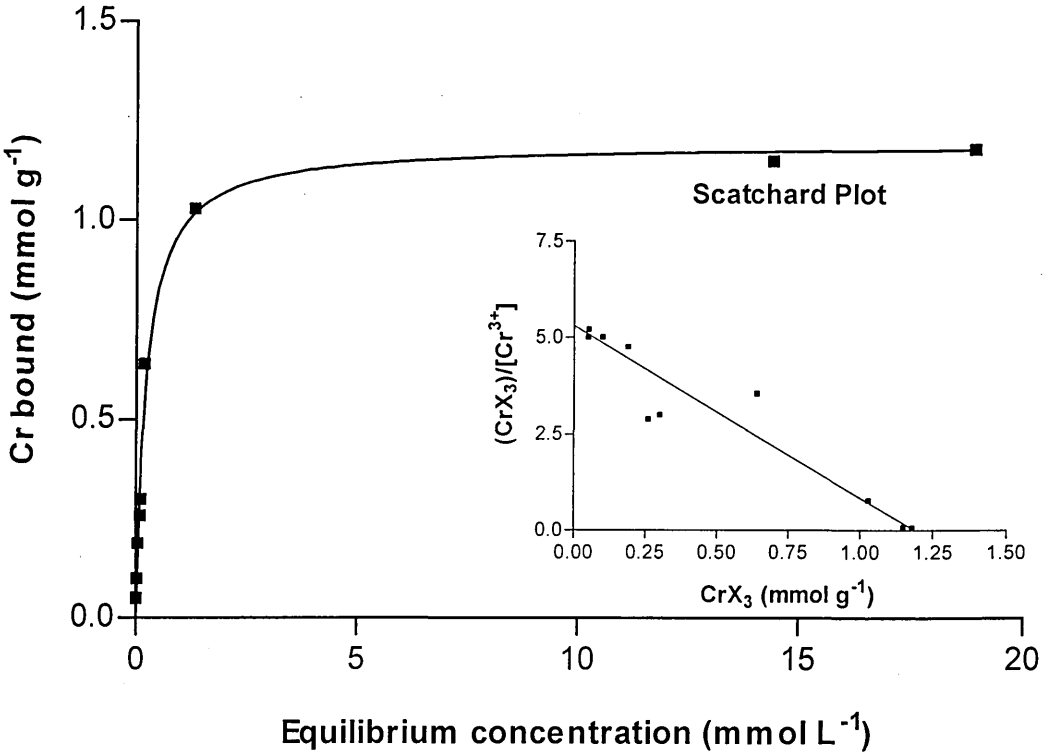

Figure 31 Al data fitted into a non-linear model and Scatchard plot

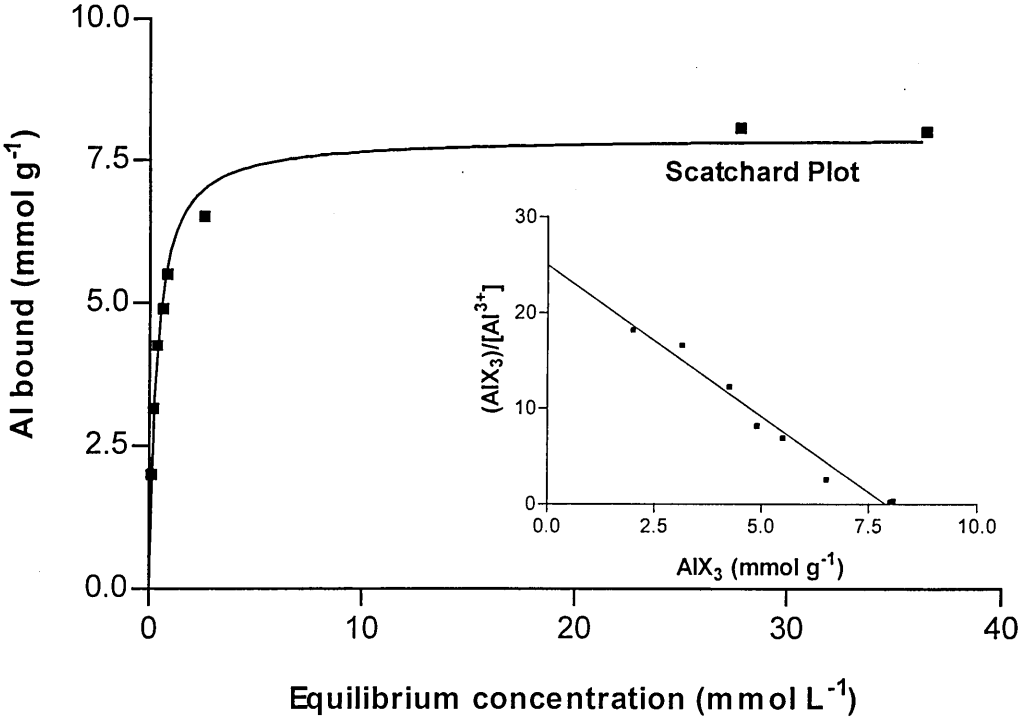

Table 6 Adsorption parameters from the non-linear regression model

Metal	B_{max} mmol g-1	K_D L mmol^{-1}	R^2
Ni	0.87	0.27	0.998
Cr	1.19	0.23	0.988
Al	7.90	0.33	0.988

The B_{max} values obtained for all metals studied using either linear or the non-linear fitting showed similarities when compared to q_{max} values, although the fitting for the non-linear model was made using a higher range of concentrations. These findings validated the uptake values obtained by the linear model, demonstrating that the capacity calculated is independent of the concentration range studied.

Comparisons between the B_{max} and q_{max} obtained by the Langmuir fitting showed differences between the values obtained for Ni, Cr, Ag and Al. The maximum capacity for Al was too low compared to the B_{max} value, and the values for Ag, Ni and Cr were very different, although these are still in the same order of magnitude. The fact that the capacities found are different suggests that the Langmuir model might not be a reasonable model to explain the overall sorption process.

3.7. Determination of ion exchange constant K_{ex}^{H}

The wide use of the Langmuir isotherm in sorption studies is mainly due to its convenience in determining maximum sorption capacity and systematising data at high concentrations. The problem with these types of models is that they do not really apply to the actual chemical process involved. Several authors (83, 86, 91, 93, 141) have demonstrated that for algae, sorption of metal ions is accompanied by displacement of protons or other cations. Therefore an ion exchange model is more consistent with the chemical system.

It has already been demonstrated that the process of sorption by dealginated seaweed is markedly affected by pH. Although the importance of protons in biosorption is generally known, it has been largely neglected in the mathematical description of the process. The application of methods used for the description of sorption in soils and ion exchange resins is a common practice, leading to the determination of separate isotherms for various pH values or

for different initial biomass saturation states. This has been necessary because the most frequently used Langmuir or Freundlich sorption models do not take into account the fact that metal biosorption is an ion exchange phenomenon (91). These models do not incorporate the behaviour or concentration of previous ions bound to the biosorbent such as hydrogen or sodium, resulting in miscalculations in the prediction of the biosorbent performance.

An approach to modelling the binding of heavy metal ions and protons, as a function of metal ion concentration and pH for a range of initial sorbent loadings with the heavy metal ion or protons was developed by Crist *et al.* (141). The model enables the prediction of the effect of protons as exchanged species on the metal ion binding. The results for the application of this model to the determination of the stoichiometry for the algae *Vaucheria*, alginic acid and humic acids showed more accurate results in establishing the ion exchange nature of the sorption mechanism.

To assess the extent of metal binding by ion exchange, the ion exchange constant K_{ex}^{H} was determined. Sorption experiments were conducted using a batch method, except that the initial solution pH was maintained at pH 6 and the solution and dealginate were in contact for 1 hr. The initial metal ion concentration was varied between 1 and 1000 mg L^{-1}. The concentrations of Cd, Pb, Cu, Ni, Cr, Ag, Au and Al in these solutions were determined by ICP-AES. In the case of Al, the study was carried out at pH 4.

Ion exchange equilibrium constants were determined using the model proposed by Crist *et al.* (141). The following reaction was assumed, at pH 6 for the Cd^{2+}, Pb^{2+}, $Cu^{2+}$and Ni^{2+} cations:

$$M^{2+} + 2(HX) \rightleftharpoons 2H^{+} + (MX_2) \qquad (18)$$

$$K_{ex}^{H} = \frac{[H^+]^2[MX_2]}{[M^{2+}][HX]^2} \qquad (19)$$

Where *(HX)* represents the number of acid sites on the solid phase, *(MX_2)* is sorbed M^{2+} and *[H^+]* was calculated from the solution pH.

The unreacted *(HX)* required for this calculation is given by:

$$(HX) = (HX)_o - H^{+}_{off} \qquad (20)$$

where $(HX)_o$ is the initial number of acids sites present at pH 6.

For Ag^+ the assumption was made using the following equilibrium:

$$M^+ + (HX) \rightleftharpoons H^+ + (MX) \qquad (21)$$

$$K_{ex}^{H} = \frac{[H^+]\,[MX]}{[M^+][HX]} \qquad (22)$$

For Cr^{3+} and Al^{3+} the assumption was made based on the equilibrium:

$$M^{3+} + 3(HX) \rightleftharpoons 3H^+ + (MX_3) \qquad (23)$$

$$K_{ex}^{H} = \frac{[H^+]^3[MX_3]}{[M^{3+}][HX]^3} \qquad (24)$$

The values of $(HX)_o$ in mmol g^{-1} used to calculate the ion exchange constants are shown in Table 7. The value of $(HX)_o$ was derived using a minimisation procedure in which the value of $(HX)_o$ was adjusted by several iterations until the values of K_{ex}^{H}, which was calculated for a series

of solutions with different initial metal concentrations, gave a minimum error. This was considered to be the optimum value of $(HX)_o$.

The values of the ion exchange constants, K_{ex}^H for the metals studied are presented in Table 7. The ion exchange constant could not be established for Au since the assumption has been developed for cations only. Crist *et al.* (131) reported a value of K_{ex}^H of 9.3 ± 0.85 x 10^{-6} for cadmium adsorption by peat moss at pH 6. The reported K_{ex}^H values for Cd and Pb were 3.3 x 10^{-2} and 3.2 x 10^{-5} respectively for sorption by *Vaucheria* at pH 6.0. The K_{ex}^H values found for dealginated seaweed are constants for all of the metals studied except for Ag and Al. Crist *et al.* (131) observed that the calculated K_{ex}^H values depend on the metal at a given pH and there is no apparent correlation between K_{ex}^H and the binding strength of a metal.

Table 7 Values of acid sites $(HX)_o$, and K_{ex}^H for dealginated seaweed

Element	$(HX)_o$ mmol g^{-1}	K_{ex}^H
Cd	2.9	3.3 ± 0.1 x 10^{-6}
Pb	2.8	4.1 ± 0.1 x 10^{-6}
Cu	2.0	6.2 ± 0.6 x 10^{-6}
Ni	2.2	1.8 ± 0.1 x 10^{-6}
Cr	2.3	2.3 ± 0.07 x 10^{-6}
Ag	6.1	2.4 ± 0.3 x 10^{-7}
Al	6.0	7.8 ± 1 x 10^{-10}

The $(HX)_o$ values found for the divalent cations were similar, but no pattern could be described for Ag^+, Cr^{3+} and Al^{3+}. The low K_{ex} value for Ag compared to those for divalent metals could be explained by the fact that only one proton is displaced. The values of the initial amount of acid sites $(HX)_o$ calculated by iteration showed them to be higher than the total amount of binding sites at low pH determined by titration of dealginated seaweed for Ag, Cd and Al. Schiewer (142) compared the use of this model against the Langmuir model and a two-sites binding

model respectively, and established that although this ion exchange approximation tends to overestimate the initial amount of sites, due to the fact that its value has to be estimated from a series of iterations, the model can be advantageous at low metal concentrations.

3.8. Simulation of the solution conditions by PHREEQC and MINEQL+

Several authors (83, 142 - 144) have employed well know computer programme to simulate chemical equilibrium in aqueous solutions. Some of the most widely used programmes are PHREEQC and MINEQL+.

PHREEQC is a computer programme for simulating chemical reactions and transport processes in natural or polluted water. The programme is based on the equilibrium chemistry of aqueous solutions interacting with mineral, gases, solid solutions, exchangers and sorption surfaces, and includes the capability to model kinetic reactions with rate equations that are completely user-specified in the form of basic statements. PHREEQC was written in the C program language and was used as a speciation programme to calculate the distribution of aqueous species. Analytical data for mole balances were defined for a combination of valence states for each element studied (145).

PHREEQC employs three databases for the simulations. Surface complexation constants for two of the databases distributed with the programme (phreeqc.dat and wateq4f.dat) were taken from Dzombak and Morel (146); surface complexation constants for the other database distributed with the programme (minteq.dat) were taken from MINTEQA2. Ion exchange reactions are modelled with the Gaines-Thomas convention and equilibrium constants derived from Appelo and Postma (147) were included in two of the databases distributed with the programme.

MINEQL+ is a chemical equilibrium modelling system that can be used to perform calculations on low temperature (0-50°C), low to moderate ionic strength (<0.5 M) aqueous systems. MINEQL+ is a data driven programme that can be used by selecting chemical components from a menu, scanning the thermodynamic database and running the calculation. However, MINEQL+ also provides tools that allow the user to take control of the reaction data, create a thermodynamic database, perform synthetic titrations and automatically process multiple samples (such as field data). MINEQL+ uses a thermodynamic database that contains the entire USEPA MINTEQA2 database plus data for chemical components that the EPA did not include, so all calculations produce results compatible with EPA specifications (148).

The results obtained for Cd are shown in Figure 32. Cadmium has one principal oxidation state Cd(II). The chemistry of Cd in an aqueous system describes all the possible hydroxyl ions formed by Cd hydrolysis, however, at the concentration studied, three species seem to be the most important Cd^{2+}, $Cd(OH)^{+}$ and $Cd(OH)_2$. For the range of pH evaluated between 3 $x10^{-3}$ and 1x 10^{-9} M, Cd^{2+} ions predominant in solution and the hydroxide compound starts to precipitate at pH 8.2. At concentrations higher than 1 x 10^{-3} M the ion $Cd(OH)^{+}$ is not present.

Pb speciation in aqueous solution is shown in Figure 33. Pb^{2+} ions remain in solution until pH 6.4. Pb hydrolyses to give initially the dissolved hydroxide complex $Pb(OH)^{+}$ which finally forms the $Pb(OH)_2$ precipitate at pH values higher than 7.2. Although other species have been reported for Cd and Pb (14) these do not occur in the concentration range studied.

Figure 32 Distribution diagram for Cadmium hydroxide species in solution

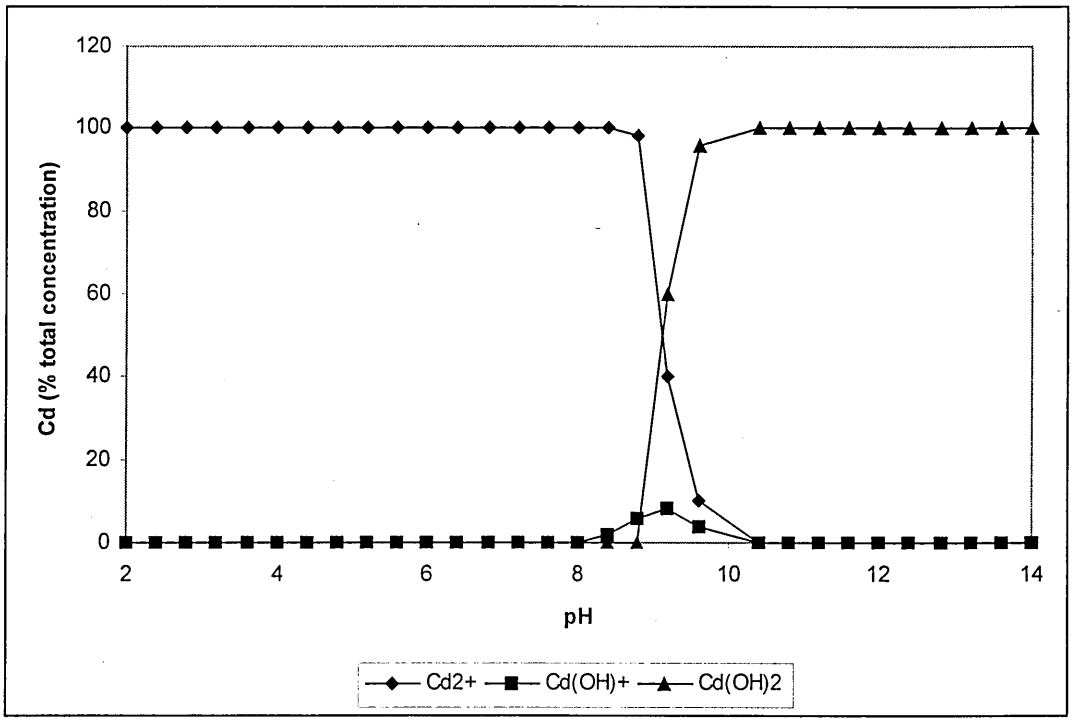

Figure 34 shows the Cu speciation diagram obtained from the solution simulation. The Cu^{2+} ions are present in solution until pH 6.0. At pH 6.2, the $Cu(OH)_2$ rapidly starts to form. The transition species $Cu(OH)^+$ was not observed at 2×10^{-5} M. At concentrations higher than 1×10^{-3} M $Cu(OH)^+$ exists at a low percentage and $Cu(OH)_2$ precipitation takes place at pH values around 4.8-5.0. Although Cu^+ species exist at low concentrations, anions or other ligands present in solution to make the formation of other complexes favourable were not observed. Ni and Cu results were similar (Figure 35). The main difference is that approximately 20% of $Ni(OH)_2$ species are present at pH 6.8.

Figure 33 Distribution of Pb species with pH

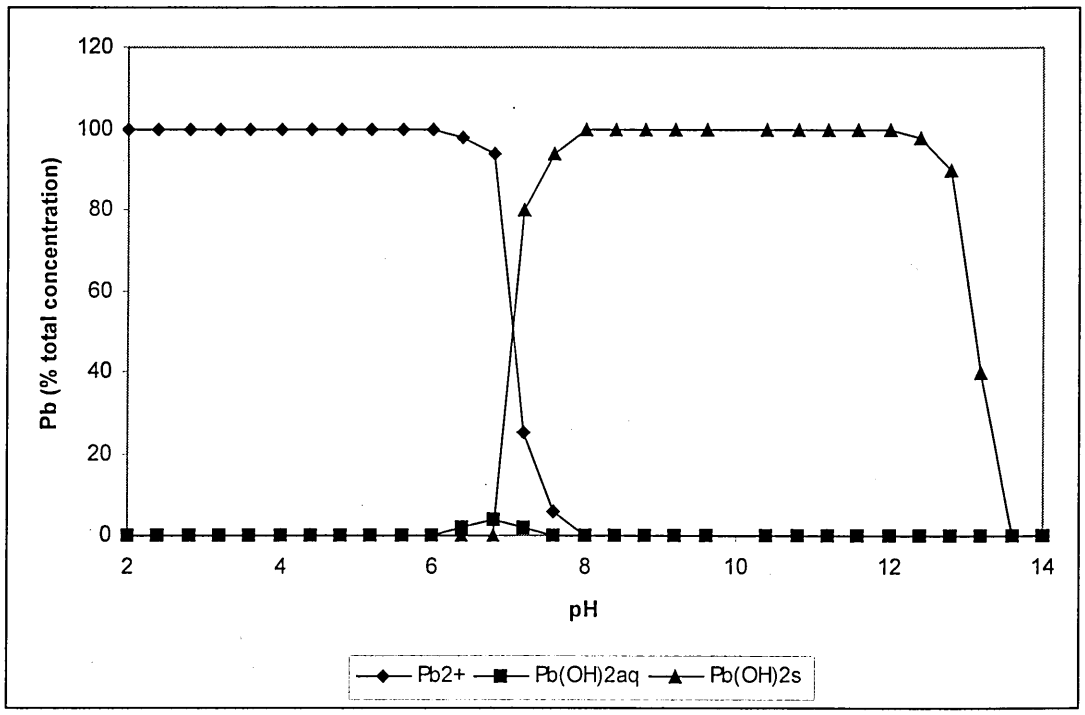

Figure 34 Distribution of Cu species with pH

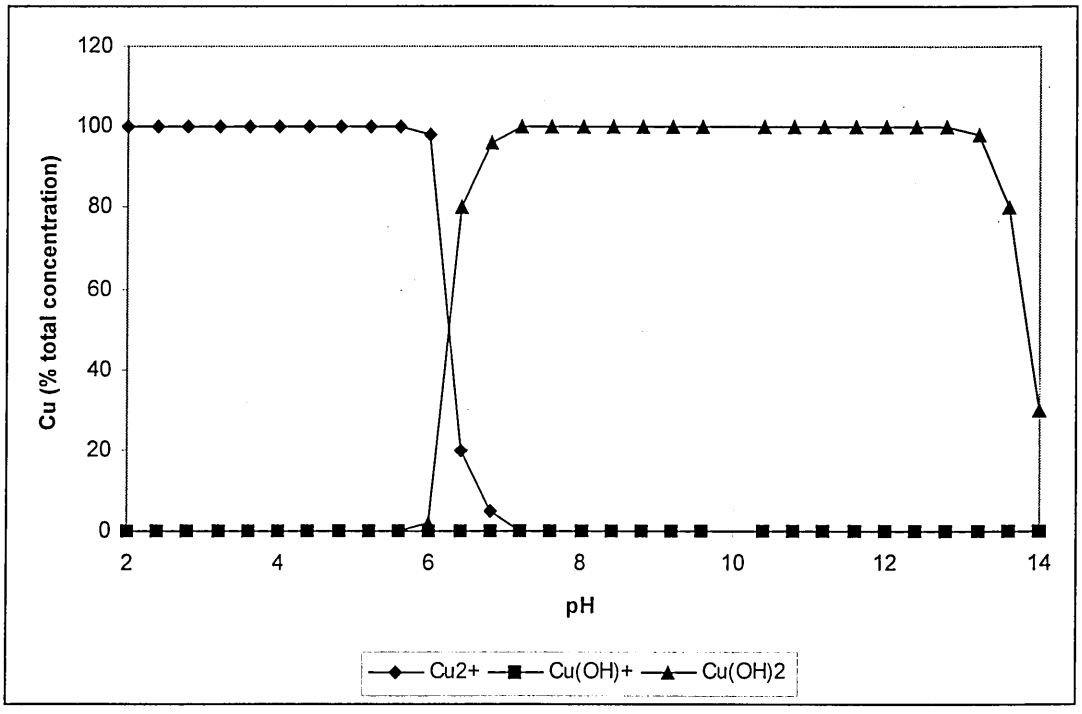

The speciation diagram obtained for Cr species in solution is shown in Figure 36. Three species were found to predominantly exist between 3 x 10^{-3} and 1 x 10^{-5} M. 40% of Cr^{3+} ions started to disappear at pH 5.8, and $Cr(OH)^{2+}$ is the main species at this pH. PHREEQC results showed that approximately 60% of the Cr (III) ions present in solution at pH 6 are $Cr(OH)^{2+}$ ions and the remaining 40% are $Cr(OH)_2^{+}$ ions. Beyond this pH value, the equilibrium is displaced to form Cr_2O_3. According to Stumm and Morgan (14) $Cr(OH)^{2+}$ and $Cr(OH)_2^{+}$ are the predominant species across a wide range of concentration and pH. This behaviour of Cr (III) in aqueous solution may explain the results obtained for the Cr ion exchange constant. The results have shown that Cr (III) behaves like Ni (II), which is a divalent cation. Furthermore, Cr ions seem to be bound through the same mechanism and gave similar results for *K* as the other divalent cations. Therefore, the fact that the results for Cr can be grouped with the other divalent cations is because it has a similar charge in the range of pH and concentration studied.

Figure 35 Distribution of Ni species with pH

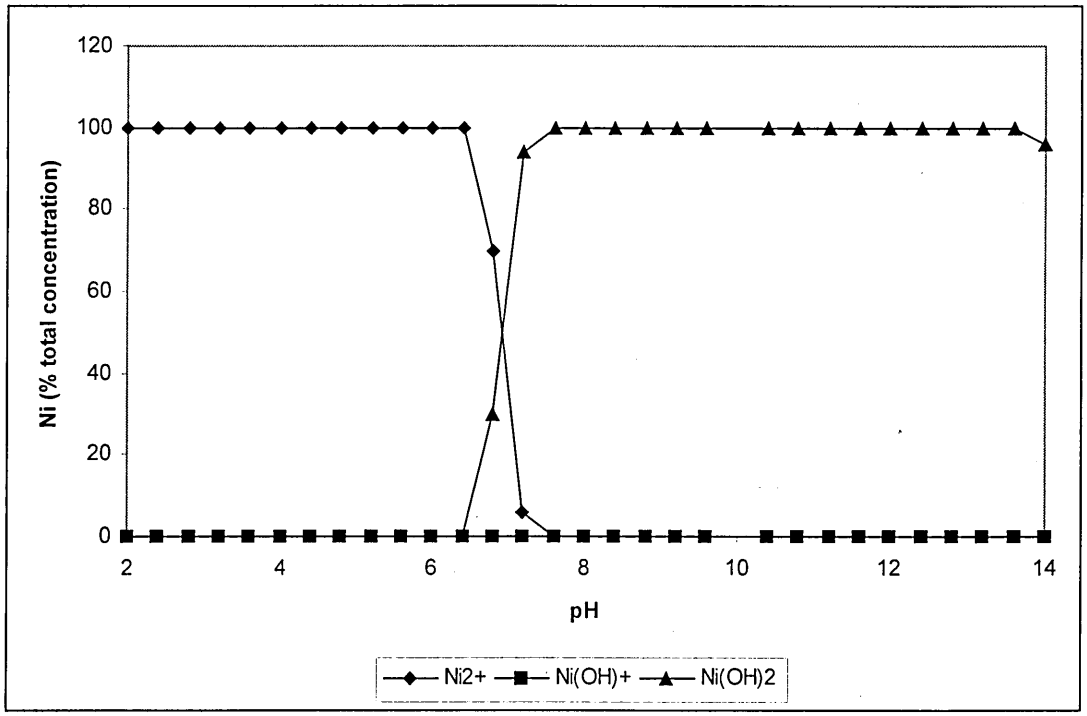

Figure 36 Distribution of Cr species with pH

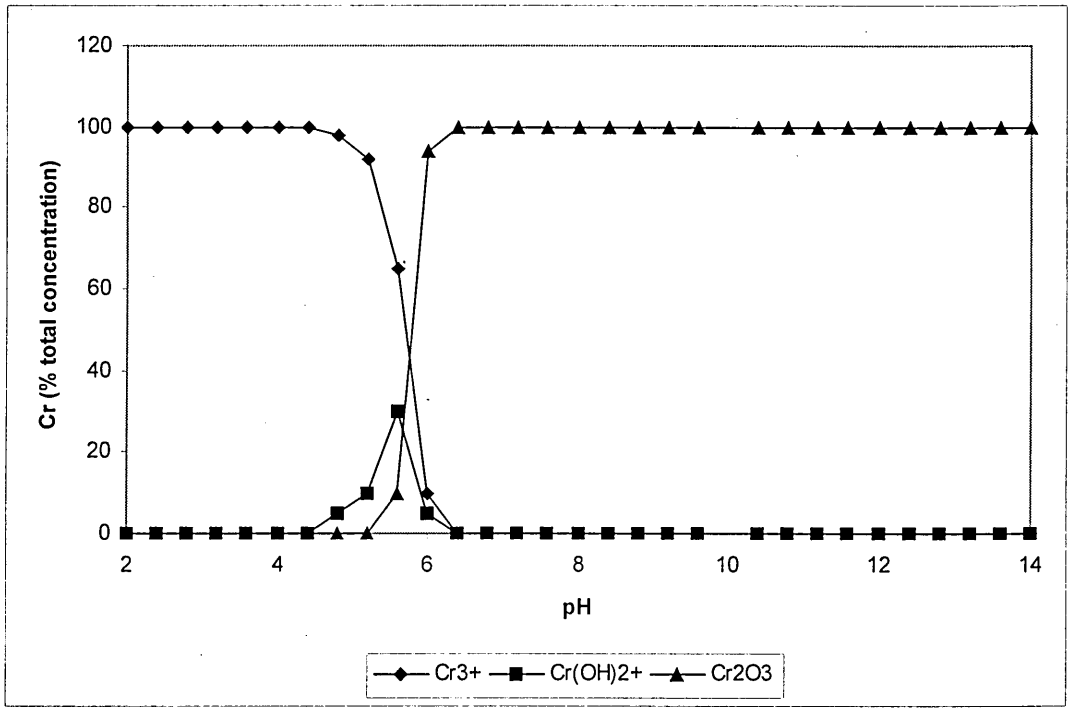

The results found for Ag speciation are shown in Figure 37. At concentrations between 1 x 10^{-3} and 9 x 10^{-5} M, three predominant species, Ag^+, $Ag(OH)_2^-$ and Ag(OH) are present. The hydrolysis of Ag in aqueous solutions gave approximately 100% Ag^+ ion in solution until pH 10. The other species appear at much higher pH. At concentrations higher than 1 x 10^{-3} M $Ag(OH)_2^-$ is not found.

The diagram obtained for Al speciation (Figure 38) showed that at low pH (pH < 4) hydroxide complexes are not significant. Their importance increases towards higher pH values, greater than 7 the hydroxide complex completely dominates the solubility of Al. Although the simulation shows that at pH 4.6 the Al^{3+} ion completely disappears. It has been reported that the ion exists in solution up to pH 8 at concentrations between 1 x 10^{-4} and 1 x 10^{-16} M (147).

Figure 37 Distribution of Ag species with pH

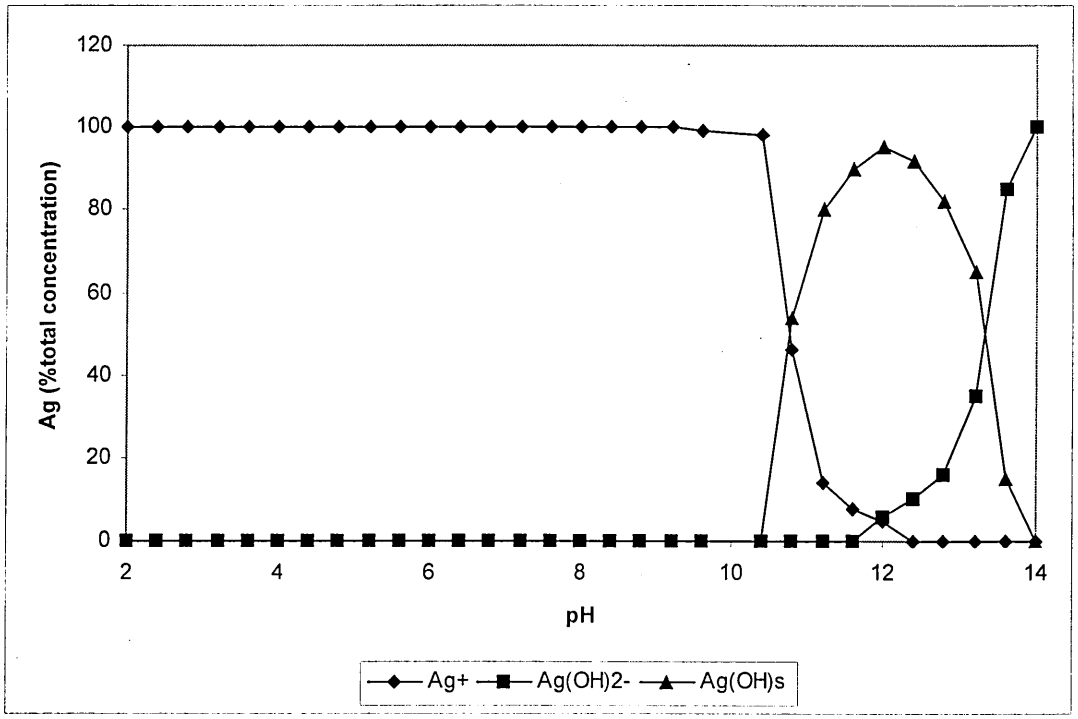

Figure 38 Distribution of Al species with pH

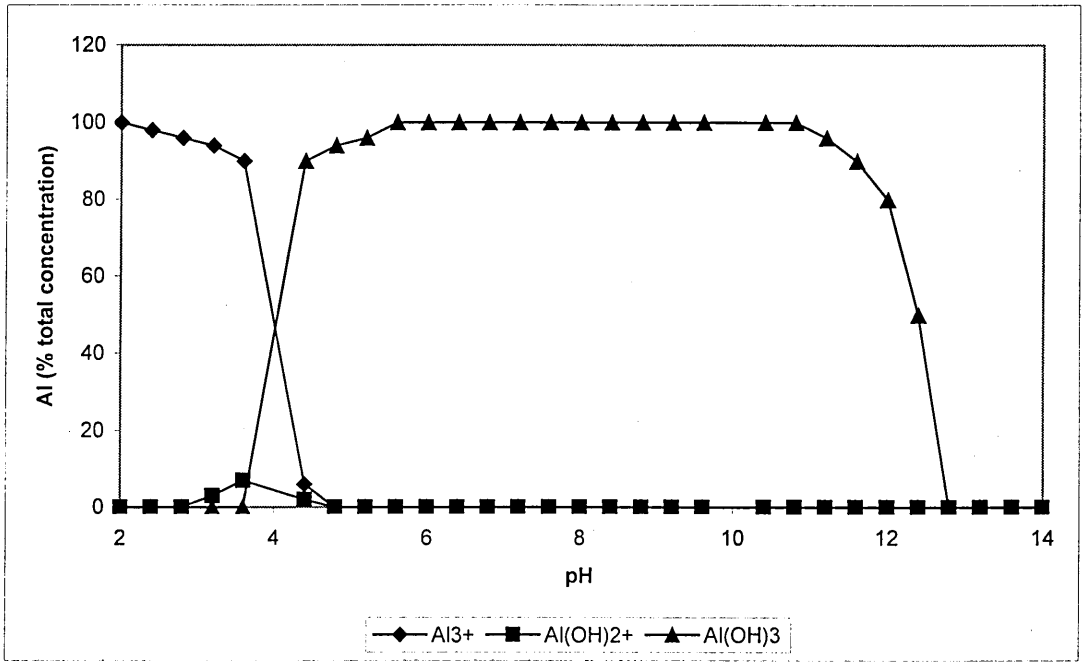

Results for the simulation of Au (I) are shown in Figure 39. Unfortunately, the databases employed by the two programmes used do not include Au (III). Au+ ions do not exist in solution, except in complexes. Gold (III) also is complexed in all solutions, usually as an anionic species.

Figure 39 Distribution of Au species with pH

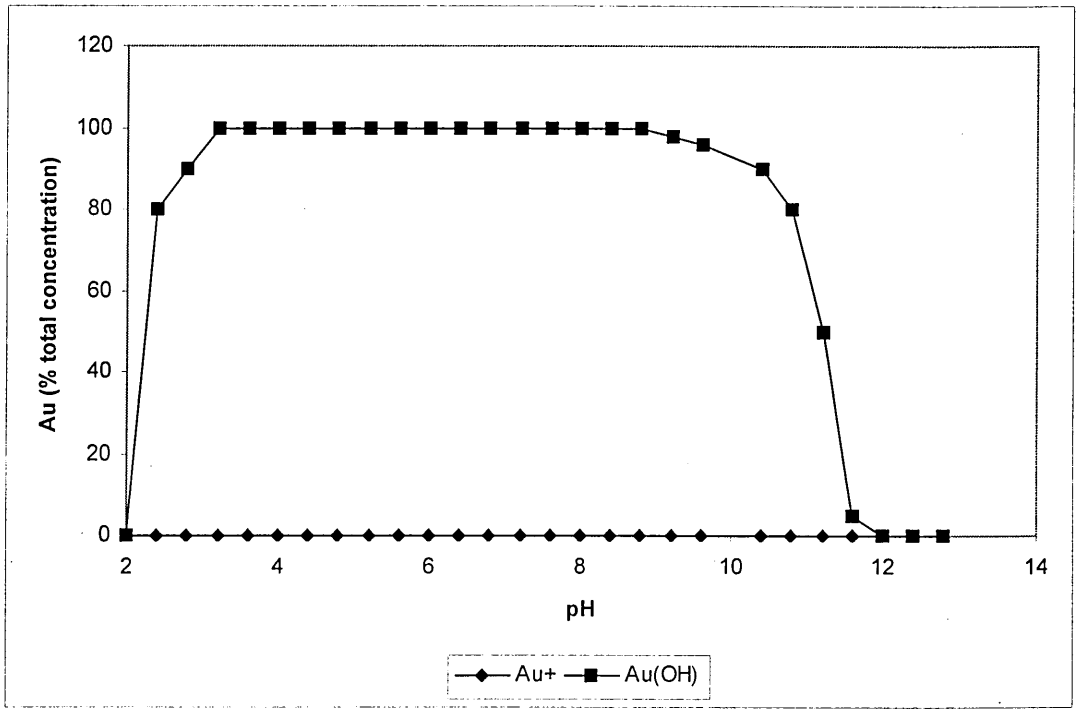

3.9. Proton and Calcium displacement investigation

In order to investigate the nature of the cadmium dealginate interaction, the dealginate was contacted with a solution containing calcium and then, solutions of cadmium at known concentrations were added to the samples until equilibrium, during a 2h period. The amount of protons or calcium displaced was then estimated. This allowed the relationship between proton and calcium displacement and cadmium sorption to be determined.

Results for a typical set of experiments with dealginated seaweed are shown in Table 8. The value of K_{ex}^{H} was calculated using this set of data. As described before the amount of acid sites at equilibrium *(HX)* is the difference between $(HX)_o$, the initial amount of acid sites and the amount of proton reacted (H_{off}). H_{off} was based on the amount of LiOH used to keep the pH at 6. Values for K_{ex}^{H} calculated from these data are comparable with the values calculated from the ion exchange data as has been previously shown. K_{ex}^{H} was found to be constant over the given Cd concentration range.

Table 8 Proton displacement experiment

	EXPERIMENT				
	1	2	3	4	
Cd, mM	0.5	1.0	2.0	4.0	
H_{OFF}, μequiv g^{-1}	75	144	158	200	
Ca_{OFF}, μequiv g^{-1}	449	655	847	959	
(CdX_2), μequiv g^{-1}	524	799	985	1159	
(CaX_2), μequiv g^{-1}	488	225	111	111	
[Cd], mequiv L^{-1}	3.3	934	17.4	40.0	
(HX), μequiv g^{-1}	225	156	142	100	
$K_{ex}^{H} \times 10^{6}$	3.1	3.5	2.8	2.9	$\bar{x} = 3.1 \pm 0.3 \times 10^{-6}$

The ratio of calcium displaced from dealginated seaweed per equivalent of Cd sorbed was calculated. The data is shown in Table 9. The ratios of calcium displaced to cadmium sorbed showed that approximately 1 mole of calcium was displaced when one mole of cadmium was sorbed, regardless of the initial cadmium concentration. These results confirm that ion exchange may be one of the mechanisms for the retention of cadmium by dealginate.

Table 9 The effect of calcium displacement on cadmium sorption by dealginate

Parameter	Value			
Initial Cd Concentration (mM)	0.5	1	2	4
Ca displaced (μmol g^{-1})	225	225	450	675
Cd adsorbed (μmol g^{-1})	300	369	588	875
Ratio Ca/Cd	0.80	0.70	0.77	0.77

Crist *et al.* (86, 141) showed that the stoichiometry for *Vaucheria* is approximately 2 protons displaced per Cd sorbed in the proton reaction and 1 Ca displaced per Zn sorbed in the calcium reaction, suggesting that the bonding is primarily electrostatic in nature. Schiewer *et al.* (90 - 92) proposed and used a model to determine the stoichiometry of metal binding to algal biomass. The model demonstrated a binding stoichiometry of either $BM_{0.5}$ or BM_2 for protons, and reassured the ion exchange nature of the binding for a range of metals, including Cu, Ni, Zn, Ca, Cd, and Na. These findings suggested that at low ionic strength a significant portion of the binding is electrostatic, however, at higher metal concentrations all sites would be occupied by metal until "no" free sites were left and then the metal binding would be exclusively coordinative and not electrostatic (90).

The fact that metal binding on the dealginate occurs via proton exchange supports the assumption of the presence of carboxylic groups on the biomass surface as shown before. This has been also demonstrated by Schiewer *et al* (92). for Cu binding constants for brown and green algae. Virtually no covalent metal binding occurred, for the green alga *Ulva*, because of its low content of alginate, which resulted in a lack of carboxyl groups spaced at a suitable distance for bridging of one metal ion between two binding sites.

3.10. Esterification of dealginated seaweed

In an attempt to identify the nature of the functional group responsible for metal sorption, the carboxyl groups were esterified using the procedure described by Gardea-Torresdey *et al.* (77).

The procedure involves chemically blocking the carboxyl groups by transforming them into methyl esters:

$$R\text{-}COOH + CH_3OH \rightleftharpoons R\text{-}COO\text{-}CH_3 + H_2O \qquad (25)$$

Figure 40 shows the results from the adsorption experiments. It was observed that the amount of cadmium bound was reduced from 95% to 17%, suggesting that cadmium ions bind to carboxyl groups. However, the residual sorption after esterification is indicative of the presence of other cadmium binding sites. The same behaviour was observed for all the metals studied. However, there were differences depending on the metal. In the case of Ni, Cu Cr and Ag results were similar to those reported for Cd, 82%, 80%, 80%, 83%, respectively. Values of 72%, 57% and 48% were found for Pb, Au and Al, respectively. These values strongly suggest that other type of sites are involved in the sorption of Pb, Au and Al. In the case of Au and Al, the other type of site is responsible for nearly 50% of the sorption process, indicating that the presence of these sites may be important for the retention of these metals.

Although this material has been produced from a mixture of seaweeds, which have been chemically treated, it could still contain residues of polyuronates (alginates). According to the manufacturers, the waste contains about 1% alginic acid. The decrease in the affinity for the studied cations is analogous to that reported for Ca in which its affinity for polyuronates decreases with increasing esterification. Schweiger (150) has proposed two possible mechanisms by which divalent cations bind to polyuronates (see Figure 41). It is to be expected that in either case esterification of the carboxyl groups will result in diminished affinity

for cations. However, some metal binding will still remain presumably due to the interaction with the vicinal hydroxyl groups.

Figure 40 Metal sorption on the untreated and esterified dealginated seaweed

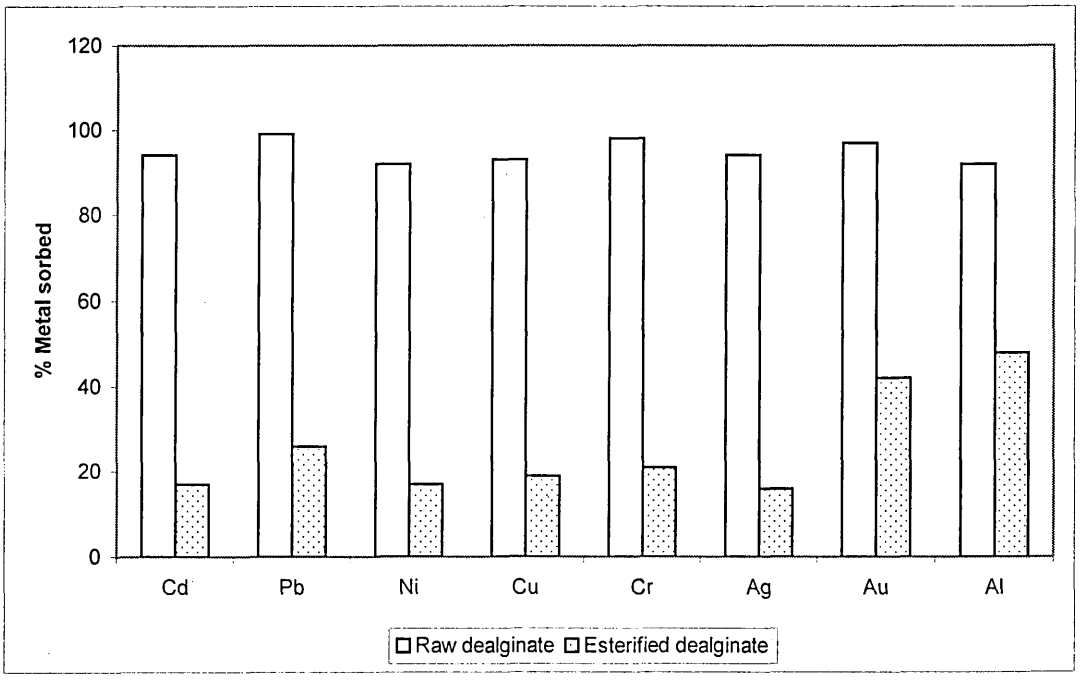

Figure 41 Possible Metal binding sites on polyuronates (after Schweiger (150))

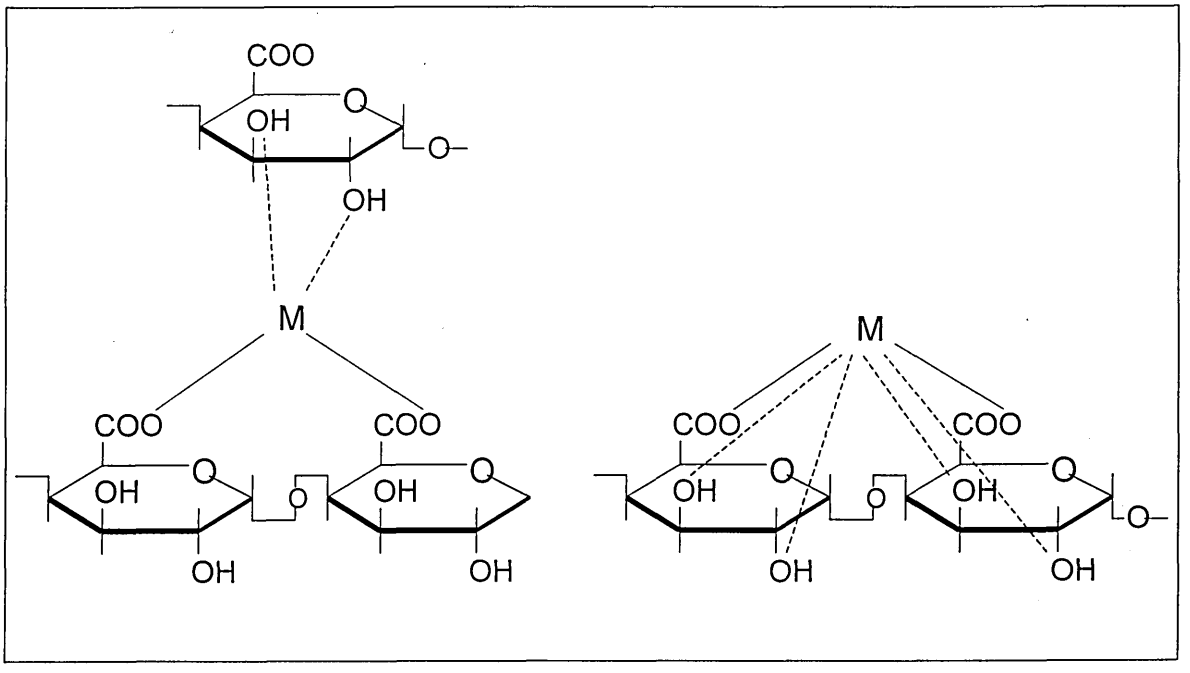

Although carboxylic groups have been identified as the main chemical group responsible for the sorption of metal by algae and other biomasses (36, 61, 80, 82 - 84, 86, 139, 142, 151) the titration study has shown that other groups might be present and need to be taken into consideration in order to fully explain the sorption process. These groups may be responsible for the remaining sorption that occurs in the presence of blocked carboxylic groups.

The presence of sulphonate groups has been quantitatively demonstrated, and although it has been difficult to establish their contribution to the sorption process, they have been identified as being responsible for the sorption of metals at very low pH (61, 82, 142). It has been suggested (36, 141) that sulphydryl groups are mainly involved in Ag sorption by algae biomass. The binding is probably covalent in nature making it independent of the pH. A reduction in Cu, Cd and Pb sorption was shown when amine groups in fungi biomass were modified (84). Crist *et al.* (86) also suggested that Cu bound to algae through amine groups via covalent bonding. The binding of Au to the biomass was shown to be less affected by the reduction in carboxylic groups on the surface, suggesting the involvement of other groups, or even other mechanisms. It has been shown that colloidal Au could be formed when Au(III) is reduced to Au(0) on dealginate. Watkins *et al.* (139) suggested that Au was most probably bound to S or N than to carboxylate groups. Gardea-Torresdey (124) also suggested an electrostatic interaction between amine residues and Au.

In order to establish the efficiency of the esterification process the reverse reaction was applied, and the biomass was hydrolysed via the hydrolysis reaction:

$$R\text{-}COO\text{-}CH_3 + NaOH \rightleftharpoons R\text{-}COO^- + CH_3OH \qquad (26)$$

The dealginate was placed in contact with the metal ion solution and the resulting uptake percentage is shown in Figure 42. The process was demonstrated to be reversible, since the

hydrolysed dealginate showed a similar removal capacity to that of the untreated biomass. A slight increase in dealginate sorption was observed for Cd, Pb, Ni, Cu and Al. In the case of Ag there was little difference in the sorption by the untreated and hydrolysed dealginate and the sorption by hydrolysed dealginate was slightly lower for Cr and Au.

Figure 42 Metal sorption on untreated and hydrolysed dealginate seaweed

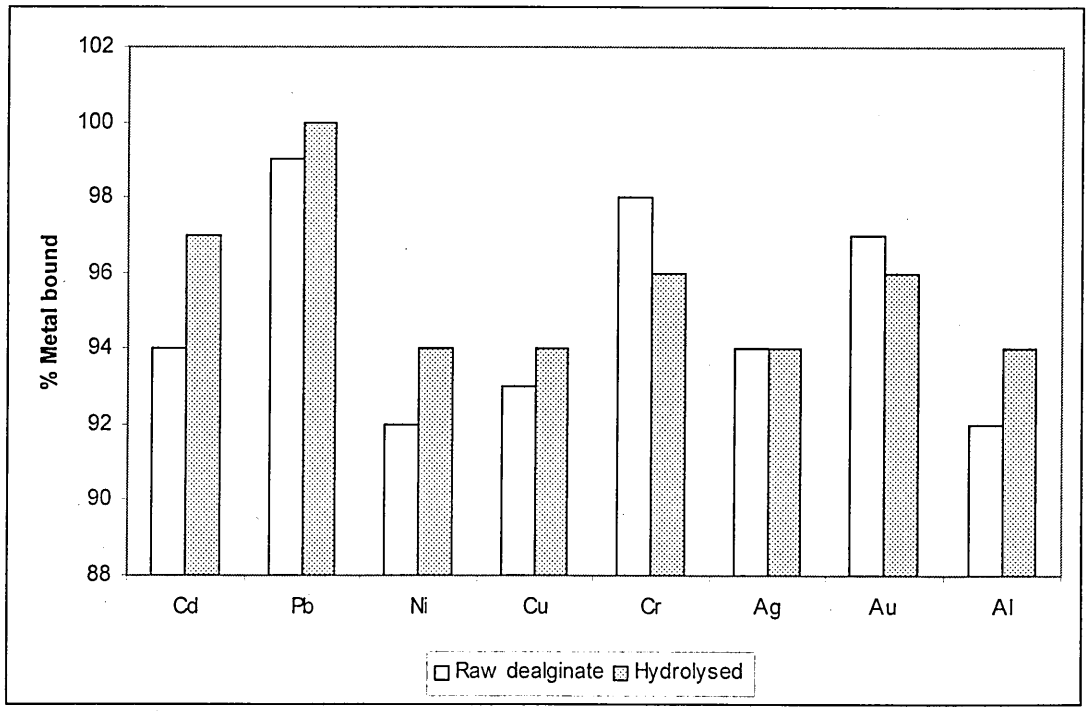

These results are in agreement with metal binding studies performed using *Datura innoxia*, algal biomass and alfalfa biomass (61, 77, 80). In these studies, the binding of Ni, Cu, Sr and Cr was increased by saponification of the biomass and decreased in the case of Cd. This means that the overall binding capacity of the biomass was regained, and the slight variations present after the treatment may be due to the nature of the binding to specific metals.

3.11. Saturation of Dealginated Seaweed

In order to ascertain the saturation capacity of the dealginated seaweed, a batch procedure using a high concentration of metal ion solution (500 mg L^{-1}) was employed. A sample of dealginated seaweed was repeatedly placed in contact with this solution for over 9 cycles and the Cd, Pb, Ni, Cu, Cr, Ag, Al and Au concentrations were determined by ICP-AES. The results are shown in Figures 43 and 44.

Figure 43 The Cd, Pb, Ni and Cu uptake by dealginated seaweed over 9 consecutive cycles

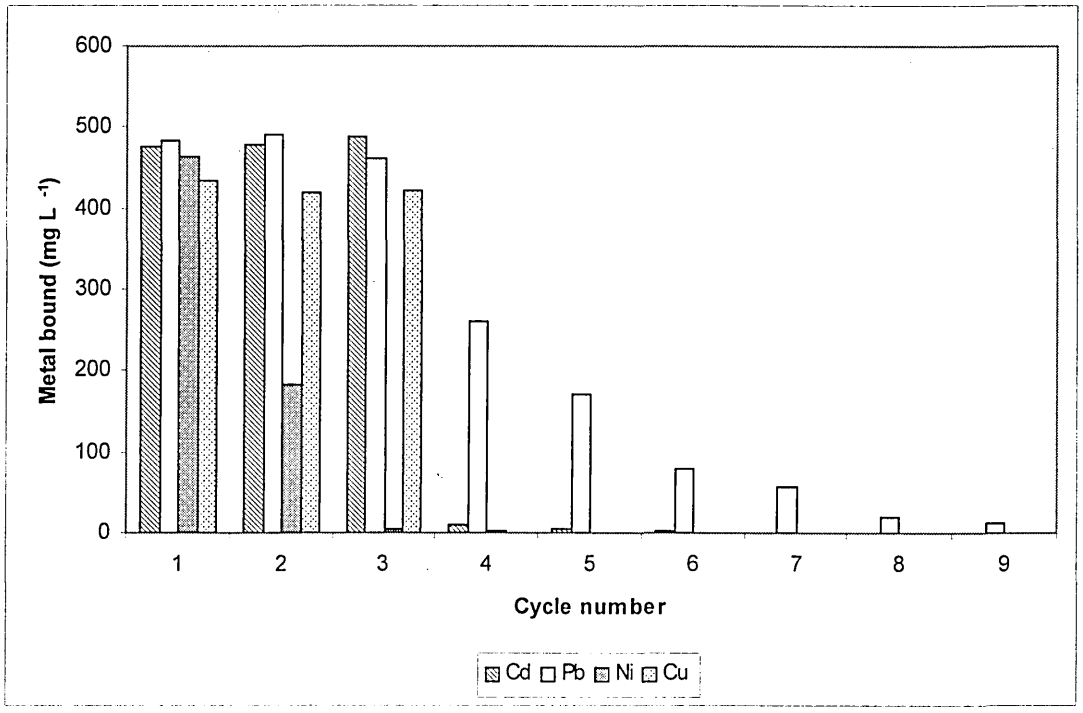

Figure 44 The Cr, Ag, Al and Au uptake by dealginated seaweed over 9 consecutive cycles

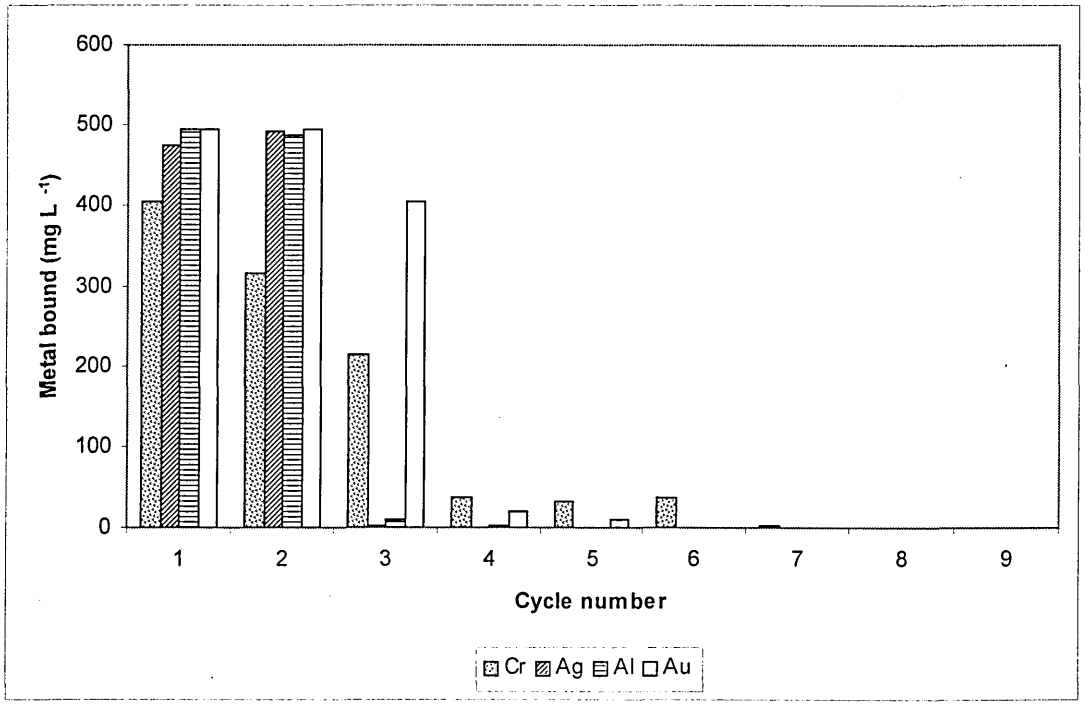

It was observed that for the majority of the metals studied the dealginate was saturated with metal ions from the solution after the third cycle. The sorption of Ni and Ag was no longer observed after the fourth cycle and a small proportion of Cd, Cu, Cr, Al and Au were still bound during the 4th, 5th and 7th cycles. Total saturation was not achieved for Pb, since some sorption still occurred in the 9th cycle.

The capacities calculated from the saturation point were 1.31, 0.71, 1.57, 2.03, 1.56, 0.92, 3.67, 0.75 mmol g^{-1} for Cd, Pb, Ni, Cu, Cr, Ag, Al and Au, respectively. The value for Pb was calculated assuming that the maximum saturation was achieved during the 3rd cycle, the remaining binding over subsequent cycles was not considered. The values found were in good agreement for Cd, Cu, Cr and Ag with the previously estimated capacities obtained using the linear regression, which were 1.24, 0.45, 0.75, 1.59, 1.18, 1.14, 0.94 and 0.40 mmol g^{-1}, respectively.

3.12. The speciation of cadmium, lead and silver ions in the adsorption process

The speciation of Cd ions in the solutions collected during the isotherm experiments was determined by comparative analysis of the samples by ICP-AES and by ion selective electrode (ISE). The results of these analyses are shown in Table 10. The ISE technique is the only analytical technique available that can measure the concentration of free metal species.

The results from the ISE analysis provide a measure of the concentration of free Cd^{2+} ions in the dealginate supernatant solution. It should be noted that while the results of the determination of Cd by the two techniques in the initial solution are similar, once dealginate is added only about 30 per cent of the Cd left in solution was in the free form.

These results show that despite extensive washing before use, ligands, which bound cadmium, are introduced into the solution. Therefore, only a fraction of the Cd in equilibrium with the dealginate is available for exchange. The amount of Cd in this fraction was less than 10% of the initial concentration. This could explain the residual Cd concentration in solution even after 24 h of contact.

Table 10 The Cd concentration before and after addition of dealginate as determined by ICP-AES and ISE

Initial Cd concentration by ICP-AES (mg L^{-1})	Initial Cd concentration by ISE (mg L^{-1})	Cd concentration by ICP (mg L^{-1}) after adsorption	Cd concentration by ISE (mg L^{-1}) after adsorption
1.02	0.99	0.17	0.03
5.10	5.02	0.49	0.17
9.96	9.87	0.68	0.22
24.99	25.30	1.20	0.71
49.93	49.48	2.09	0.60
79.80	80.01	3.56	1.31
100.30	100.02	4.49	1.65

Results for Pb are shown in Table 11. In the case of Pb a comparison between the values obtained by the two techniques showed that all the Pb remaining in solution was Pb^{2+}. The total amount of Pb^{2+} ions present represents 2% of the total initial Pb concentration, as was expected from the Pb speciation. This also demonstrated a better performance for the removal of Pb ions by dealginate.

Table 11 The Pb concentration before and after addition of dealginate as determined by ICP-AES and ISE

Initial Pb concentration by ICP-AES (mg L^{-1})	Initial Pb concentration by ISE (mg L^{-1})	Pb concentration by ICP (mg L^{-1}) after adsorption	Pb concentration by ISE (mg L^{-1}) after adsorption
1.07	1.09	0.11	0.13
4.98	5.21	0.14	0.17
10.06	10.53	0.23	0.26
25.01	25.17	0.35	0.31
50.12	51.03	1.05	1.16
80.05	80.65	1.35	1.13
100.61	99.41	2.44	2.52

The speciation of Ag^{+} ions in solution was found to be similar to the results obtained for Pb. All of the Ag remaining in solution after the dealginate was added was Ag^{+}. It is more likely that these Ag^{+} ions were left in solution after the dealginate removed a considerable proportion of Ag, although the possibility of dynamic exchange may not be discarded.

Table 12 The Ag concentration before and after addition of dealginate as determined by ICP-AES and ISE

Initial Ag concentration by ICP-AES (mg L^{-1})	Initial Ag concentration by ISE (mg L^{-1})	Ag concentration by ICP (mg L^{-1}) after adsorption	Ag concentration by ISE (mg L^{-1}) after adsorption
1.14	0.98	0.09	0.15
5.13	4.93	0.16	0.21
10.00	10.39	0.28	0.31
25.11	24.96	0.75	0.69
50.22	49.87	2.15	2.21
79.63	80.18	2.28	2.23
99.97	99.77	3.43	3.51

3.13. Summary

The main mechanism of metal sorption by dealginated seaweed is ion exchange, featuring fast sorption kinetics and metal ion removal from solution between 92-97%. The sorption process is pH dependent and a negative surface charge was established. Three types of binding sites were identified on the dealginate surface: sulphonates, carboxylates and phenolic OH groups. The stoichiometry of the sorption process was found to be a B_2M type. The esterification of the dealginated surface showed a reduction in the ability of the biosorbent to bind metal ions, indicating that carboxyl groups are mainly responsible for the sorption process. The efficiency of the sorption process was demonstrated to be dependent on the metal species used.

On-Line Preconcentration and Chemical Speciation of Trace Metals using Dealginated Seaweed Packed Microcolumn with Inductively Coupled Plasma Spectrometry Detection

Chapter 4

4.1. Introduction

The performance of dealginated seaweed for metal preconcentration was evaluated in a continuous flow column system. The ability of the biosorbent to remove metal ions from dilute solutions was developed and optimised for a wide range of metals. The data presented here represent the average of 5 measurements in all cases except for the blank samples, for which 10 measurements were collected.

4.2. Development and validation of the analytical procedures

4.2.1. Effect of the amount of adsorbent

The retention of the elements studied was evaluated in relation to the amount of dealginated seaweed, which was varied from 0.05 g to 0.5 g. It was found that above 0.1 g the recovery of Cd, Pb, Ni, Cr and Cu was gradually increased, and at about 0.3 g of adsorbent the metals reached a plateau. Values above 0.3 g caused clumping and hindered the control of a uniform flow rate through the column. Therefore 0.3 g was chosen as the optimum amount of dealginate to be packed into the column for preconcentration experiments.

4.2.2. Effect of the strength and volume of the elution solution

HCl was chosen for the elution of the sorbed metals because it was found to be less destructive to the biosorbent compared with HNO_3 or H_2SO_4. The elution studies were performed with 0.1, 1.0 and 5.0 M HCl. The eluate volumes evaluated were 0.5, 1.0 and 5.0 mL. As can be seen in Table 13, 0.5 mL of 1.0 M HCl was found to be satisfactory.

Table 13 Effect of HCl volume on recovery of Cd by dealginated seaweed

Concentration mol L^{-1}	Volume mL	Recovery (%)
0.1	0.5	93
	1.0	94
	5.0	91
1.0	0.5	96
	1.0	96
	5.0	97
5.0	0.5	97
	1.0	97
	5.0	96

4.2.3. Effect of the flow rate of sample solution

The flow rates were controlled using a peristaltic pump and were in the range of 0.1 – 3.0 mL min^{-1}. For flow rates lower than 0.7 the analysis time became too long, although the equilibrium and recoveries found were satisfactory. Flow rates higher than 2.0 mL min^{-1} caused the biosorbent to clump at the end of the column, impeding the circulation of solution after a few hours analysis. Flow rates between 0.8 and 1.5 mL min^{-1} proved to be suitable, with recoveries for Cd in the range of 96-98%. In order not to compromise the performance of the column, a 0.8 mL min^{-1} flow rate value was chosen as the optimum.

4.2.4. Effect of the volume of the sample

Different volumes of a mixed standard solution at pH 6 containing 5 mg L^{-1} of each metal were preconcentrated and desorbed from the column using dilute HCl solutions. Up to 5 mL sample solutions could be injected and about 90% of the metals desorbed with 1.0 mL 1.0 M HCl. The

preconcentration and desorption cycles were repeated for a period of up to four months without adverse effects on the performance of the column.

Up to 5 mL of the 5 mg L^{-1} mixed standard could be injected into the column, and mean recoveries of 96, 97, 94, 93, 93, 94 and 97% obtained for Cd, Pb, Cu, Ni, Cr, Ag and Au, respectively, when 0.5 mL of 1.0 M HCl was used for desorption.

It is important to emphasise that no reconditioning of the column is necessary after the initial column preparation. Analysis of the multi element solution was achieved using the ICP-AES, 1 mL sample loop was used and the metals desorbed with 500 μL, 1.0 M HCl. With this set up, a two-fold increase in sensitivity compared to when no column is used was obtained for all seven elements. This preconcentration factor is adequate for the analysis of the samples used in this study.

A slight increase in the biosorption performance from 96 to 98% removal was observed after several sorption-desorption cycles, which was attributed to the fact that the acidic wash may generate more available sites on the surface. This behaviour has been reported for immobilised sphagnum peat moss (45), which showed an increase in retention of Cd, Zn and Mn after 5 runs.

4.2.5. Calibration graph and detection limit

The calibration graphs in the range 0.1 – 1 mg L^{-1} obtained from mixed metal standard solutions were rectilinear with correlation coefficients (r^2) of 0.9982, 0.9954, 0.9984, 0.9932, 0.9995, 0.9991, 0.9975 for Cd, Pb, Cu, Ni, Cr, Ag and Au, respectively and corresponding detection limits of 0.069 mg L^{-1}, 0.077 mg L^{-1}, 0.018 mg L^{-1}, 0.023 mg L^{-1}, 0.077 mg L^{-1}, 0.058 mg$L^{-1}$and 0.083 mg L^{-1}($n = 5$).

Typical chromatograms for the column elution are shown in Figures 45 and 46. The results are split for visualisation purposes. The negatively charged ions, Au, Se, As and V showed shorter retention times, appearing first in the chromatogram, as expected because of their poor affinity towards the biosorbent surface. It was observed that most of the divalent cations were stripped at the same time, with little separation between them. However, the retention time for Ag was shorter and for Sc the retention time was slightly longer, allowing their differentiation from the rest of the metals. The difference in retention time for Ag could be due to the single positive charge that this metal holds, resulting in more Ag ions being needed to fill the available sites in a shorter time. The separation observed indicates the potential use of the column for metal speciation. The overall retention time was short, demonstrating that the column performance is rapid.

Figure 45 Chromatogram for the separation of metals in dealginated seaweed column

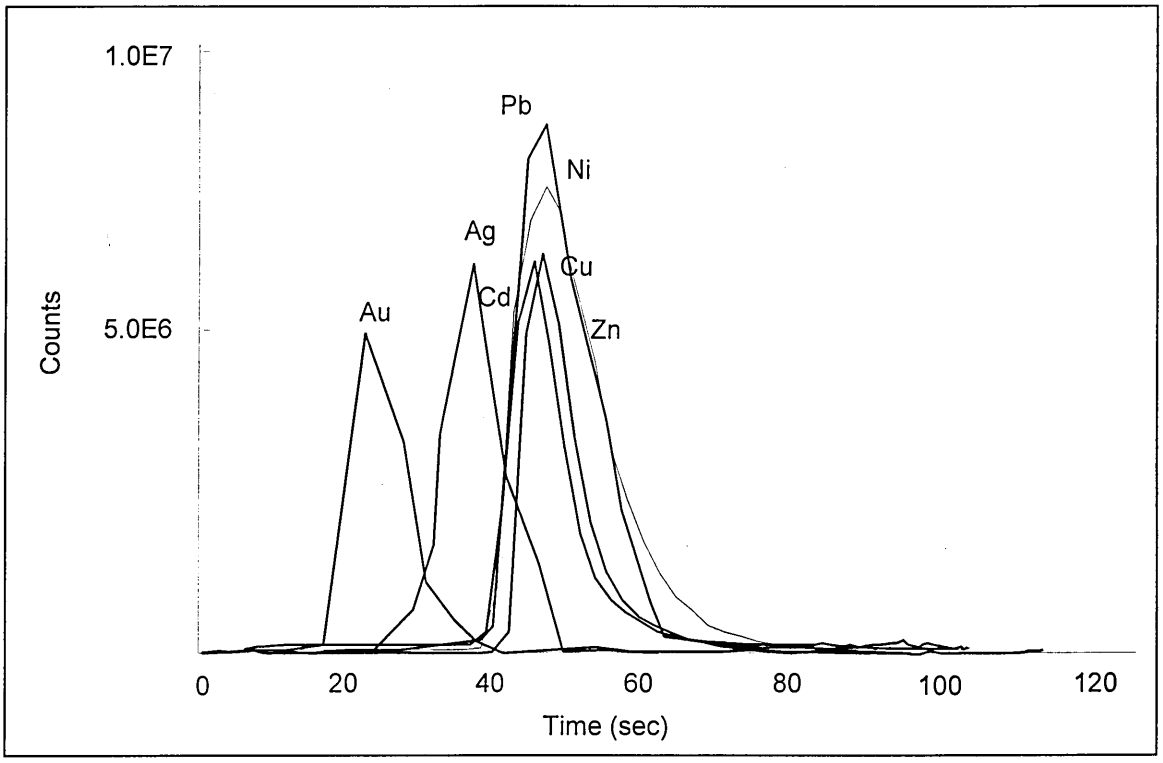

Figure 46 Chromatogram for the separation of metals in dealginated seaweed column

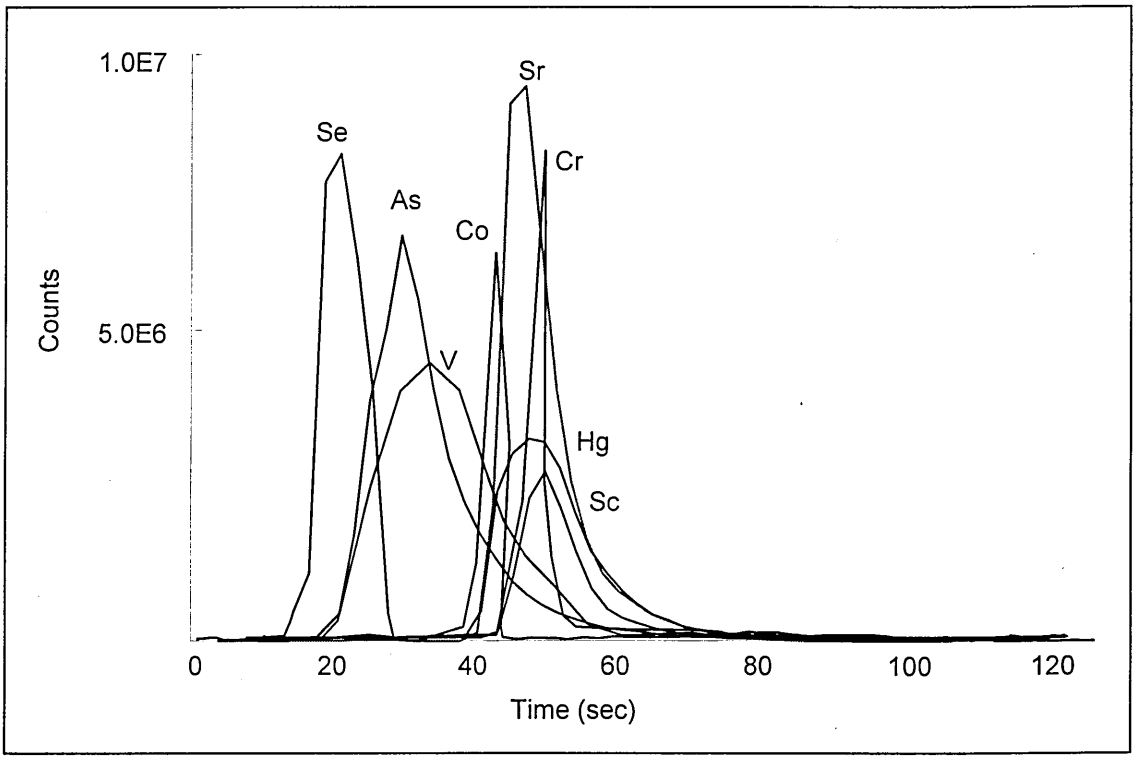

4.3. Column Capacity

The dealginated seaweed packed column was evaluated for the simultaneous preconcentration and separation of several metal ions from solution. The experiments were performed at pH 6 for all metals except for Au and Al, which were examined at pH 3 and 4, respectively.

The exchange rate of biosorbent may be defined as the time taken to reach half of the maximal sorption of a metal ($t_{1/2}$). This parameter along with measurement of capacity for metal sorption after a period of 2 min could be taken as a practical measure of the exchange rate for satisfactory column operation (42). Results from batch studies indicate that dealginated seaweed meets the requirements for satisfactory column operation with

favourable sorption kinetics compared with a low capacity resin for all metals studied. The relationship between contact time and equilibrium capacity showed a $t_{1/2}$ value of 1 min and a capacity greater than 60% for all metal ions studied.

The breakthrough curves which were obtained separately for Cd, Pb, Ni, Cu, Cr, Ag, Al and Au are shown in Figures 47 to 54. The eluted metals were detected by ICP-AES. Except for Pb, the shapes for all breakthrough curves were similar, a typical S shape. For Ni, Cr, Ag, Al and Au, the flat top is a straight line indicating saturation, when the influent concentration equals the outlet concentration. In the case of Cd and Cu the line approaches total saturation exponentially. For Pb, saturation was not achieved after 60 mL, and the dealginate seemed to keep sorbing Pb ions from solution, even after passing 120 mL of solution.

In experiments performed with single 5 mg L^{-1} element solutions, the breakthrough volumes were 17.0, 57.3, 29.0, 31.0, 34.8, 14.2, 19.8 and 9.0 ml for Cd, Pb, Ni, Cu, Cr, Ag, Al and Au, respectively. The ability of the dealginate to sorb Pb ions is clearly shown in the shape of the breakthrough curve and the value of the breakthrough volume, since a large volume of Pb solution was required to fill the sites on the surface (see Figure 48).

The differences in breakthrough volumes suggest that the binding sites for Pb are different from those of the other metals. In contrast, because of its weaker affinity for dealginate Au broke through the column faster than any of the other metals studied. The low breakthrough volume obtained indicates that the sites available for Au sorption are rapidly filled, and may be different in nature to those preferred by the other metals. The natural selectivity of the biosorbent for some metals reflected in the results obtained using the column makes it suitable for metal separation and speciation.

Figure 47 Column breakthrough curve for Cd

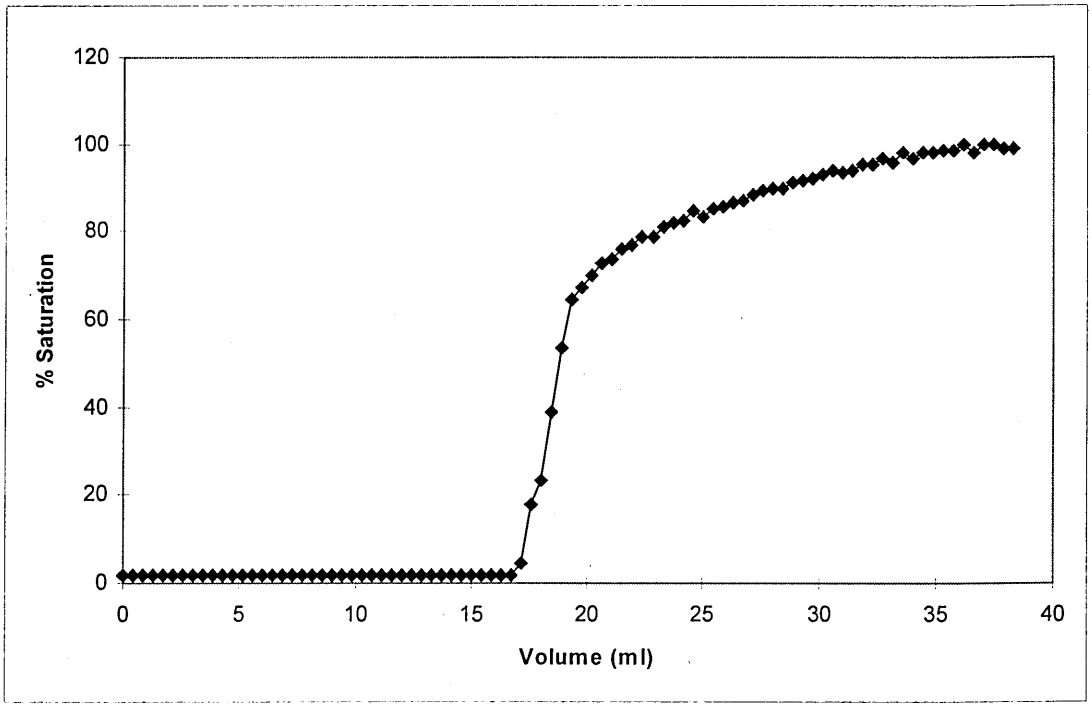

Figure 48 Column breakthrough curve for Pb

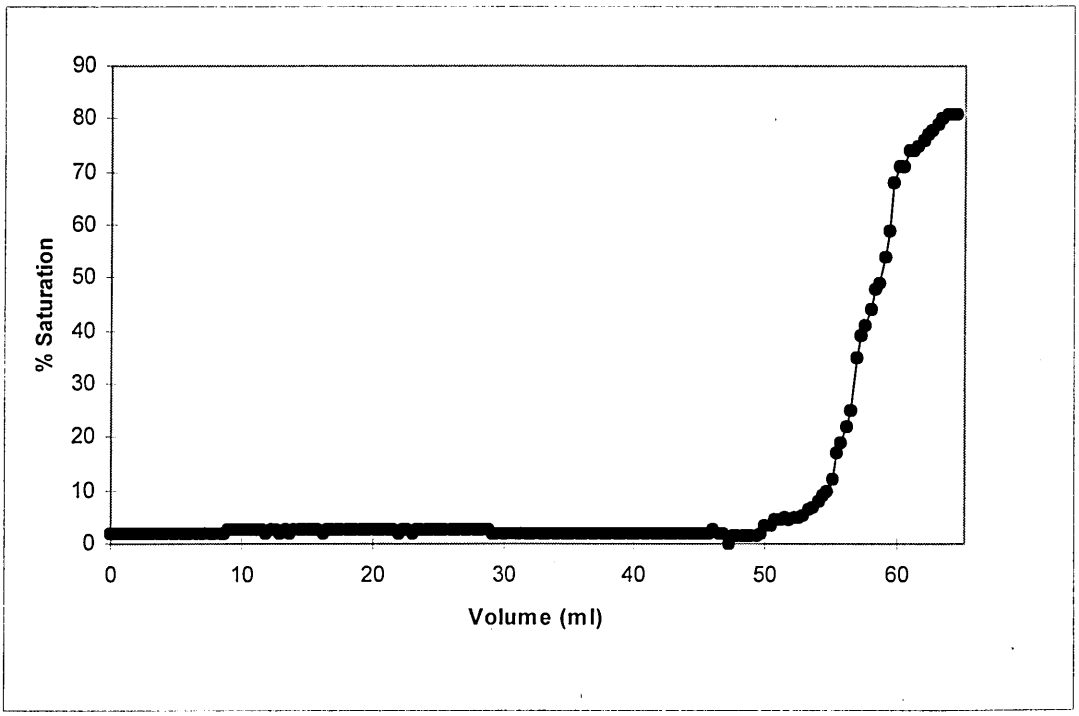

Figure 49 Column breakthrough curve for Ni

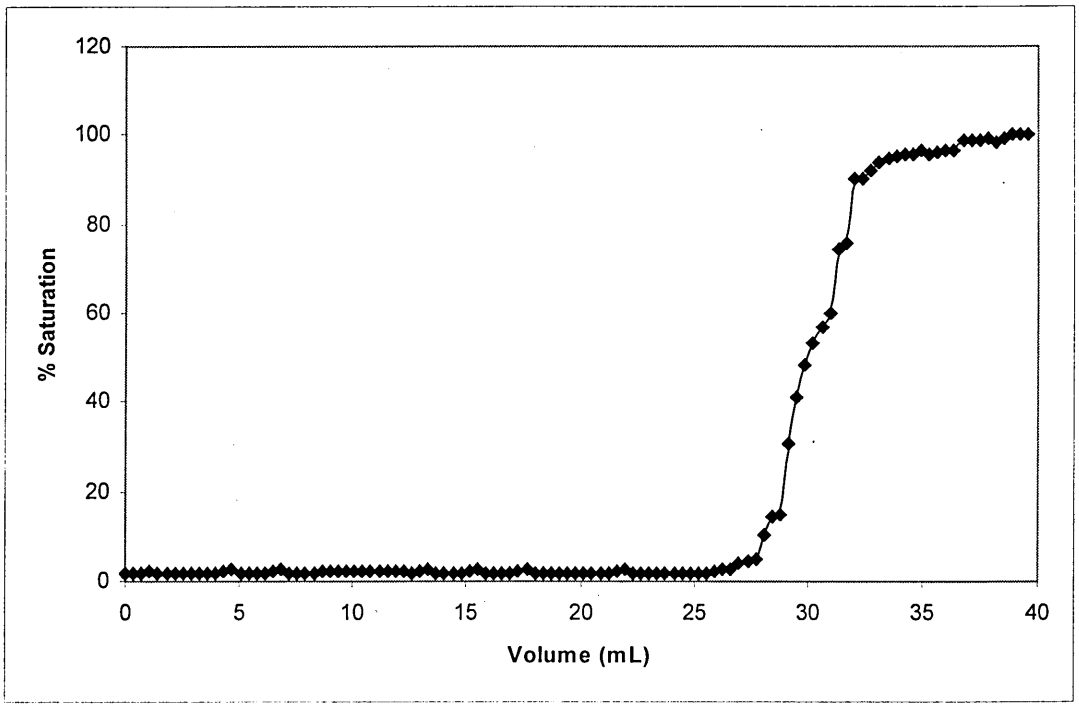

The column capacities obtained from single element experiments were 8.0, 12.0, 24.7, 26.2, 33.7, 11.0, 18.2 and 3.80 μmol g^{-1} for Cd, Pb, Ni, Cu, Cr, Ag, Al and Au, respectively. For the preconcentration of trace metals the available column capacity is more than adequate. It is important to note that the uptake of the metals by the column from the solution pumped in at 0.8 mL min^{-1} was complete until the breakthrough point suggesting that the metal uptake by the biomass at that flow rate is not limited by kinetic factors.

Similar experiments were performed using a multi element solution. The experiment was performed at pH 5, in order to keep all the studied species in solution. Due to the effect of pH in the diminution of Al, this metal was not included in this study. Au was included because maximum sorption was observed at this pH. The results obtained are shown in Figure 55 and 56.

The shapes of the curves obtained were similar to those reported using single metal ion solutions. The affinity of the biosorbent towards Pb is maintained even in a multi element solution. It can be seen that the sites for Pb are still available long after the sites for the other elements have become saturated, indicating the greater affinity of the biosorbent towards Pb. The affinity for Cu and Ag is similar, although a separation is clearly noted in the curves. There are no apparent differences in affinity towards Cr, Cd and Ni, and these metals seem to fill a similar type of site. As was shown previously, Au breaks through first in the series. The differences between the breakthrough volumes for individual solution and for the multi element solution indicate that there is competition between the metals for the available sites. No overshoots were observed for the metals studied. This could be explained by the fact that the metals that have higher affinities towards dealginate break through later, resulting in a minimum interference from the metals with fewer affinities in the sorption process.

Similar breakthrough volumes of 7.8 mL were obtained for both Cd and Cr, and the values for Pb, Cu, Ni, Ag and Au and were 28.0, 8.7, 6.3, 8.3 and 3.2 mL, respectively, using a 5 mg L^{-1} multielement solution buffered at pH 5. Based on the volumes at which saturation was obtained, the effective column capacity for each of the elements were: 3.5, 6.8, 5.3, 6.9, 7.5, 3.9 and 0.8 μmol g^{-1} for Cd, Pb, Ni, Cu, Cr, Ag and Au, respectively.

The lower capacity obtained for the mixed standard indicates that the column capacity for each element is affected by the presence of the other elements.

Figure 50 Column breakthrough curve for Cu

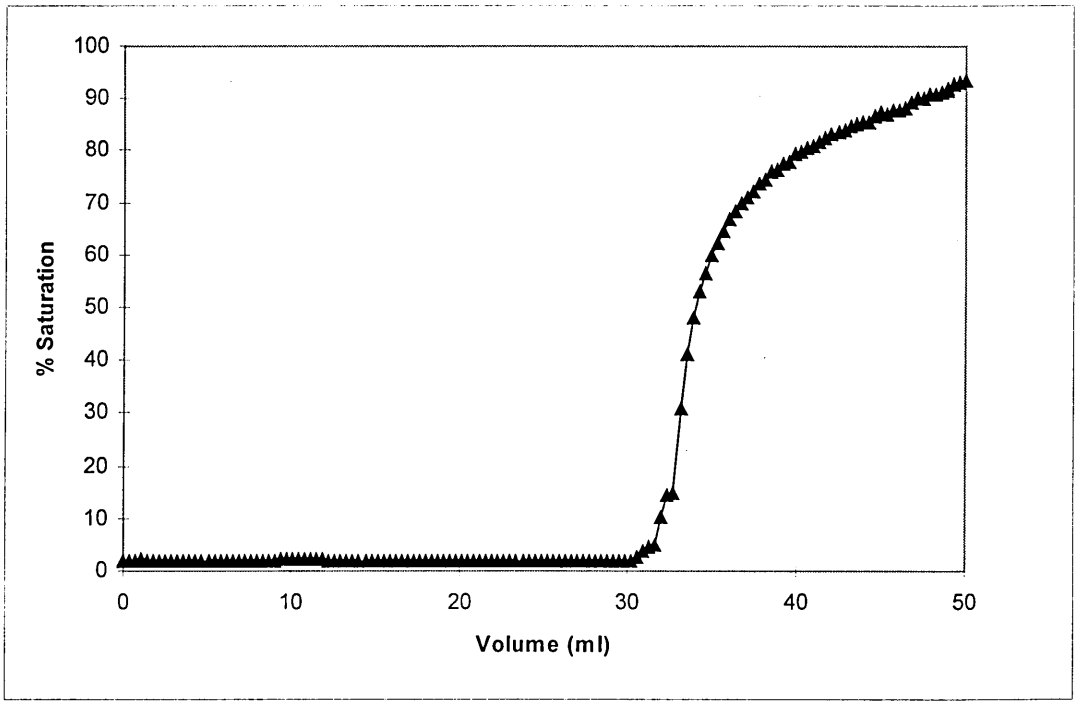

Figure 51 Column breakthrough curve for Cr

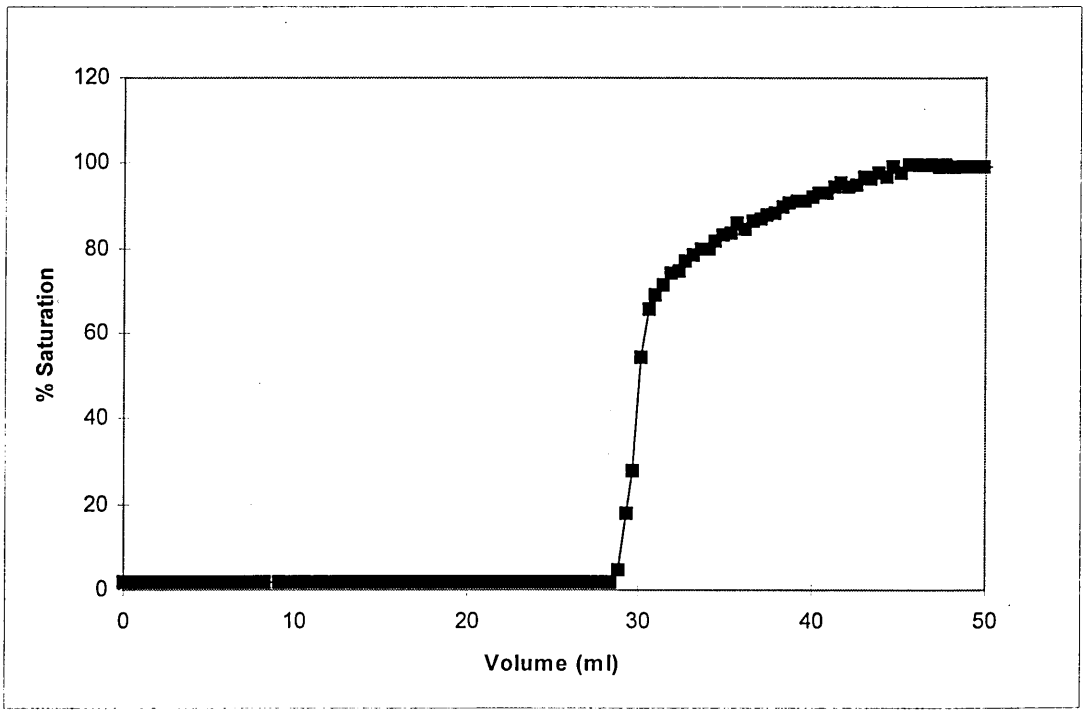

Figure 52 Column breakthrough curve for Ag

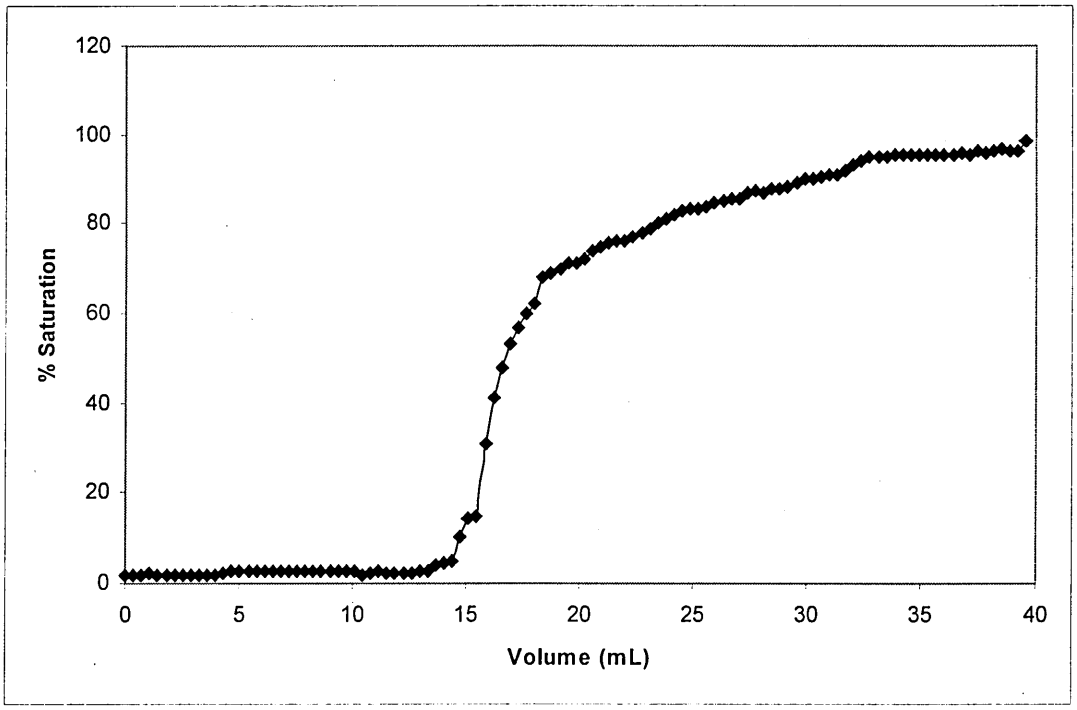

Figure 53 Column breakthrough curve for Al

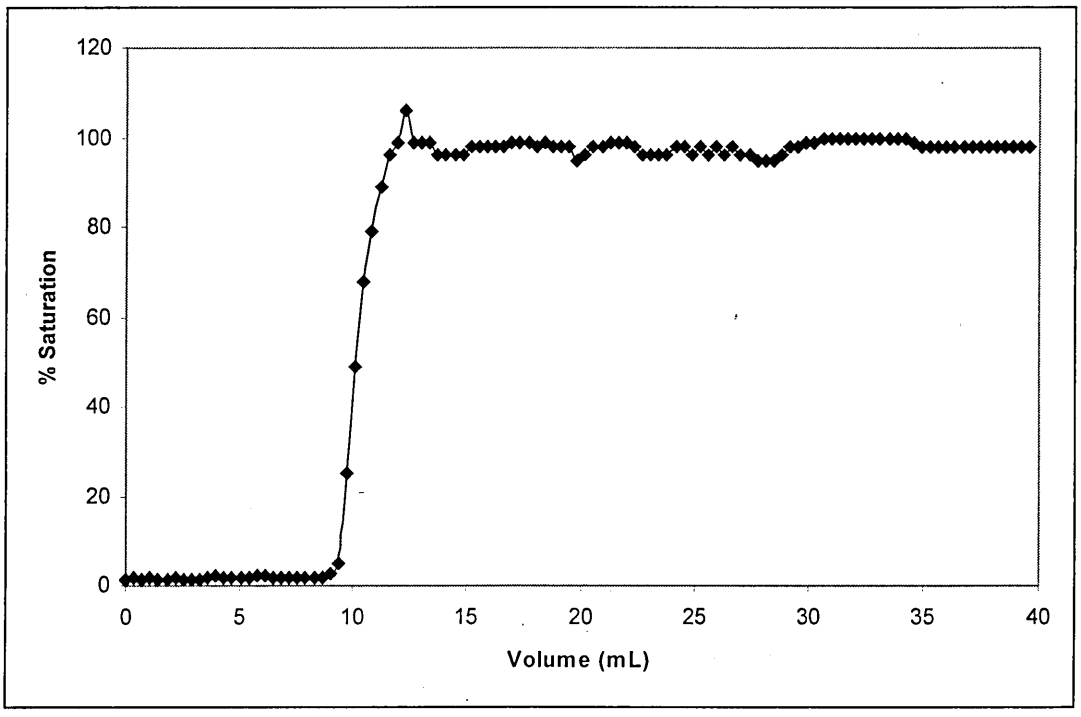

Figure 54 Column breakthrough curve for Au

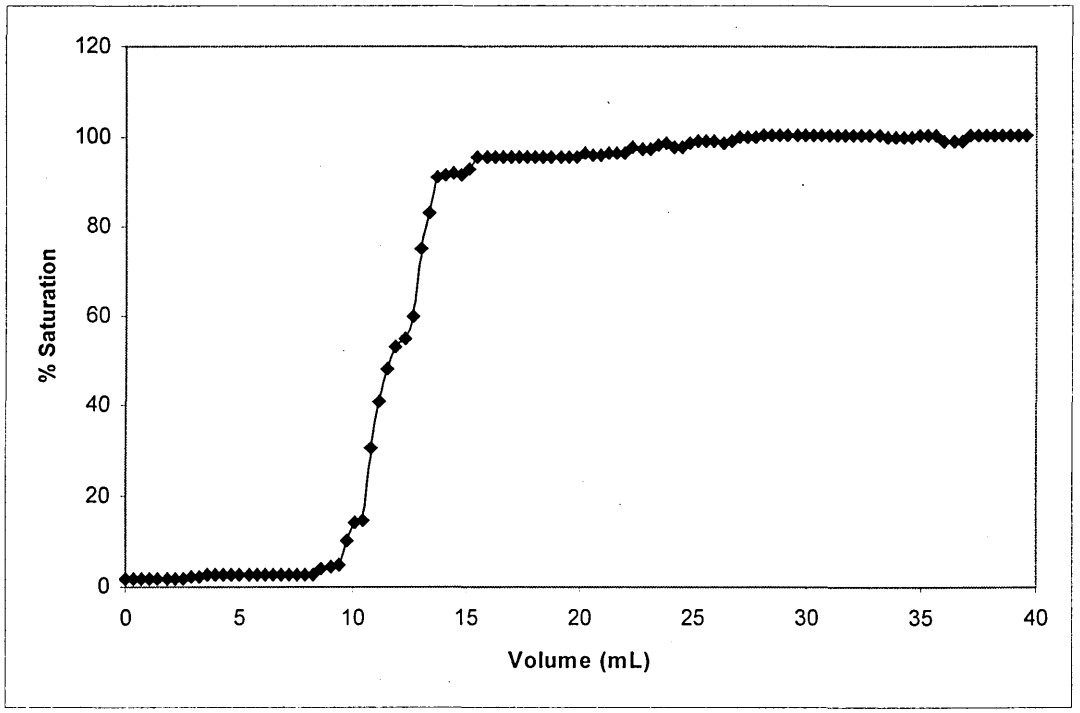

Figure 55 Column breakthrough for metal studied in a mixed metal solution

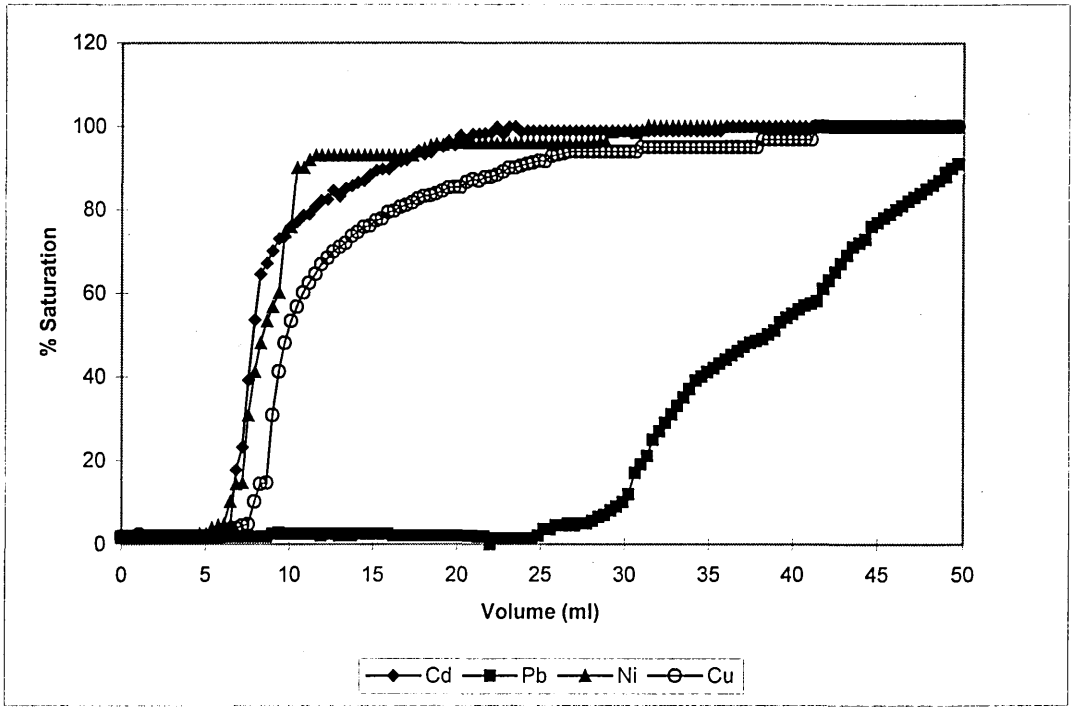

Figure 56 Column breakthrough for metal studied in a mixed metal solution.

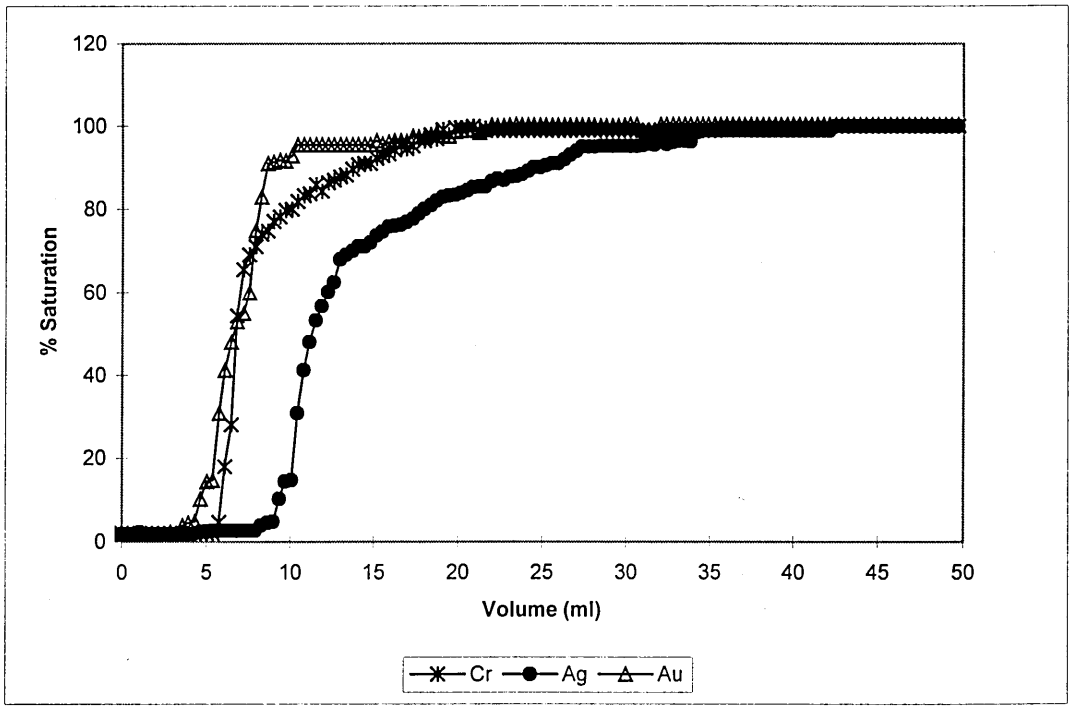

In order to evaluate other possible applications for the dealginate column, a multi-element solution containing a wider range of metal ions was used. The multi-element solution included Zn, Sc, Sr, Co, Mn, Hg, Sb, As, Se and V in addition to the previously studied metals. The breakthrough curves obtained using a 500 $\mu g\ L^{-1}$ multielement solution are shown in Figures 57 - 60.

The breakthrough curves were split for better visualisation. Similar results previously obtained were observed for Cd, Pb, Ni, Cu and Cr and Ag. In contrast, a slight overshoot was detected for Au. The biosorbent showed good affinity towards Sr^{2+} ions, which showed a similar retention as Pb^{2+} ions, but showed a less steep breakthrough curve. This behaviour could be compared to the affinity of the biosorbent to Cd^{2+} ions, since these two elements have similar characteristics.

A more straight and favourable breakthrough was observed for Mn and Hg. In the case of Mn a clear overshoot was seen in the curve, demonstrating that the sorption of this metal by dealginate is markedly influenced by the presence of other metals. The biosorbent showed poor retention of Co^{2+} ions compared to the other divalent ions studied. In addition it was easily removed compared to similarly charged cations.

The affinity of dealginate for As, Se, V and Sb was lower than for other metal ions studied. As can be seen from the Figures 59 and 60 these metals broke through first along with Au. These metal ions are negatively charged in solution, forming the species $H_2AsO_4^-$, $H_2SeO_3^-$, $H_2VO_4^-$ and SbO_3^-, respectively. Considering that the dealginate performance is dominated by a negatively charged surface, the affinity is likely to be lower towards negatively charged species. However, the presence of positively charged groups on the biosorbent surface could not be discarded, and any small retention of these metal ions could be accounted for by sorption at those sites.

Figure 57 Column breakthrough from a 500 μg L^{-1} mixed metal solution using ICP-MS detection

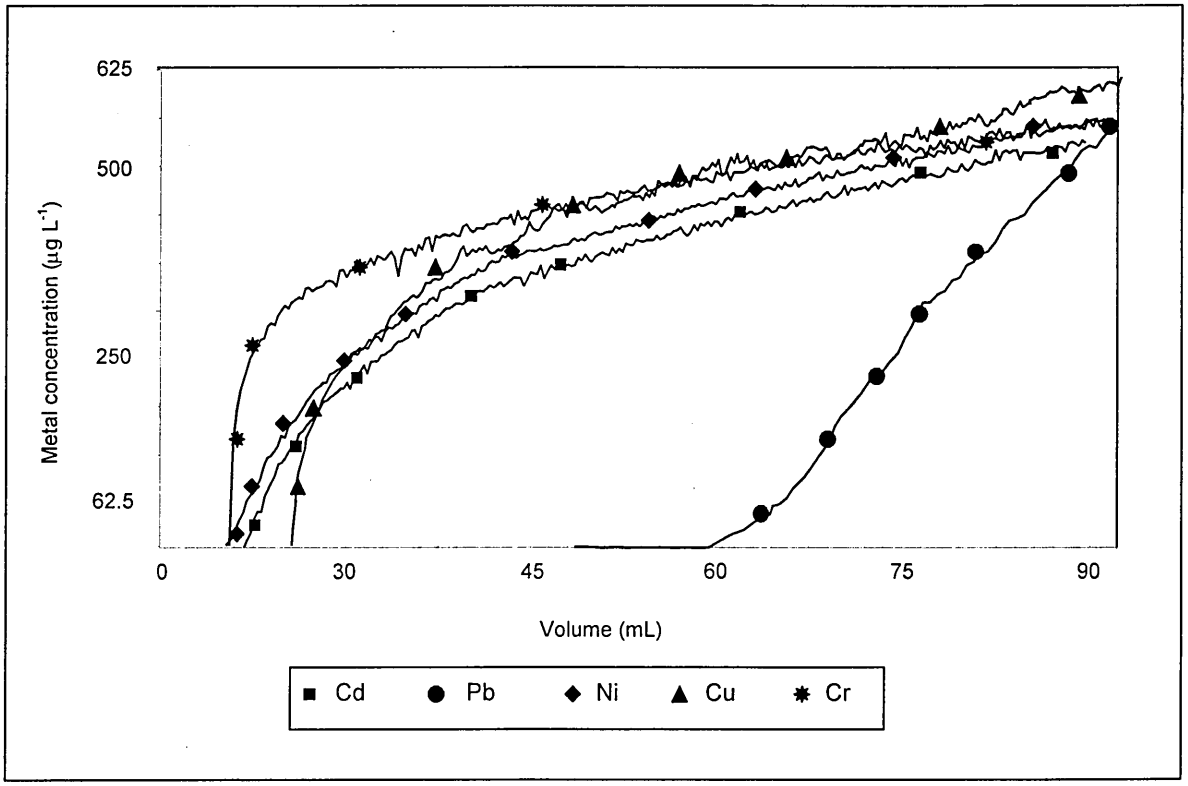

Figure 58 Column breakthrough from a 500 μg L^{-1} mixed solution using ICP-MS detection.

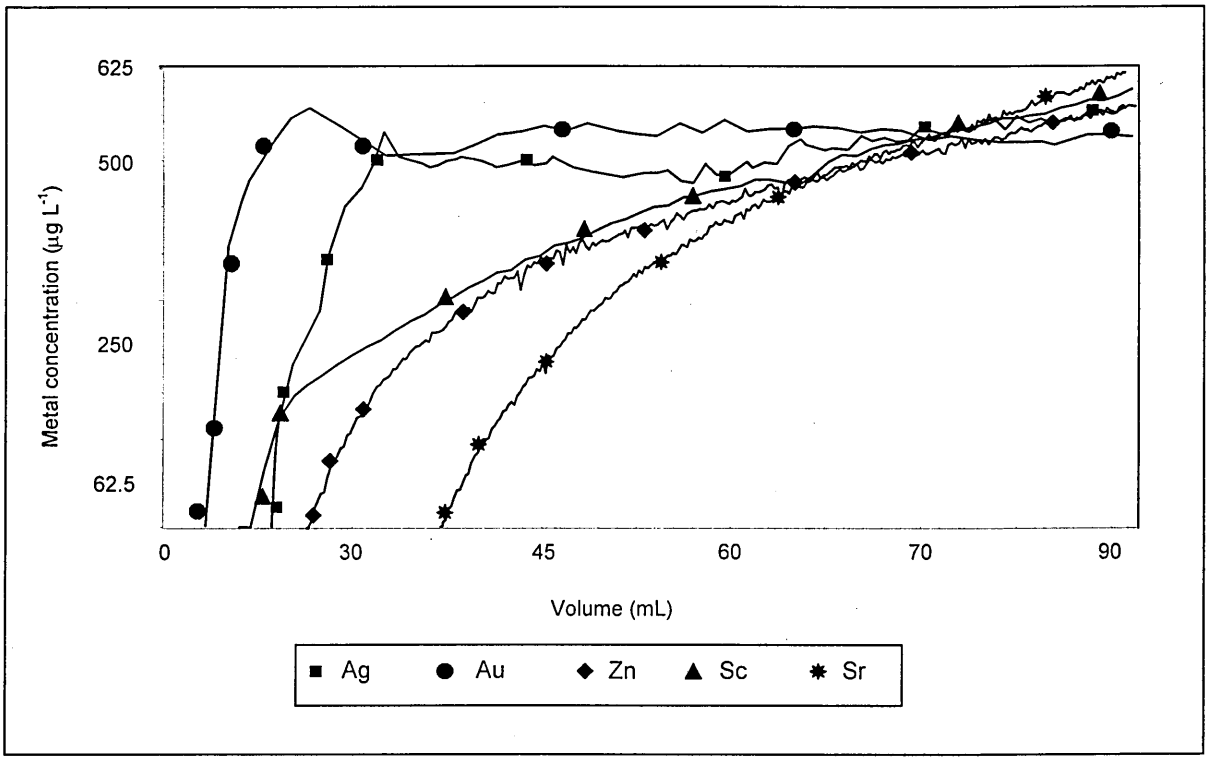

Figure 59 Column breakthrough from a 500 μg L^{-1} mixed solution using ICP-MS detection.

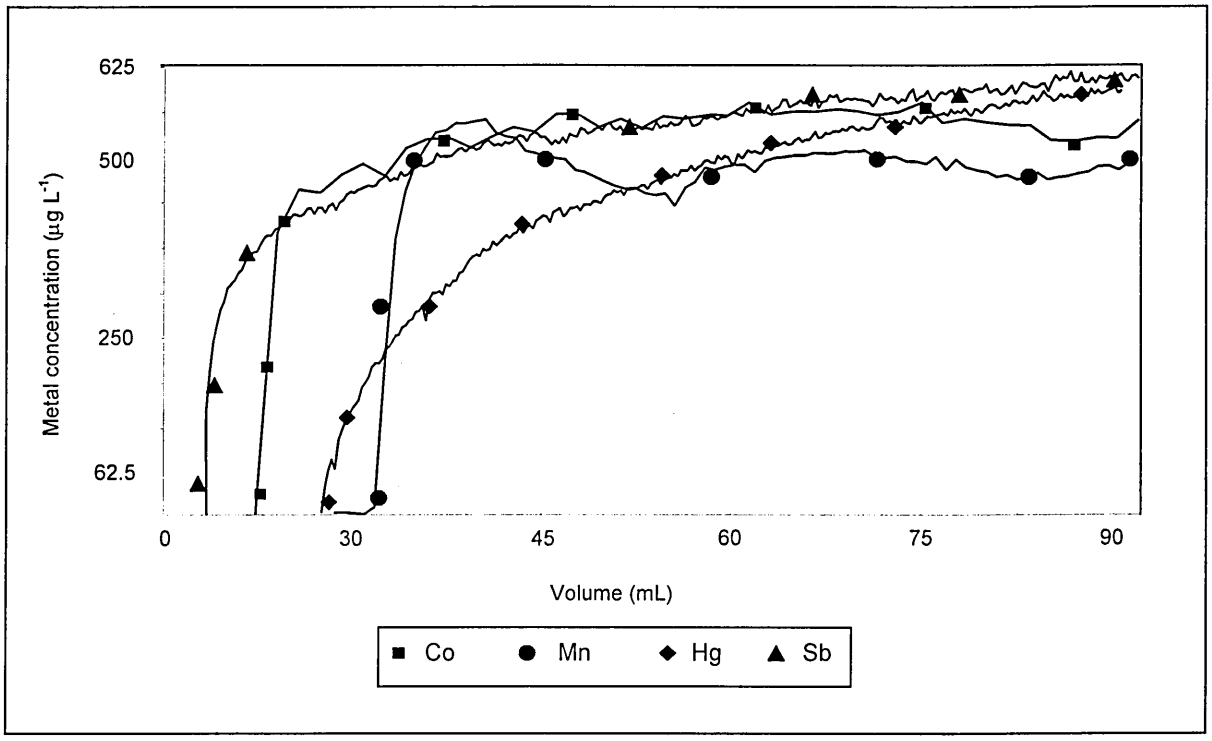

Figure 60 Column breakthrough from a 500 μg L^{-1} mixed solution using ICP-MS detection.

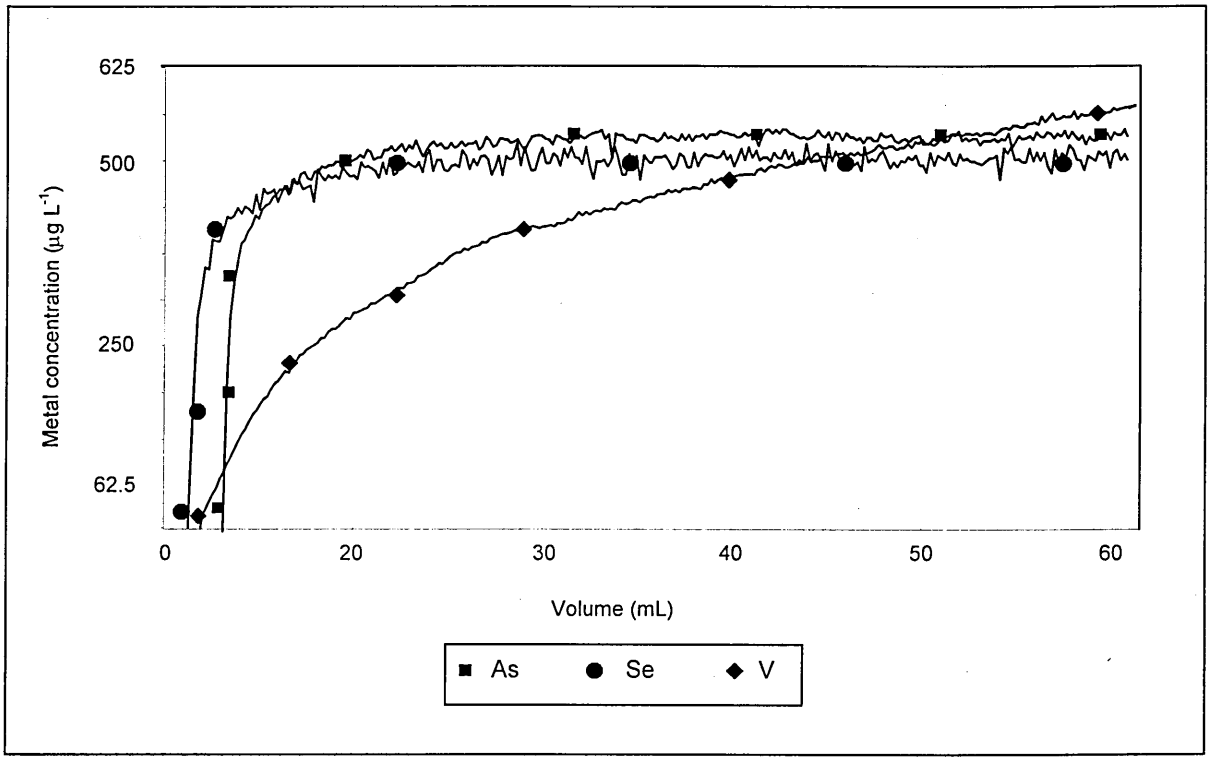

Using the breakthrough curves obtained, capacities at the saturation point were calculated for all the metals studied. The results are shown in Table 14. Comparison of the capacities calculated using the breakthrough to the capacities obtained after acid stripping of the metals in solution using 1.0 M HCl showed no significant differences at the 95% confidence limit.

The capacity values obtained were lower than those calculated using a single metal solution, and in some cases even lower than those obtained from the initial mixed multi element solution. This also indicates the competition between the metals for the available sites.

Table 14 Capacities for the metal sorbed in the column experiment

Metal Ion	Breakthrough capacity $\mu mol\ g^{-1}$	Acid stripping capacity $\mu mol\ g^{-1}$
Cd^{2+}	1.7	1.1
Pb^{2+}	8.4	8.0
Ni^{2+}	3.4	2.7
Cu^{2+}	2.4	1.1
$Cr(OH)^{2+}$	2.2	1.1
Ag^{+}	4.0	5.0
$AuCl_4^-$	0.2	3.7
Zn^{2+}	1.2	1.5
Sc^{3+}	1.0	0.9
Sr^{2+}	2.7	2.6
Co^{2+}	0.9	0.2
Mn^{2+}	6.4	5.3
Hg_2^{2+}	1.4	1.3
SbO_3^-	0.4	0.3
$H_2AsO_4^-$	0.8	0.6
$HSeO_3^-$	0.5	0.4
$H_2VO_4^-$	1.0	0.8

The observed overshoots also indicate that the affinity for certain metals such as Pb or Sr, forces the dealginate to free already sorbed metal ions to enable it to bind preferred metal ions that appear subsequently. This causes interferences in the sorption process of the metal sorbed earlier. The capacity values also reflect the preference of the dealginate for some metals, especially the divalent cations.

Experiments were performed using the same set up for Au, Zn, Sb and Hg single metal solutions. The breakthrough curve shapes were similar, but the breakthrough volumes were slightly higher, since there were no other metals present. However, the capacities obtained for Au and Sb, 0.5 and 0.3, respectively, were very similar to those calculated previously, since the capacity itself relies more on the affinity of the dealginate towards these species. In the case of Zn and Hg, the values obtained were 3.2 and 1.8, respectively. The increased capacity of Zn compared to the multi element solution, indicates that the sorption of Zn by dealginate is affected by the presence of other metals in solution. Kratochvil *et al.* (29) previously described this behaviour with respect to Zn. An overshoot was observed for Zn in a multi-component solution, and the biosorption of Zn was markedly affected by the presence of Cd, Cu and Ca.

4.4. Preconcentration of multi element solution

A diluted multi-element solution, containing the metal ions previously studied was employed to evaluate the ability of the column as a preconcentrator. A 500 mL aliquot of 1.0 ng L^{-1} multi element solution was passed through the column and stripped off using 5 mL of 0.5 M HCl. The experiment was carefully monitored to avoid saturation of the metals in the column.

The results are shown in Table 15. A 100-fold preconcentration factor was achieved with this set up for all the metals and saturation was not observed during the experiment.

Table 15 Preconcentration of 1.0 ngL^{-1} multi element solution

Metal Ion	Concentration $\mu gL^{-1} \pm$ S.D
Cd^{2+}	121.1 ± 0.7
Pb^{2+}	114.6 ± 0.6
Ni^{2+}	116.9 ± 0.7
Cu^{2+}	114.0 ± 1.6
$Cr(OH)^{2+}$	111.2 ± 3.5
Ag^{+}	109.0 ± 1.1
$AuCl_4^-$	127.8 ± 5.1
Zn^{2+}	112.0 ± 2.1
Sc^{3+}	92.0 ± 0.5
Sr^{2+}	101.1 ± 0.3
Co^{2+}	92.9 ± 4.2
Mn^{2+}	112.5 ± 0.6
Hg^{2+}	125.6 ± 0.9
SbO_3^-	90.8 ± 6.5
$H_2AsO_4^-$	117.7 ± 5.6
$HSeO_3^-$	115.9 ± 4.6
$H_2VO_4^-$	112.5 ± 3.8

4.4.1. Analysis of Water Reference Materials

In order to test the suitability of the procedure for the determination of the elements in real samples two Lake Ontario water reference materials (National Water Research Institute, Canada) TMDA 51.2 and TMDA 54.2 and a synthetic seawater were analysed.

The results obtained for the simulated seawater can be found in Table 16. The metal recoveries were between 93 – 96% at pH 6.0 for the Cd, Pb, Cr and Cu, even though the ratio of Ca, Mg, Na and K ions to the other elements were in most cases in excess of 100:1. In this configuration, the major cations Ca, Mg, Na and K in the sample were not retained by the column, and eluted well ahead of the preconcentrated metals.

Table 16 Recoveries of Cd, Pb, Cu and Cr in simulated seawater

Metal	Values found, $\mu g\ L^{-1}$ (n = 3)	Certified values, $\mu g\ L^{-1}$ (n = 3)
Cu	257 ± 51	250 ± 1
Cd	221 ± 13	250 ± 1
Cr	243 ± 6	251 ± 2
Pb	249 ± 17	252 ± 4

For these determinations, the pH of the Lake Ontario water reference materials was adjusted to 5.0 before metal preconcentration of the column. Comparisons of the results obtained with the certified values are given in Table 17. The differences between the two sets of results, except for Cd in TMDA 51.2, are not statistically significant at the 95% confidence limit except for As, Se and V.

The values for As, Se and V found were considerably lower compared to the certified values. The poor retention of these metal ions is mainly due to the metal species in solution. As, Se and V were in solution as negatively charged species and this diminished their affinity towards the biosorbent surface. As a result the retention observed was very low.

The poor retention for negatively charged species forms the basis for the separation of different metal species. Because of the surface of the biosorbent is mainly negatively charged, as shown by the titration results, the repulsion force created between the negatively charged species and the surface of the biosorbent resulted in low values found for these types of metal specie.

Table 17 Results of the determination of metal content in two Lake Ontario Water Reference Material.

Sample	Element determined	Values found, $\mu g\ L^{-1}$ (n = 3) x ± 1 S.D.	Certified values, $\mu g\ L^{-1}$ (n = 3) x ± 1 S.D.
TMDA 51.2	Cd	25 ± 3	72 ± 18.9
	Pb	67 ± 13	72.9 ± 10.6
	Cu	101 ± 6	91 ± 10.2
	Ni	66.7 ± 7.4	62.7 ± 4.6
	Cr	60 ± 8	62.5 ± 6.6
	Zn	106.0 ± 15.0	105.9 ± 1.6
	Co	71.9 ± 6.3	68.0 ±1.1
	Mn	82.0 ± 10.2	80.9 ± 2.1
	As	5.3 ± 3.4	14.5 ± 1.7
	Se	6.0 ± 3.0	12.9 ± 1.9
	V	27.7 ± 7.7	45.8 ± 0.8
TMDA 54.2	Cu	457 ± 65	460 ± 41.9
	Cd	172 ± 33	165 ± 16.1
	Cr	450 ± 34	432 ± 32.1
	Pb	498 ± 66	531 ± 54.4

4.4.2. Speciation Studies

It has already been demonstrated that dealginated seaweed was suitable for carrying out speciation studies, since it is mainly a cation exchanger, it could be used to study the cation and anion species of given metal.

Figure 61 shows that a broad chromium peak identified as Cr (VI) or CrO_4^{2-} is eluted first and on subsequent injection of 500 µL, 1.0 M HCl a much sharper peak corresponding to Cr (III) is observed. The point at which acid is injected could be chosen such that sample throughput is increased. For these experiments the acid was injected at 350 s, but as can be seen in the

chromatogram anytime between 250-350 s could have been chosen. The microcolumn was reused immediately after the elution of Cr (III), in contrast to the system based on using activated alumina where three injections were required to completely strip the adsorbed Cr (VI) species (5). A throughput of about fifty samples per day could be achieved using the system described here.

Figure 61 Chromatogram of 25 μg L^{-1} of a mixed Cr (III) and Cr (VI) standard solution.

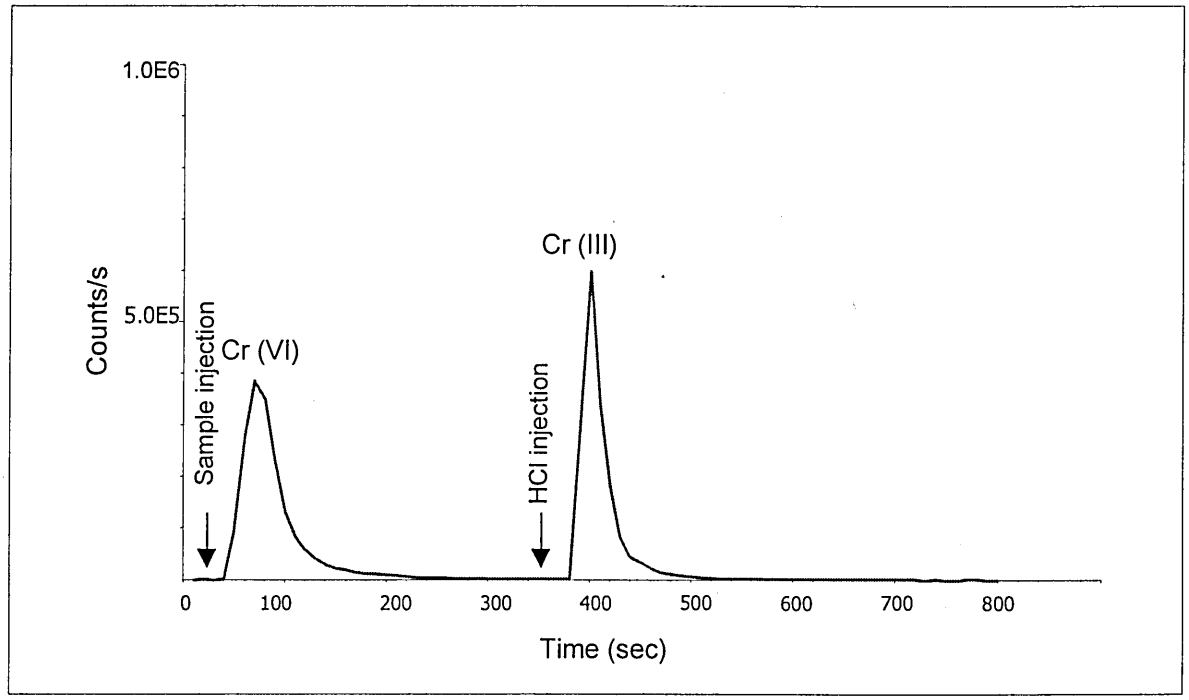

The results of the determination of the two chromium species were 39 ± 0.3 μg L^{-1} and 20 ± 0.2 μg L^{-1} for Cr (VI) and Cr (III) respectively; to give a total chromium value of 59 ± 0.4 μg L^{-1}, compared to a total certified value of 62.5 ± 6.6 μg L^{-1}. Similar analysis of TMDA 54.2 (n = 3) found 299 ± 1 μg L^{-1} and 162 ± 1 μg L^{-1} Cr (VI) and Cr (III), respectively; and a total of 461 ± 0.2 μg L^{-1}, compared to a certified total value of 432 ± 32.1 μg L^{-1}. Detection limits calculated as three times the standard deviation of the background noise levels, were 0.97 μg L^{-1} and 0.28 μg L^{-1} (n = 10) for Cr (VI) and Cr (III), respectively.

In order to demonstrate that chromium speciation was not altered when the sample is in contact with the column material, the Cr (VI) and total Cr levels were determined spectrophotometrically. The complexing agent 1,5 diphenylcarbohydrazide reacts with Cr (VI) to form a coloured complex the absorbance of which is measured at 540 nm. Total Cr is determined after oxidation of Cr (III) to Cr (VI) with nitric acid. Comparison of the results obtained by both methods is presented in Table 18. The precision of the 1, 5 diphenyl carbohydrazide method is rather poor particularly at low concentrations. However, the comparisons of the results show that the differences in the values obtained by both methods are not statistically significant at the 95% confidence limit.

Table 18 Comparison of the chromium speciation results obtained by the proposed and the 1,5 diphenylcarbohydrazide methods

Method		1,5 diphenylcarbohydrazide method Average ± 1 S.D. (n = 3)		Proposed method Average ± 1 S.D. (n = 3)	
Sample	Reference value (µg/L)	Cr (III) (µg/L)	Cr (VI) (µg/L)	Cr (III) (µg/L)	Cr (VI) (µg/L)
TMDA 51.2	62.5 ± 6.6	12 ± 5	54 ± 31	20 ± 0.2	39 ± 0.3
TMDA 54.2	432 ± 32.1	132 ± 12	313 ± 16	162 ± 1	299 ± 1

It has been reported in the literature that Cr (VI) may be reduced by biosorbents, including oat biomass and immobilised *Saccharomyces cerevisiae* (19, 3). The researchers claim that the Cr (VI) biosorption is via reduction to Cr (III) with subsequent sorption of Cr^{3+} ions, since carboxylates are proposed as major binding sites. However, the separation observed in this work is based on the fact that Cr (VI) species, CrO_4^{2-} was not retained by dealginate due to its negative charge. This result could invalidate the biosorption observed for other anions, such as $H_2AsO_4^-$, $H_2SeO_3^-$, $H_2VO_4^-$, but the possibility of the presence of positively charged sites, which

would be able to bind anions with a single negative charge, instead of larger anions such as chromates is still strong.

4.5. Summary

In summary, these results have shown the ability of dealginated seaweed to bind several metal ions in a column set up under continuous flow conditions. The selectivity towards specific metal ions, which enables its use of the column for speciation and metal preconcentration from solution, was demonstrated. One of the main advantages compared to ion exchange resins is that dealginated seaweed is less subject to interference from alkaline-earth metals. The ability of the biosorbent to preconcentrate metals was comparable with those of other types of plant-derived materials, immobilised algae and bacteria (8, 24, 115). In these cases, preconcentration of Cd (II), Pb (II), Cu (II), Be (II), Se (IV), Hg (I), Al (III) and Au (III) was achieved with enhancement factors between 5 and 1000, similar to those obtained with dealginate (2 and 100). However, the fact that there is no need to immobilise the dealginate makes it more suitable for use in a column system, compare with other biosorbents such as algal and bacterial cells (8, 115). It is also important to highlight the excellent durability of the biosorbent over a long period. The proposed method is simple, sensitive and accurate, making it suitable for further application in effluent treatment and sample preparation for atomic spectrometric methods.

Identification of Functional Groups on Dealginated Seaweed by Fourier Transform Infrared (FT-IR) Spectroscopy

Chapter 5

5.1. Fourier Transform Infrared Spectroscopy

To better understand the nature of the functional groups responsible for metal binding, FT-IR spectra of preparations of untreated dealginate, metal bound and esterified samples were obtained.

The FT-IR spectra of the dried HCl washed, alginic acid and Ca-containing dealginate are shown in Figures 62 and 63. The band assignments are shown in Table 19. In the fingerprint region (below 2000 cm^{-1}) bands at 1605, 1205, 1159, 1112, 1055, 1030 and 868 cm^{-1} overlap in all the samples. The band at 1413 is not present in the alginic acid spectra, and is very strong and sharp in the Ca-bound spectra compared with HCl washed dealginate. The band at 1314 cm^{-1} is similar in the HCl and Ca spectra. The strong band at 1716 cm^{-1} observed in the alginic acid spectra assigned to carbonyl may be compared to the band at 1605 cm^{-1}observed for HCl and Ca dealginate, possibly shifted towards lower wave number as an effect of metal interaction with the biosorbent.

The spectrum of the HCl washed dealginate shows similar characteristics to that of mannuronic acid rich calcium alginate as reported by Dupuy *et al.* (155) (see bracketed figures in Table 19). The wave number difference between the two bands assigned to the asymmetric and symmetric vibrations of the carboxyl group in both calcium alginate and dealginate are similar, 189 cm^{-1} and 186 cm^{-1}, respectively. Although the dealginate sample has been acid washed to remove metals bound to the material there is no evidence of the presence of nonionised carboxyl groups as seen at 1716 cm^{-1} in the alginic acid spectrum (Figure 62).

Evidence from the FT-IR spectrum of dealginate suggests that functional groups contributing to the dealginate spectrum may be similar to those in calcium alginate. Mannuronic and guluronic acid units make up alginate and the dealginate spectrum is similar to that for the

mannuronic acid rich calcium alginate. According to Kohn (156), the affinity of the monomers of the two acids for calcium is identical suggesting that the nature of the calcium interactions with both is similar. This is possible because all polyuronates have to some extent similar primary structures. The results observed are also in agreement with the functional groups described by Sartori *et al.* (157) for sodium and calcium alginates.

Table 19 Assignments of infrared absorption bands for hydrochloric acid washed dealginate, alginic acid and calcium dealginate. Figures in brackets are those of mannuronic acid rich calcium alginate

Wavenumber (cm^{-1})	Intensity-shape	Assignment
3500-3000	strong-broad	O-H stretching C-H stretching
2892 (2904)	medium-shoulder	C-H stretching O-H stretching
1716	strong-sharp	C=O
1605 (1609)	medium-shoulder	COO^- stretching (asymmetric)
1413 (1420)	strong-shoulder	COO^- stretching (symmetric)
1314 (1328)	strong-shoulder	C-O stretching
1205 (1200)	medium-shoulder	C-C stretching
1159 (1155)	medium-sharp	C-C stretching C-O stretching C-C-C bending
1112 (1115)	strong-shoulder	C-C stretching C-O stretching
1055 (1047)	v strong-shoulder	O-H bending
1030 (1027)	strong-sharp	C-C
868 (882)	strong-sharp	C-C-O C-O-C
821 (811)	medium-sharp	C-O

Figure 62 FT-IR spectra of (i) alginic acid and (ii) HCl washed dealginate

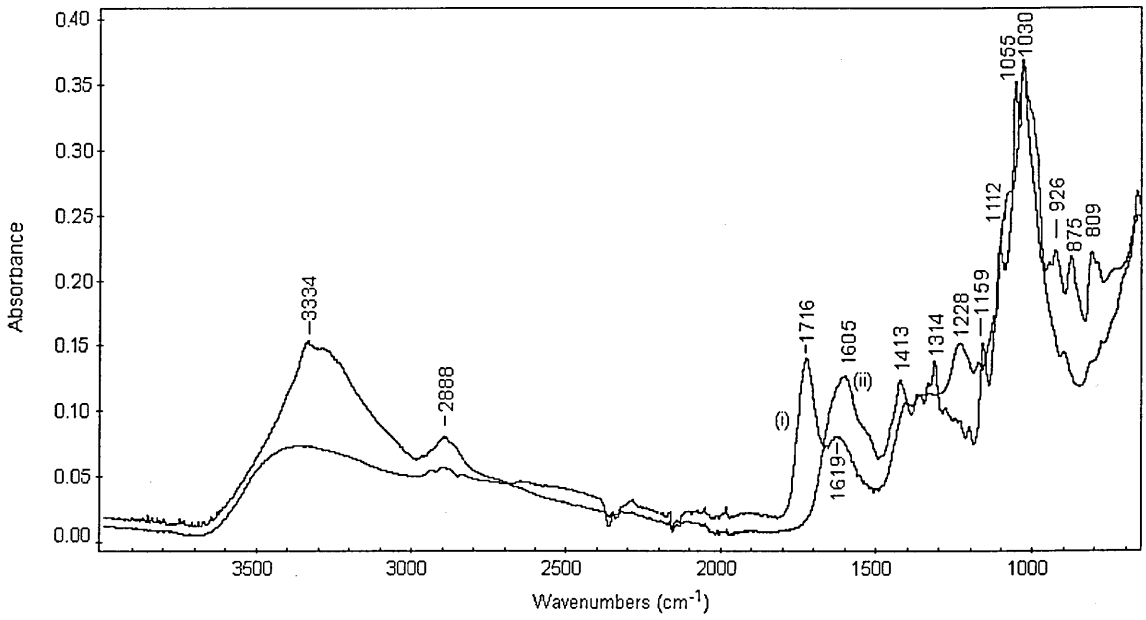

Figure 63 FT-IR spectra of (i) Ca bound dealginate and (ii) HCl washed dealginate

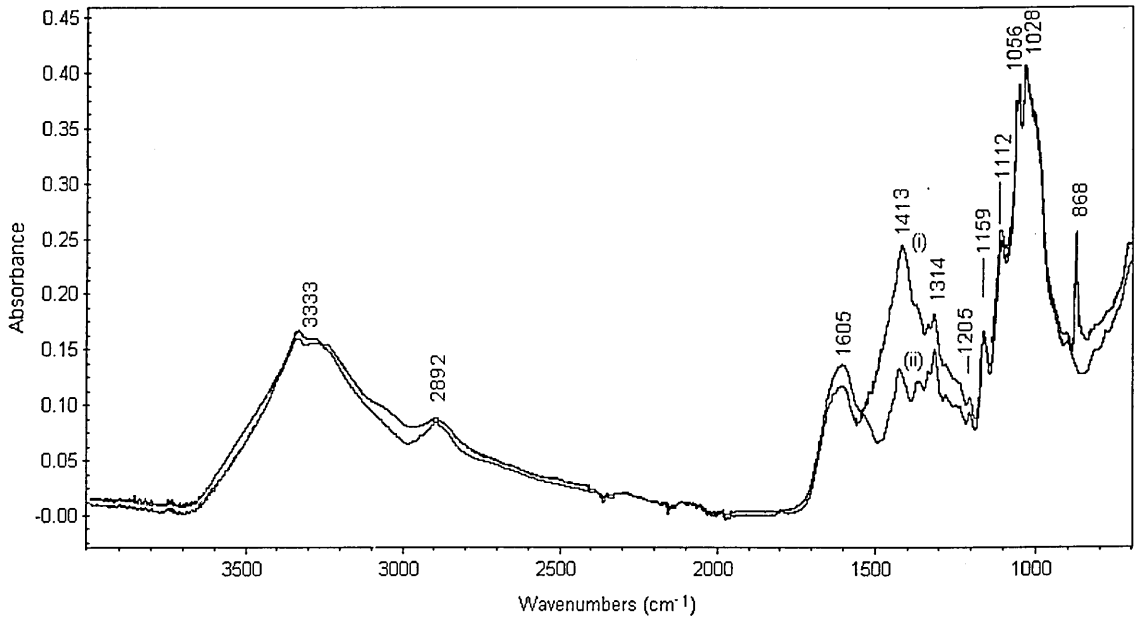

Tables 20 shows a summary of the infrared common bands observed for cadmium acetate, Cd-, Pb-, Ni-, Cu-, Cr- and Ag-dealginate samples at pH 2 and 6, as well as Al- and Au-dealginate samples prepared at pH 4 and 3, respectively. Table 21 shows a summary of the infrared common bands observed for esterified dealginate and metal-esterified samples. Differences in the intensity, shape and presence of other bands are discussed individually in the following sections.

Table 20 Assignments of infrared absorption bands for metal-bound dealginate and cadmium acetate

Wavenumber (cm^{-1})	Intensity-shape	Assignment	Observed
3500-3000	strong-broad	O-H stretching C-H stretching	All metal-dealginate samples $Cd(CO_2CH_3)_2$
2904-2885	medium-shoulder	C-H stretching O-H stretching	All metal-dealginate samples
1605-1600	medium-shoulder	COO^- stretching (asymmetric)	All metal-dealginate samples at pH 6 and Ag pH 2
1424-1413	strong-shoulder	COO^- stretching (symmetric)	All metal-dealginate samples except Pb and Cu pH 2
1315- 1310	medium-shoulder	C-O stretching	All metal-dealginate samples
1160-1154	medium-sharp	C-C stretching C-O stretching C-C-C bending	All metal-dealginate samples
1106-1115	strong-shoulder	C-C stretching C-O stretching	All samples except Pb, Cu pH 6 and Cr pH 2
1055-1053	v strong-shoulder	O-H bending	All metal-dealginate samples
1030-1028	strong-sharp	C-C	All metal-dealginate samples
893	strong-shoulder	C-C-O C-O-C	Cd, Pb, Ni, Cr and Ag pH 6, Ag pH 2, Al and Au

Table 21 Assignments of infrared absorption bands for esterified and metal-bound esterified dealginated seaweed

Wavenumber (cm^{-1})	Intensity-shape	Assignment	Observed
3500-3000	strong-broad	O-H stretching C-H stretching	All samples except Cr
2904-2885	medium-shoulder	C-H stretching O-H stretching	All samples
1604-1595	medium-shoulder	COO^- stretching (asymmetric)	All samples
1417-1414	strong-shoulder	COO^- stretching (symmetric)	All samples
1310- 1303	strong-shoulder	C-O stretching	All samples
1160	medium-sharp	C-C stretching C-O stretching C-C-C bending	All samples except Pb and Au
1106-1115	strong-shoulder	C-C stretching C-O stretching	All samples except Pb, Cu pH 6 and Cr pH 2
1054	v strong-shoulder	O-H bending	All samples
1030-1028	strong-sharp	C-C	All samples
871	strong-sharp	C-C-O C-O-C	All samples except Cd

5.1.1. Cadmium

The spectra of Cd-dealginate samples prepared at pH 6 and 2 are shown in Figures 64 and 65. The assignments for the observed bands have been made in Table 20. Both spectra showed similar characteristics to those HCl washed dealginate and most of the bands observed overlap in the three samples. The increased intensity of the bands at 1413 and 1314 cm^{-1} in the Cd-bound pH 6 spectra indicates the interaction of the metal with the carboxylate groups. The intensity of the Cd-dealginate pH 2 spectra was weaker, suggesting less Cd bound

to dealginate. The band at 1600 cm^{-1} was shifted towards higher wave numbers and could be attributed to a C=O stretching vibration, which has been associated with complexation of the carbonyl group by dative coordination (82).

Figure 66 shows the spectra of Cd-dealginate at pH 6 and cadmium acetate. The shape of the spectra were similar in the majority of the bands observed, with the bands shifted towards lower wave numbers on the Cd-dealginate sample. This result indicates that the binding of Cd to dealginate is through carboxylate groups forming acetate type complexes.

Comparison of the spectra obtained from esterified dealginate with and without cadmium addition show prominent new bands at 3244, 3059, 1303 and 828 cm^{-1} respectively in the former. The intensity of the band at 1303 cm^{-1} in the cadmium-containing nonesterified and esterified dealginate samples respectively, point to the presence of another cadmium binding site in addition to the carboxyl groups (see Figure 66).

In a review of ion binding on polyuronates, Kohn (156) proposed that divalent cations were bound by ionic exchange through binding to carboxyl groups. The FT-IR results show that cadmium binds to the carboxyl groups. This is confirmed by the disappearance of the strong band and the appearance of a shoulder at 1414 cm^{-1}, when the cadmium esterified sample was examined (Figure 67). Similar results were described for *D. innoxia* samples treated with acidic methanol (61).

Figure 64 FT-IR spectra of (i) Cd bound at pH 6 dealginate and (ii) HCl washed dealginate

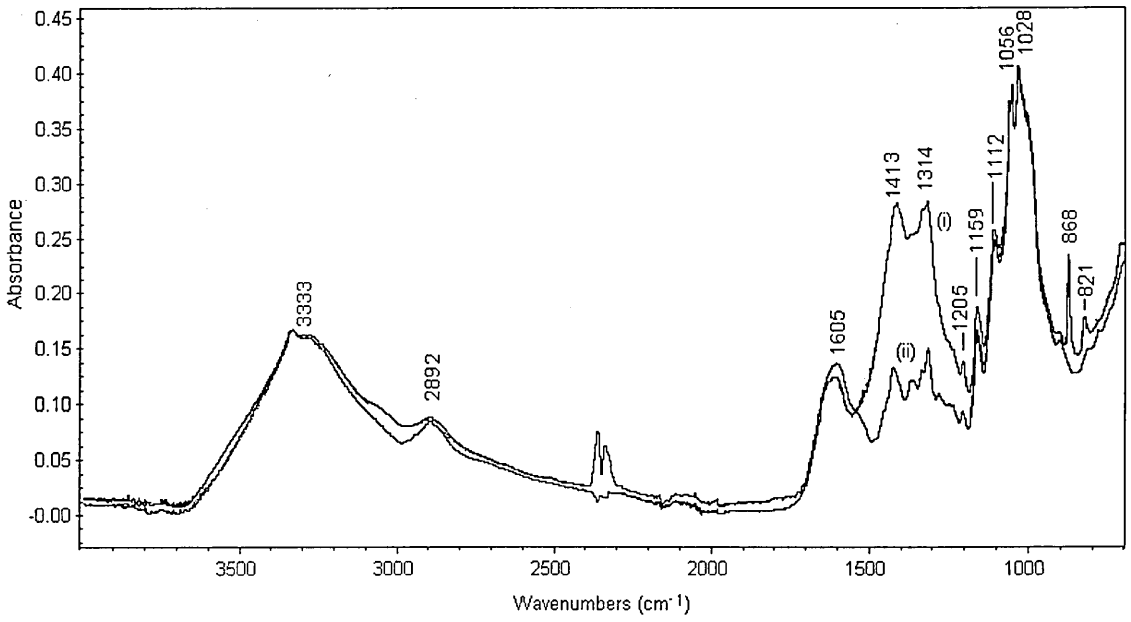

Figure 65 FT-IR spectra of (i) Cd bound dealginate at pH 2 (ii) HCl washed dealginate

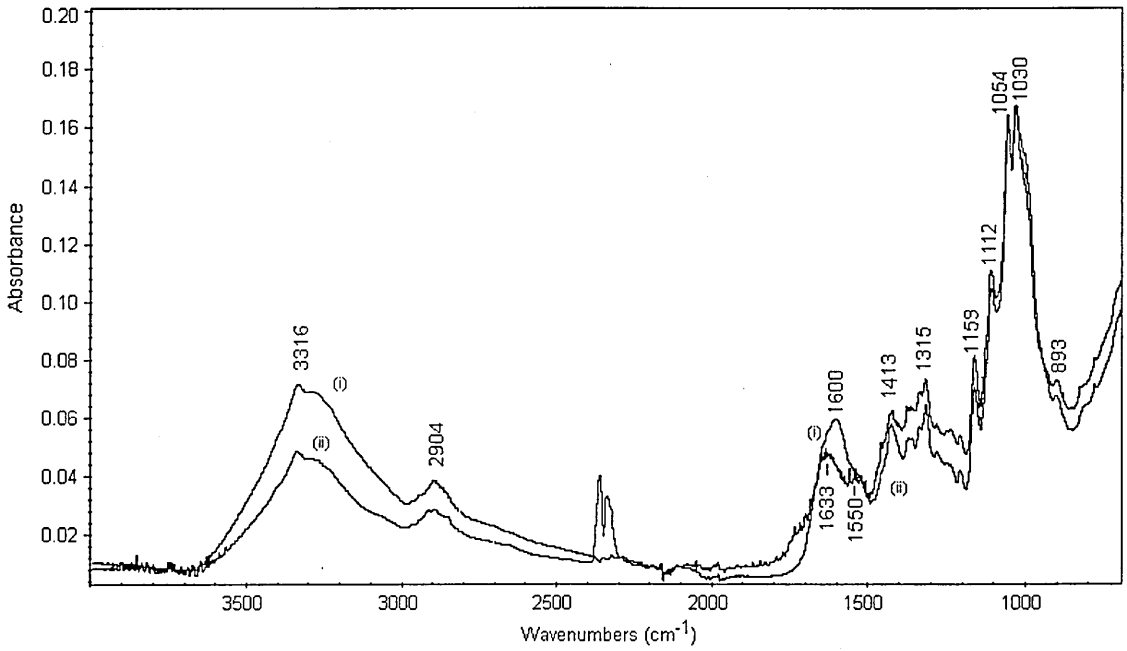

Figure 66 FT-IR spectra of (i) Cd-bound dealginate and (ii) Cadmium acetate

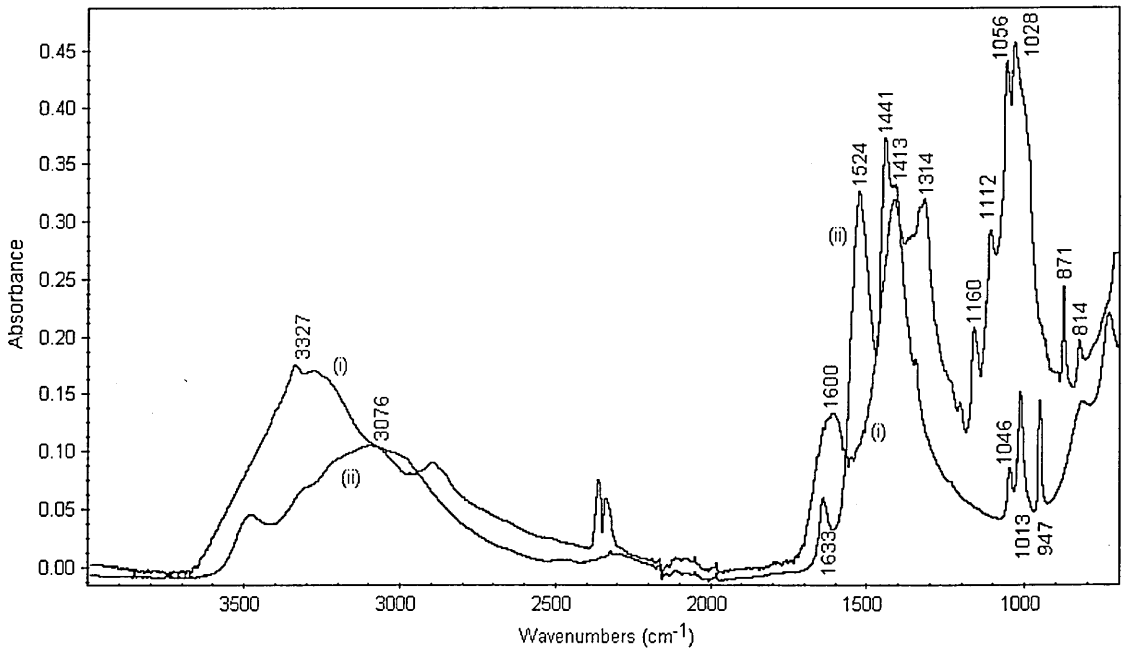

Figure 67 FT-IR spectra of (i) Cd-bound esterified dealginate and (ii) esterified dealginate

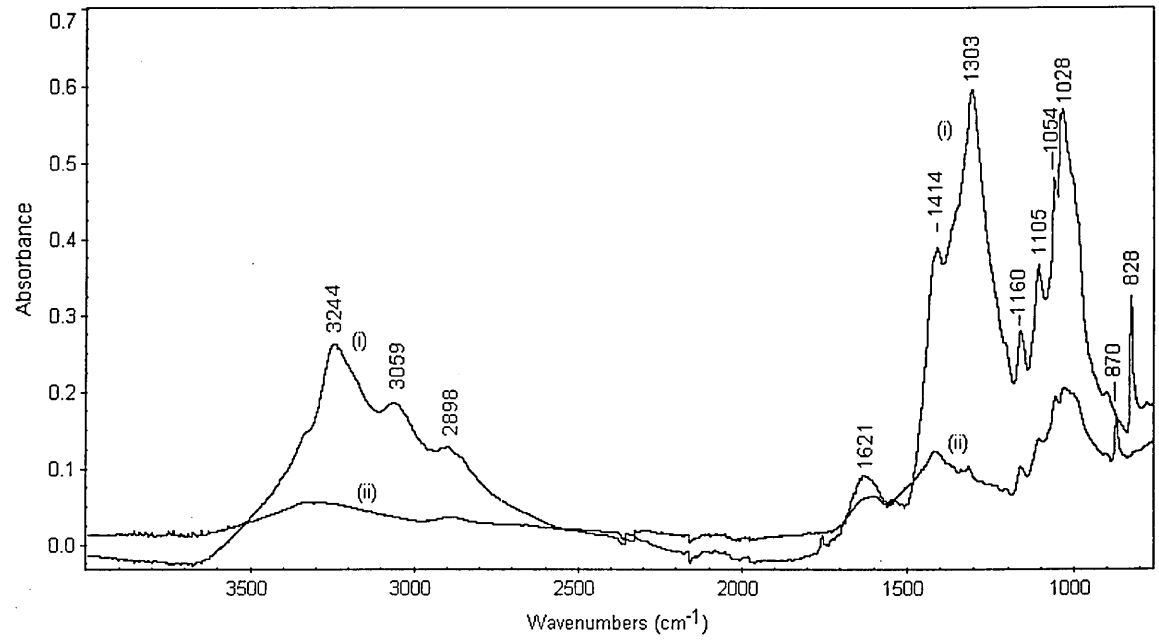

5.1.2. Lead

The spectra of Pb-dealginate showed significant differences when compared with HCl washed dealginate (Figure 68). The bands at 1417 and 1312 cm^{-1} became one very intense band at 1352 cm^{-1}, because of the interaction of Pb with carboxylate groups. Similarly, the bands at 1054 and 1030 cm^{-1} disappeared to form a single less intense band at 1023 cm^{-1}. The doublet has been attributed to the C-O stretching vibrations of alcoholic groups in carbohydrate component of the cell walls of green algae (109). Therefore, this could be attributed to the interaction of Pb with carboxylate groups.

There were no marked differences between the spectra for Pb-dealginate pH 2 and HCl washed dealginate (Figure 69). The band at 1602 cm^{-1} was slightly shifted towards higher wave numbers, and the intensity was weaker. This could be the result of no Pb being bound to the biosorbent at pH 2. The Pb-esterified spectra was identical to the esterified dealginate spectra, indicating very low amounts of Pb sorbed on dealginate due to the blocked carboxylate groups (Figure 70).

5.1.3. Nickel

The spectra for Ni-dealginate pH 6 showed differences mainly in the region between 1650 and 1150 cm^{-1} when compared with HCl washed dealginate spectra,. A broadening of the band at 1600 cm^{-1}, as well as the increase of the intensity of the bands at 1424 and 1315 cm^{-1} indicates the effect of the Ni bound to dealginate (Figure 71).

The Ni-dealginate spectra at pH 2 (Figure 72) showed the presence of unique bands at 1728, 1638 and 1533 cm^{-1}, resulting from the splitting of the band at 1600 cm^{-1}. This might be due to the effect of Ni bound to carboxylate groups on the biosorbent surface.

Figure 68 FT-IR spectra of (i) Pb bound dealginate and (ii) HCl washed dealginate

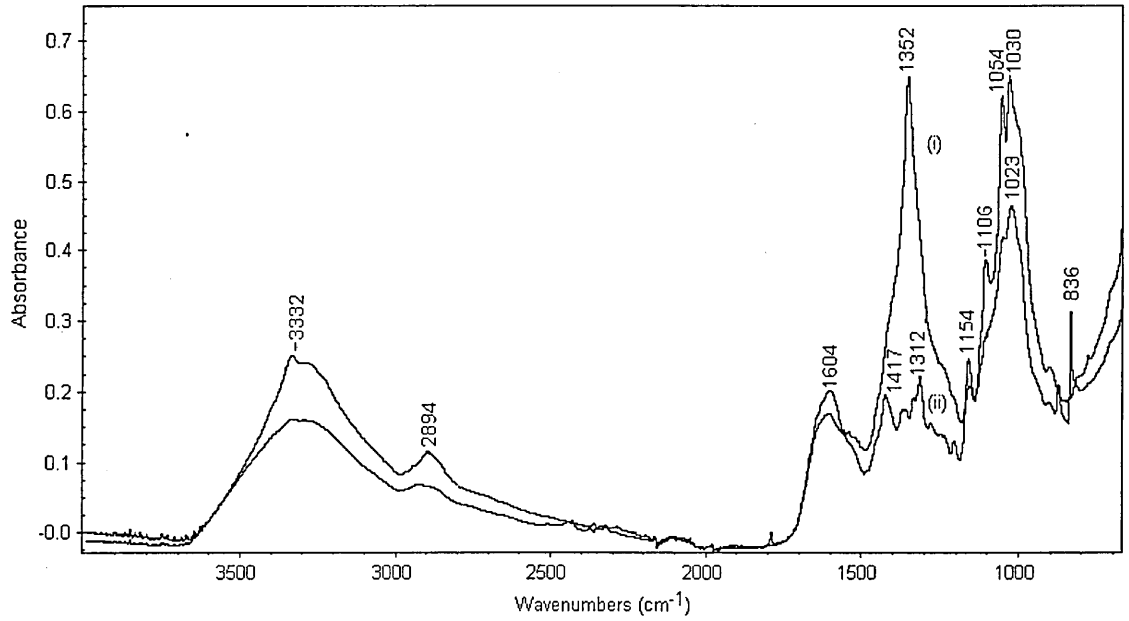

Figure 69 FT-IR spectra of (i) Pb bound dealginate at pH 2 (ii) HCl washed dealginate

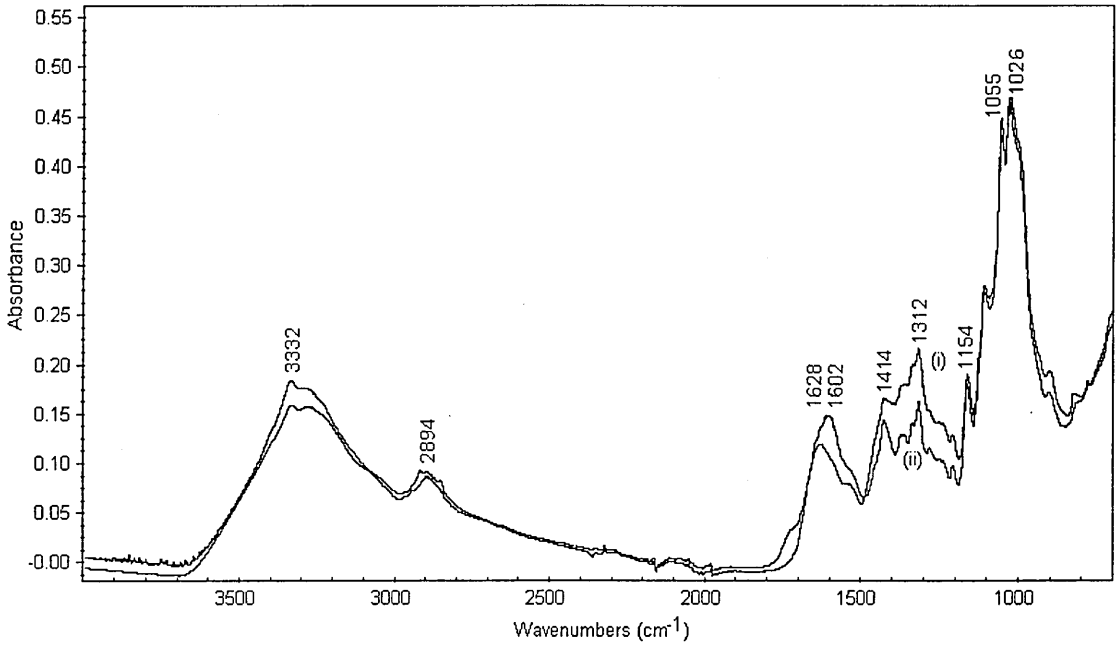

The spectrum of the green algae *Cyclotella cryptica* and *Chlamydomonas reinhardtii* showed similar bands at 1623 and 1548 cm-1, which were attributed to C=O stretching, C-N stretching and N-H deformation (84, 109), probably revealing new binding sites for Ni on dealginate. Although the optimum sorption pH was demonstrated to be 6, the result observed for Ni-dealginate pH 2 sample suggests Ni sorption at pH 2. The increased intensity of the band located at 1315 cm-1 could indicate the presence of another binding site for Ni. A weak band was observed in Ni spectra at817cm^{-1} that could be a result of the presence of metal on the sample.

No differences were observed between the spectra for the Ni-esterified and esterified dealginate, nearly all the bands observed overlap in the two samples (see Table 21). This result suggests very low sorption of Ni when the carboxylate groups are blocked on the biosorbent surface.

Figure 70 FT-IR spectra of (i) Pb-bound esterified dealginate and (ii) esterified dealginate

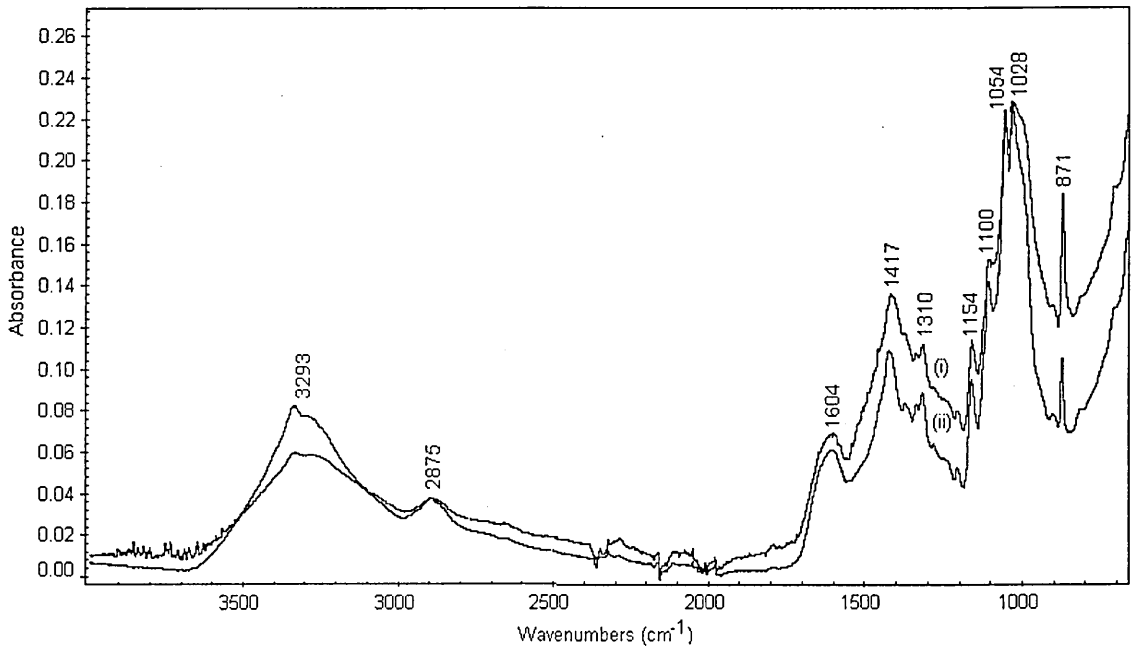

Figure 71 FT-IR spectra of (i) Ni bound at pH 6 dealginate and (ii) HCl washed dealginate

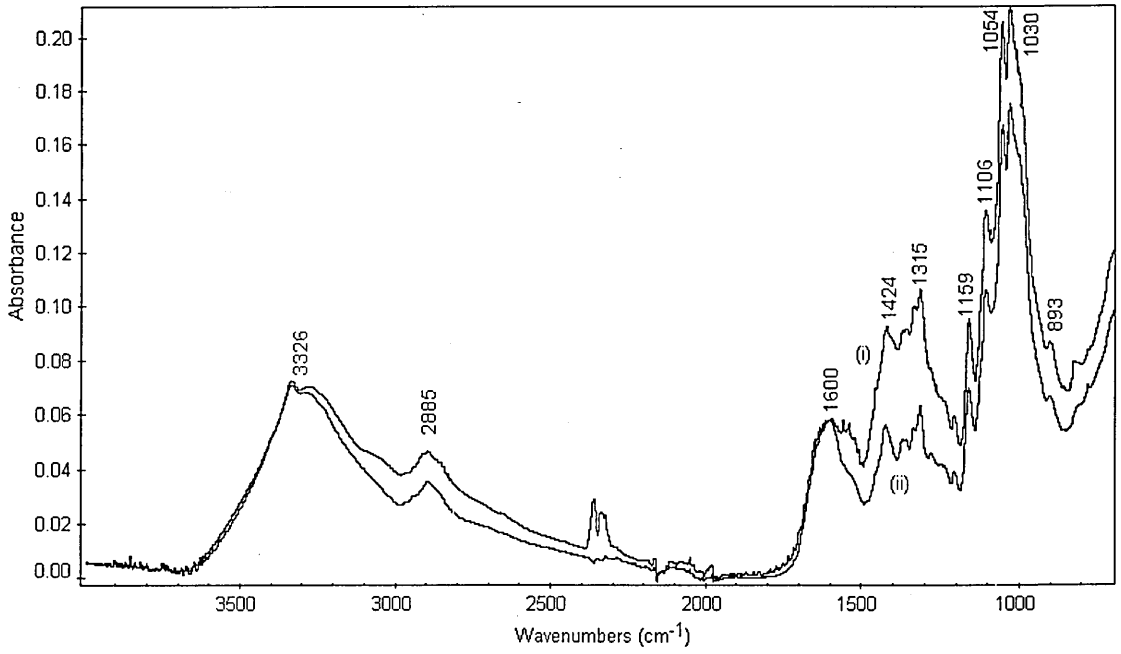

Figure 72 FT-IR spectra of (i) Ni bound at pH 2 dealginate and (ii) HCl washed dealginate

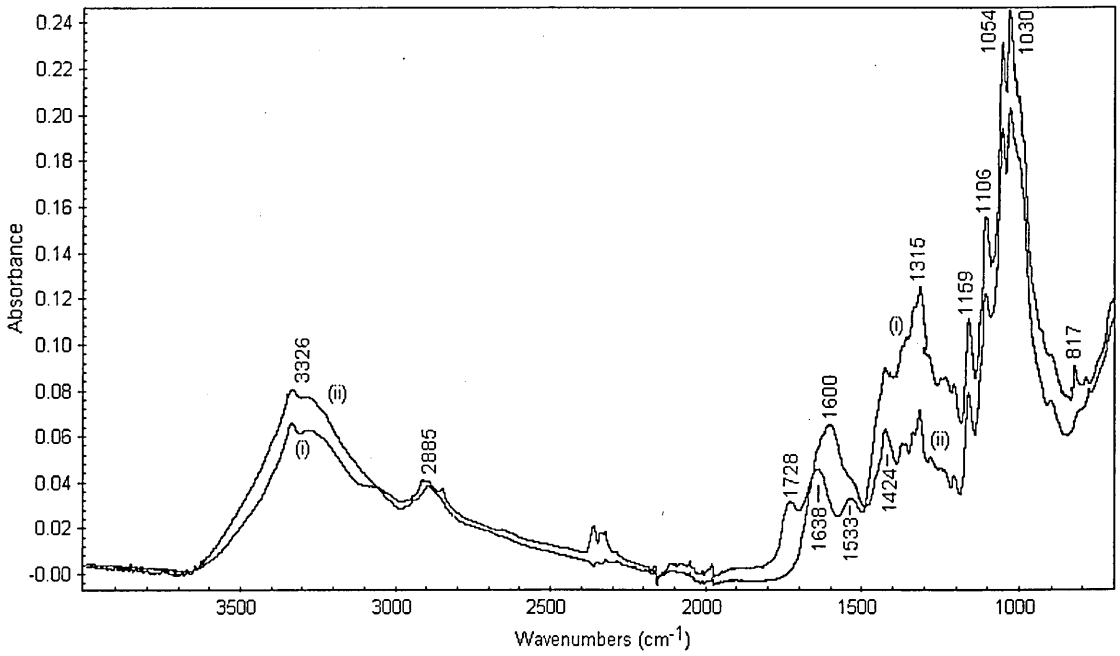

Figure 73 FT-IR spectra of (i) Ni-bound esterified dealginate and (ii) esterified dealginate

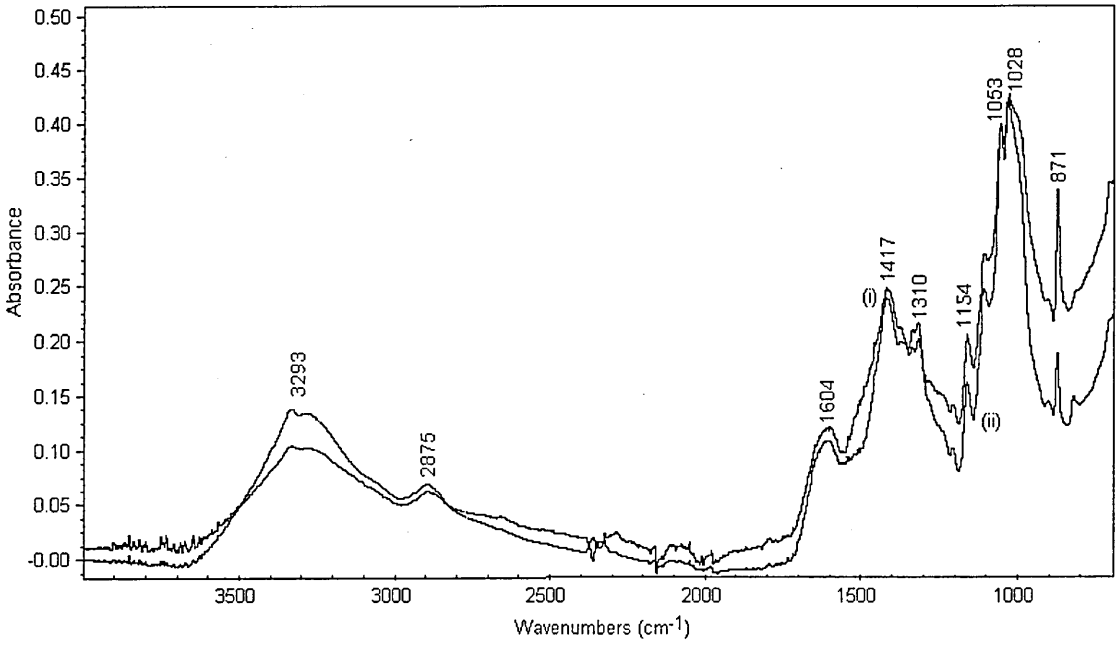

5.1.4. Copper

The FT-IR spectra of Cu-dealginate sample at pH 6 (see Figure 74) showed similar bands as the HCl washed dealginate spectra, described in Table 20. The differences were observed mainly in two bands. The band at 1602 cm^{-1} appeared slightly shifted to 1629 cm^{-1}, showing lower intensity and the presence of a small shoulder around 1530 cm^{-1}. The intensity of the band at 1315 cm^{-1} was increased, and the band at 1417 cm^{-1} virtually disappeared. These changes could be attributed to the effect of Cu bound to carboxylate groups on the biosorbent. These results were observed previously for the sorption of Cu on Sphagnum peat moss and *Datura innoxia* biomass (61, 78)

The spectra of Cu-dealginate at pH 2 showed similar changes, but the intensity of the bands was lower compared with the pH 6 sample. Although the bands were weaker, some Cu

sorption was observed at pH 2. The Cu-esterified spectrum was very similar to the esterified spectra, showing little sorption of Cu (see Figures 75 and 76).

Figure 74 FT-IR spectra of (i) Cu bound at pH 6 dealginate and (ii) HCl washed dealginate

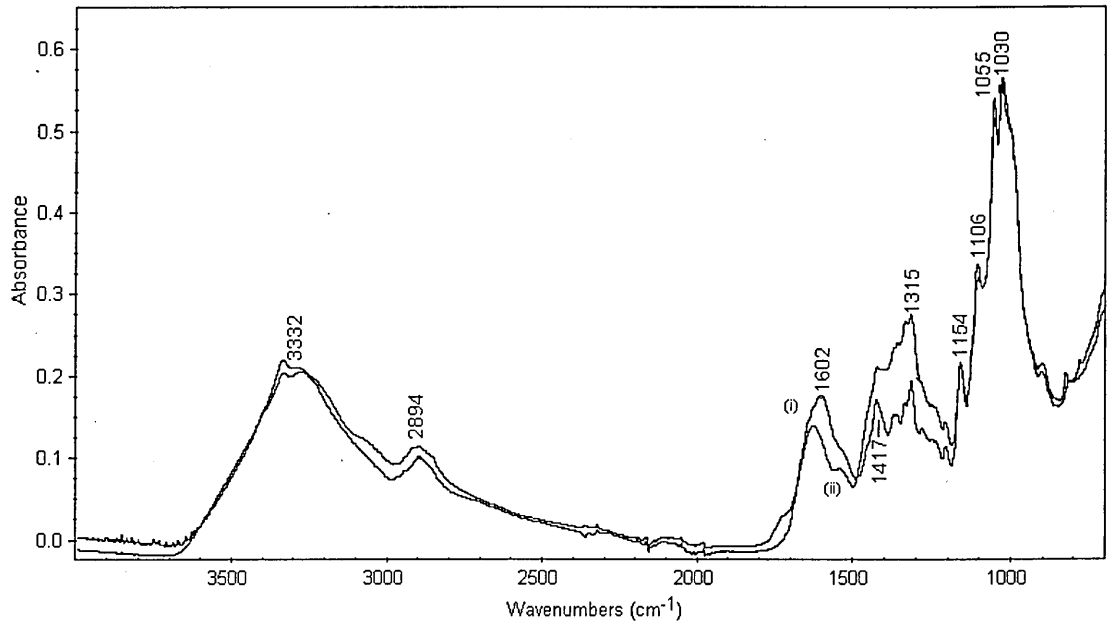

Figure 75 FT-IR spectra of (i) Cu bound at pH 2 dealginate and (ii) HCl washed dealginate

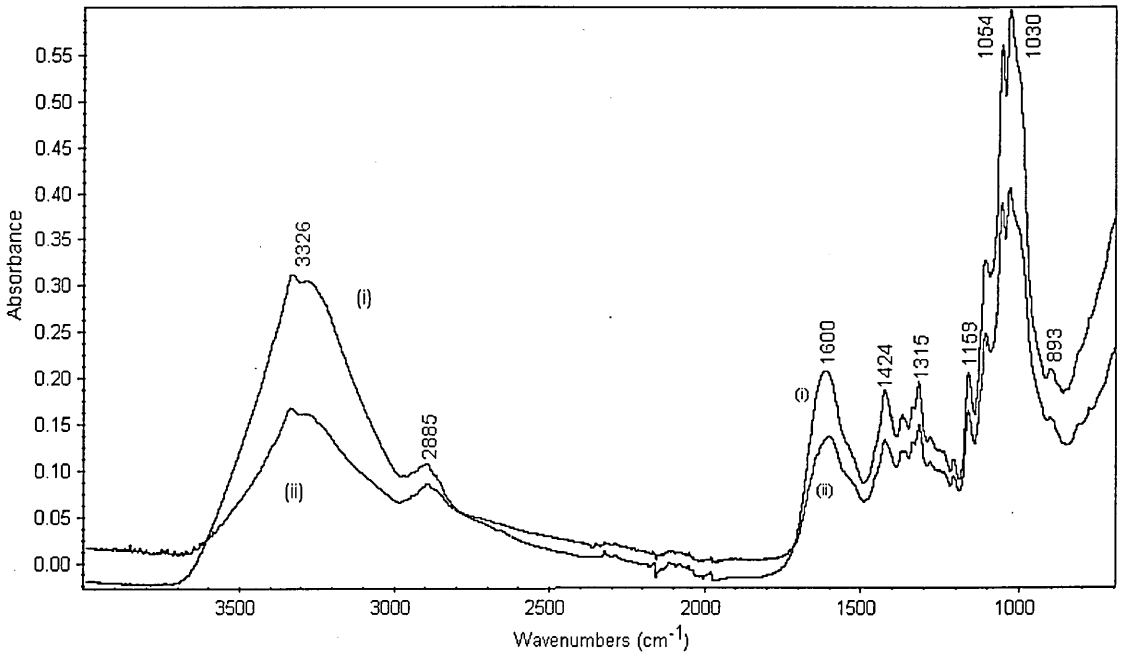

Figure 76 FT-IR spectra of (i) Cu bound esterified dealginate and (ii) esterified dealginate

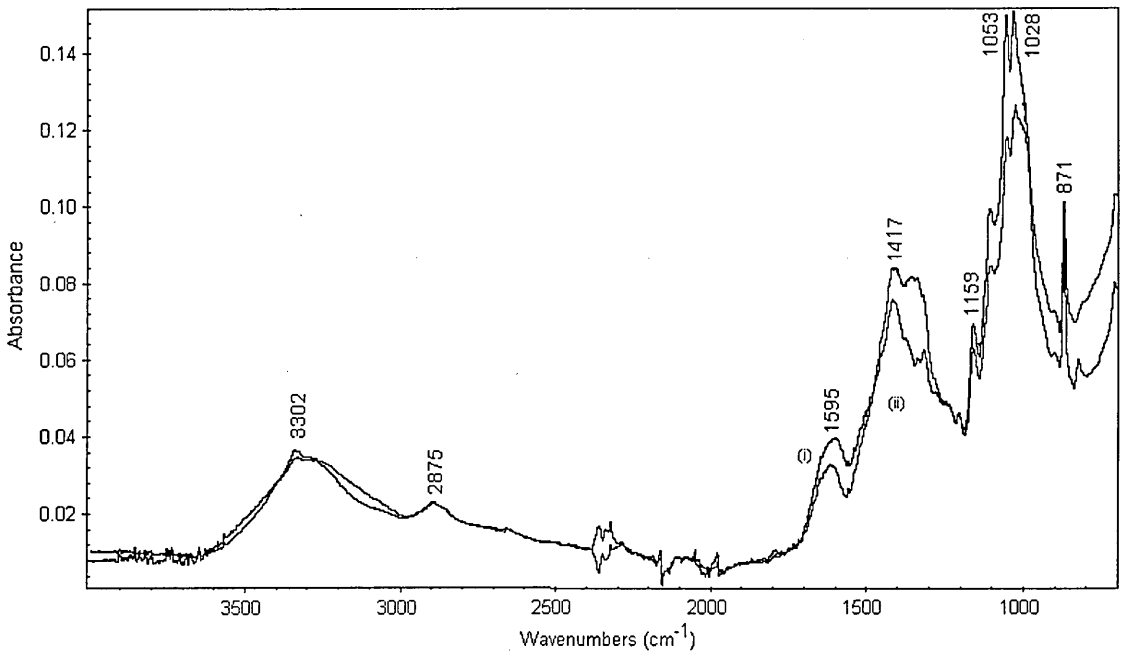

5.1.5. Chromium

Figure 77 shows the spectra of Cr-dealginate at pH 6. Marked differences were observed in the fingerprint region when compared with the HCl washed dealginate spectra. The band at 1600 cm^{-1} was split, resulting in two more intense bands at 1628 and 1519 cm^{-1}. The intensity of the band at 1310 cm^{-1} increased. The band at 1424 cm^{-1} and the shoulder located at 1106 cm^{-1}disappeared due to the interaction of Cr with the biosorbent. The changes on the carboxylate region of the spectra indicate that the binding of Cr is through these types of group.

There were little changes in the spectra of Cr-dealginate at pH 2 indicating low metal sorption by the biosorbent. The very low intensity of the spectra of Cr-esterified suggests no sorption of Cr by the esterified biosorbent (Figure 78).

Figure 77 FT-IR spectra of (i) Cr bound at pH 6 dealginate and (ii) HCl washed dealginate

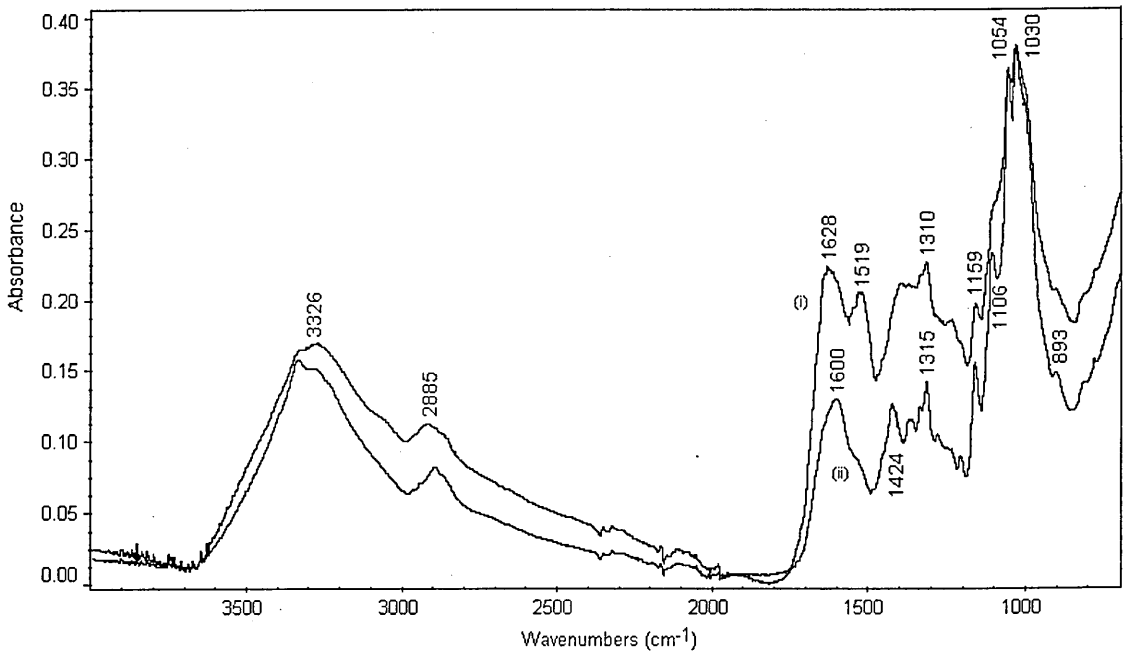

Figure 78 FT-IR spectra of (i) Cr bound at pH 2 dealginate and (ii) HCl washed dealginate

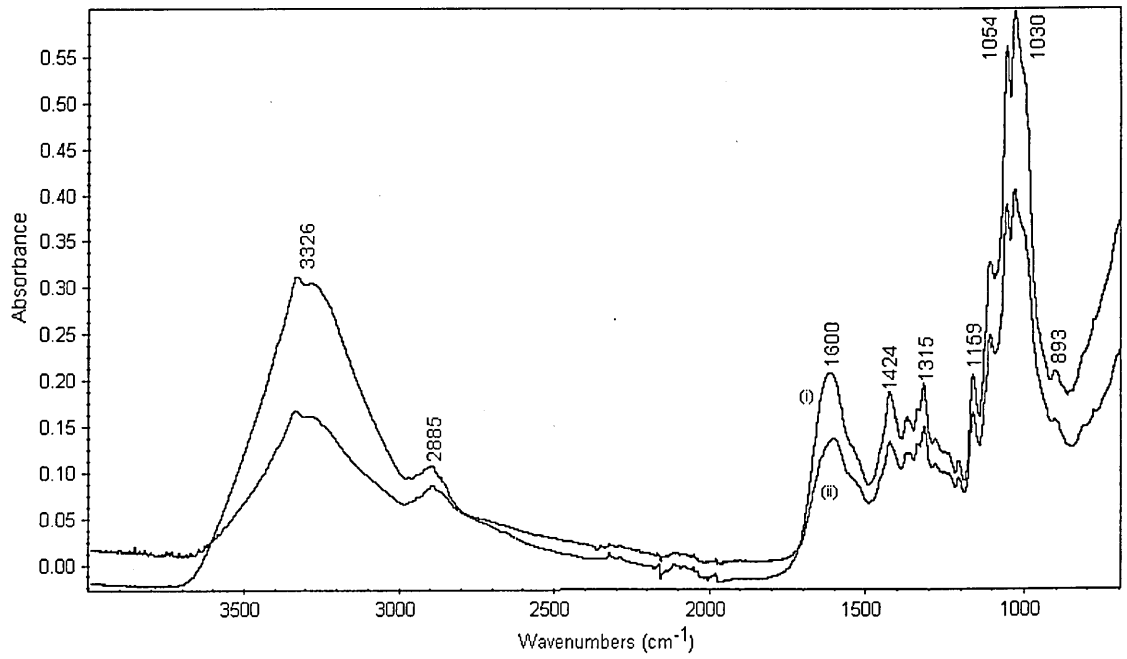

Figure 79 FT-IR spectra of (i) Cr bound esterified dealginate and (ii) esterified dealginate

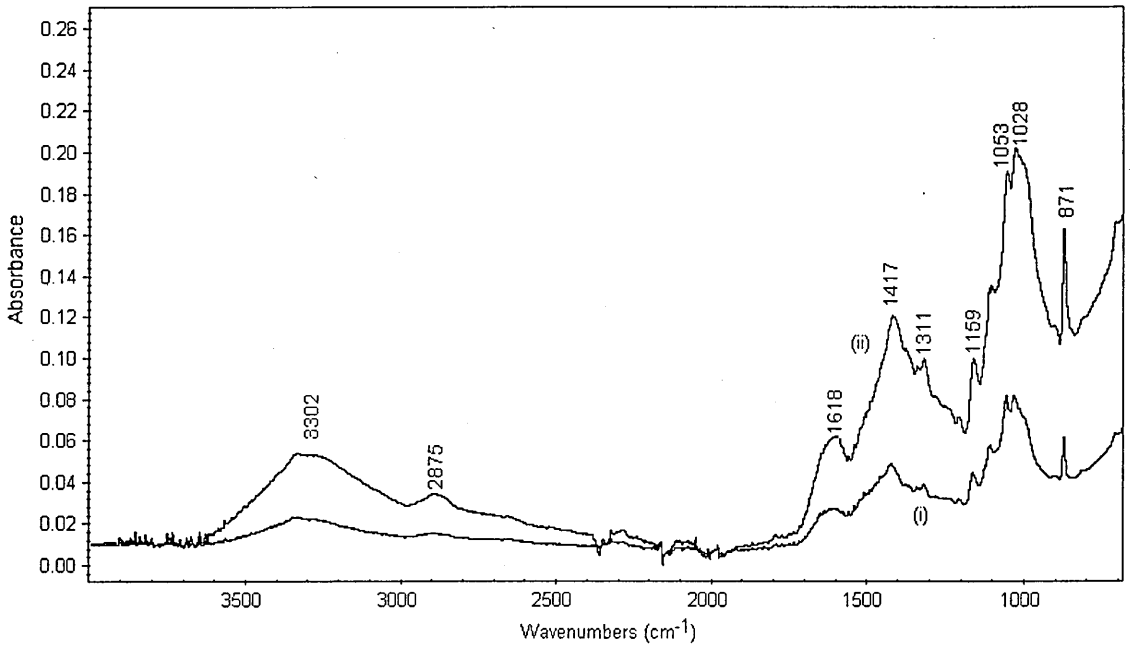

5.1.6. Silver

The main differences between the Ag-dealginate pH 6 sample and HCl washed dealginate was observed in the presence of a strong sharp band at 1419 cm^{-1} and the diminishing of the existing band at 1315 cm^{-1}(Figure 80). Similar to the previous metals studied, these changes in the shape of the spectra could be attributed to the effect of Ag binding to the biosorbent. These results corroborate the indication of carboxylate groups as being mainly responsible for metal binding on dealginated seaweed.

As expected there were very little changes in the spectra of Ag-dealginate at pH 2, since the sorption process is not favourable at this pH. The reduction on the Ag bound to dealginate was observed in the shape of the Ag-esterified spectra. Apart from an increase in the intensity of the band at 1595 cm^{-1} caused by the interaction of Ag, no other changes were observed (Figure 82).

Figure 80 FT-IR spectra of (i) Ag bound at pH 6 dealginate and (ii) HCl washed dealginate

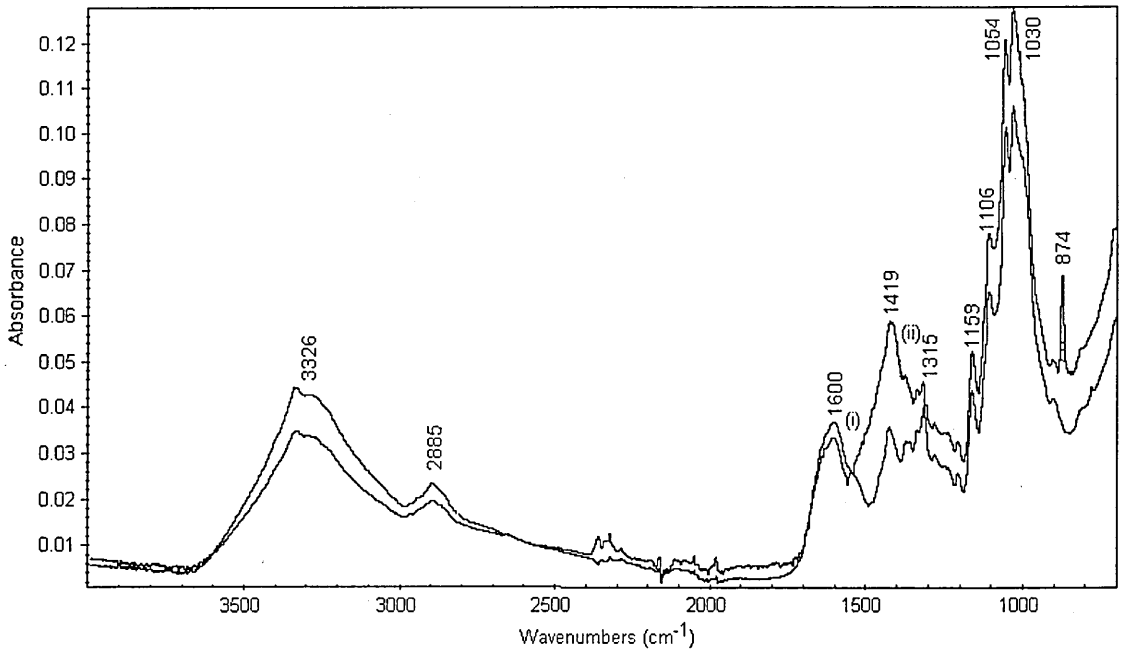

Figure 81 FT-IR spectra of (i) Ag bound at pH 2 dealginate and (ii) HCl washed dealginate

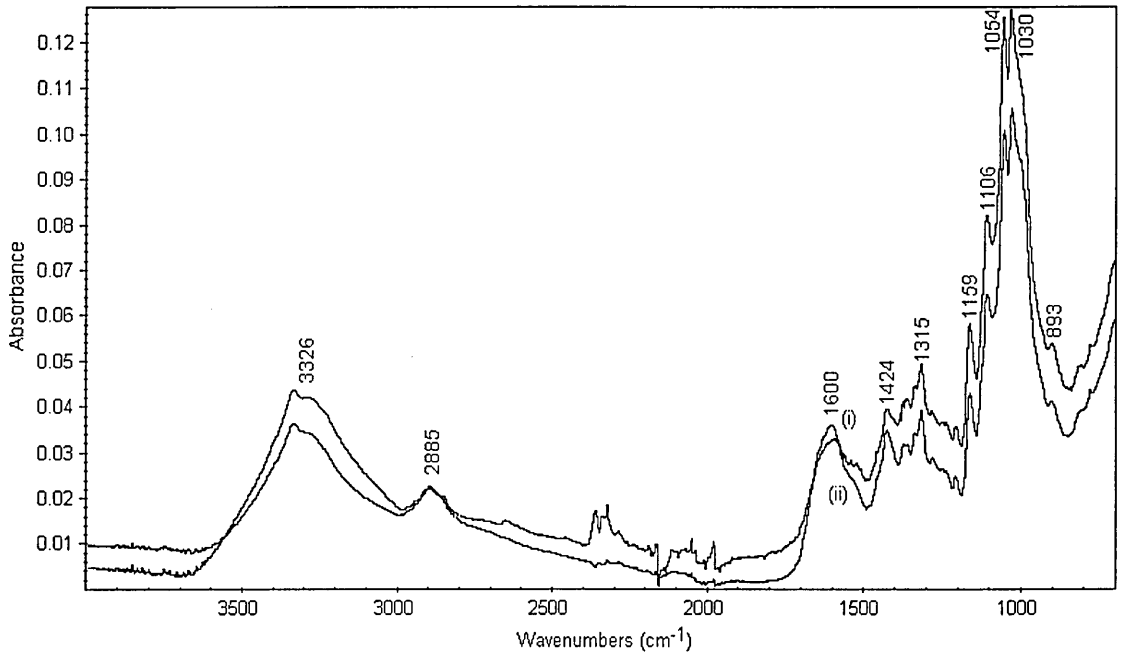

Figure 82 FT-IR spectra of (i) Ag bound esterified dealginate and (ii) esterified dealginate

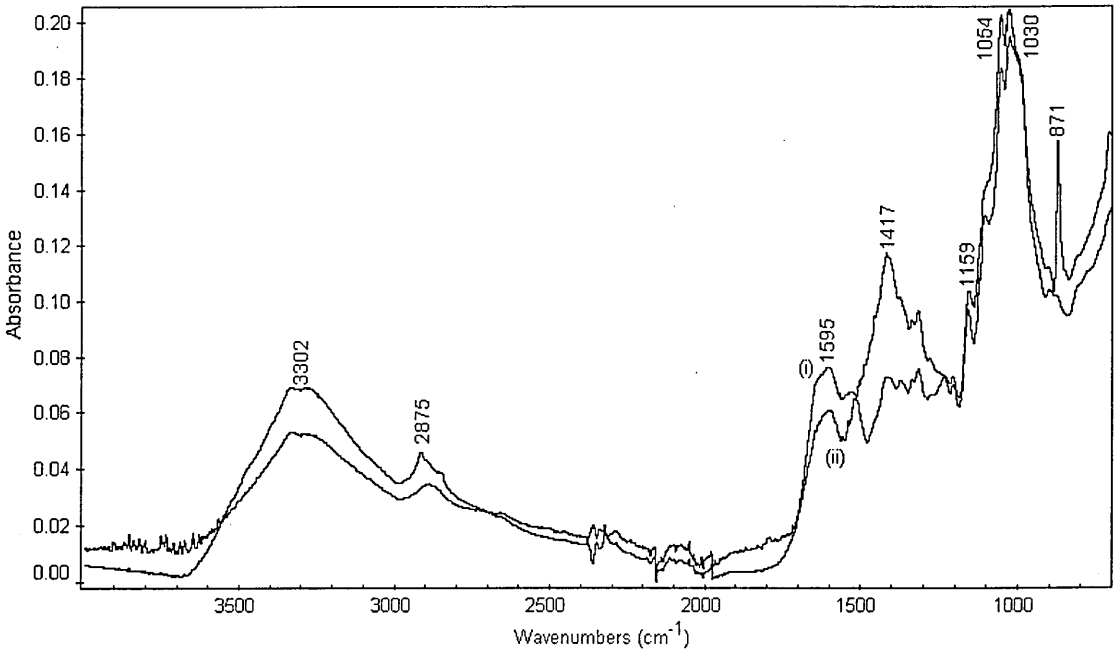

5.1.7. Aluminium

Figure 83 shows the spectra of Al-dealginate at pH 4. There were no differences when compared with the HCl washed dealginate, indicating that no Al was retained by the biosorbent. Similar results were observed for the Al-esterified sample (Figure 84). These results indicate that no sorption process occurred in the Al study.

Figure 83 FT-IR spectra of (i) Al bound at pH 4 dealginate and (ii) HCl washed dealginate

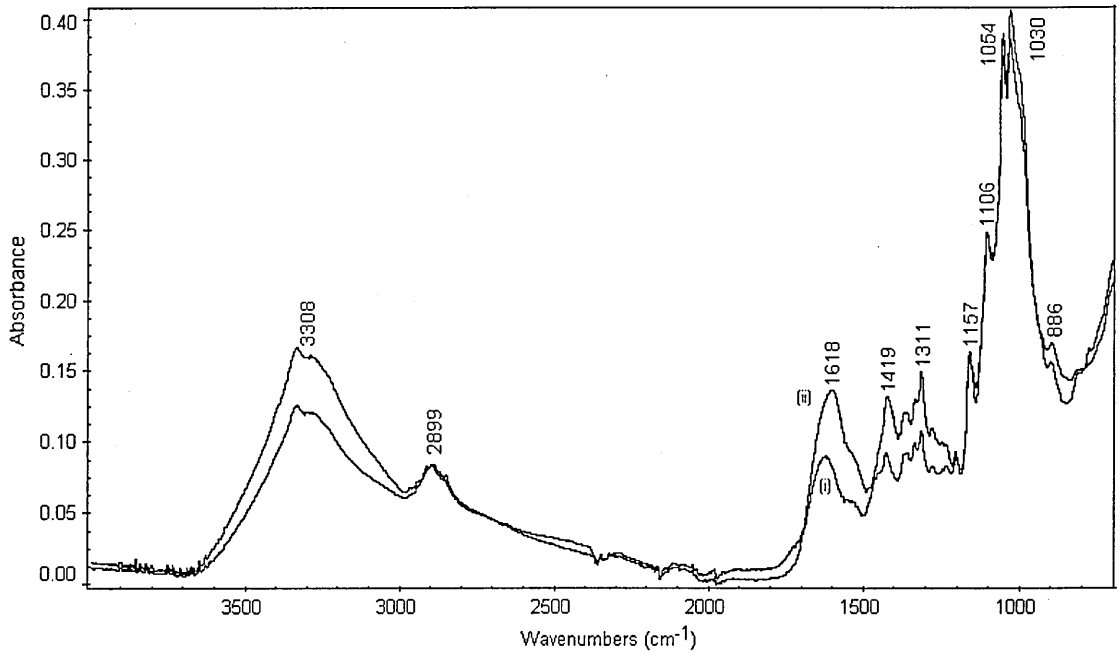

Figure 84 FT-IR spectra of (i) Al bound esterified dealginate and (ii) esterified dealginate

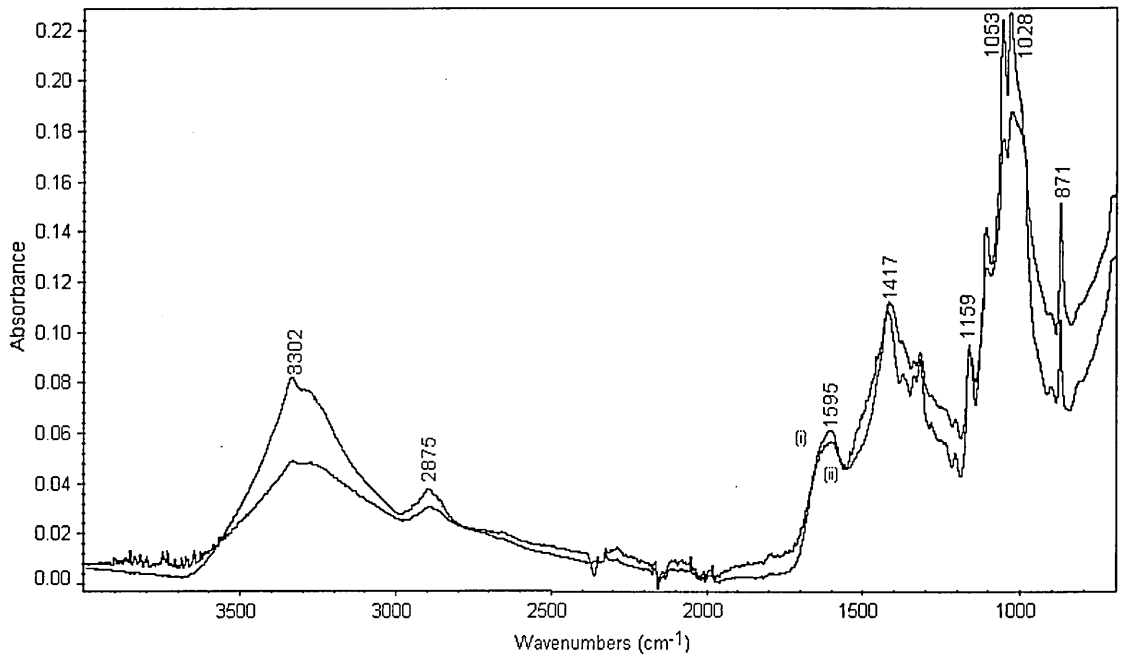

5.1.8. Gold

The spectra of Au-dealginate at pH 3 are shown in Figure 85. As observed previously for Ni and Cr, the band at 1600 cm^{-1}splits in to three, to give shoulders at 1728, 1638 and 1528 cm^{-1}. The intensity and shape of the band at 1424 cm^{-1} remains the same, and the intensity of the bands at 1315 1159, 1104, 1054 and 1030 cm^{-1} increased. The changes in the shape of the spectra are attributed to the interaction of the Au with the carboxylate groups present on the surface of the biosorbent. Similar results were described for the sorption of Au by *S. natans* (108). The results showed IR peaks attributed to carbonyl groups, which were shifted towards lower wave numbers due to the chemical coordination.

Figure 86 shows the spectra of Au-esterified and esterified dealginated seaweed. The increase in the intensity of the bands at 1595 and 1417 cm^{-1} along with the appearance of a band at 871 cm^{-1} suggests the presence of other types of binding sites for Au.

Figure 85 FT-IR spectra of (i) Au bound at pH 3 dealginate and (ii) HCl washed dealginate

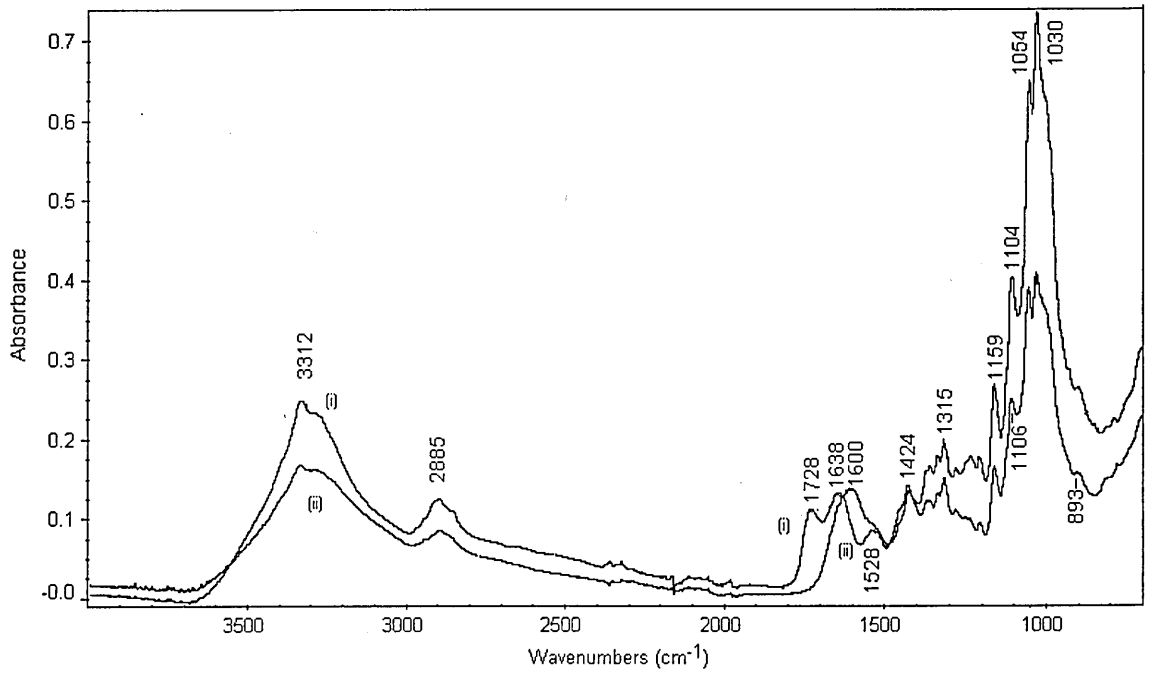

Figure 86 FT-IR spectra of (i) Au bound esterified dealginate and (ii) esterified dealginate

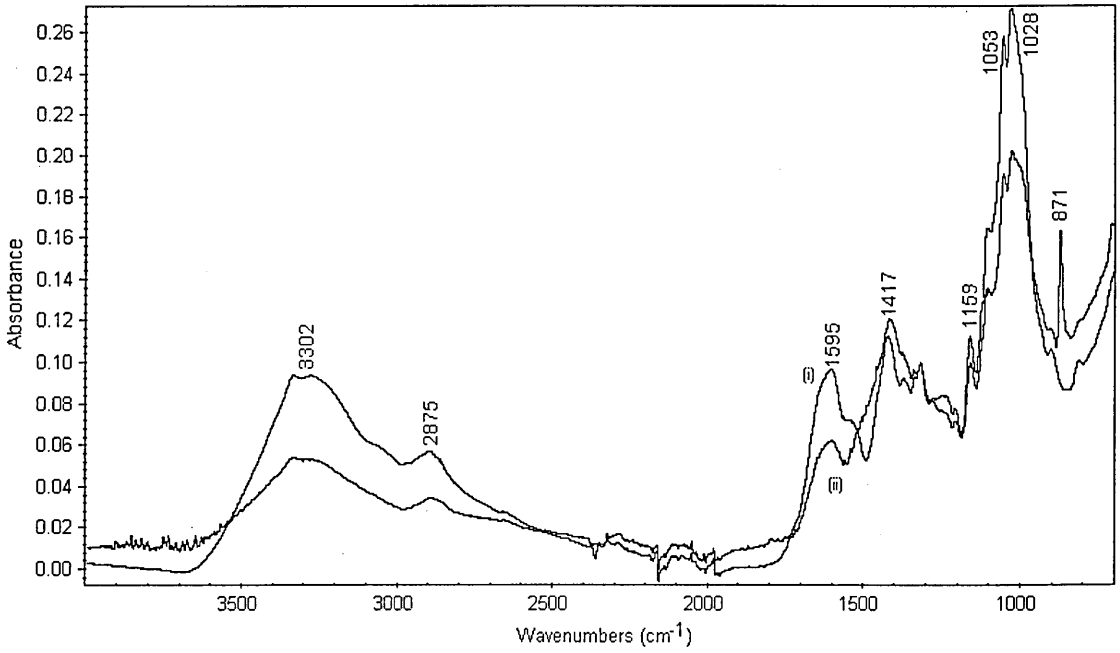

5.2. Summary

The participation of carboxylate group in the uptake of metal ions by dealginated seaweed was demonstrated by use of Fourier transform infra-red spectroscopy. It was possible to elucidate the presence of carboxylate groups on the surface of the biosorbent, and the effect that uptake of metals causes on the carboxylate groups. The effectiveness of the esterification process was demonstrated with the reduction of carboxylate bands in the fingerprint region. In the case of Al, the possibility of precipitation instead of sorption occurring at the biosorbent surface was suggested. The use of FT-IR as a powerful tool for the characterisation of the nature of metal binding sites on dealginate was demonstrated.

Surface Morphological Characterisation of Dealginated Seaweed using Environmental Scanning Electron Microscopy (ESEM)

Chapter 6

6.1. Direct observation of hydrated specimens

A programme of environmental scanning electron microscopy (ESEM) techniques, combined with elemental Energy Dispersive X-Ray analysis, was developed to assess the distribution of metal on the seaweed surface.

The advantages of ESEM over conventional SEM for this application include the minimal amounts of sample preparation (and surfaces artefacts); no requirement for conductive coatings and the ability to look at surfaces under fully hydrated conditions at high resolution (113).

The secondary electron detection process employed in this study is shown in Figure 87.

Figure 87 Hydration in the ESEM, chamber configuration and secondary electron amplification

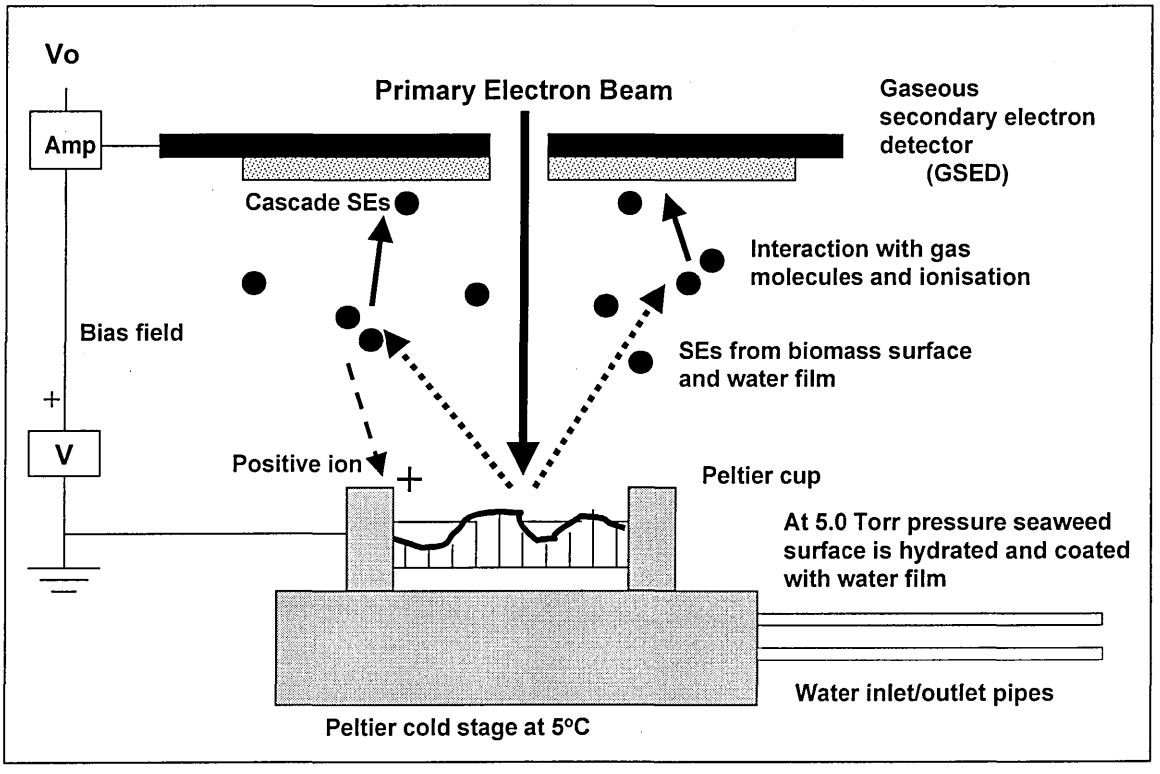

The gaseous secondary electron detector (GSED) is positioned around the pole piece and final pressure-limiting aperture. A voltage is applied between the specimen surface and the GSED, accelerating both secondary and derived electrons towards the detector (see Figure 87) (114). Three different types of collisions are created between secondary electrons and gas molecules: elastic, ionising (creating electron-ion pairs) and excitatory (transferring energy to gas molecules), all of which contribute to the amplification process.

The creation of electron-ion pairs by ionising collisions leads to amplification of the scanned electron signal with a residual cloud of positive ions around the sample. The presence of a gaseous atmosphere in the specimen chamber allows examination of the biological specimen with no need for a conductive coating, whilst at the same time maintaining the specimen in a fully or partially hydrated state.

The surface of dealginated seaweed was examined in the hydrated state using the ESEM. Untreated, esterified and Pb, Ag, Au and Al saturated samples were observed using this technique. Metals such as Ni and Cr could not be studied due to interference caused by the components of the peltier cup. The Cd and Cu lines were too weak to be monitored during the X-ray analysis.

Environmental scanning electron micrographs showed that the wet-state surface of the untreated dealginate was covered with porous particles (see Figure 88). The microstructure of the biosorbent was found to consist of cell walls ending in round tips, formed by intersecting and overlapping layers (see Figure 89). A more detailed examination revealed the presence of fibre-like areas (Figure 90) surrounded by round particles, similar to beads, distributed alongside the fibres.

Figure 88 Electron micrograph of the Dealginated seaweed surface

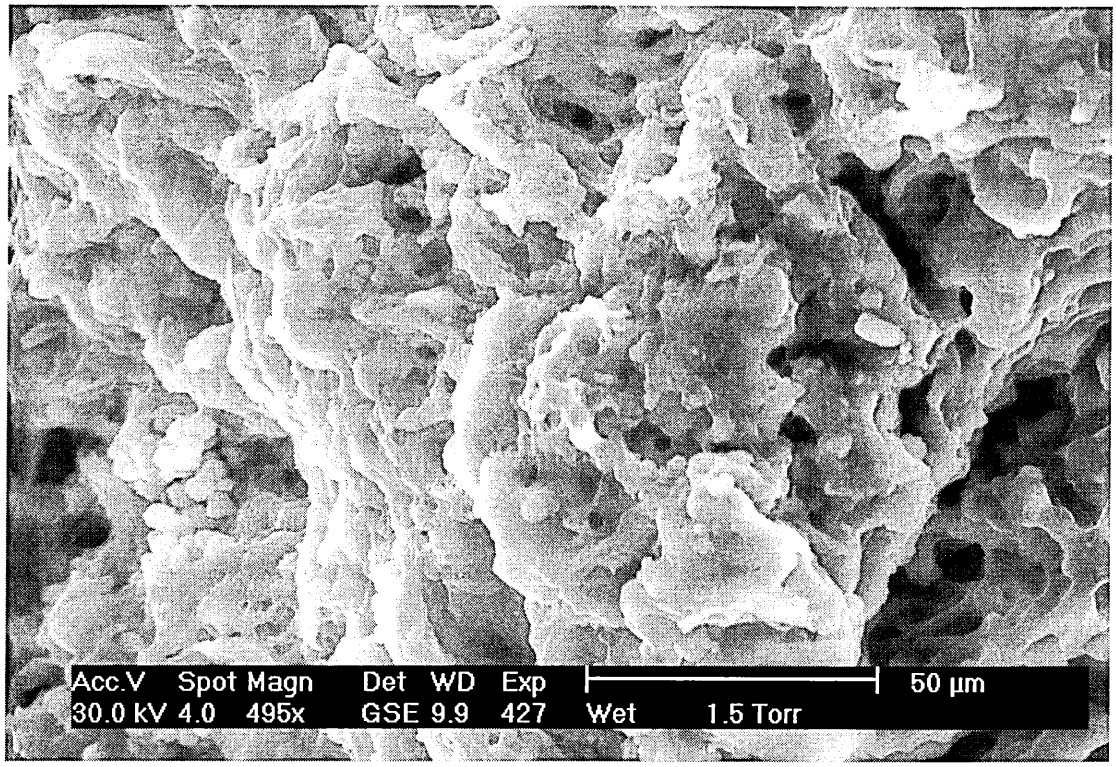

Figure 89 Electron micrograph of the details on the dealginated seaweed surface

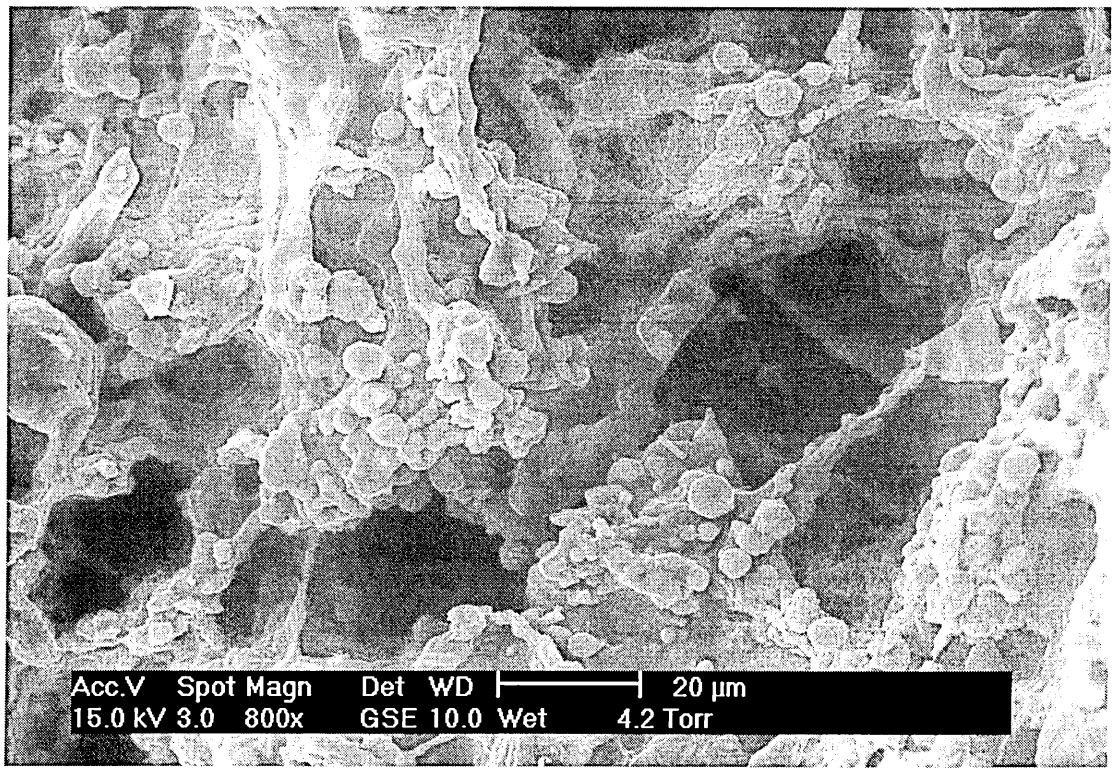

Although the biosorbent has undergone the processes of chopping, milling and precipitation with salts, the cell structure was still evident in large areas of the surface, as it can be seen in Figures 91 and 92. The micrographs showed a lack of plant tissue organisation with only the cell wall being distinguishable. This is most likely to have resulted from the dehydration and exposure to acids and salts during the extraction of alginates. Similar results were reported for *Sargassum fluitans* examined using Transmission Electron Microscopy (TEM) (118).

The presence of beads "sitting" inside the cells was observed on the surface of the entire specimen (Figure 92). Figure 93 shows the X-ray spectra of the beads showing a high Ca content, which confirmed the presence of Ca from the alginate removal process.

The dealginated seaweed surface was examined following the cleaning procedure used to prepare the biomass for sorption. The surface showed no damage as a result of the use of the HCl solution that was used to remove Ca, Na, Mg and K present from the untreated material. The surface retained its original structure, as shown in Figure 94.

The removal of the cations present on the surface was confirmed by ESEM since there was no presence of the beads observed previously. Figures 95 to 97 show secondary electron (SE) images of the surface after the cleaning procedure. Figure 97 shows the detail of the cell walls free of beads. This confirms the efficiency of the cleaning procedure.

Figure 90 Detail of fibre type areas on dealginated seaweed surface

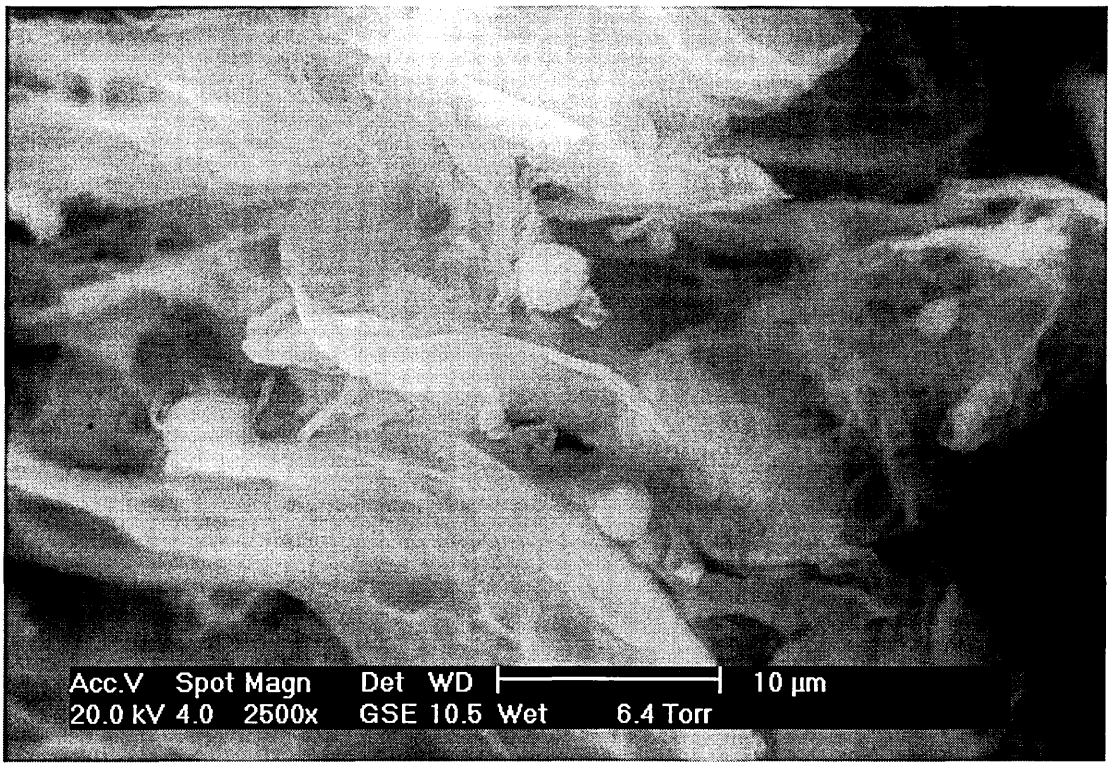

Figure 91 Typical cell areas on dealginated seaweed surface

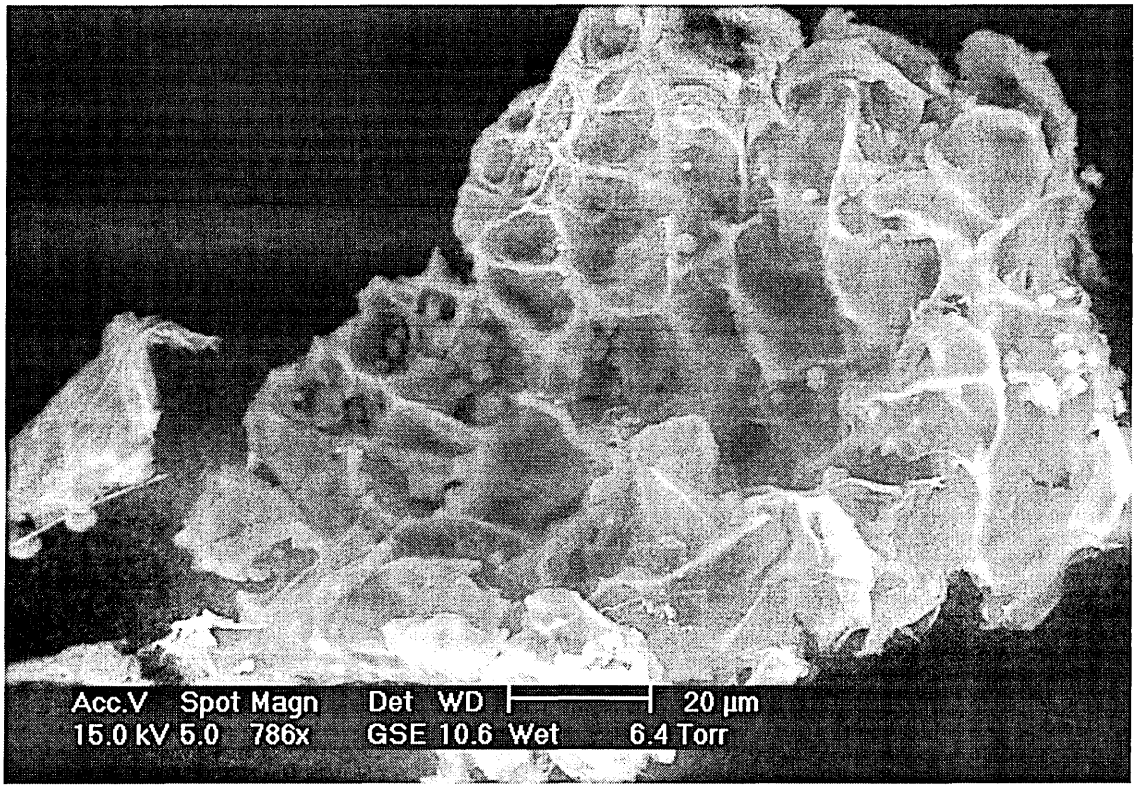

Figure 92 Detail of cells on dealginated seaweed surface

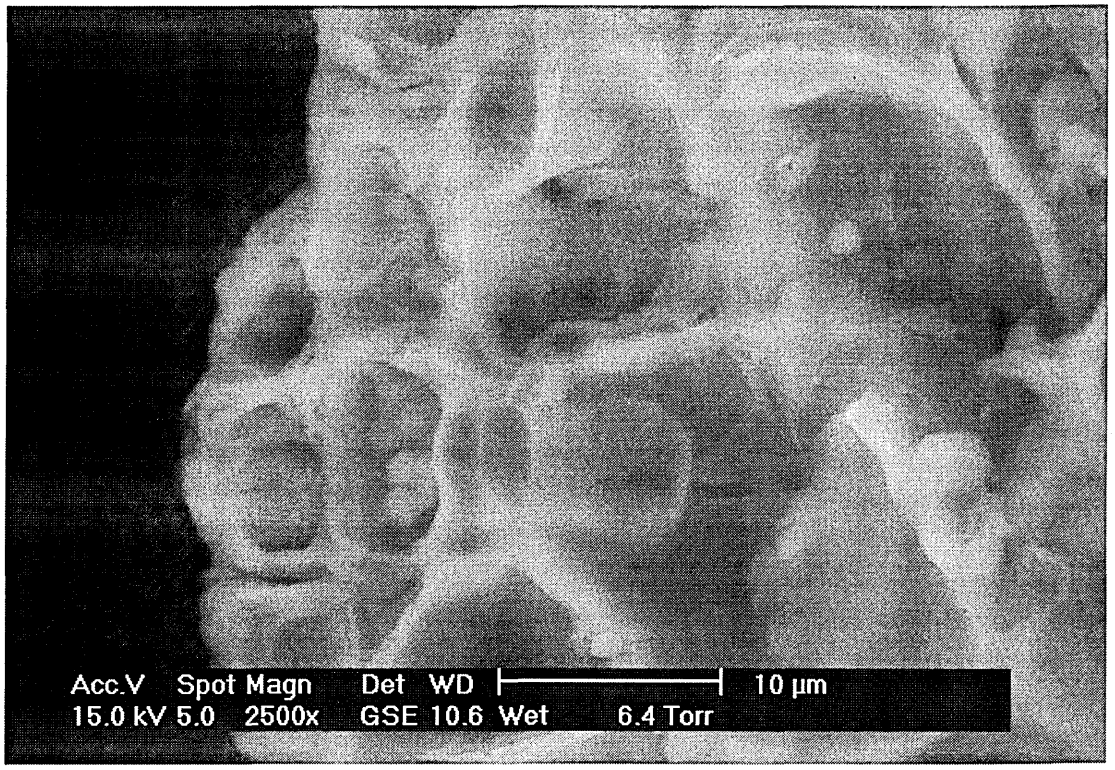

Figure 93 X-ray analysis of a detail of Ca beads in cells on dealginated seaweed surface

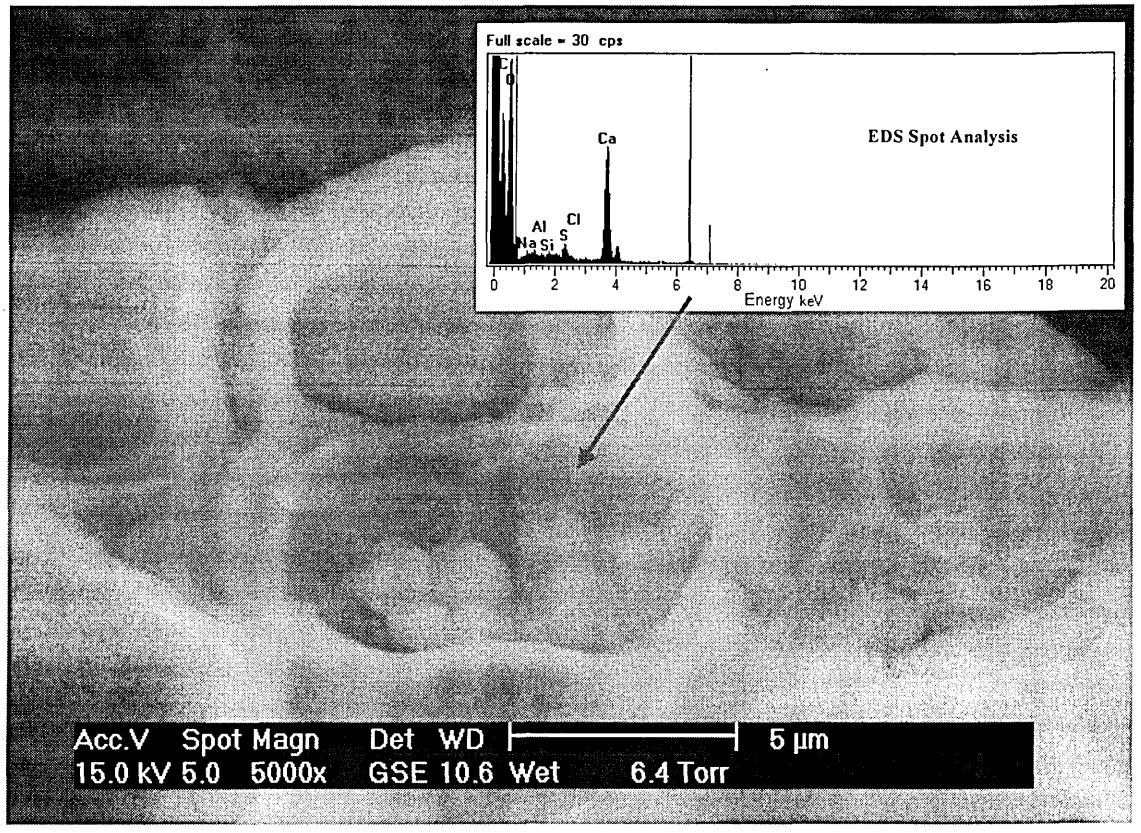

In order to establish whether there were observable changes on the surface of the material after the esterification of the carboxylate groups treated samples were analysed. As shown in Figures 98 and 99 no changes to the surface were observed, even after the acidic methanol digestion. Furthermore, no Ca beads were observed. Similarly, possible changes on the surface of dealginate after repeated use as column packing material were evaluated. As shown in Figures 100 and 101 no changes were observed.

Examination of *Durvillaea potatorum* using SEM showed no significant differences between biomass loaded with Cu^{2+} and Cd^{2+} when compared to untreated biomass (117). In contrast, morphological changes were observed during the binding of Cu^{2+} by *Mucor rouxii* (116).

Figure 94 SE image of HCl washed dealginated seaweed

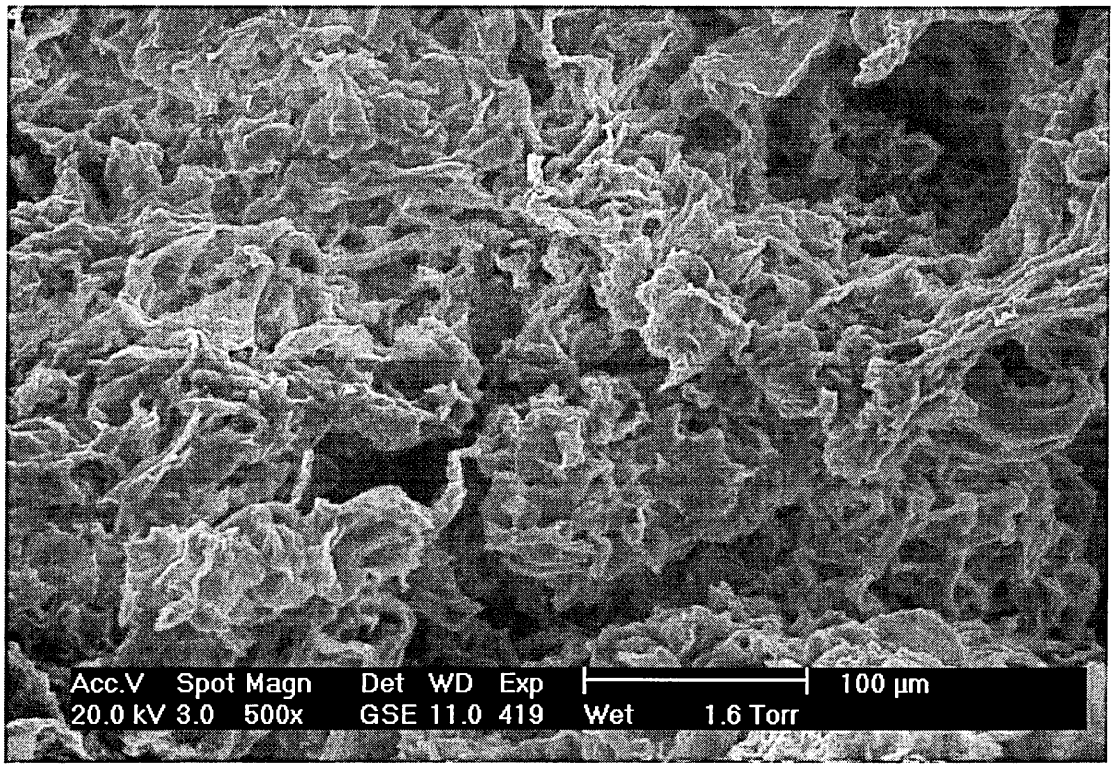

Figure 95 SE image of HCl washed dealginated seaweed

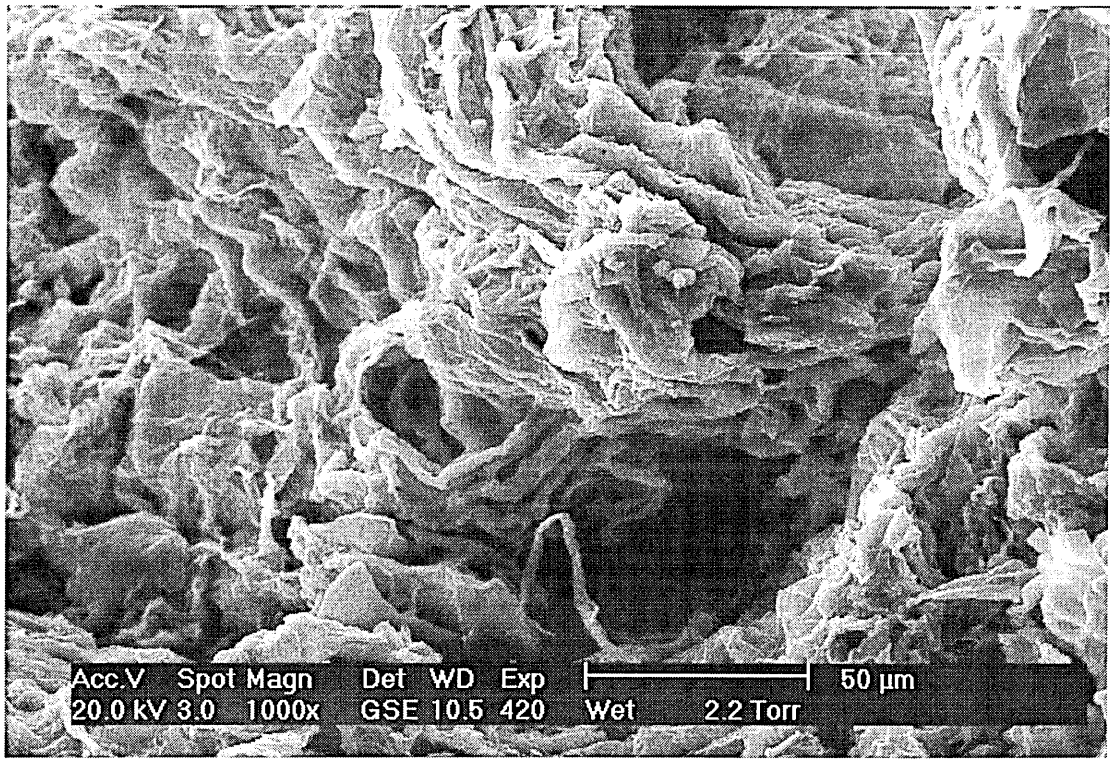

Figure 96 Detailed image of HCl washed dealginated seaweed

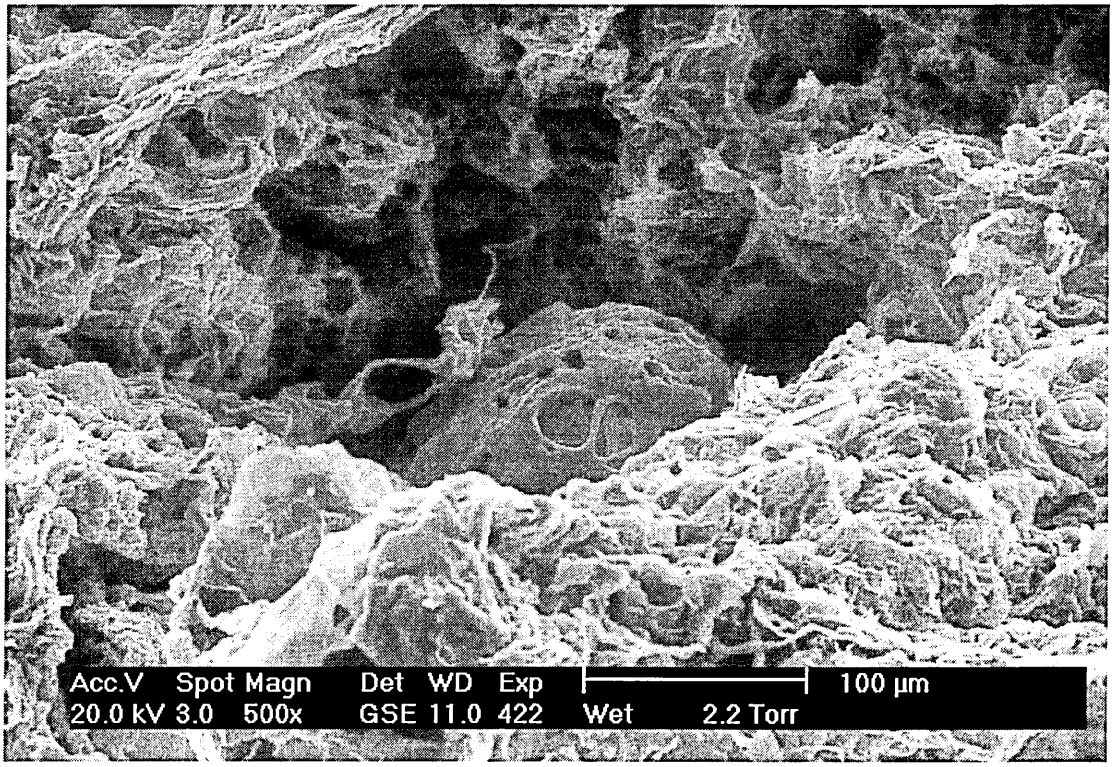

Figure 97 Detailed of clean cell walls on dealginated seaweed surface

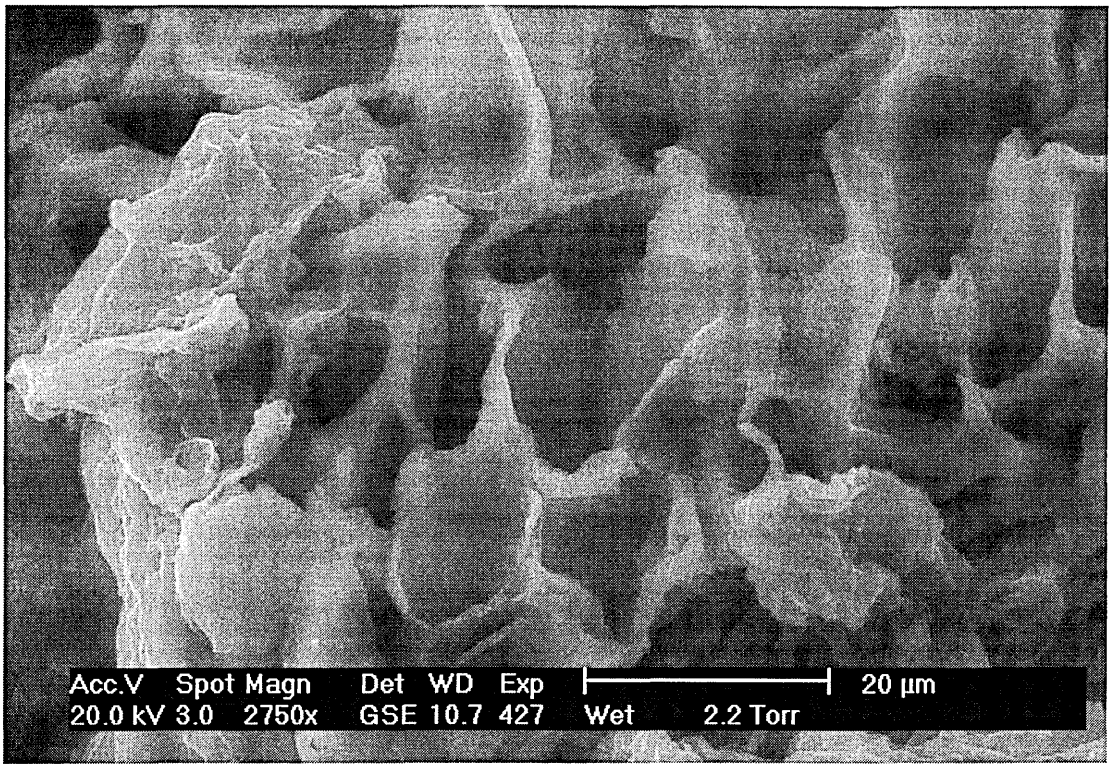

Figure 98 SE micrograph of esterified dealginated seaweed

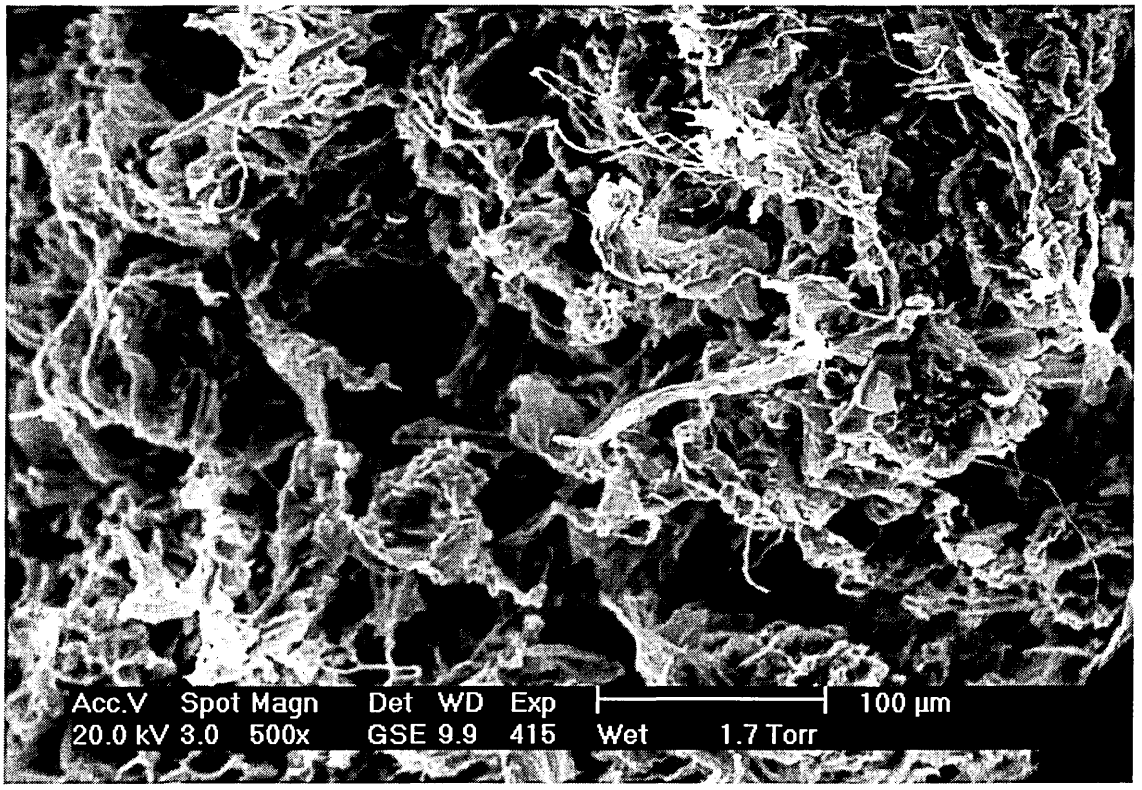

Figure 99 Detailed SE micrograph of esterified dealginated seaweed

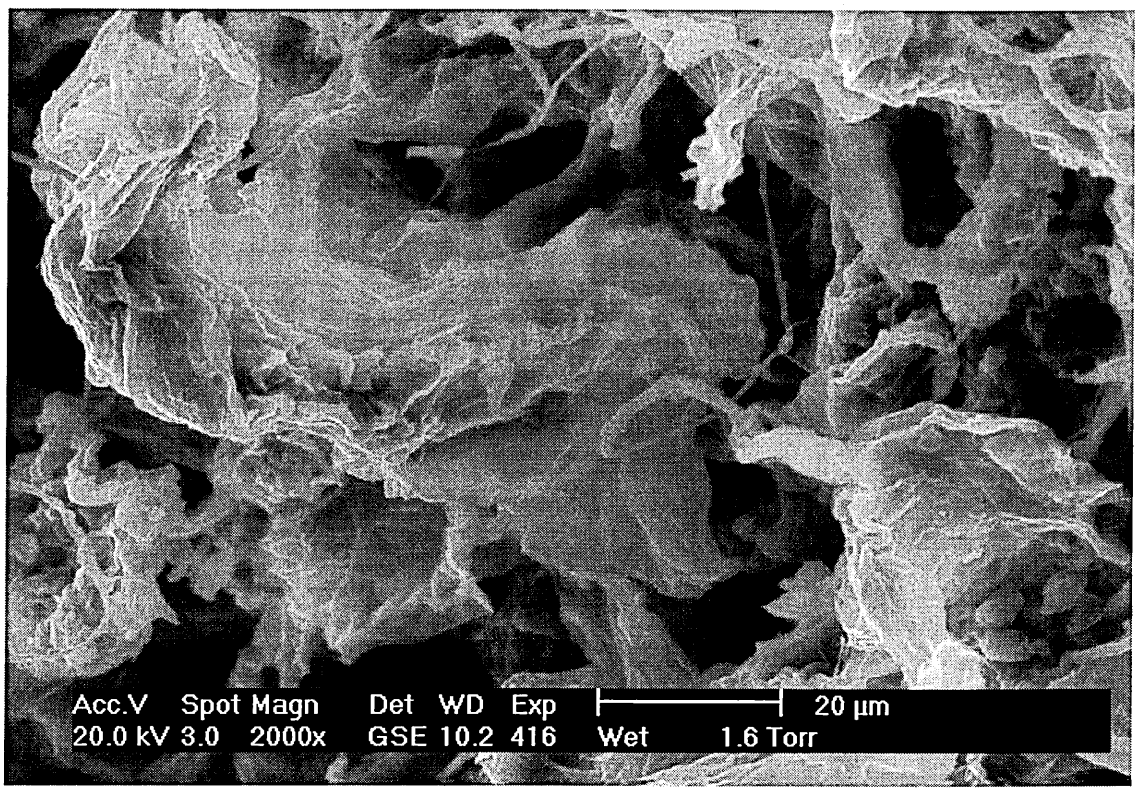

Figure 100 SE image of dealginated seaweed column packing

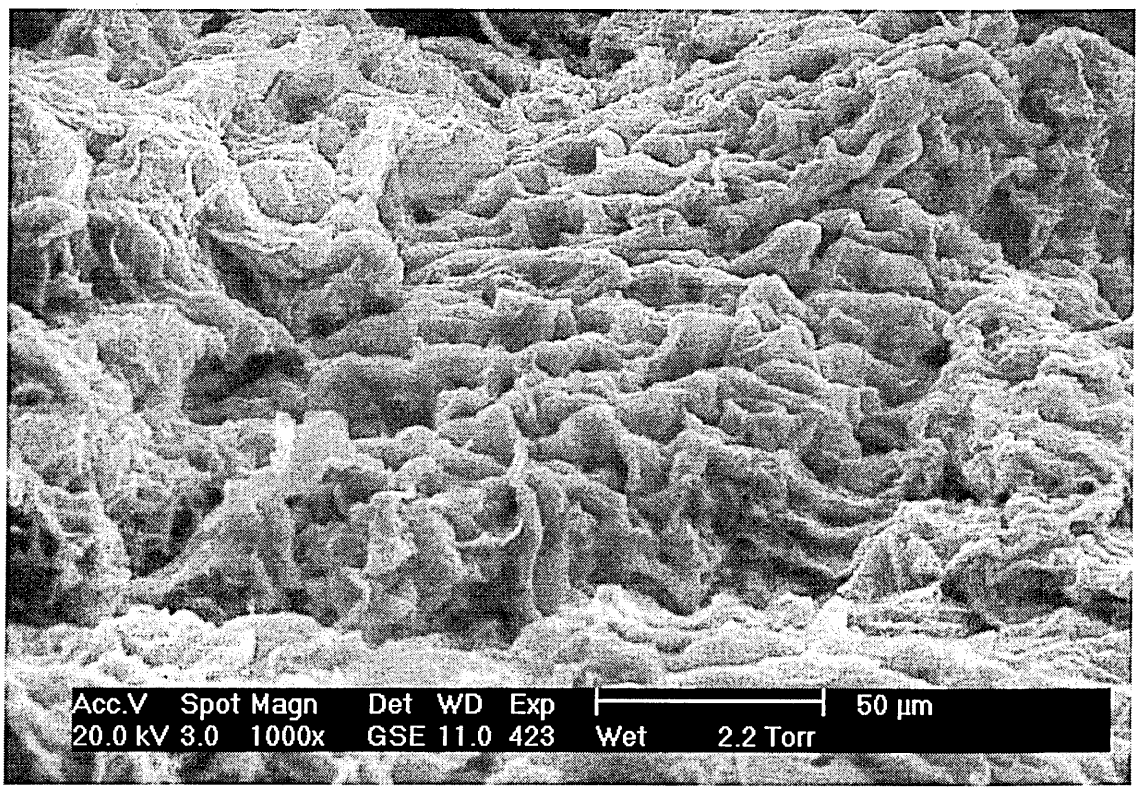

Figure 101 Details of dealginated seaweed used for column packing

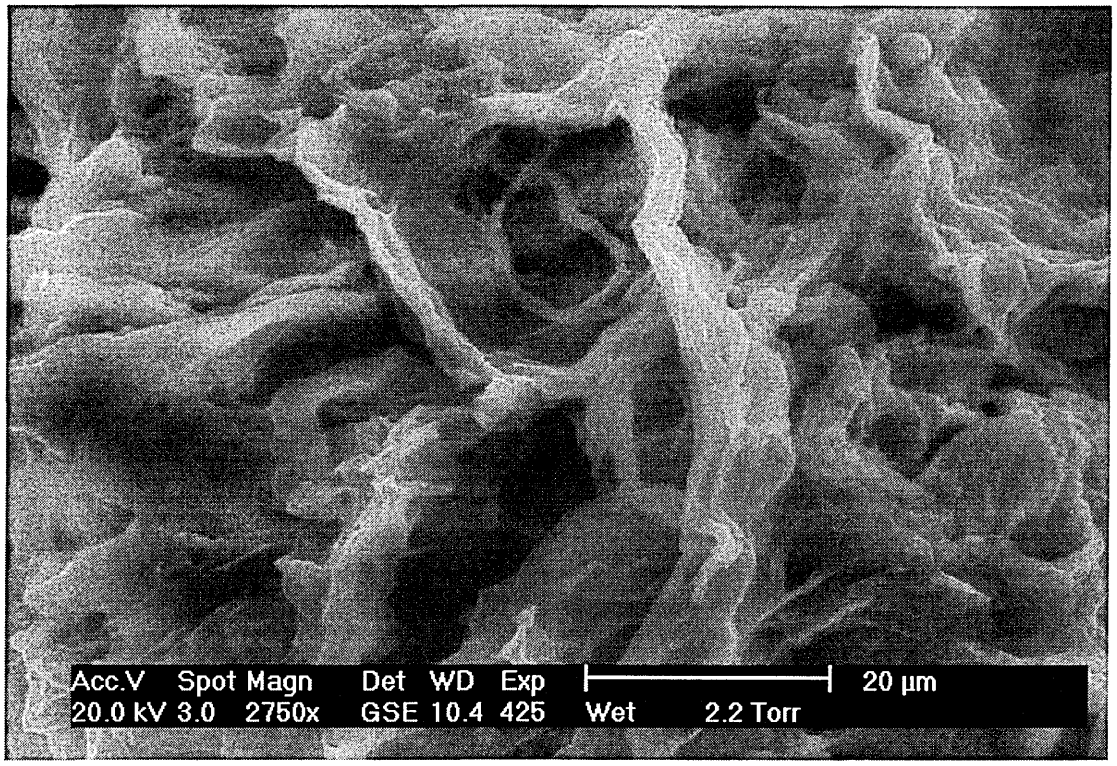

Sets of micrographs for the progressive removal of surface water film from wet untreated dealginated seaweed are shown in Figures 102 - 107.

Initially, the chamber was saturated with water vapour at 6.8 torr of pressure and 3°C, since at a particular temperature, higher water vapour pressures resulted in water condensation. As shown on Figure 102, a water film was lying over the surface. An examination of the surface at higher magnification (Figure 103) revealed the dealginated surface was covered with water, and the characteristic surface was not visible.

Figure 104 shows a view of same field after the pressure was reduced to 4.2 torr and the temperature increased to 5°C. Some water was removed from the surface film allowing the surface to be partially exposed. Figure 105 shows a detailed image at higher magnification, where the water film is clearly visible with only a strand above the liquid surface.

Following a further 5 minutes of exposure further free water was removed (Figure 106). Finally, as shown in Figure 107, the pressure was reduced to 3 torr and the temperature was increased to 17°C, causing water evaporation, until the material appeared completely dry.

Since it is important not to dehydrate the specimen the micrographs were taken so as not to cause morphological distortion by using a temperature of 4°C and a chamber pressure between 1 and 4 torr when the surface of dealginate was completely exposed.

Figure 102 SE Image of surface of dealginated seaweed

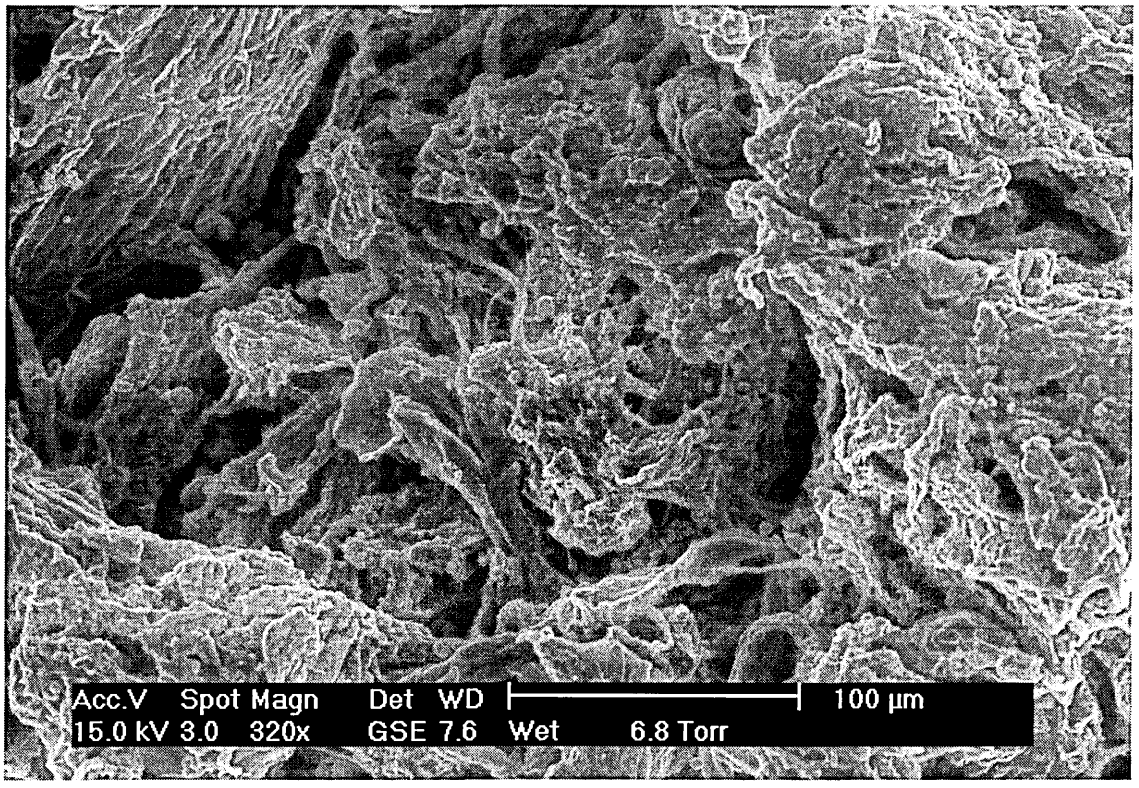

Figure 103 SE Image of surface water film on dealginated seaweed

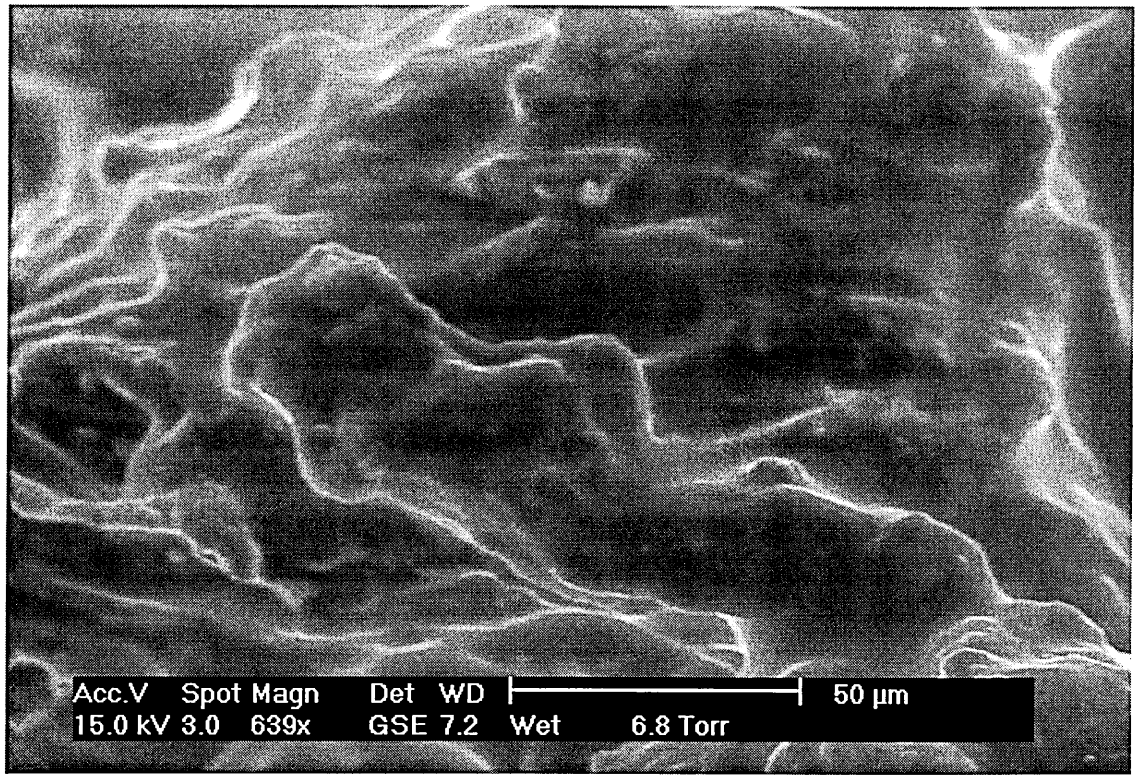

Figure 104 Image of the water film on dealginated seaweed surface at 4.8 torr pressure

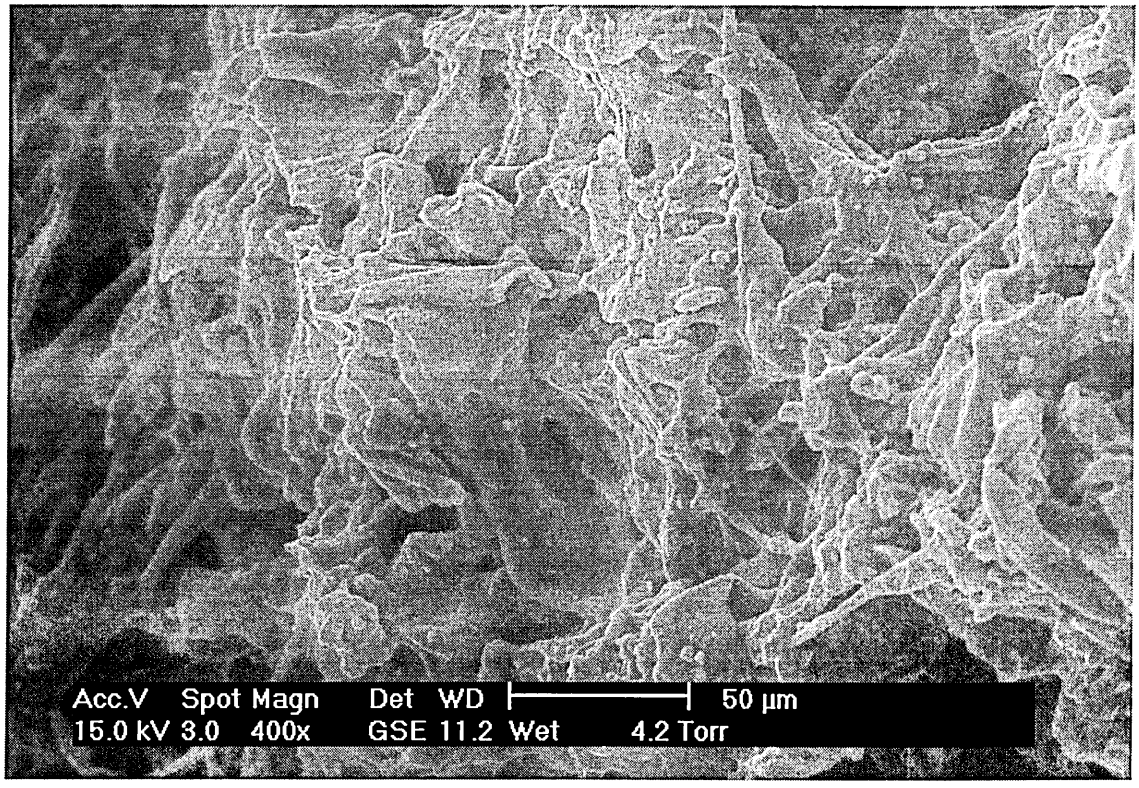

Figure 105 Detail of surface water film on dealginated seaweed surface

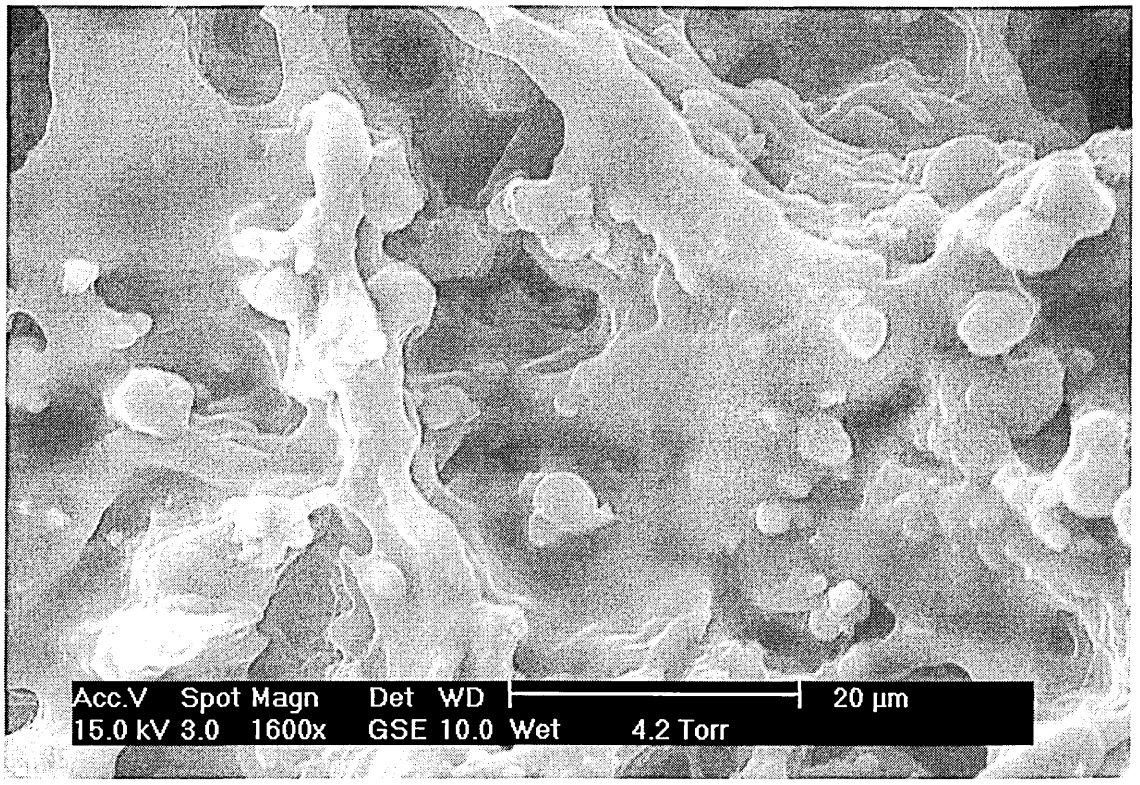

Figure 106 SE image of water film on dealginated seaweed surface at 4.2 torr pressure

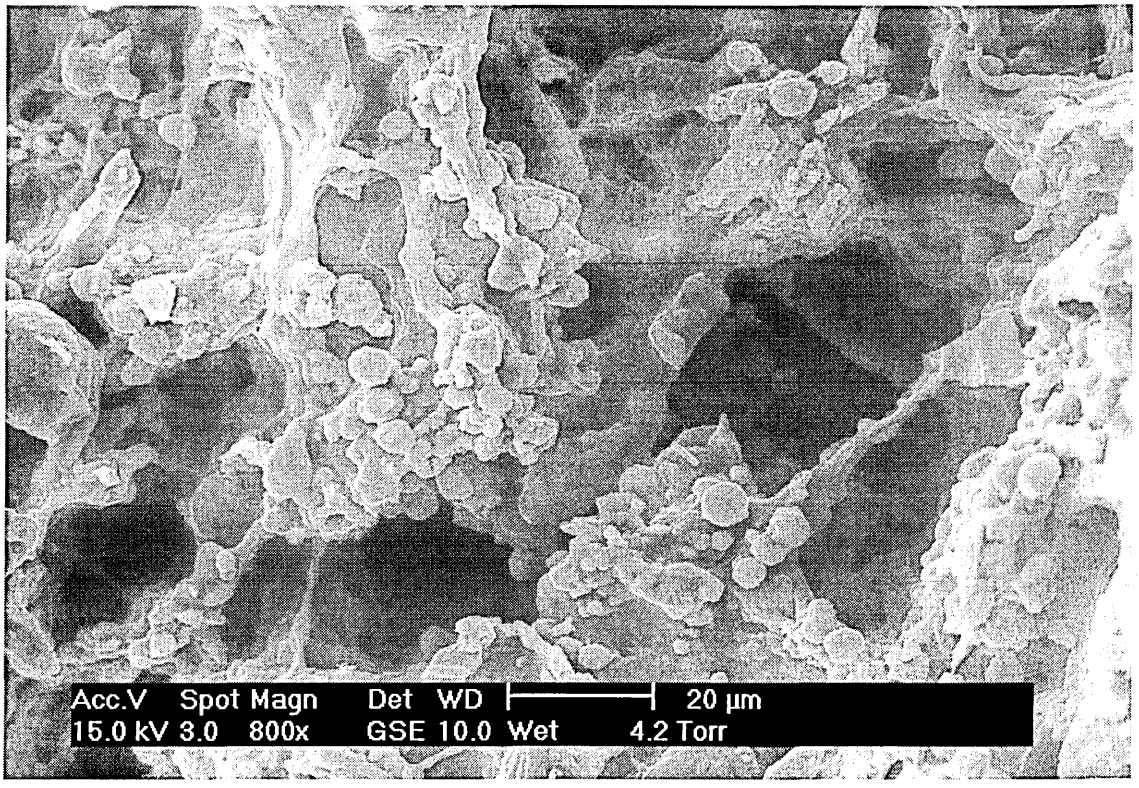

Figure 107 SE Image of dry dealginated seaweed surface

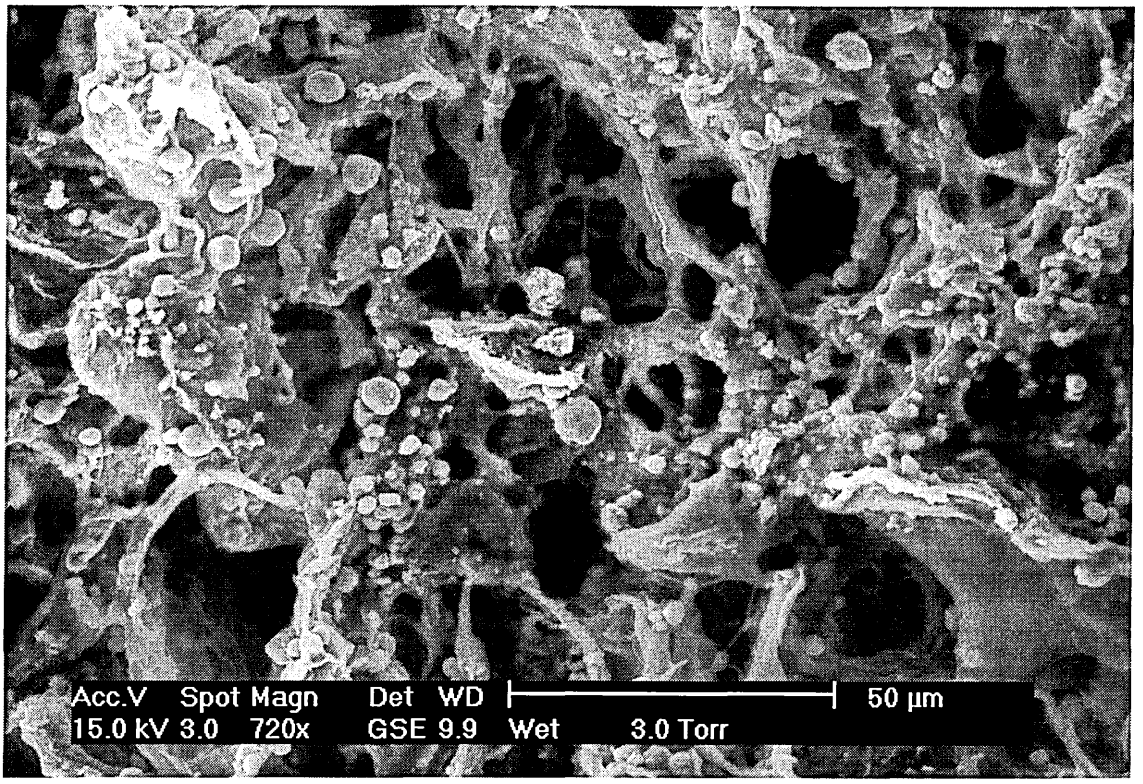

6.2. Metal distribution on dealginated seaweed surface

Energy dispersive X-ray analysis was employed to determine distribution of Pb, Ag, Al and Au on the surface of dealginated seaweed. The samples were saturated with metal ion solution, air-dried and examined under the microscope.

6.2.1. Lead

The micrographs showed that Pb distribution on the dealginate surface was homogeneous when the sample was examined under fully hydrated conditions at 5°C. Although, it has been reported (158) that Pb is sizeable in patches on the surface of green algae, localised Pb was not observed on dealginated seaweed.

Figure 108 and 109 shows the presence of Pb detected by X-ray analysis. No changes were observed in the surface of the biosorbent when compared to untreated dealginated or treated dealginated.

With certain optimisation of EDS collection method and slit minimisation, it was possible to quantify the Pb concentration in the sample. Table 22 shows the percentage distribution of elements in the sample, showing that approximately 5% of the sample was composed of Pb, as was expected from the initial concentration of Pb removed by the dealginated during the sorption process.

The presence of S and Cl observed were typical of the biomass composition. Chloride is a major component of seaweeds. Although S was found to represent only 1.3% of the elemental composition, its presence on the biosorbent was suggested by the titration results shown in Chapter 3, section 3.3.

Table 22 Elemental composition of the Pb saturated dealginate sample by EDS

Element	Element %
C	14
O	67
N	11
S	2
Cl	2
Pb	5

Figure 108 SE image of Pb saturated dealginated seaweed

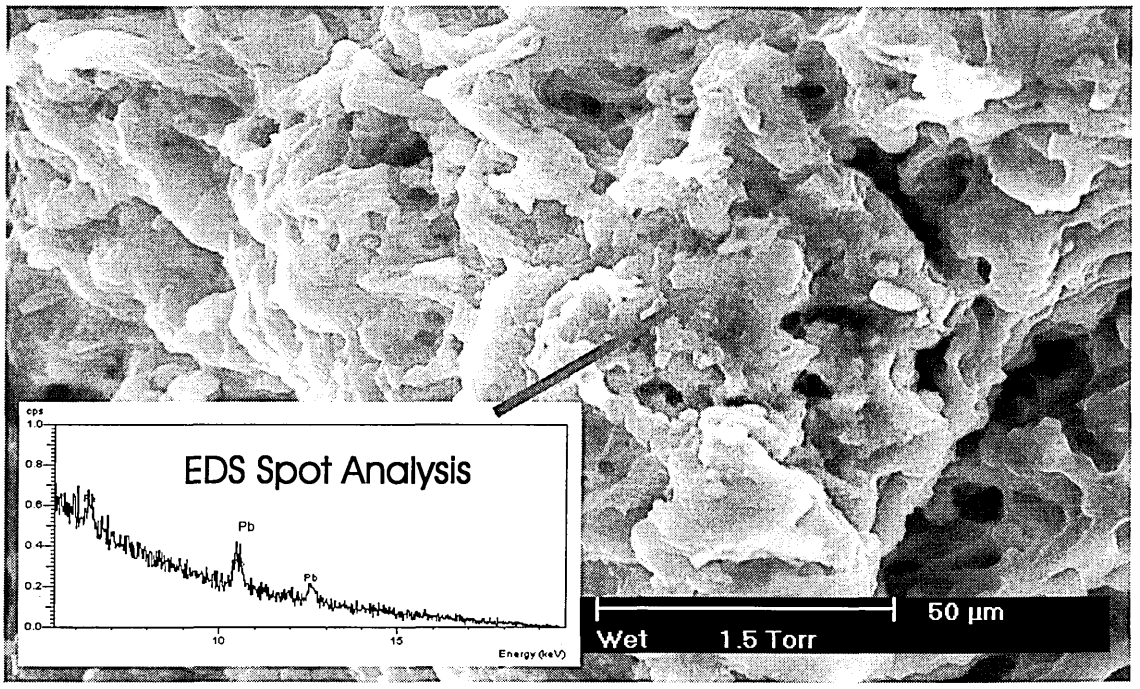

Figure 109 SE image of Pb saturated dealginated seaweed

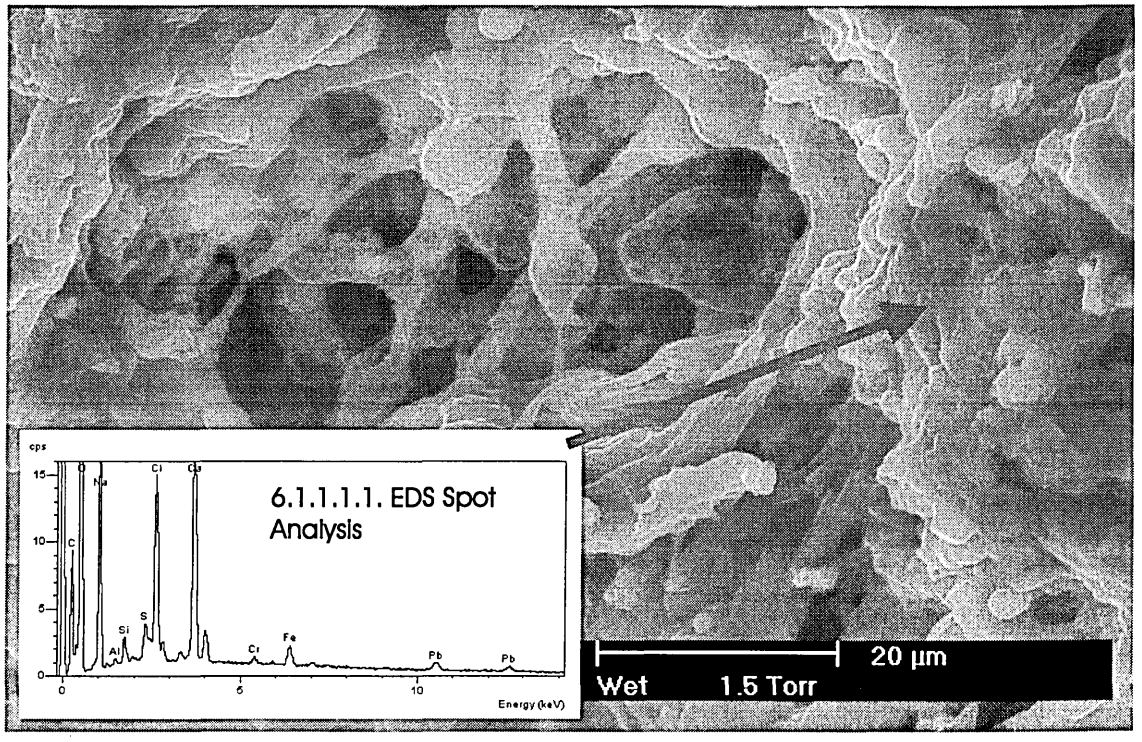

6.2.2. Silver

Images for Ag showed texture changes on the surface of the dealginate material. The presence of beads in some areas was also observed. The cell characteristics were not easily observed. The surface looked like all the components had clumped together (see Figure 110). Occasionally beads were found mixed in the flattened surface, as shown in Figure 111.

Figures 112 and 113 showed the EDS analysis of the beads. The EDS spot analysis showed a high content of Ag, demonstrating the nature of the new beads formed during the Ag saturation. The accumulation or precipitation of Ag may be due to interaction with elements present on the surface of the dealginate material.

An X-ray intensity map was taken of the surface of the Ag dealginated sample, showing the presence of silver, which was easily matched with the sulphur map obtained from the same sample (see Figure 114). No other elements such as oxygen or nitrogen matched the silver distribution.

6.2.3. Aluminium

There was no evidence of changes in the surface morphology in the Al-dealginate samples. As is shown in Figure 115 the structure was similar compared with the untreated biosorbent. Figure 116 shows the presence of Al determined by EDS analysis and the element seemed to be homogenously distributed.

The X-ray intensity map for Al matched that of S. The possibility of aluminium sulphate compounds may therefore be considered.

Figure 110 SE image of Ag saturated dealginate surface

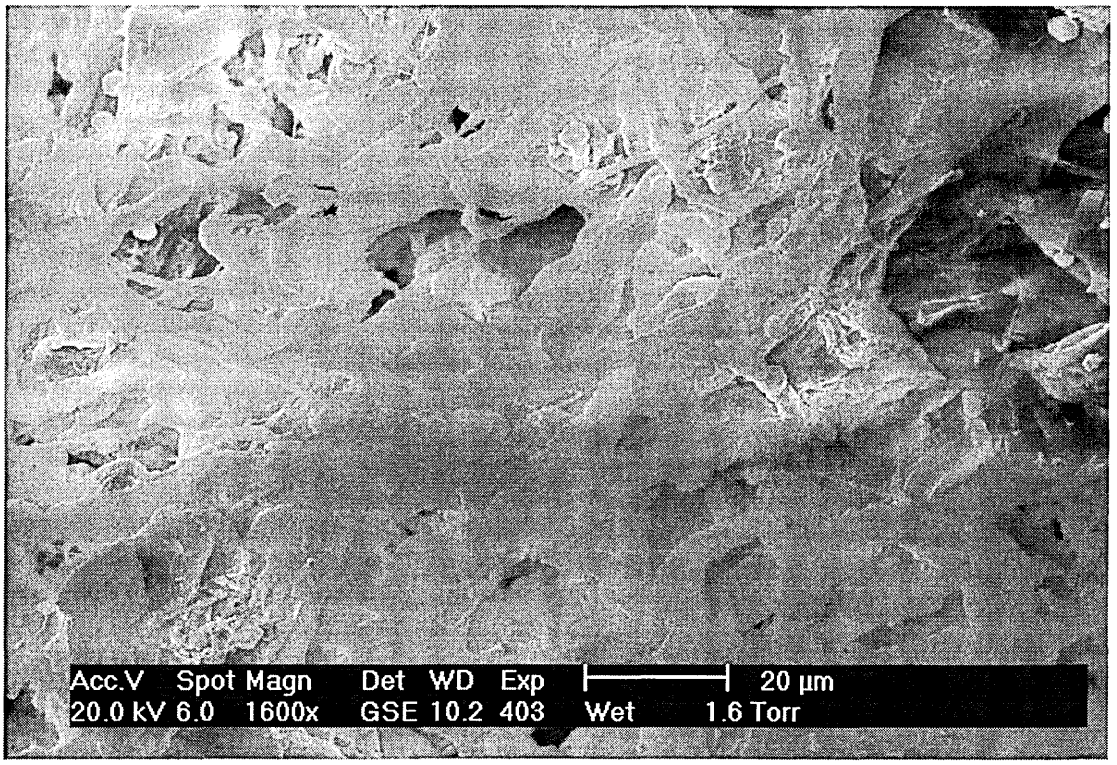

Figure 111 Detail of beads on Ag saturated dealginate surface

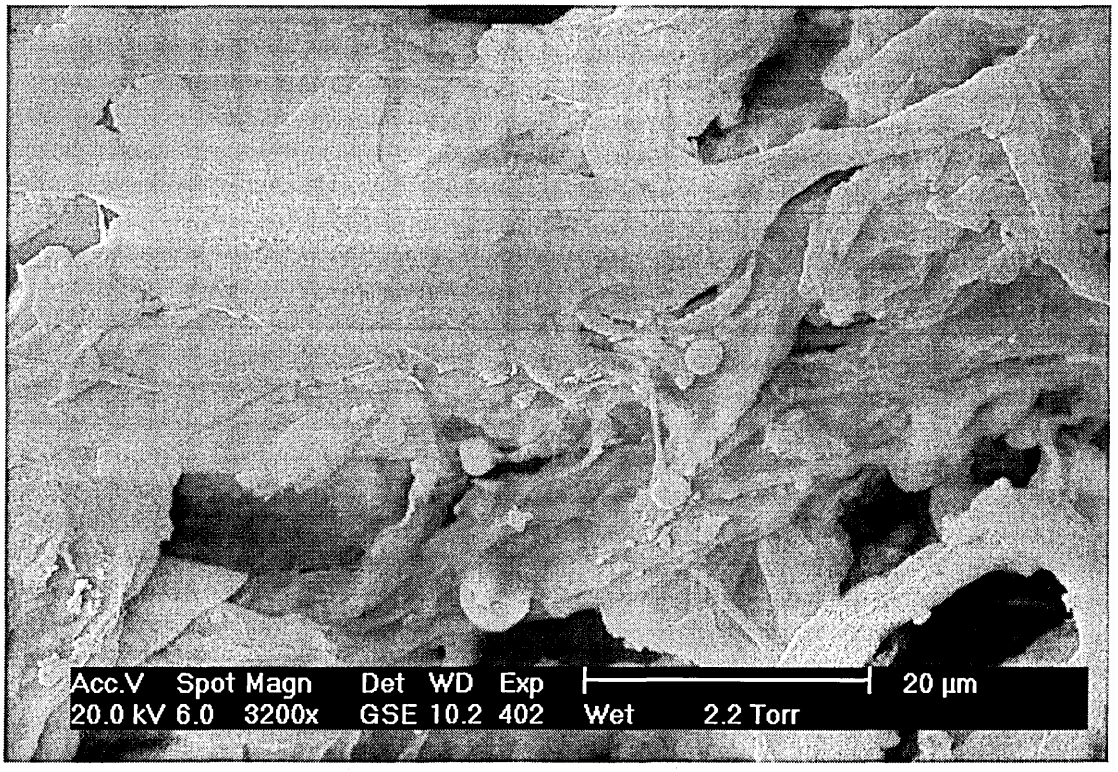

Figure 112 SE image of Ag beads accumulated on dealginated seaweed surface

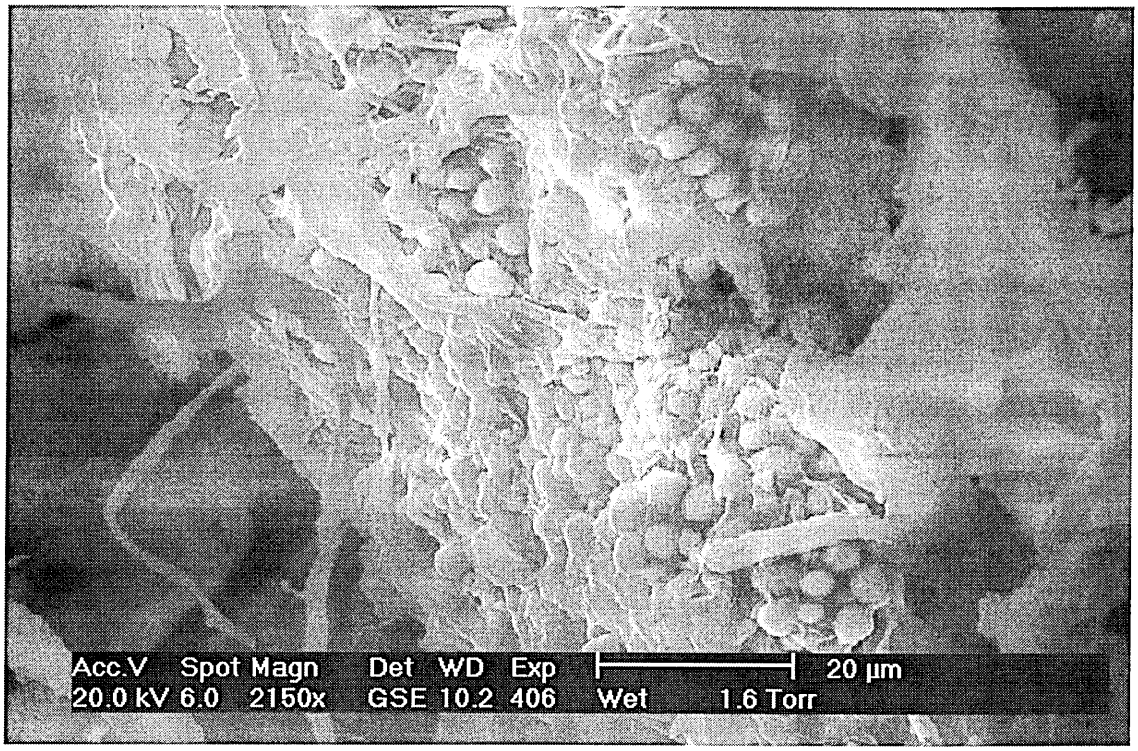

Figure 113 EDS spot analysis of beads on Ag saturated dealginate surface

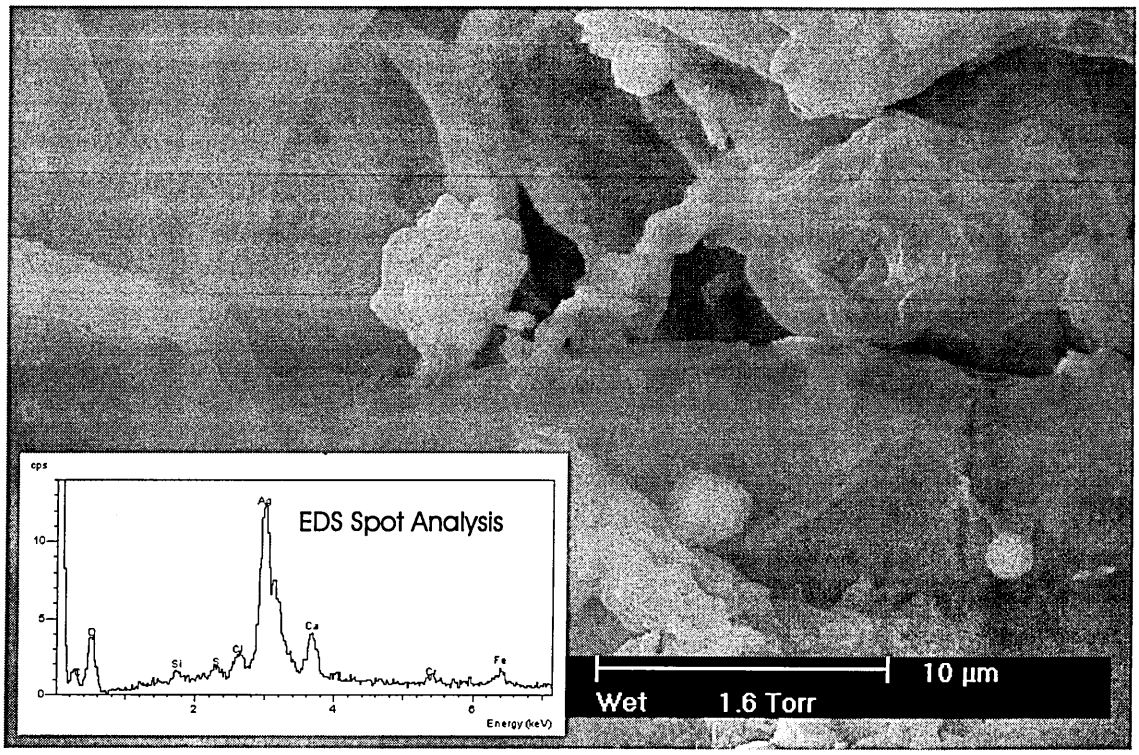

Figure 114 Se image and X-ray intensity elemental maps for Ag saturated dealginate

Acc.V	Spot	Magn	Det	WD	Exp
20 0 kV	6.0	800x	GSE	9 0	405

Figure 115 SE image of Al saturated dealginated seaweed surface

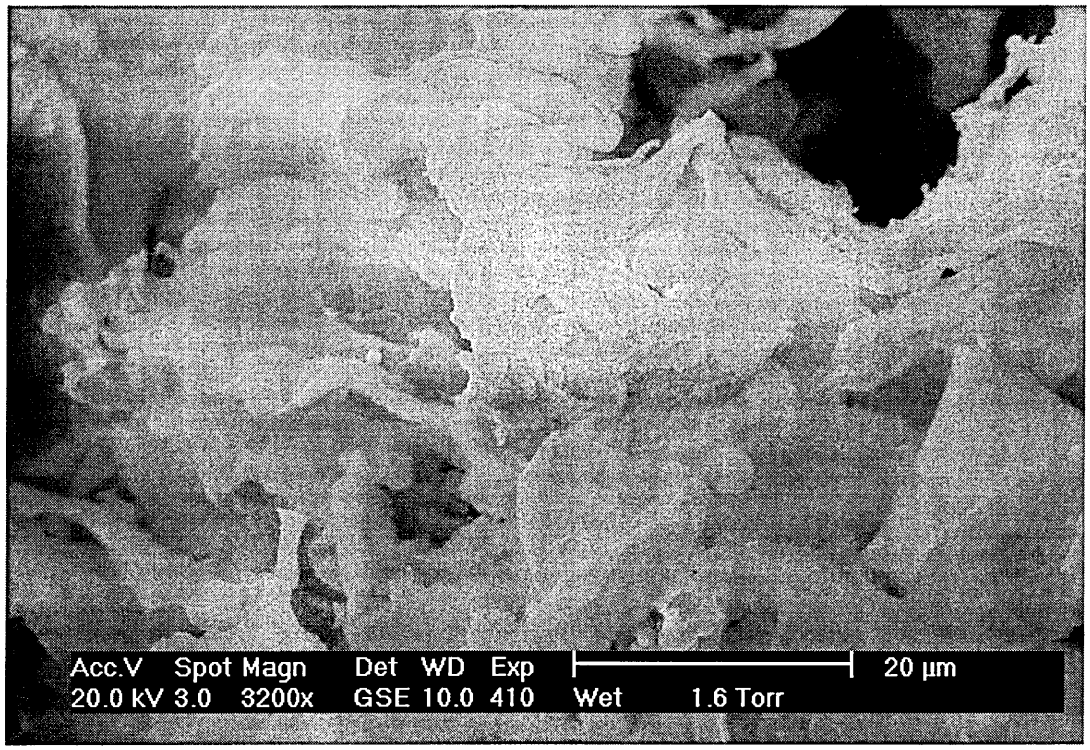

Figure 116 EDS spot analysis for Al saturated dealginate

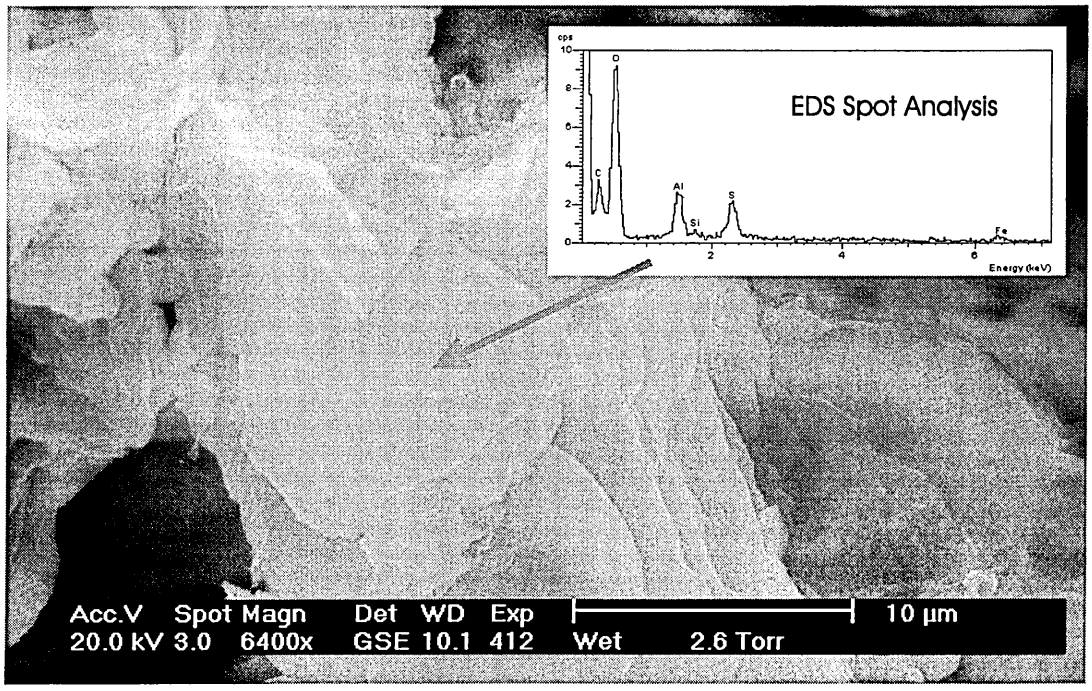

Figure 117 SE image and X-ray intensity elemental map for Al saturated dealginate

6.2.4. Gold

Examination of the Au saturated dealginate samples showed the deposition of Au particles on the biomass surface, as shown in Figure 118. No structural changes were observed on the dealginate surface, since the fibre type and the cell structures were still visible after contact with the Au solution (see Figure 119). However, the Au saturated dealginate sample was observed to be purple in colour.

Two types of Au deposits were found on the surface. Figure 120 shows the detail of one type of Au compound. Highly organised crystalline structures, with recognisable shapes were observed to be homogenously distributed over the surface. The other type of deposits can be seen in Figure 121. Round bead shaped precipitates, covering specific sites of the biosorbent surface were observed. EDS analysis of these structures showed that both contained high amounts of Au (see Figures 122 and 123).

Due to the visible presence of Au colloid on the surface, quantification analysis was made, revealing that Au was present in around 10% of the bulk sample. Table 23 shows the results for the elements analysed. No significant residues of elements present originally on the sample, as Na or K were found.

Table 23 Element composition of the Au saturated dealginate sample by EDS bulk analysis

Element	Element %
O	84
Si	2
Cl	2
Au	11

Figure 118 SE image of Au saturated dealginate seaweed surface

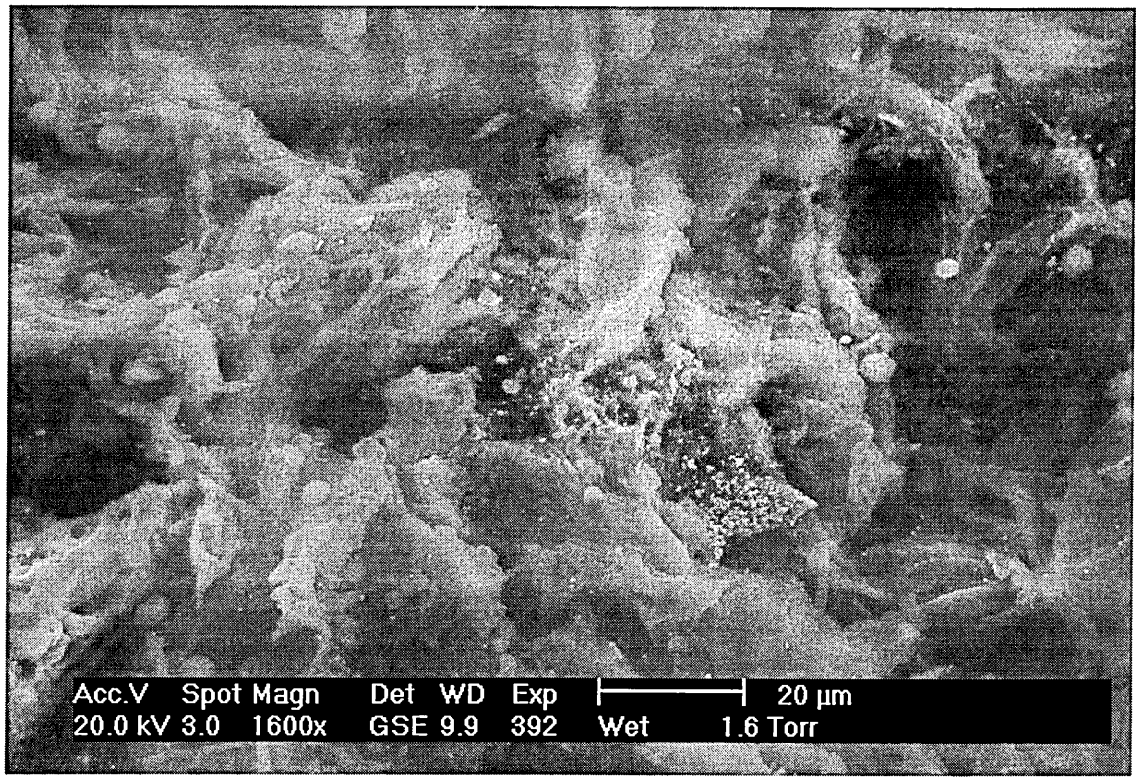

Figure 119 Detail of Au deposition on dealginated seaweed surface

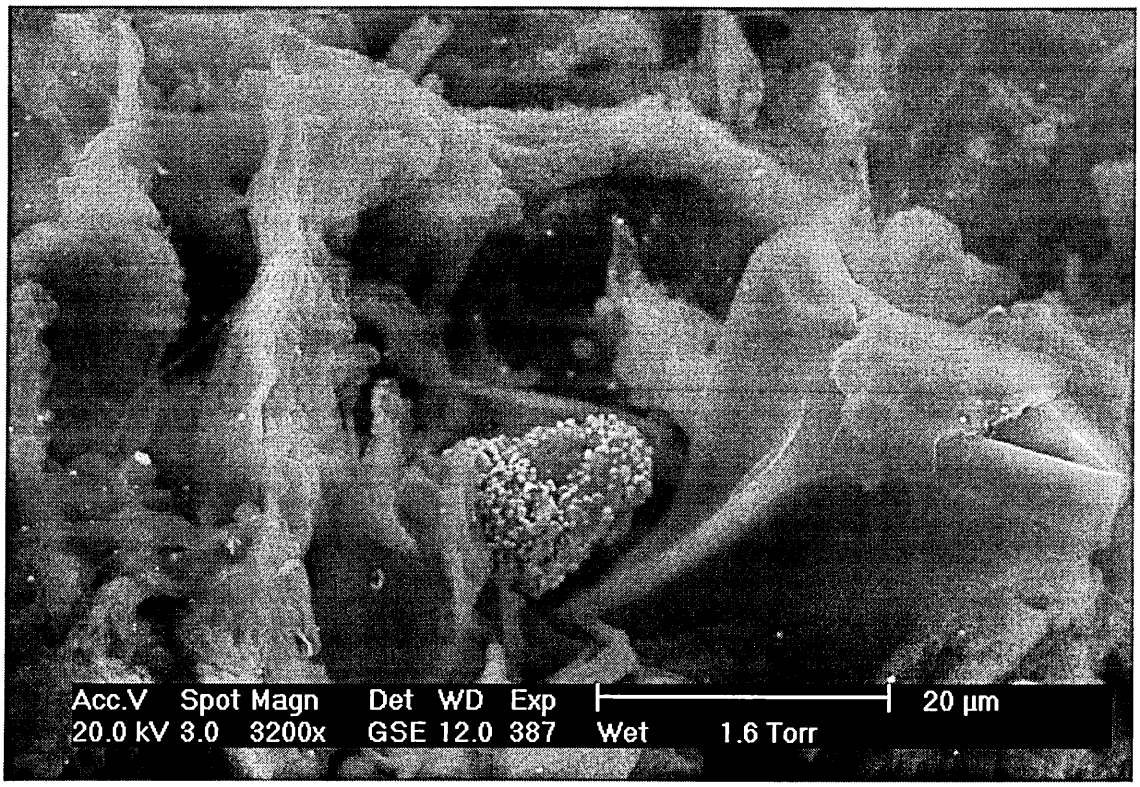

Figure 120 Au deposits on dealginate surface

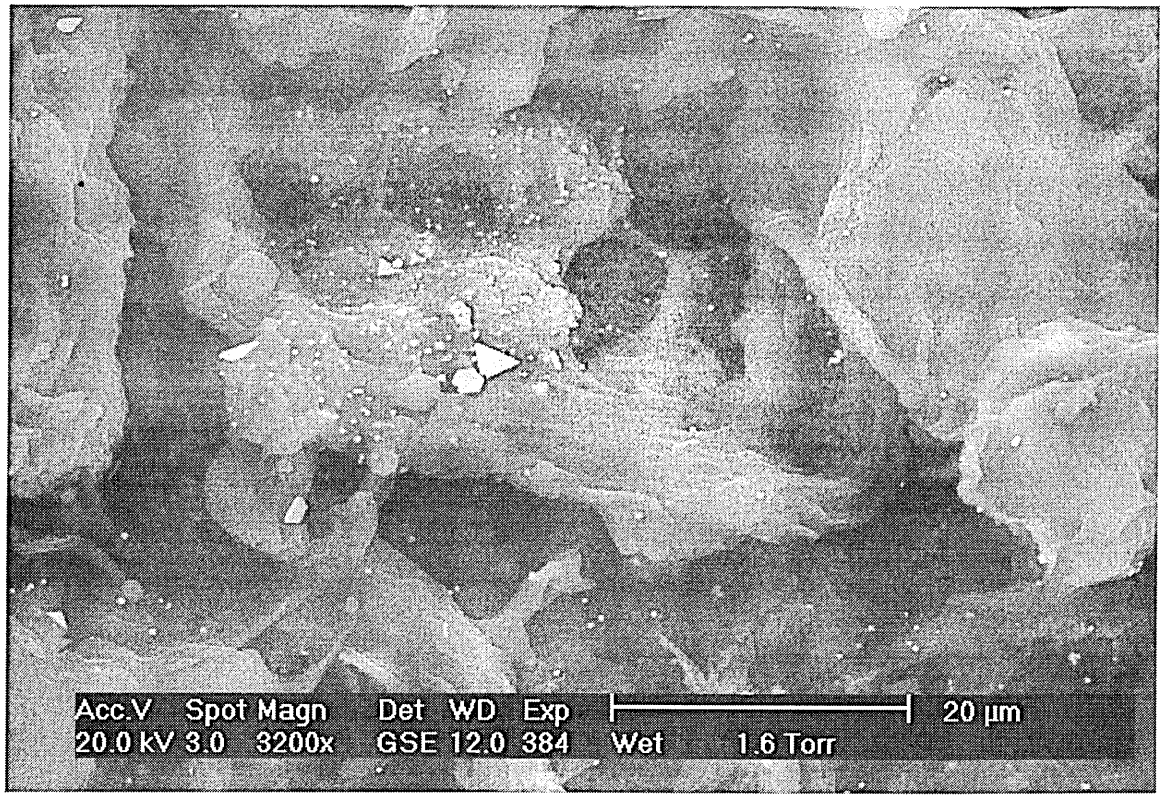

Figure 121 Au beads on dealginated seaweed surface

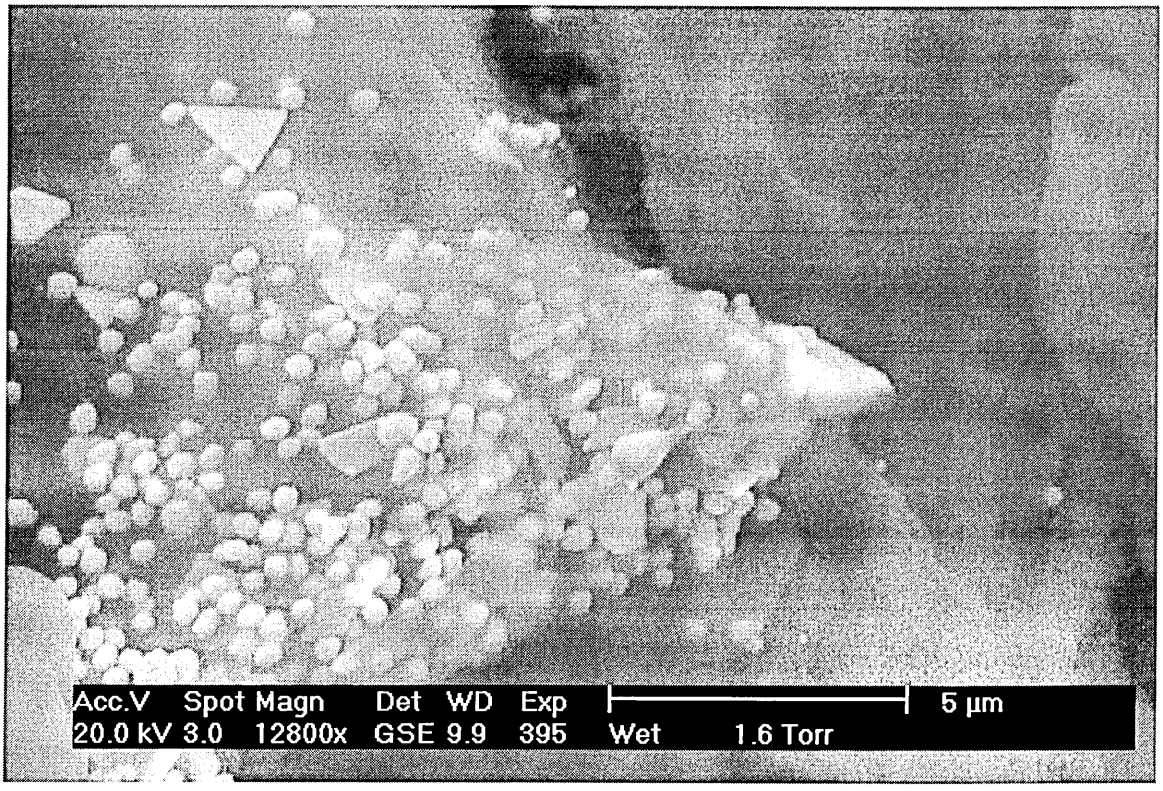

Figure 122 EDS analysis of Au deposits on dealginated seaweed surface

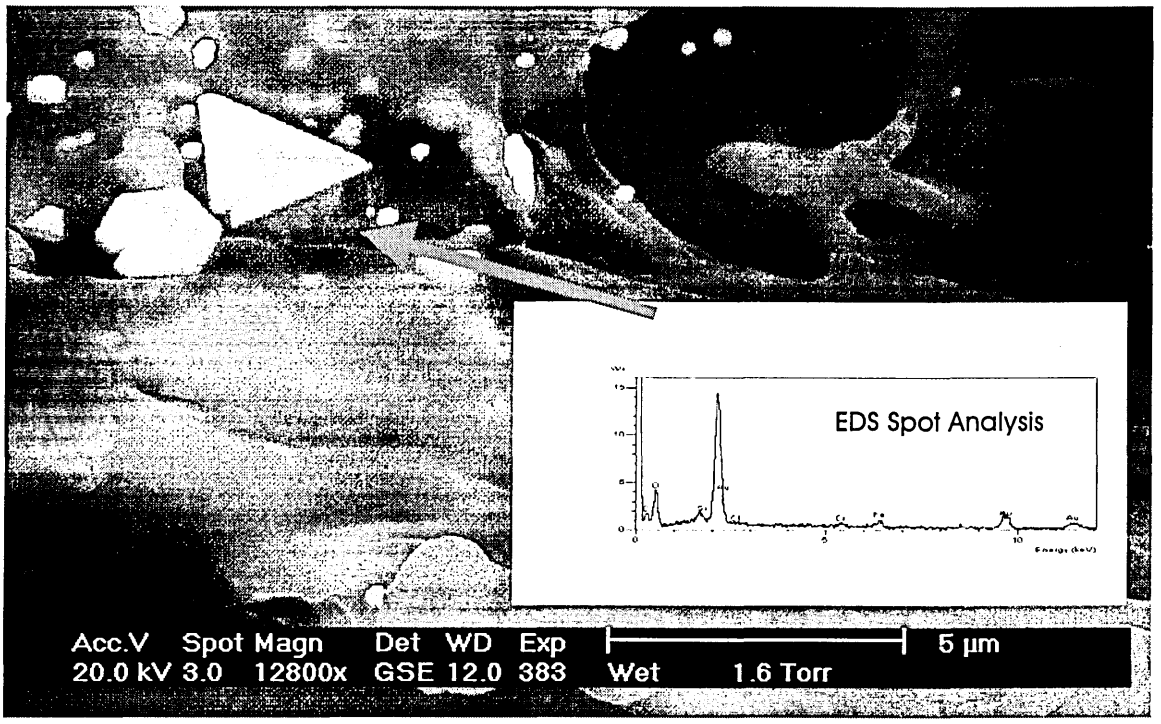

Figure 123 EDS analysis of Au beads on dealginated seaweed surface

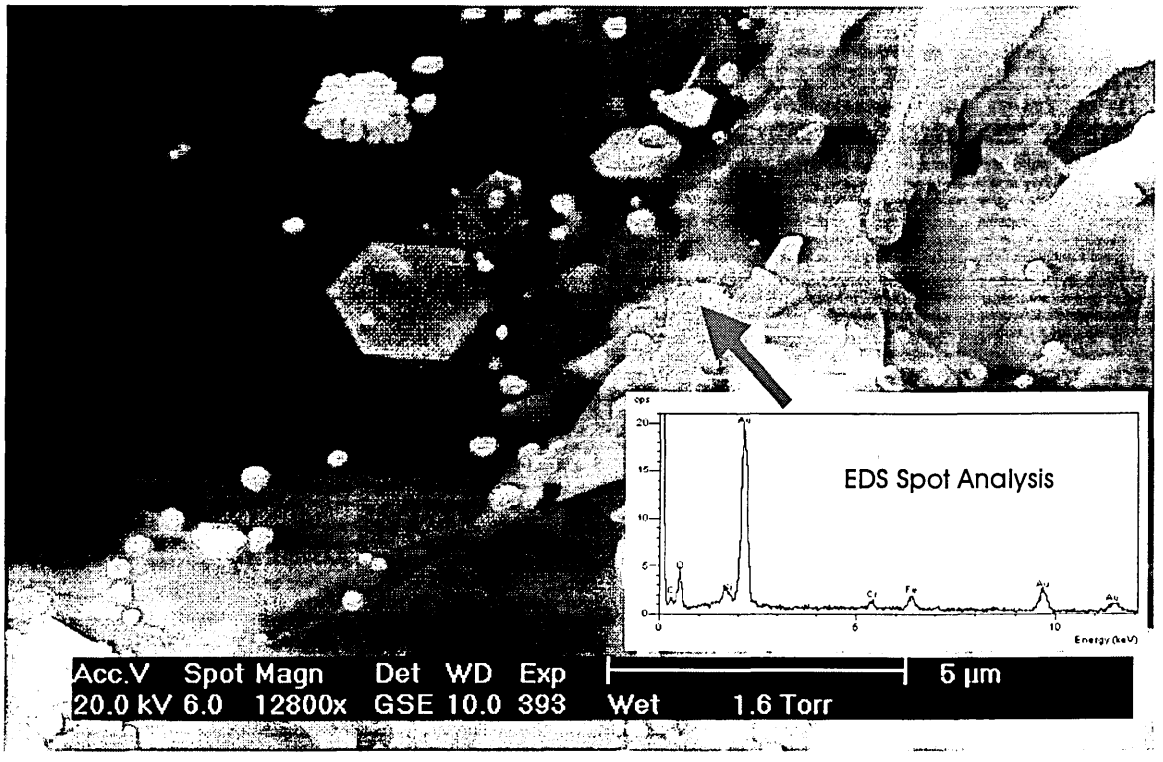

Two different areas of the Au saturated dealginate samples were scanned to produce X-ray elemental maps. Figure 124 shows the X-ray elemental intensity map for an area of the Au saturated dealginate sample which was mainly comprised of a mixture of the two types of Au particles described previously.

The bright colour on the maps indicated higher concentration of atoms in a certain area, which produced higher intensities during the X-ray analysis. The Au distribution in the sample was highly concentrated in the bottom right hand corner of the picture, where the bead type particles were located, as was clearly indicated by the concentration of bright red points on the X-ray bulk map. An attempt to correlate the presence of Au on the surface with that for other element studied was unsuccessful since no other map showed a similar distribution to that the Au map.

Figure 125 shows the map of an area predominantly formed by Au beads. The Au concentration in the map could be clearly compared to the Au particles in the micrograph. Of the other elements analysed, only S showed a similar distribution to the Au. This finding suggests the association between Au and S.

Siegge (159) reported that the definition of X-ray maps is limited at water vapour pressures required to keep the sample in a wet state. However, the results obtained here shows that the element mapping could be performed at pressures as low as 1.6 torr with high resolution.

Figure 124 SE image and X-ray intensity elemental maps for Au saturated dealginate

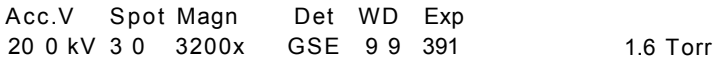

Figure 125 SE image and X-ray intensity elemental maps for Au saturated dealginate

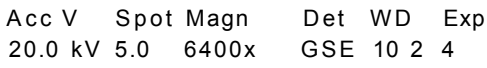

6.3. Analysis of Au saturated dealginate using Backscattered Electrons Detector

In order to complete the examination of Au on the dealginate surface, the sample was observed using the backscattered electron (BSE) imaging. Backscattered electrons are electrons emitted from the specimen at high energies and have been backscattered through angles approaching 180° within the sample. The yield of BSE varies monotonically with the atomic number, Z of the specimen; therefore, the number of BSE produced is greater than the number of SE (112).

Because of the yield of BSE varies with the atomic number of the element, its widely used for the determination of high atomic number elements. Au posses a high atomic number making it suitable for this type of study (112).

Figure 126 shows the SE image of an area of the Au saturated dealginate sample, which apparently shows no Au deposition on the surface, and only the biosorbent surface is observable. Although the SE image showed the biosorbent surface as being homogeneous, the same sample observed using BSE imaging revealed the presence of Au particles on the surface. Figure 127 clearly shows the bright Au particles on the surface of the dealginate. The phases are readily distinguished because the dealginate essentially formed by C, H and O produces significantly fewer backscattered electrons than the Au precipitates.

The detector allowed a more detailed study of the distribution of Au in the sample providing a convenient method of examining the distribution of the elements within dealginated seaweed. Figure 128 shows a different area that was not observed previously using the SE detector.

Figure 126 SE image of Au saturated dealginate seaweed

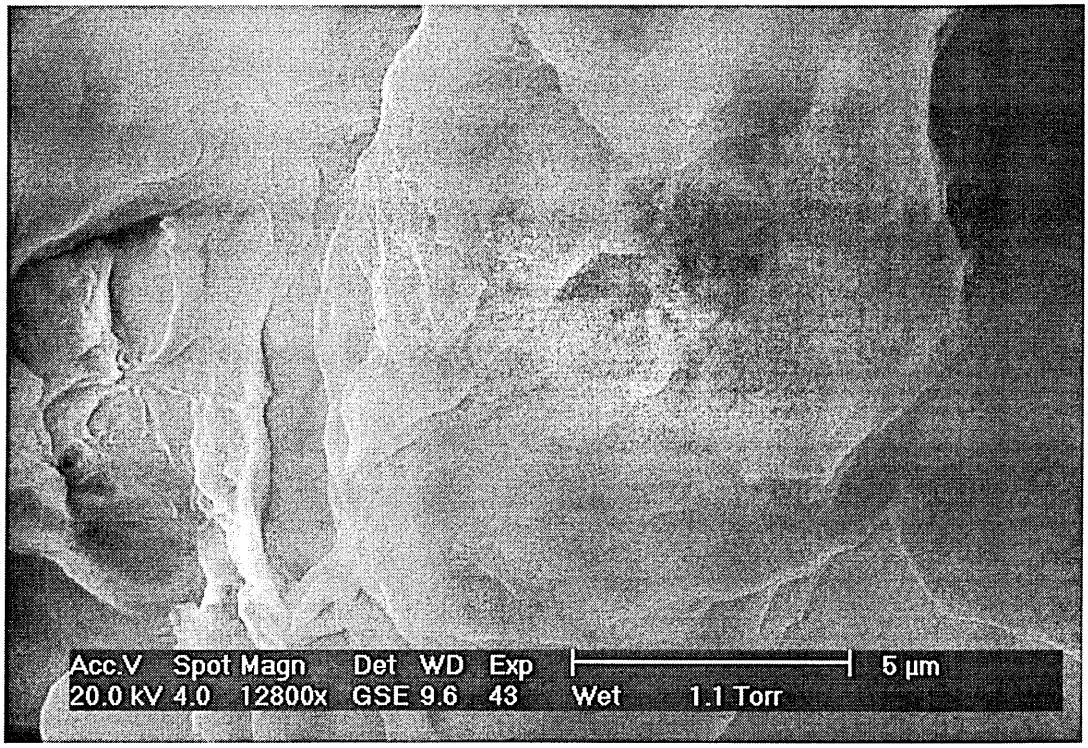

Figure 127 BSE image of Au saturated dealginated seaweed

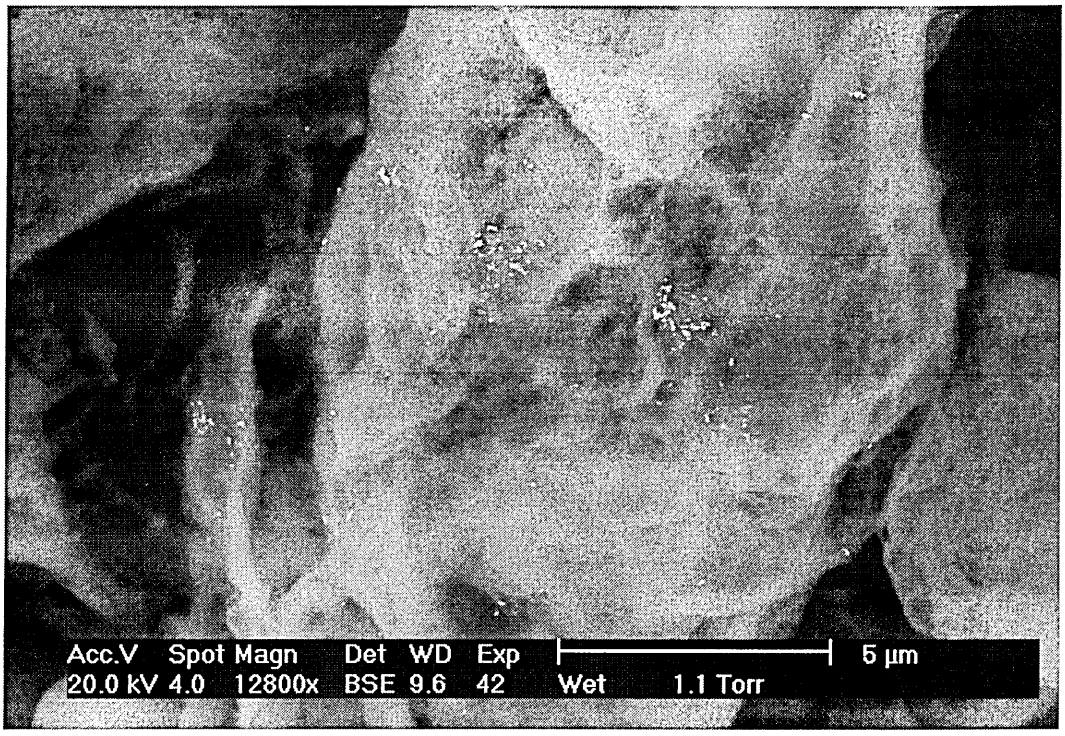

Figure 128 BSE image of Au layer on dealginate surface

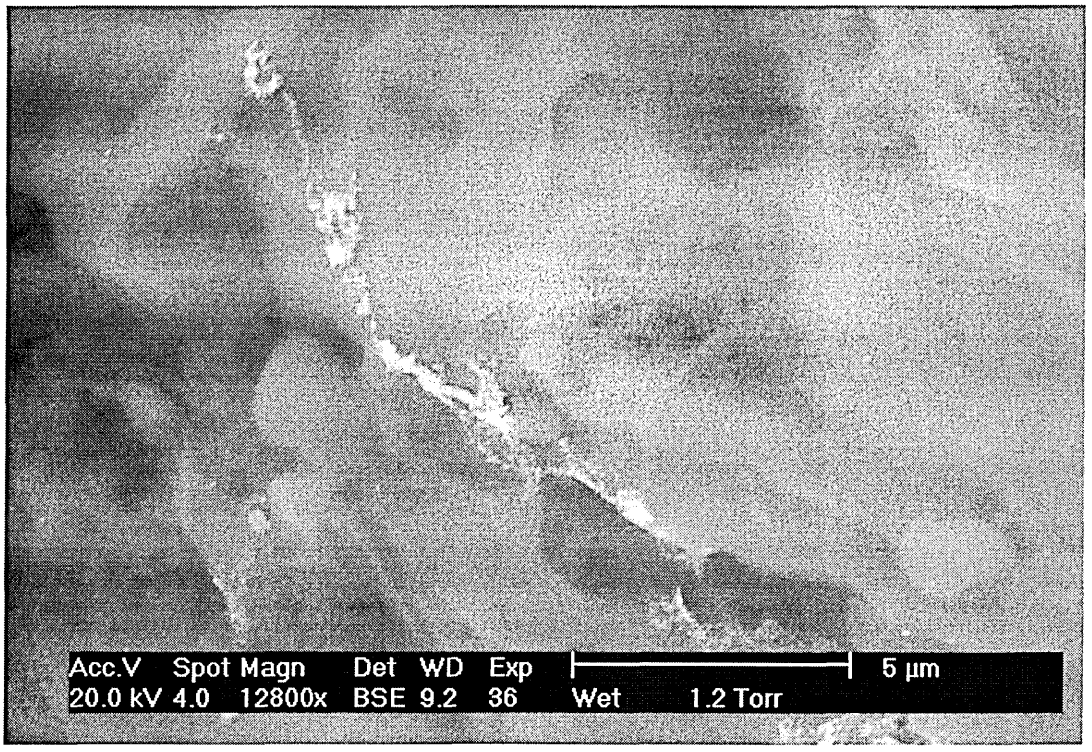

Figure 129 Detail of BSE image of Au layer on dealginated seaweed

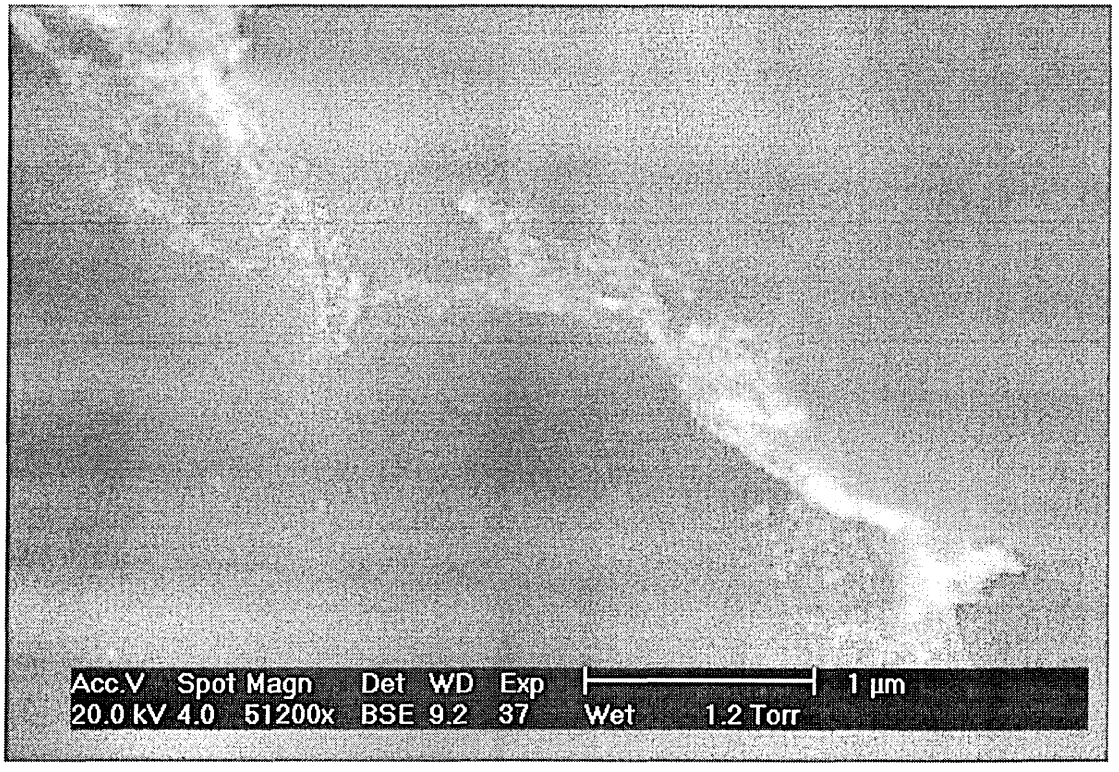

Au particles in this zone had not shown specific shapes, like the larger particles observed previously. Instead, Au seems to be laid down on the surface in a layer, coating the surface of certain areas of the biosorbent. A detailed image of the area can be seen in Figure 129, where the Au layer is clearly visible. By comparing the BSE image with the SE image, the binding locations can be unambiguously located. These findings suggested the possibility of a different mechanism of colloidal Au deposition on the surface.

6.4. Summary

The analysis of fully hydrated dealginated seaweed has shown that the application of environmental scanning electron microscopy for the characterisation of biosorbent surface is possible. The X-ray microanalysis quantitatively revealed the elemental content of the dealginate seaweed. Elemental mapping showed the distribution of the element on the dealginated surface. SE images observed in combination with elemental mapping, localised the binding sites on the dealginate surface. Results obtained by BSE images suggested that Au is bound to sites on the surface, as well as in the interior of the biosorbent.

Study of Dealginated Seaweed Binding Sites using X-ray Absorption Fine Structure (EXAFS) Spectroscopy

Chapter 7

7.1. Extended X-ray Absorption Fine Structure (EXAFS). Data analysis

The characterisation of the metal binding sites on dealginated seaweed was performed using the Extended X-ray absorption fine structure (EXAFS) technique.

EXAFS data was obtained using the synchrotron radiation source at CLRC Daresbury Laboratory. The data was calibrated, background-subtracted and analysed using the standard Daresbury packages EXCALIB, EXBACK and EXCURV98 respectively.

EXCALIB converts monochromator positions to X-ray energy and allows signals from poor detectors to be removed from the data. It is also used to sum spectra. EXBACK fits the pre- and post-edge regions of the spectra by low-order polynomials in the standard manner to extract the oscillatory EXAFS signal.

The package EXCURV98 utilises a least squares curve-fitting procedure to compare theoretical and experimental spectra with the structural parameters (distance, coordination number, Debye-Waller factor and atom type) as fitting parameters. The theoretical spectra were calculated using first curved wave theory (160). The Hedin-Lundquist exchange potential and the von Barth ground state potential were used in the calculation of scattering data within the programme. Multiple scattering (161) was included if deemed necessary. The standard metal foil was used to determine the amplitude reduction factor (AFAC), which should be close to unity for the potentials used (162). The programme also determines the uncertainties in the fitted parameters and whether a shell significantly improved the fit, using the Joyner (163) method. The uncertainties quoted here were always $\pm 2\sigma$ (95% confidence). All shells described improved the fit index significantly.

7.2. Metal Ions in solution by EXAFS

In order to understand the coordination binding of metal ions to dealginated seaweed, EXAFS data were collected for several diluted solutions, approximately 10 mM concentrations of single metal ion solution of Cd, Pb, Ni, Cu, Ag and Au. The results are shown in Table 24.

Gold exists as a complex ion, $AuCl_4^-$, and its behaviour was very different from the other metals studied. The other metals were found to exist in a very well ordered oxygen environment. The coordination of 5-10 oxygens is typical in aqueous solution and the metal-oxygen distances are similar to those found in solids.

Table 24 Bonding distances of metal-ligand in solution obtained by EXAFS analysis

Metal	Concentration (mM)	Charge	N	Type	R Å	σ^2 x10^{-4} Å^2	C_3 x10^{-4} Å^3
Cd	8	2^+	8.7 ± 1.8	O	2.26	120 ± 30	-100 ± 120
Pb	14	2^+	6.6 ± 4.6	O	2.51	340 ± 210	65 ± 10
Ni	33	2^+	6.9 ± 0.6	O	2.02	85 ± 10	10 ± 5
Cu	25	2^+	5.0 ± 0.5	O	1.96	85 ± 20	0 ± 4
Ag	8	1^+	4.9 ± 2.7	O	2.34	200 ± 120	10 ± 40
Au	5	3^+	4.0 ± 0.6	Cl	2.27	20 ± 10	—

The mean square variations in distance, σ^2, are very similar to those found in solid samples with ionic bonding, such as the solid salts, indicating similar bonding in solution. The third C_3, which measures the asymmetry of the distribution, was always consistent with zero. Thus, the nearest-neighbour peak is accurately Gaussian, suggesting that a harmonic oscillator potential is appropriate.

If a harmonic oscillator potential $v = \frac{1}{2}K(r - r_0)^2$ is used, then a classical analysis gives:

$$\sigma^2 = kT / k = kT / 4\pi^2 \mu \upsilon^2 \quad (27)$$

where ν is the stretch frequency. If the description is extended to calculate unharmonic terms, an analysis of the partition function gives:

$$v = \frac{1}{2}K(r - r_0)^2 + b(r - r_0)^3 \quad (28)$$

$$\sigma^2 = kT / K \quad C_3 = -6b(kT)^2 / K^3 = -6(b / k)\sigma^4 \quad (29)$$

Since $b/k \sim 1$ Å^{-1}, therefore the two terms in v are comparable, C_3 will only be significant for σ^2 values greater than about 0.1 Å^2. The results showed that C_3 was equal to zero, as was expected for this type of analysis, since σ^2 value is approximately 0.01 Å^2.

The results enabled the evaluation of the force constant K (in J m^{-2}) and hence the stretch frequency, ν, since the effective mass, μ is known. Taking μ to be the oxygen atomic mass, on the assumption that the heavy metal atoms do not move much, K was calculated for the metal studied. The results showed (see Table 25) that the force constants and the stretch frequencies were reasonable and were to be found in the far infrared region.

Table 25 Force constants and frequencies for the metals studied by EXAFS

Metal	σ^2 x10^{-4} Å^2	K J m^{-2}	K ev Å^{-2}	$\bar{\lambda}$ cm^{-1}
Cd	120 ± 30	35 ±10	2.5 ±0.7	190
Pb	340 ± 210	12 ± 8	0.8 ± 0.5	115
Ni	85 ± 10	50 ± 10	3.5 ± 0.7	220
Cu	85 ± 20	50 ± 15	3.5 ± 1.0	220
Ag	200 ± 120	20 ± 10	1.5 ± 0.7	140
Au	20 ± 10	200 ± 100	14 ± 17	300

7.3. Modelling the potential

In order to further understand these results, the potential was modelled. A steep repulsion, representing the atomic cores, in addition to a Coulomb attraction was used. Assuming a purely ionic bond, the potential may be written as:

$$V(r) = \frac{A}{r^n} - \frac{e^2}{4\pi t_0}\frac{Z_1 Z_Z}{t}\frac{1}{r} \quad (30)$$

Where: Z_1 = the metal ion charge

Z_Z = the oxygen (or chlorine) atom charge

t = mean dielectric function

To connect this to an oscillator model, the equilibrium separation r_o has to be expanded:

$$V(r) = V(r_0) + \frac{dV}{dr}\Big|r_0 (r - r_0) + \frac{1}{2}\frac{d^2V}{dr^2}\Big|r_0 (r - r_0)^2 + \frac{1}{6}\frac{d^3V}{dr^3}\Big|r_0 (r - r_0)^3 \ldots\ldots (31)$$

At $r = r_0$ $dV/dr = 0$. Thus,

$$\frac{dV}{dr} = -\frac{nA}{r^{n+1}} + \frac{e^2}{4\pi t_0}\frac{Z_1 Z_2}{t}\frac{1}{r^2} \qquad A = \frac{1}{n}\frac{e^2}{4\pi t_0}\frac{Z_1 Z_2}{t} r_0^{n+1} \quad (32)$$

$$V(r) = \frac{e^2}{4\pi t_0}\frac{Z_1 Z_2}{t}\left[\frac{r_0^{n-1}}{n r^n} - \frac{1}{r}\right] \quad (33)$$

It is then found:

$$\frac{d^2V}{dr^2}\Big|r_0 = k = \frac{e^2}{4\pi t_0}\frac{Z_1 Z_2}{t}\frac{(n-1)}{r_0^3} \quad (34)$$

$$\frac{d^3V}{dr^3}\Big|r_0 = 6b = -\frac{e^z}{4\pi t_0}\frac{Z_1Z_2}{t}\frac{(n+4)(n-1)}{r_0^4} \quad (35)$$

$$V(r_0) = \frac{e^z}{4\pi t_0}\frac{Z_1Z_2}{t}\frac{i-n}{nr_0} \approx -\frac{e^z}{4\pi t_0}\frac{Z_1Z_2}{t}\frac{1}{r_0}, \quad \text{n large} \quad (36)$$

The last formula shows that the bond strength is essentially equal to the Coulomb attraction at the equilibrium spacing. This also gives:

$$V(r_0) = -\frac{kr_0^2}{n-1} \quad b = -\frac{n+4}{6}\frac{k}{r_0} \quad (37)$$

The index of repulsion n is of order 10 therefore $b/a \sim -1$Å^{-1} as noted above for normal distances. Using the values of k and r_o given above, the values of ionic strengths for n=11 were calculated. The results are shown in Table 26.

Table 26 Bond strength for the metals studied

Metal	r_0 Å	K ev Å^{-2}	$V(r_0)$ ev	b ev Å^{-3}
Cd	2.26	2.5	1.3	2.8
Pb	2.51	0.8	0.5	0.5
Ni	2.02	3.5	1.4	4.3
Cu	1.96	3.5	1.35	4.5
Ag	2.34	1.5	0.85	1.6
Au	2.27	14	7.3	15

The bond strengths were all of the correct order. The value for Ag was weak since Z = 1, and the value for Pb was very low because Pb is a large atom. The Au-Cl value is large, perhaps due to the more complete ionisation of Cl atoms compared to O atoms in H_2O. The values of *b* for all the metals gave C_3 values, which were very small, in the order of 10 x 10^{-4} $Å^3$. The results found by the model were in good agreement with the findings from the EXAFS analysis, corroborating the structures previously proposed for the metals in solution.

7.4. Metal studies on Dealginated Seaweed

7.4.1. Cadmium

For all the samples studied, the edge step was calculated as:

$$\Delta\mu = \Delta\sigma \times nt \quad (38)$$

The structural parameters obtained by the data analysis appearing on the Tables in the following description of the EXAFS results are: *N*, which is the number of scattering atoms; the type of atom found; *r* is the distance at which the atom was found. The Debye-Waller factor σ^2 is the mean square variation in interatomic distance between the emitting and scattering atoms and FI is the fit index.

Transmission and fluorescence data were collected for Cd saturated dealginate samples without a monitor foil, because it was not available. The Cd K edge was studied. The edge steps observed for the three Cd dealginate samples were very similar. The metal mass calculated for the samples was similar as well, as can be seen in Table 27. A concentration value of 8 mM was found for the $Cd(NO_3)_2$ solution. The $\Delta\sigma$ used for Cd was 0.81 x 10^{-24} m^2 $atom^{-1}$ (164).

Table 27 Transmission edge steps for Cd samples on dealginated seaweed

Sample	$\Delta\mu$ (Cd)	nt (m-2)	t (μm)	n (m^{-3})	Mass ($mg\ cc^{-1}$)
Cd foil	1.0	1.23×10^{24}	25	4.9×10^{28}	9200
Cd solution	~0.002	2.5×10^{21}	500	5×10^{24}	1
Cd at pH 2	0.04	5×10^{22}	500	10×10^{25}	19
Cd at pH 6	0.04	$5x\ 10^{22}$	500	10×10^{25}	19
Cd esterified	0.06	7.5×10^{22}	500	14×10^{25}	28

Analysis of EXAFS data collected for Cd metal foil, $Cd(NO_3)_2$ solid and $Cd(NO_3)_2$ solution are shown in Table 28. The results obtained for the foil were comparable to the crystal structure, which shows 6 Cd atoms in a plane at 2.98 Å plus a further six out of plane atoms 3.21Å, although the precision for N and σ^2 was rather poor. The correlated Debye theory gave a value for σ^2 of 120 at temperature, θ_0 of 209 K. The data suggested 6 in-layer atoms with out-layer atoms being less well bound.

Table 28 EXAFS results for Cd foil, $Cd(NO_3)_2$ solid and solution

Sample	N	Atom type	r ± 0.02 Å	σ^2 10^{-4} Å^2	K_{max} Å^{-1}	E_F	FI
Cd foil	6 ± 3	Cd	2.97	120 ± 30	10	-10.9	7.0
	7 ± 6	Cd	3.21	260 ± 180	10	-10.9	
$Cd(NO_3)_2$ solid	7.1 ± 0.9	O	2.30	120 ± 20	10	-0.9	11.7
	6.6 ± 2.2	O	2.31	100 ± 70	10	-2.3	10.0
	0.9 ± 2.4	O	2.53	0 ± 150	10	-2.3	
$Cd(NO_3)_2$ solution	8.7 ± 1.8	O	2.26	120 ± 30	10	-2.3	27.2

The $Cd(NO_3)_2$ solid sample showed a significant split in the first shell. A coordination number of approximately 7 was found, which can be compared to the crystal structure: 6 O atoms at 2.26-2.43 Å and 2 O atoms at 2.59 Å. No evidence of N atoms at approximately 3.0 Å was observed, as in crystals. Two split 6 + 1 fits significantly better. A value of $\sigma^2 = 100 \times 10^{-24}$ m^2 was calculated, which corresponds to a Cd-O stretch frequency of 210 cm^{-1} if the full oxygen mass is used. The data for the $Cd(NO_3)_2$ solution showed no indication of splitting. A higher coordination number compared to the solid data was observed.

The EXAFS data collected for the Cd dealginate samples showed very good signal intensity. The results of the fitting analysis are shown in Tables 29 and 30. Three atom types were fitted for the Cd pH 2 sample: oxygen, carbon and nitrogen, all of them giving equally good fits. Sulphur atoms could not be fitted into the data. The distances found strongly suggest that an O atom is the nearest neighbour, if cadmium nitrate composition is to be considered. Other molecule distances, such as cyanide crystals give Cd-C at 2.10 Å and Cd-N at 2.20 Å. The difference with respect to these distances is slightly higher, therefore an O atom is considered to be the nearest neighbour.

Table 29 EXAFS results for Cd pH 2 samples

N	Atom type	r ± 0.02 Å	σ^2 10^{-4} Å^2	K_{max} Å^{-1}	E_F	FI
6.6 ± 0.6	O	2.29	140 ± 15	10	-4.0	6.5
9.0 ± 0.6	C	2.34	120 ± 10	10	-2.5	4.8
7.4 ± 0.5	N	2.32	120 ± 15	10	-3.2	5.2
7.6 ± 0.7	O	2.31	180 ± 20	10	-5.6	4.6
2.0 ± 1.1	C	2.66	50 ± 60	10	-5.6	
6	O	2.30	60 ± 5	10	-6.0	5.2
3	C	2.66	85 ± 30	10	-6.0	

Assuming oxygen as the nearest neighbour a second shell was fitted, which significantly improved the fit index, as can be seen in rows 4 and 5 of Table 29. The coordination therefore is 6 + 3, and it was found to be within experimental errors. The σ^2 values also improved, corresponding to a Cd-O stretch frequency of 270 cm^{-1}. These findings suggested an environment of three bidentated CO_2 units. Attempts were made to simulate the experimental spectrum by assuming a fixed coordination number of 6 + 3. The results obtained are shown in rows 6 and 7 of Table 29. The fit index was found to be slightly higher, but still comparable to the best fit. The calculated distances gave a good structure for three-fold symmetry, if the distance for C-O bound is 1.36 Å.

The data obtained for the Cd pH 6 sample were essentially the same as Cd pH 2 sample (see Table 30). The fitting of a second shell significantly improved the results. The C atom shell gave a low coordination number and σ^2 values, suggesting the 6 + 3 arrangement, as described in the previous sample.

Table 30 EXAFS results for Cd-dealginate samples

Sample	N	Atom type	R ± 0.02 Å	σ^2 10^{-4} Å^2	K_{max} Å^{-1}	E_F	FI
PH 6	5.6 ± 0.5	O	2.28	60 ± 10	10	-4.7	7.8
	5.8 ± 0.8	O	2.30	60 ± 15	10	-6.5	5.9
	1.5 ± 1.2	C	2.65	20 ± 50	10	-6.5	
esterified	6.4 ± 0.6	O	2.29	70 ± 10	10	-5.9	7.1
	6.5 ± 0.5	O	2.30	70 ± 15	10	-7.5	5.8
	3.0 ± 2.0	C	2.65	90 ± 90	10	-7.5	

In comparison with the two previous samples, the Cd esterified sample fitted better to a second atom shell, with significant improvement in the data. Again, a 6 + 3 structure was clearly observed (rows 5 and 6 of Table 30), corroborating the aforementioned results. The

Cd^{2+} ion exhibits a d^{10} configuration, which shows no stereochemical preferences from ligand field effects, allowing a variety of coordination numbers and geometries, based mainly on the importance of electrostatic forces, covalence and size factors. Because of its size, Cd^{2+} is more often found with a coordination number of 6 compared with other metals in the same group (127).

These findings indicated three fold symmetry for Cd surrounded by O atoms as nearest neighbour, bound to a C atom. Figure 100 depicts a possible structure for the Cd dealginate sample, based on the distances calculated using the EXAFS results. This indicates a slightly different outline with respect to the previously proposed structure shown in Figure 32 (Chapter 3.1). However, the assumption that the bonding is Cd-O-C remains essentially the same. The proposed angles were 62° and 118° for the O-Cd-O and O-C-O respectively, giving an octahedral geometry type structure. Structural analysis of the compound $Cd(CO_2CH_3)_2(H_2O)_2$ has shown that it contains acetate groups that are monatomically bridging (165). Therefore, the Cd binding mechanism by dealginated seaweed may be an ion-exchange type, with Cd being bound to the biosorbent surface by O atoms from carboxyl groups.

Figure 87 Proposed Cd-dealginate structure from EXAFS analysis.

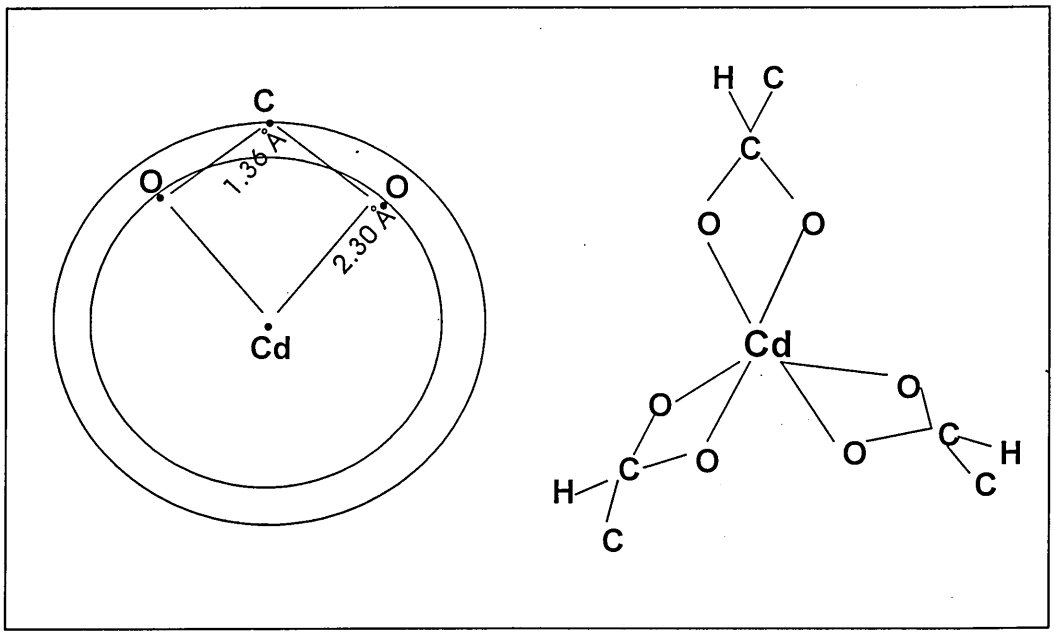

7.4.2. Lead

EXAFS data for Pb was collected in transmission and fluorescence mode using $Pb(CH_3COO)_2$ salt as a monitor, the Pb L_3 edge was studied.

The results for the transmission edge steps are shown in Table 31. Samples showed an absorption edge for Br in dealginated seaweed. The $\Delta\sigma$ value from tables (164) was 3.5×10^{-24} and 1.8×10^{-24} m^2 $atom^{-1}$ for Pb and Br respectively. The edge step of Br was used to approximately correct for peak differences, assuming that is a constant amount. The concentration of the $Pb(CH_3COO)_2$ sample was determined to be 14 mM.

All three samples showed similar metal masses. The edges showed similar values between the Pb dealginate samples and similar values when compared to the Pb solution sample. The three Pb dealginate samples showed an edge shift of –1.7 eV relative to the solid Pb acetate. The main transition for the L_3 edge is p $\rightarrow$ d, which is largely independent of the charge state.

Table 31 Transmission edge steps for Pb samples on dealginated seaweed

Sample	Δμ (Pb)	Δμ (Br)	Δμ (Pb) scaled	nt (m-2)	N (m^{-3})	Mass (mg cc^{-1})
$Pb(CH_3COOH)_2$	0.015	–	0.015	$0.43x10^{22}$	$0.086x10^{26}$	3
Pb at pH 2	0.18	0.01	0.18	5.1	1.02	35
Pb at pH 6	0.19	0.01	0.17	4.9	0.98	34
Pb esterified	0.04	0.006	0.07	2.0	0.40	14
Br		0.01		0.55	0.11	1.5

Analysis of the transmission spectra collected for $Pb(CH_3COO)_2$ showed that there are presumably two nearest neighbours for Pb^{2+} and two acetate ions were present. Table 32 indicates the possibility that two O atoms are present in the environment. The value of σ^2 was as expected, corresponding to $\bar{\lambda}$ ~ 140 cm^{-1}. The fit was improved by splitting the shell into two distances. This procedure showed the presence of one O atom each time (see Table 32). The new $\bar{\lambda}$ values calculated were 270 and 210 cm^{-1} respectively. Two further light atom shells could be fitted at 3.5 Å and 3.8 Å, lowering the fit index significantly. These results are in good agreement with X-ray diffraction data reported for basic Pb acetate compounds (166).

Table 32 EXAFS results for $Pb(CH_3COO)_2$ solid and solution

Sample	N	Atom type	r ± 0.02 Å	σ^2 10^{-4} Å^2	K_{max} Å^{-1}	E_F	FI
$Pb(CH_3COOH)_2$ solid	1.6 ± 0.6	O	2.34	220 ± 90	8	-0.1	54.5
	1	O	2.29	60 ± 25	8	-1.9	38.8
	1	O	2.57	100 ± 50	8	-1.9	
$Pb(CH_3COOH)_2$ solution	6.6 ± 4.6	O	2.51	340 ± 210	8	2.5	88.8

Fluorescence scans similar to those for solids were taken for Pb acetate in solution. The results (Table 32) showed higher Pb-O bond lengths compared to the solid. Ionic radii from a high coordination number crystal gives a Pb-O distance value of 2.52 Å, suggesting that the increase in the bond length value observed may be a higher coordination number effect. Pb often has a distorted oxygen environment. A 4+2 split fits at distances of 2.31 Å and 2.56 Å with no significant improvement in fit index. σ^2 for single shell fit implies RMS deviation σ = 0.18 Å, suggesting around 6 atoms spread between 2.33 and 2.69 Å, very similar to two shell fit.

Data from the Pb at pH 2 transmission spectra showed a clear improvement with a split shell. Two clear peaks are visible in the Fourier Transform. The use of an asymmetric single peak gave no improvement in fit index. The values in the last two rows in Table 33 clearly showed a 4+2 light atom environment, suggesting the presence of 6 neighbours.

Table 33 EXAFS results for Pb pH 2 sample

N	Atom type	r ± 0.02 Å	σ^2 10^{-4} Å^2	K_{max} Å^{-1}	E_F	FI
5.7 ± 1.3	O	2.41	310 ± 60	8	13.8	27.1
4.4 ± 2.0	O	2.50	200 ± 130	8	5.9	20.6
1.4 ± 1.6	O	2.79	40 ± 120	8	5.9	
4	O	2.50	180 ± 20	8	4.8	22.5
2	O	2.78	90 ± 25	8	4.8	

The Pb at pH 6 sample showed a constant presence of four neighbours (see Table 34), clearly confirmed from the asymmetric or split peak. No other peaks were observed on the Fourier Transform. The split peak has mean radii of 2.52 Å while the asymmetric peak has mean radii of 2.61 Å, suggesting the presence of four light atoms in a moderately asymmetric peak.

Table 34 EXAFS results for Pb pH 6 sample

N	Atom type	r ± 0.02 Å	σ^2 10^{-4} Å^2	K_{max} Å^{-1}	E_F	FI
3.2 ± 0.8	O	2.47	240 ± 70	8	0.2	37.0
0.9 ± 6.0	O	2.37	70 ± 900	8	-1.2	27.0
2.7 ± 8.2	O	2.59	480 ± 1800	8	-1.2	
3.1	O	2.61	220 ± 40	8	-2.6	23.7

EXAFS results for the Pb esterified sample are shown in Table 31. A second weak peak was observed in the Fourier transform. The degree of fit based on the asymmetric or split peak gave improved results. It can be seen that the structure was essentially identical to Pb pH 6, with approximately four light atoms being present in a moderately asymmetric peak.

Most divalent Pb complexes exhibit octahedral geometry for a coordination number 6 and square planar geometry for coordination number 4 although other geometries can be achieved with particular ligands. The structure of the Pb binding could be similar to that proposed for Cd.

7.4.3. Nickel

Transmission and fluorescence data for Ni K edge were collected. The results obtained for transmission edge steps are shown in Table 35. The amount of Ni present in the pH 6 sample was considerably lower compared to the amount of Ni at pH 2 and in the esterified samples. The absorption edges were similar for the three samples, and a shift of approximately 2.3 eV from Ni foil was calculated. The concentration of the $Ni(NO_3)_2$ solution was 33 mM, and $\Delta\sigma$ value from tables was 2.9×10^{-24} m^2 $atom^{-1}$ (164).

Analysis of EXAFS data for Ni metal foil (Table 36) showed that the distances for Ni were as expected, with an average of 11 neighbours when AFAC 1.0 was used for the calculation.

Table 35 Transmission edge steps for Ni samples on dealginated seaweed

Sample	$\Delta\mu$ (Ni)	nt (m-2)	T (μm)	n (m^{-3})	Mass (mg cc^{-1})
Ni foil	1.25	4.3×10^{23}	5	0.9×10^{28}	9000
Ni solution	0.03	0.1×10^{23}	500	0.02×10^{29}	2
Ni at pH 2	0.25	0.86×10^{23}	500	0.17×10^{27}	17
Ni at pH 6	0.05	0.17×10^{23}	500	0.034×10^{27}	3.4
Ni esterified	0.15	0.52×10^{23}	500	0.10×10^{27}	10

The analysis was improved when AFAC 0.92 was employed (see Table 36), giving approximately 12 neighbours surrounding the Ni environment and a reduction of the fitting index from 25.6 to 6.4. Since the results were improved using AFAC 0.92, this value was used throughout the rest of the calculation. The correlated Debye theory gave a σ^2 value of 70 x 10^{-24} m^2 for the first shell, rising to 100 x 10^{-24} m^2 for the most distant shell.

Table 36 EXAFS results for Ni foil, $Ni(NO_3)_2$ solid and solution

Sample	N	Atom type	r ± 0.02 Å	σ^2 10^{-4} Å^2	K_{max} Å^{-1}	E_F	FI
Ni foil							
AFAC 0.1	11.0 ± 2.4	Ni	2.47	65 ± 15	15	-10.9	25.6
AFAC 0.92	11.9 ± 0.4	Ni	3.48	65 ± 5	15	-11.1	6.4
	6	Ni	3.48	120 ± 35	15	-11.1	
	24	Ni	4.33	100 ± 10	15	-11.1	
	11.9 ± 0.4	Ni	4.98	75 ± 20	15	-11.1	
$Ni(NO_3)_2$ solid	6.4 ± 0.5	O	2.03	80 ± 10	12	3.7	6.9
$Ni(NO_3)_2$ solution	6.9 ± 0.6	O	2.02	85 ± 10	12	5.9	8.1
	6	O	2.05	75 ± 10	12	4.7	8.5
	6	O	2.06	75 ± 10	12	3.3	7.7
Single scattering	6	O	2.05	75 ± 10	12	4.7	8.5
O_h multiple scattering	6	O	2.06	75 ± 10	12	4.7	7.7

In the case of $Ni(NO_3)_2$ solid, a prominent peak at 4.5 Å was observed. XRD measurements show 6 oxygens at 2.06 Å or 2.08 Å for hydrated crystals, which can be compared to the value of 2.03 Å found for this sample. A value of λ of 240 cm^{-1} was determined when the total oxygen mass was used. A well-ordered environment was found for the Ni solution. The value of σ^2 determined was similar to that calculated for the solid sample. A significant peak was found at 4.5 Å, although this was much weaker compared to the solid sample. This peak gave rise to a characteristic shape around 3 Å^{-1} in the spectrum, which was visible in all spectra described

here. This peak was considered to be long for a second neighbour contribution, and could not be fitted. The presence of the peak might be due to a multiple scattering path of the type Ni-O-Ni-O-Ni with forward scattering through the central atom. A centro-symmetric Ni site is the only possible explanation for this effect, giving a regular octahedral geometry for O_h point group.

The data was improved by fitting a defined cluster for O_h symmetry, with the coordination number fixed at 6. The results were found to be significant, showing a good peak at 4.5 Å and a very good shape at approximately 3 $Å^{-1}$ in the spectrum. These findings suggested a well-ordered octahedral Ni environment as is found in the solid nitrate salt.

The most common geometry for Ni complexes at a coordination number 6, as observed for Ni solid and Ni solution samples is octahedral (127). The $Ni(NO_3)_2$ salt occurs most commonly as the hydrate, containing the green hexaaquanickel (II) ion in an octahedral environment. Tienmann *et al.* (80) reported similar results to those illustrated before, the fitting of 6 O atoms at 2.05 Å for the $Ni(H_2O)_6(NO_3)_2$ complex, but no further peaks or shells were described.

EXAFS results for the Ni-dealginate samples are shown in Table 37. There were marked differences in the edges between the samples and compared to the $Ni(NO_3)_2$ samples that may be attributed to differences in symmetry.

Ni in the pH 2 sample was fitted in three different atom type environments: oxygen, nitrogen and sulphur. The distances found for S atoms were too long to consider this type of atom as the nearest neighbour. The presence of four O atoms at 2.04 Å was observed. Although the bond lengths suggested oxygen as the nearest neighbour, N cannot be discarded since σ^2 corresponds to stretch frequency λ of 240 cm^{-1}. No evidence for further shells at 2.5 – 3.0 Å was found. A significant peak at approximately 4.5 Å was observed, as for the Ni solid sample.

This peak can be fitted well by including multiple scattering in C_{4h} cluster, as can be seen in rows 4 and 5 of Table 37. The fitting index was significantly lower compared to the single scattering, strongly suggesting a square planar Ni environment.

The planar geometry is preferred for the majority of four-coordinated Ni complexes, due to the d^8 configuration of this element. The planar ligand set causes one of the d orbitals to be high in energy leaving the remaining eight electrons to occupy the other four d orbitals, giving it preference over the tetrahedral geometry (127).

Table 37 EXAFS results for Ni-dealginate samples

Sample	N	Atom type	r ± 0.02 Å	σ^2 10^{-4} Å^2	K_{max} Å^{-1}	E_F	FI
pH 2	4.0 ± 0.3	O	2.04	75 ± 10	12	-0.4	7.1
	4.6 ± 0.3	N	2.07	70 ± 10	12	0.6	6.8
	8 ± 1	S	2.21	200 ± 25	12	13.5	13.3
Single scattering	4	O	2.04	80 ± 5	12	0.3	6.9
C_{4h}	4	O	2.05	80 ± 5	12	-0.5	5.1
pH 6	5.2 ± 0.7	O	2.05	80 ± 20	12	-0.2	15.3
esterified	4.9 ± 0.4	O	2.05	80 ± 10	12	-0.6	7.8
Single scattering	6	O	2.05	115 ± 10	12	0.6	9.3
O_h cluster	6	O	2.06	120 ± 10	12	-1.1	8.5
Single scattering	4	O	2.05	65 ± 10	12	-0.3	8.6
D_{4h} cluster	4	O	2.05	65 ± 10	12	-1.1	6.4

The data for the Ni pH 6 sample showed that Ni is surrounded by five O atoms at 2.05 Å. A significant peak at 4.5 Å was also observed as well for the Ni pH 6 sample. This peak fitted well with multiple scattering, giving a coordination number 5. This coordination number implies that Ni is embedded in a square planar environment, with the presence of one O atom above the plane.

The Ni esterified dealginate showed approximately five O atoms as nearest neighbour, located at 2.05 Å. A similar peak at 4.5 Å was observed for this set of data. There was no evidence of a further shell between 2.5 and 3.0 Å. Single scattering fits suggest first shell coordination of five atoms. Attempts made to fit the peak at 4.5 Å resulted in data fitted by defining cluster, including multiple scattering. The 4.5 Å peak was best fitted with a D_{4h} cluster (index fit of 6.4) implying a most likely square planar Ni with one additional O atom above the plane, as was found for Ni pH 6 sample. The symmetry is possibly C_{4v}. This conformation clearly differs from the results found for the Ni pH 2 sample.

For coordination number 5, the Ni complex tends to adopt the trigonal bipyramidal geometry, but a number of square pyramidal complexes occur as well (127). Cyanide salts of Ni ions usually adopt the square pyramidal geometry, and a number of five-coordinated complexes with weak field oxygen ligands have been described to form square pyramidal high-spin complexes. Figure 88 depicts the proposed geometry for Ni at pH 2 and pH6 and Ni in the esterified sample, based on the EXAFS results. Tienmann *et al.* (80) found no other shell could be fitted to complete the picture, but assumptions based on previous findings of this study indicate that a C atom is the nearest neighbour to the O atom. In addition in Ni acetate complexes containing unidentate acetate ligands, no forming bridges have been described (167), making this type of structure the most probable.

Figure 88 Proposed Ni-dealginate structure from EXAFS analysis

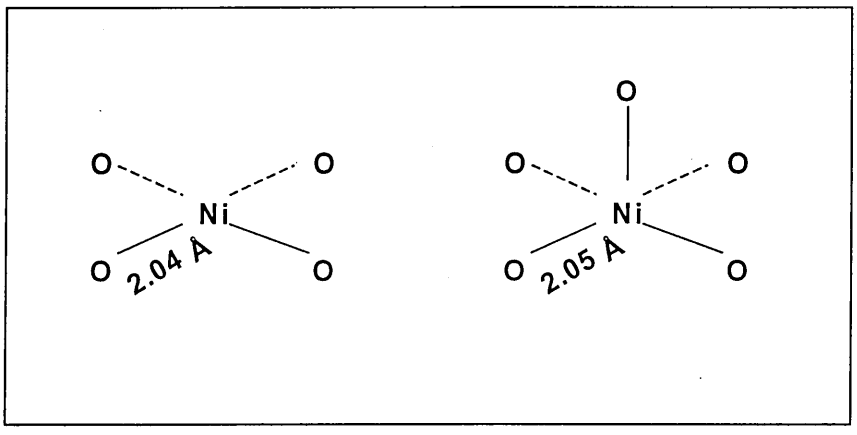

7.4.4. Copper

EXAFS transmission and fluorescence data for Cu K edge was collected using a Cu foil as a monitor. The absorption edges showed significant variation in edge shape, although the edge shape and the white line height were similar for the three Ni dealginate samples. A similar metal content was found for all the samples (see Table 38). The concentration of Cu solution was 25 mM and the $\Delta\sigma^2$ value used was 2.7×10^{-24} m^2 $atom^{-1}$ (164).

Table 38 Transmission edge steps for Cu dealginated seaweed samples

Sample	$\Delta\mu$ (Cu)	Nt (m-2)	t (μm)	n (m^{-3})	Mass (mg cc^{-1})
Cu foil	1.05	3.9×10^{23}	5	7.8×10^{28}	8500
Cu solution	0.00	0.74×10^{22}	500	1.5×10^{25}	1.6
Cu at pH 2	0.25	9.3×10^{22}	500	19×10^{25}	20
Cu at pH 6	0.25	9.3×10^{22}	500	19×10^{25}	20
Cu esterified	0.14	5.2×10^{22}	500	10.4×10^{25}	11

The single transmission spectrum for the 5 μm Cu foil gave good distances and scattering parameters (see Table 39). When an AFAC value of 1.0 was used the correct coordination numbers of 12, 6 and 24 for Cu-Cu interactions were produced, therefore, this value was used for subsequent analysis. The correlated Debye theory gave a σ^2 value of 77×10^{-24} m^{-2} for the first shell, rising to 115×10^{-24} m^{-2} for the distant shells.

The EXAFS data collected for the $Cu(NO_3)_2$ solid was good, but produced low coordination symmetry. This low coordination could be a result of a poor background subtraction during the transforming process. The crystal has four O atoms in a square planar configuration located at 1.96 Å (see Table 39).

The results showed no improvement when coordination number value was fixed to four atoms, but if multiple scattering is included in the calculations, a square planar, D_{4h} symmetry type structure is observed. The fit index value obtained is 16.1 and a good peak appears at approximately 3.8 Å. No evidence for other significant shells was observed. The coordination number 4 is often found in Cu(II) complexes (127). Although the d^9 configuration makes Cu (II) subject to the Jahn-Teller effect if placed in a regular octahedral or tetrahedral environment, with a few exceptions is not very often observed in these environments.

Furthermore, the $Cu(NO_3)_2$ salt cannot be fully dehydrated and two different forms of the solid can exist, both possessing complex structures in which Cu(II) ions are linked together by nitrate ions in an infinite array.

Table 39 EXAFS results for Cu foil, $Cu(NO_3)_2$ solid and solution

Sample	N	Atom type	r ± 0.02 Å	σ^2 10^{-4} Å^2	K_{max} Å^{-1}	E_F	FI
Cu foil	11.5 ± 1.4	Cu	2.54	90 ± 10	15	-14.2	8.2
	6	Cu	3.60	120 ± 30	15	-14.2	
	24	Cu	4.46	120 ± 10	15	-14.2	
	11.5 ± 1.4	Cu	5.00	90 ± 120	15	-14.2	
$Cu(NO_3)_2$ solid	2.4 ± 0.3	O	1.97	90 ± 15	11.5	-12.6	12.3
	4	O	1.96	120 ± 15	11.5	-11.1	18.0
	4	O	1.96	120 ± 15	11.5	-11.0	16.1
$Cu(NO_3)_2$ solution	5.0 ± 0.5	O	1.96	85 ± 20	11.5	-10.9	11.4
	6	O	1.96	110 ± 20	11.5	-10.5	12.7
	6	O	1.97	115 ± 20	11.5	-10.5	

The results for $Cu(NO_3)_2$ solution sample produced a good value for σ^2 when five O atoms were fitted at 1.96 Å, suggesting a coordination number 5 (see Table 35). No improvement was observed when coordination number 6 was used, or by adding multiple scattering to the

calculation, with observed values of fit index of 11.4, 12.7 and 12.8 for the three analyses. The peak in Fourier transform at approximately 3.8 Å was not observed for this set of data, suggesting the possibility of five fold coordination with no definite centro-symmetric unit.

Copper salts are soluble in water forming the hexaaquocopper (II) ion. Successive additions of ligands leads to the formation of complexes by displacement of water molecules. As observed for the ammonia complexes, that four molecules are bound to Cu in the normal way, the fifth molecule is possible in aqueous solution, but the addition of the sixth molecule occurs under extreme conditions, showing that with Cu 5 and 6 coordination number are possible. This behaviour is caused by the Jahn-Teller effect, because the Cu does not bind the fifth or sixth ligand very strongly (127).

The EXAFS results for the three Cu dealginate samples studied are shown in Table 40. A very well ordered environment without any sign of asymmetry was observed for the pH 2 sample, showing four O atoms at 1.95 Å. A small value of σ^2, corresponding to λ of 280 cm^{-1} was established. Because the calculated bond lengths strongly suggested an O atom as the nearest neighbour, it was not necessary to include other metals in the fitting. A strong peak was observed at approximately 3.8 Å.

Table 40 EXAFS results for Cu-dealginate samples

Sample	N	Atom type	R Å	σ^2 10^{-4} Å^2	K_{max} Å^{-1}	E_F	R ± 0.02 Å
pH 2	3.9 ± 0.3	O	1.95	60 ± 10	11.5	-11.4	6.9
	4	O	1.95	60 ± 5	11.5	-11.3	6.9
	4	O	1.95	60 ± 5	11.5	-11.2	4.9
pH 6	3.7 ± 0.2	O	1.93	60 ± 10	11.5	4.1	3.7
	4	O	1.94	70 ± 5	11.5	4.3	3.8
	4	O	1.93	70 ± 5	11.5	3.7	2.7
esterified	4.1 ± 0.3	O	1.94	70 ± 20	11.5	-11.3	4.7
	4	O	1.94	65 ± 5	11.5	-11.4	4.7
Multiple scattering	4	O	1.94	65 ± 5	11.5	-11.3	3.0

A significant improvement was observed when multiple scattering was included, lowering the fit index value to 4.9 and a good peak was observed at approximately 3.8 Å. This result suggests the occurrence of a square planar environment, D_{4h} symmetry, with a centro-symmetric atom, as suggested for the $Cu(NO_3)_2$ solid sample.

The values obtained for the pH 6 and esterified samples were very similar to the pH 2 sample, also suggesting a square planar geometry. Identical to the pH 2 sample, four O atoms were located at 1.94 Å. An improvement was observed when D_{4h} cluster multiple scattering was included, giving a peak at 3.8 Å, for both Cu pH 6 and the esterified samples.

The three Cu dealginate samples provided good data and a clear four fold oxygen coordination, most likely in square planar configuration. No evidence of asymmetry or any further significant shells were observed. The Cu environment observed on the samples was very well ordered, similar to $Cu(NO_3)_2$ with a σ^2 value corresponding to λ of 280 cm^{-1}. The edges shapes for the three Cu dealginated samples were very similar to the $Cu(NO_3)_2$ solid.

Although the results indicated a square planar geometry, similar to Ni, the geometry for Cu bound to dealginated seaweed, other structures have been proposed for copper carboxylate complexes, which are also possible. Binuclear complexes, with four carboxylate bridges that may have end groups (127) and linear or near linear crystalline groups type Cu-X-Cu (168) are among the complexes described. The known structure of copper (II) acetate monohydrate possesses four bridging acetate groups linking Cu ions in pairs to afford centrosymmetric eight-membered rings (168). Crystal structure studies (169, 170, 171) have shown that the majority of copper (II) carboxylates are in fact carboxylate-bridged dimers with two Cu atoms at 2.6 – 2.7 Å distance. Taking into account these structures, and the EXAFS findings for the Cu dealginate samples, the structure depicted in Figure 102 is proposed for Cu bound to dealginate. Unfortunately, no other shells were observed in the data collected for Cu to elucidate if the second shell contains two or four C atoms, which could have helped in the definition of a structure. The structure shows a binuclear type of molecule, with carboxylate groups acting as bridges for the Cu atoms.

Figure 89 Proposed structure for Cu bound to dealginated seaweed

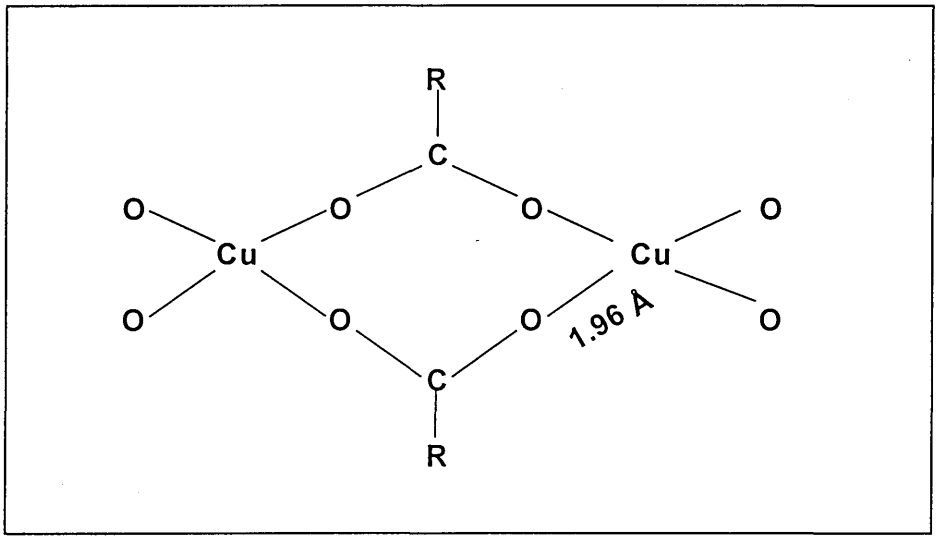

7.4.5. Silver

Transmission and fluorescence data for Ag K edge was collected using a Ag metal foil as a monitor. The transmission edge steps of the three Ag dealginate samples were very similar, showing a weak white line and an edge shift of about –1.5 eV with respect to the metal foil. The solution showed a shift of +0.2 eV. The masses found were different between the three Ag dealginate samples (see Table 41), probably due to differences in packing or thickness. A concentration value of 8 mM was calculated for the $AgNO_3$ sample. The value of $\Delta\sigma$ used was 0.84×10^{-24} m^2 $atom^{-1}$ (164).

Table 41 Transmission edge steps for Ag dealginate seaweed samples

Sample	$\Delta\mu$ (Ag)	nt (m-2)	t (μm)	n (m^{-3})	Mass (mg cc^{-1})
Ag foil	1.2	1.43×10^{24}	25	5.7×10^{28}	10300
Ag solution	0.0002	2.4×10^{21}	500	4.8×10^{24}	0.86
Ag at pH 2	0.14	1.7×10^{23}	500	3.4×10^{26}	61
Ag at pH 6	0.05	6.0×10^{21}	500	12×10^{24}	2.2
Ag esterified	0.02	21×10^{21}	500	42×10^{24}	8.6

Data from 25 μm Ag foil with $\Delta\mu$ of 1.2 was used to optimise the parameters in the programme. The results showed that using an AFAC value of 0.9 the accuracy of the parameters increased, therefore, this value was used for further calculations (see Table 42). With these settings, a coordination number 12 was obtained for the Ag configuration. No improvement was observed when other shells were added by multiple scattering for coordination numbers of 6, 12 and 24, since the fit index value slightly changed from 4.2 to 4.3. The correlated Debye theory gave a value of σ^2 of 110×10^{-24} Å^2 rising to 140×10^{-24} Å^2 for most distant shells.

Data from transmission scans for $AgNO_3$ solid showed an edge shift of –1.1 eV with respect to the metal foil (see Table 42). The crystal structure for this solid shows 3 oxygen atoms at 2.48 Å and 2 additional oxygen atoms at 2.57 Å, giving an average of 5 oxygen atoms at 2.51 Å. This value is in good agreement with 5 oxygen atoms fitted at 2.49 Å in the $AgNO_3$ solid sample. Similarly, the value of Ag found is comparable to the value of Ag in the crystal structure, which is located at 3.2 Å. When the oxygen mass is used, a σ^2 value of 200 x 10^{-24} $Å^2$ was calculated, corresponding to Ag-O stretch frequency of approximately 140 cm^{-1}.

Table 42 EXAFS results for Ag foil, $AgNO_3$ solid and solution

Sample	N	Atom type	r ± 0.02 Å	σ^2 10^{-4} $Å^2$	K_{max} $Å^{-1}$	E_F	FI
Ag foil							
AFAC 1.0	10.7 ± 1.1	Ag	2.07	90 ± 10	12	-8.8	6.5
AFAC 0.9	11.6 ± 1.0	Ag	2.87	90 ± 5	12	-9.0	4.2
	6 ± 5	Ag	4.04	140 ± 60	12	-9.0	
	16 ± 1.4	Ag	5.00	130 ± 40	12	-9.0	
	11.6 ± 1.0	Ag	5.64	120 ± 30	12	-9.0	
	12	Ag	2.87	90 ± 5	12	-9.1	4.3
	6	Ag	4.03	130 ± 25	12	-9.1	
	24	Ag	5.01	160 ± 20	12	-9.1	
	12	Ag	5.63	120 ± 30	12	-9.1	
$AgNO_3$ solid	5.5 ± 0.9	O	2.49	240 ± 40	10	-8.1	22.5
	5.5 ± 0.6	O	2.49	200 ± 25	10	-8.5	11.5
	3.2 ± 1.1	O	2.82	270 ± 100	10	-8.5	
	6.7 ± 5.3	Ag	3.12	590 ± 2800	10	-8.25	
	5	O	2.49	200 ± 15	10	-8.5	14.3
	2	O	2.82	200 ± 70	10	-8.5	
	1	Ag	3.12	320 ± 200	10	-8.5	
$AgNO_3$ solution	4.9 ± 2.7	O	2.34	200 ± 125	10	-5.7	71.4

The bond lengths for Ag-O in solution were much shorter compared to those found in the solid samples. This might be caused by the fact that Ag-N lies at 2.22 or 2.37 Å and Ag-S appear at 2.43 Å in solids, increasing the distance of Ag-O. Furthermore, a five or six O atom is a common environment for metal atoms in aqueous solution, and both geometries are possible for Ag complexes (127). A well-ordered environment was observed for the solution as well as the solid sample, and σ^2 values between both samples were comparable. No further shells gave significant improvement in the fit index.

The EXAFS results for the Ag pH 2 samples are shown in Table 43. A higher content of Ag was found in this sample, with values around 60-70 mg g^{-1}. No fitting could be obtained using 5 atoms, since the signal was found to be π out of phase. Three different atoms were fitted, O, N and S all of them gave good fit for the Ag samples, suggesting a wide variety of possibilities compared to the other metals studied. The distances suggested that an O atom was most likely to be the nearest neighbour, located at 2.33 Å.

Table 43 EXAFS results for Ag pH 2 samples

N	Atom type	r ± 0.02 Å	σ^2 10^{-4} Å^2	K_{max} Å^{-1}	E_F	FI
2.7 ± 0.5	O	2.33	180 ± 50	10	-7.1	29.5
2.8 ± 0.6	N	2.34	170 ± 40	10	-6.1	30.5
3.0 ± 0.6	C	2.37	140 ± 40	10	-5.3	31.1
1.9 ± 0.8	O	2.30	100 ± 60	10	-8.4	19.9
1.9 ± 1.1	C	2.62	120 ± 120	10	-8.4	
1.4 ± 1.0	S	3.19	220 ± 110	10	-8.4	16.1
1.3 ± 0.5	C	3.00	40 ± 40	10	-8.4	15.2
0.8 ± 0.5	Ag	2.82	190 ± 90	10	-8.4	16.8

Adding a second light atom shell significantly improved the fit index, as shown in rows 4 and 5 of Table 42. It also lowered the O atom coordination distance to approximately 2.3 Å due to interference between overlapping shells. The second shell was assumed as C, but N or S could equally be bound, especially because Ag has a relatively low affinity for oxygen donors, and forms numerous complexes with the donor atoms S and N (127). If the O atom and C atom form a unit with the same coordination number, and the distance of C-O is assumed to be 1.36 Å, like in the case of Cd, then the angle Ag-O-C is about 90°, which produces a very rigid structure. The possibility of an Ag environment of 2 + 2 formed by four different bonding units cannot be discarded.

The three last rows of Table 42 show the results of a new fit using a peak observed at approximately 3.0 Å in the Fourier transform of the data. The values suggested that all the atoms form possible structures with Ag. The coincidence of distance and the Debye-Waller factor suggested Ag from Ag metal (12 nearest neighbours at 2.87 Å). This coordination represents 7 ± 4 % of Ag as metal and is probably due to photo reduction. This could be verified by comparing data early and late in the exposure of the sample to the beam.

In addition crystal structure studies of some Ag-carboxylate compounds (172, 173) have shown the presence of centrosymmetric binuclear units containing bridging carboxylate groups. The units were described as being linked into polymeric structures by weak Ag-O interactions, and the Ag-Ag bond length was observed to be at 2.90 Å distance.

The Ag content in the Ag pH 6 sample possesses the lower concentration of Ag of all the Ag dealginate samples studied, diminishing the quality of the data acquired. The results found were comparable to the Ag pH 2 sample (see Table 44). A lower coordination than the Ag pH 2 sample was observed, and fitting of five atoms was not possible. The calculated bond lengths were shorter compared to Ag pH 2 sample. Shorter distances suggest a Ag-N, since

this bond distance is 2.22 Å in AgSCN, when the coordination is to one N atom and one S atom and 2.37 Å in AgCNO when the coordination is to two N atoms. Because Ag (I) configuration is d^{10}, when coordination number 2 is fitted the stereochemistry shows a pronounced tendency to form linear twofold coordination in most of the complexes (127). There was no evidence of the presence of the peak at 3 Å observed in the pH 2 sample, suggesting that the Ag is not photo-reduced to Ag metal. No further shells could be fitted.

Table 44 EXAFS results for Ag pH 6 samples

N	Atom type	r ± 0.02 Å	σ^2 10^{-4} Å^2	K_{max} Å^{-1}	E_F	FI
1.1 ± 0.4	O	2.19	120 ± 70	8	-1.4	58.0
1.3 ± 0.5	N	2.22	110 ± 70	8	-1.7	58.0
1.4 ± 0.9	O	2.19	190 ± 140	10	0.9	82.4
1.6 ± 1.0	N	2.22	170 ± 130	10	0.1	81.9

The EXAFS data obtained for Ag esterified sample showed a low Ag content. It was not possible to perform a five atom fit using this data. The results (see Table 45) clearly showed one light atom bound to Ag, or possibly two atoms bound at approximately 2.25 Å. The distances suggested N atom as nearest neighbour, similar to the Ag pH 6 sample. A further peak was observed at approximately 3.0 Å, giving the possibility of N or Ag as the nearest neighbour (see rows 5 and 6 of Table 44). The significant improvement in the fit and the value of σ^2 obtained indicated approximately 6 ± 4 % of Ag metal. The similarity of this result to the aforementioned presence of Ag metal in the pH 2 sample strongly indicates the possibility of photo-reduction during the analysis.

Analysis of a shorter range of data showed the possibility of S atom as nearest neighbour at 3.22 Å (row 11 of Table 45). As previously found, N is the likely nearest neighbour at 2.26 Å, but

instead of one, two N atoms are suggested. In addition, a signal from a small fraction of Ag metal was observed. No evidence of a second shell was found.

Table 45 EXAFS results for Ag esterified samples

N	Atom type	r ± 0.02 Å	σ^2 10^{-4} Å^2	K_{max} Å^{-1}	E_F	FI
1.7 ± 0.6	O	2.23	150 ± 70	10	-7.2	56.2
1.8 ± 0.6	N	2.26	130 ± 70	10	-6.6	57.1
2.1 ± 0.7	C	2.29	120 ± 70	10	-5.9	58.0
1.3 ± 0.7	S	2.48	160 ± 80	10	-4.0	70.5
1.9 ± 0.6	N	2.26	160 ± 70	10	-6.6	44.5
0.7 ± 0.5	Ag	2.84	90 ± 60	10	-6.6	
1.6 ± 0.5	N	2.25	110 ± 100	8	-7.0	50.8
1.7 ± 0.5	N	2.26	130 ± 70	8	-7.0	39.8
0.8 ± 0.6	Ag	2.83	100 ± 100	8	-7.0	
1.6 ± 0.4	N	2.26	110 ± 50	8	-7.4	40.5
0.8 ± 0.8	S	3.22	80 ± 130	8	-7.4	
1.6 ± 0.5	N	2.24	110 ± 50	8	-5.7	44.2
2.2 ± 1.9	C	3.56	40 ± 130	8	-5.7	

A specific structure for the binding of Ag to dealginated seaweed was not possible from the analysis of the Ag nearest neighbour, since all the samples produced different results. However, the coordination number proposed and the bond lengths are in good agreement with the stereochemistry of Ag described in the literature (127). However, ESEM results indicated the possibility of Ag being bound to S atoms on the biosorbent surface, since the intensity of the X-ray maps clearly showed a match between the location of Ag and S atoms. In addition, the microphotographs indicated the presence of possible Ag complexes on the surface, in the form of beads, which could be related to the photoreduction reaction proposed here, giving as a result beads of Ag-Ag metal. The map showed, a more extensive area covered by Ag than by S indicating that the photoreduction reaction might have occurred.

7.4.6. Gold

Transmission and fluorescence data for Au L_3 edge was collected using an Au 5 μm metal foil as monitor. The transmission edge steps calculated are shown in Table 46. The edge step as well as the concentration was different for the Au dealginate samples. This result is expected, since less Au would be bound to the biosorbent on the esterified sample, if a carboxylate binding type were considered. An estimated 5 mM was obtained as concentration value for the $AuCl_4H$ solution. The value used for $\Delta\sigma$ was 3.5×10^{-24} m^2 $atom^{-1}$ (164).

Table 46 Transmission edge steps for Au dealginated seaweed samples

Sample	Δμ (Au)	nt (m-2)	t (μm)	N (m^{-3})	Mass (mg cc^{-1})
Au foil	0.9	2.6×10^{23}	5	5.2×10^{28}	17100
Au solution	0.005	1.5×10^{21}	500	3×10^{24}	1.0
Au at pH 3	0.19	5.4×10^{22}	500	11×10^{25}	36
Au esterified	0.06	1.7×10^{22}	500	3.4×10^{25}	11

EXAFS results for metal foil, $AuCl_4H$ solid and solution are in Table 46. Initially, single transmission scan and AFAC 1.0 were used to test parameters in the programme. However, better results were obtained using AFAC 0.8. Therefore, this value was used throughout the calculations. It was necessary to include multiple scattering to fit the 4th shell. The correlated Debye theory gave σ^2 value of 105×10^{-24} m^2. The results for the metal foil were as expected giving coordination numbers of 6, 12 and 24, all in good agreement with the Au metal crystal structure.

Table 47 EXAFS results for Au foil, $AuCl_4H$ solid and solution

Sample	N	Atom type	r ± 0.02 Å	σ^2 10^{-4} Å^2	K_{max} Å^{-1}	E_F	FI
Au foil	12	Au	2.87	80 ± 10	12	-10.8	10.9
	6	Au	4.08	80 ± 20	12	-10.8	
	24	Au	4.98	130 ± 20	12	-10.8	
	12	Au	5.67	80 ± 10	12	-10.8	
$HAuCl_4$ solid	3.7 ± 1.0	Cl	2.26	80 ± 30	10	-8.1	41.6
	3 ± 1	O	2.08	20 ± 30	10	-8.1	59.0
$HAuCl_4$ solution	4 ± 0.6	Cl	2.27	20 ± 10	12	-11.8	14.5
	4.7 ± 0.8	O	2.17	20 ± 100	12	-27.8	19.4

An edge shift of 2.7 eV from metal foil was observed for the Au solid sample. The results showed the Cl atom as the nearest neighbour located at 2.26 Å. Distances found were comparable to XRD distances for the Au-Cl bond which is 2.29 Å. The coordination number was lower compared to XRD (6 atoms) but the square planar type molecular geometry is appropriate for the $AuCl_4^-$ complex (127).

The edge for Au solution sample was very similar to that obtained for the Au solid sample, a weak white line and an edge shift of 2.3 eV from the metal foil. Similar to the Au solid sample, the Cl atom is the nearest neighbour, suggesting the presence of $AuCl_4^-$ complex in aqueous solution. The similarities of the edge shapes strongly indicated that Au is forming a negatively charged complex with Cl^- in solution. It has been reported that the only possible form of Au in solution is this type of complex (127). Values of σ^2 corresponding to stretch frequencies of 140 and 300 cm^{-1} were calculated when Cl atom mass is used for the oscillator.

The spectrum obtained for the pH 3 sample was very similar to the spectrum for Au foil. A first shell could be fitted for Au metal structure (see Table 48). The coordination number obtained indicated that approximately 75% of the Au present on the sample was colloidal metal. The

fitting of an additional extra shell showed the possibility of S atom as the nearest neighbour, since the distances calculated are appropriate. The binding with O was also possible, but the second S atom shell significantly improved the results, suggesting 25% of the Au bound to one or possible two S atoms.

Table 48 EXAFS results for Au pH 3 samples

N	Atom type	r ± 0.02 Å	σ^2 10^{-4} Å^2	K_{max} Å^{-1}	E_F	FI
9.1 ± 1.8	Au	2.86	80 ± 10	12	-8.8	16.1
9	Au	2.87	80 ± 5	12	-9.2	11.2
4.5	Au	4.08	100 ± 30	12	-9.2	
18	Au	4.99	120 ± 15	12	-9.2	
4.5	Au	5.66	85 ± 30	12	-9.2	
0.3 ± 0.2	S	2.33	0 ± 40	12	-9.2	8.9
0.4 ± 0.3	O	2.16	20 ± 50	12	-9.2	9.7
0.3 ± 0.2	S	2.33	0 ± 40	12	-9.2	66.8
0.3 ± 0.25	O	2.15	10 ± 90	12	-9.2	72.7

Similarly by fitting difference spectrum, the same result is achieved as shown in rows 8 and 9 of Table 49, enabling much better definition of the coordination number. The concentration of the pH 3 sample was determined as approximately 36 mg g^{-1}. The result showed that approximately 75% of the total concentration is colloidal Au, leaving about 9 mg g^{-1} bound to the dealginate surface.

The EXAFS data obtained for the Au esterified sample showed that 85% of colloidal Au was present on the sample. The data fitted the Au metal structure very well, leaving 15% of Au bound to a different type of atom from the dealginate surface. Fitting of the data (Table 49) by adding an extra shell showed that S is the nearest neighbour. As was carried out for Au pH 3, by fitting the difference spectrum the previous result was confirmed, suggesting 17% of Au

bound to one or two S atoms. The esterified sample therefore contains about 2 mg g^{-1} of Au bound to S atom.

Table 49 EXAFS results for Au esterified samples

N	Atom type	r ± 0.02 Å	σ^2 10^{-4} Å^2	K_{max} Å^{-1}	E_F	FI
10 ± 1.9	Au	2.86	80 ± 10	12	-9.3	13.9
10	Au	2.86	80 ± 5	12	-9.4	10.2
5	Au	4.06	100 ± 30	12	-9.4	
20	Au	4.97	120 ± 20	12	-9.4	
10	Au	5.67	90 ± 25	12	-9.4	
0.3 ± 0.3	S	2.34	20 ± 70	12	-9.4	9.4
0.4 ± 0.5	O	2.13	30 ± 100	12	-9.4	
0.3 ± 0.3	S	2.34	30 ± 70	12	-9.4	75.5
0.4 ± 0.4	O	2.14	30 ± 100	12	-9.4	

There was no evidence of a white line on the Au pH 3 or Au esterified sample, even after subtracting the Au foil signal from the spectra. This finding suggests the presence of Au^+ instead of Au^{3+} as in the Au solid and solution studied.

Au (III) only forms anionic complexes in solution, exhibiting a d^8 configuration, which allows it to accommodate the atoms in a high geometric structure with coordination numbers 4, 5 and 6, as was observed for the Au solution sample. The results for the Au dealginate sample consistently showed a lower coordination number two, indicating that the oxidation state for Au changed from Au (III) to Au (I). Furthermore, the fitting demonstrated that Au is bound to two S atoms. This type of configuration can only be adopted by a d^{10} configuration, which allows the coordination number 2, to give a linear geometry, resulting in an oxidation state of Au (I). Watkins *et al.* (139) reported Au(III) reduction to Au (I) on the surface of the algae *Chlorella vulgaris*, and EXAFS curve-fitting analysis described the environment as a two shell Au-S fit.

ESEM results previously showed the correlation of Au and S in a Au dealginate sample X-ray map, which strongly indicates that the binding mechanism for non-colloidal Au in dealginated seaweed is reduction to Au(I) which is subsequently bound to two S atoms in a linear geometry.

The remaining Au present on the biosorbent surface was identified as colloidal Au. Gardea-Torresdey *et al.* (124) reported Au (III) reduction to colloidal Au (0) on the surface of *Medicago sativa* by cysteine or methionine groups and the presence of colloidal Au (0) was corroborated by EXAFS analysis. The colloids formation on dealginated seaweed was also clearly shown on the SE microphotograph reported previously (Chapter 4, section 4.2).

7.5. Summary

These results have demonstrated that EXAFS is a useful tool for the elucidation of the binding mechanism of metals to dealginated seaweed. Although most of the metal studies showed a similar mechanism, the binding to the biosorbent surface strongly depends on the chemistry of the metal itself. Structures proposed for Cd, Pb, Ni and Cu corroborate the carboxylate type binding proposed previously in this study. In the case of Ag, the suggested binding could be to S atoms, but the formation of Ag-carboxylate complexes cannot be discarded. The reduction mechanism previously proposed for Au, as well as binding through S atoms was corroborated.

General Discussion

Chapter 8

8.1. Characterisation of the sorption process and elucidation of the metal binding mechanism

In order to characterise and optimise the uptake process of Cd, Pb, Ni, Cu, Cr, Ag, Al and Au by dealginated seaweed, the batch procedure was used to determine the parameters controlling the sorption process.

The results showed that the overall sorption process depends on the pH used. It was necessary to carefully control the pH during the experiments, since low metal removal was observed between pH 2 and 5. Above pH 8 most of metal ions in solution are present as hydroxides (14). The higher metal removal from solution was observed between pH 5 and 7. In order to avoid precipitation, pH 6 was considered optimum for Cd, Pb, Ni, Cu, Cr and Ag. The chemistry of Al and Au did not permit the use of this pH value, since Al and Au species start precipitating after pH 4 (14). For this reason, pH 3 and 4 were used for Au and Al, respectively.

The batch experiments showed that the kinetics of the sorption process was fast for all the metals studied. Approximately 90% of the metal in the solution was effectively removed in the first 5 minutes of contact and saturation was achieved within 24 h for all the metals except Pb.

However, the results obtained from the equilibrium experiments showed different patterns depending on the metal studied. It was observed that at low concentrations linear and non-linear models are useful to describe the sorption mechanism of Cd, Pb, Ni, Cu, Cr, Ag, and Al, based on the assumption that there is only one type of site available on the biosorbent surface. However, when the concentration is increased, the behaviour of the biosorbent is different, in the case of Cd, Pb and Cu and Ag at high concentration the curve keeps increasing, while for Ni, Cr and Al a levelling off was observed. . For Cd, Pb, Cu and Ag the best fit to a two binding sites model was obtained. Therefore, the mechanism seems to occur

in two stages, a rapid interchange with hydrogen ions from the surface, and a second step, where covalent binding slowly takes place.

The mechanism for Ni, Cr and Al differs from that proposed for the aforementioned metals. Although the results fit an ion exchange model at low concentration, the one-site type model prevails at high concentration. This suggests that Ni and Cr have affinities for homogeneous type-sites until the dealginate surface is saturated.

It was not possible to fit the Au data to the models proposed in this study. The assumption that ion exchange between cations and hydrogen ions is occurring on the surface of the biosorbent could not be applied in the case of Au, since $AuCl_3^-$ was the species used. This finding suggests a completely different sorption mechanism from the other metals studied. Two possible mechanisms could be occurring: 1) the presence of positively charged sites that allow the ion exchange of negatively charged Au species, and 2) the reaction of Au species with components on the surface of the biosorbent. Due to the range of pH used during the experiment the first mechanism is less likely to occur, since the ionic balance has to be maintained between the solution and the biosorbent surface, leaving the possibility of chemical reaction between Au and the biosorbent surface as the mechanism of Au removal from solution.

Simulation of the metal solution conditions for Cd, Pb, Ni and Cu demonstrated that the metals were bound to dealginated seaweed as divalent cations at pH 6. Ag was found to exist at this pH as the monovalent cation.

The results found for Cr showed that Cr^{3+} behaviour was very similar to the rest of the divalent cations studied. Furthermore, Cr affinity for the same type of sites as Ni indicated a similar mechanism for a divalent or a trivalent cation. However, solution simulation showed that Cr

exists as $Cr(OH)^{2+}$ at pH 6, and therefore, the sorption process might be occurring as a divalent cation. This finding explains the similarities between the Cr results and the divalent cations, and the fact that the Cr uptake follows an analogous mechanism as Ni.

The simulation of Al solution showed that approximately 50% of Al present was $Al(OH)_3$ precipitate. This finding could explain the discrepancies found when the Al data was fitted to the proposed models. Therefore, in the case of Al, precipitation appears to be playing an important role in the removal of Al ions from solution. However, high adsorption of Al by *Rhizoclonium* at pH 4 has been reported (174). The study also demonstrated Al adsorption at pH 5 from the $Al(OH)_3$ (s) suspension. The mechanism was described as an ion exchange with protons, although the kinetics were slow, attributed to a masking of $Al(OH)_3$ solid.

In order to confirm ion exchange as the proposed sorption mechanism for metal uptake by dealginated seaweed, the stoichiometry of the reaction was established, using Cd and Ca as representatives of the metals studied. The stoichiometry showed to be approximately 1:1, indicating an exchange of one divalent cation for another on the biosorbent surface.

The confirmation of the cation exchange was used to assume a B_2M stoichiometry for the ion exchange with protons. Ion exchange constants and metal capacities were calculated using this approximation. The difference in capacities found between the metals studied showed that the efficiency of the sorption process depends on the metal studied and the affinity of the biosorbent towards the metallic species.

The dealginated seaweed capacity to remove metals from aqueous solution was similar to other biomasses (23 48, 60, 76, 91,95, 100, 117, 130, 131, 140, 152) demonstrating the potential contribution to industrial processes.

Using the optimum parameters found from the batch experiments, the sorption process was extended to study a wider range of metals under continuous flow conditions. The evaluation of the removal of Cd, Pb, Ni, Cu, Cr, Ag, Au, Zn, Sc, Sr, Co, Mn, Hg, Sb, As, Se and V from solution by dealginated seaweed packed in a microcolumn showed the affinity of the biosorbent for binding specific metal ions. As was demonstrated previously in this study, the cations were retained by the biosorbent, and dealginate showed little or no retention of negatively charged species. This result demonstrates the possibility of using the biosorbent for specific metal removal in an industrial process and analytical applications.

The column packed with dealginated seaweed showed efficiencies comparable with columns filled with other types of chemical or biological sorbent without immobilisation or modification, demonstrating the advantages of direct use of the biosorbent in a column system, making the possibility of scale-up simple and easy use at low cost.

8.2. Identification of the binding sites on the surface of dealginated seaweed

Three possible binding sites were identified by titration of the dealginate surface. The calculated pKa's of 1.8, 3.63 and 9.09 were associated with sulphonate groups, carboxylic groups and phenolic groups, respectively. The amount of binding sites showed the predominance of carboxylate groups (1.5 ± 0.04 mmol g^{-1}) on the biosorbent surface.

The presence of carboxylate groups was confirmed by modification of the biosorbent surface and by FT-IR. Esterification of dealginated seaweed showed a significant reduction in the sorption capacity of the biosorbent for all the metals studied, indicating that carboxyl group are primarly responsible for the metal retention.

Hydrolysis of the biosorbent, resulted in the resumption of the sorption capabilities, confirming the previous results.

The FT-IR spectrum of dealginated seaweed showed the presence of carboxylate functional groups in the fingerprint region. The presence of other functionalities such as N or S was not confirmed. The spectra showed the dealginated seaweed to possess similar functionalities to those of alginic acid. The presence of metal bound to the biosorbent was evident in the changes observed in the fingerprint region of the spectra, indicating that the binding of Cd, Pb, Ni, Cu, Cr and Ag to the biosorbent is through carboxyl groups. Comparison of the Cd-dealginate spectra with the cadmium acetate spectra showed similarities, pointing to binding through oxygen on carboxyl to form acetate type complexes. EXAFS results allowed structures based on binding to oxygen atoms from carboxyl groups for Cd and Ni to be proposed. Results fit two shells, showing O as the nearest neighbour with the possibility of C atom as second neighbour. In the case of Cd, the suggested Cd-acetate type complex by FT-IR was confirmed. Structures of Pb and Cu bound to O atoms were also confirmed by EXAFS analysis, with coordination number 4 for both elements.

The study of the dealginate surface using ESEM showed the presence of the cell structure in the biosorbent, corroborating the similarity found between the alginic acid and dealginated seaweed FT-IR spectra. X-ray maps of the Ag-bound to dealginate sample suggested the possibility that Ag bound to the biosorbent through S sites. The occurrence of this binding is possible since S groups were identified by titration of the biosorbent surface. The binding of Ag to dealginate through O and S atoms was confirmed by EXAFS, since the data for both atoms were closely matched, corroborating the existence of two binding sites for Ag previously proposed from the equilibrium results.

The prevalence of the precipitation process over the sorption process for Al was confirmed, as no differences were found in the Al-bound dealginate compared with the dealginated seaweed spectra. In an attempt to confirm this result, the sample was analysed for Al content by ^{27}Al NMR. The results showed that the Al present was in the sulphate form, used to prepare the Al solutions. Due to these results, and the previous sorption results observed, the process of Al retention was concluded to be more a precipitation rather than sorption by the biosorbent. The precipitation resulted in the removal of Al from the solution although little sorption might have occurred. As mentioned before, the sorption results for Al did not fit the models used, suggesting a precipitation process instead sorption on dealginated. The binding of Al to S observed in the FT-IR spectra and suggested by the equilibrium and simulation results was also confirmed by X-ray maps, since the Al and S atoms were located in the same regions on the biosorbent surface.

The changes observed for Au suggested very little sorption on the biosorbent surface, at least to carboxyl moieties. X-ray maps obtained for Au-bound to dealginate indicated possible binding through S atoms. The presence of colloidal Au, formed in the biosorbent surface by reduction of Au (III) to Au (0) was observed. The EXAFS results confirmed that Au retention mechanism is very different from the rest of the metals studied. As was observed using the ESEM, the EXAFS showed that colloidal Au is formed on the surface of the biosorbent, due to reduction of Au^{3+}. This mechanism of retention accounts for approximately 85% of the Au present. The remaining Au (III) was reduced to Au (I) which was bound to the biosorbent through S atoms.

The identified binding sites on the dealginated seaweed surface were similar to those reported for a variety of biosorbents (2, 4, 11, 21, 25, 51, 56, 61, 77, 82, 92). The clear identification of the binding sites allows the modification of the surface of the biosorbent in order to improve the efficiency of the metal removal process.

CONCLUSIONS

Chapter 9

9.1. Conclusions

The study of metal retention by dealginated seaweed and the characterisation of the surface of the biosorbent demonstrated that:

- The main mechanism of metal sorption by dealginated seaweed is ion exchange.
- The sorption process is pH dependent and the efficiency of sorption process was demonstrated to be dependent on the metal species used.
- Three types of binding sites were identified on the dealginate surface: sulphonates, carboxylates and OH groups.
- The stoichiometry of the sorption process was found to be a B_2M type.
- The esterification of the dealginate surface resulted in a reduction of the ability of the biosorbent to bind metal ions, indicating that the carboxyl groups are the major binding sites.
- The ability of dealginated seaweed to bind a wide range of metal ions in a column set up under continuous flow conditions was demonstrated. The biosorbent showed excellent durability during prolonged and repeated use.
- The proposed method is simple, sensitive and accurate making it suitable for further application in effluent treatment.
- Dealginated seaweed proved useful for speciation and separation of metals from solution.
- The participation of carboxyl groups in the uptake of metal ions by dealginated seaweed was elucidated by the use of Fourier transform infra-red spectroscopy. The effect of metal uptake on the carboxyl groups indicated the importance of these moieties in the binding process.
- The analysis of fully hydrated dealginated seaweed using ESEM for the characterisation of the surface of the biosorbent was demonstrated.

- The X-ray microanalysis quantitatively revealed the element content of the dealginated seaweed.
- ESEM images observed in combination with elemental maps obtained for Pb, Ag, Al and Au were used to localise binding sites on the dealginated surface.
- EXAFS proved to be a useful tool for the elucidation of the binding mechanism of metals by dealginated seaweed. Structures proposed for Cd, Pb, Ni and Cu corroborate the carboxyl type binding previously proposed.
- Although ion exchange was proposed as the main mechanism, it was demonstrated that the binding mechanism for Au to dealginated seaweed was via covalent bond to S atoms, along with the formation of colloidal Au by reaction with the biosorbent surface.

9.2. Future Work

This study has indicated that further research in certain areas is required. In order to improve the given results it is necessary that the following are undertaken:

- To evaluate the effect of the modification of the surface of the dealginated seaweed using other methods in order to make other binding sites available. The possibility of enhancing the retention capacity by chemically modifying the biosorbent should be explored.
- To extend of the sorption process to other metals or other type of pollutants such as organic molecules or metal-organic complexes, in order to extend the range of application of the biosorbent.
- To scale-up the column system and evaluate the possible application of dealginate to clean up effluent on an industrial scale.

Postgraduate study, Presentations, Publications and References

Chapter 10

Postgraduate Study

The courses attended during the period of research studies are listed below:

- Postgraduate Certificate in Principles and Practice of Inductively Coupled Plasma (Mass) Spectrometry. Sheffield Hallam University. (35 h)

- Geochemical Modelling. Sheffield Hallam University. (16 h)

Presentations

- Williams, C. J. Romero-González, M. Gardiner, P. H. E. The treatment of metal plating wastewaters by adsorption for metal ion removal and recovery. 8th World Filtration Congress. European Federation of Chemical Engineering. Brighton, U. K. April 2000.

- Romero-González, M. E. Gardiner, P. H. E. Williams, C. J. On-line preconcentration and chemical speciation of trace metals using a dealginated seaweed packed microcolumn with inductively coupled plasma spectrometry detection. Tenth Biennial National Atomic Spectroscopy Symposium. Royal Society of Chemistry. Analytical Division. Sheffield, U. K. July 2000.

- Habesch, S. M. Romero-González, M. A combined study of trace metal cation concentration and surface morphological characteristics on seaweed surfaces under hydrated conditions using environmental scanning electron microscopy (ESEM). Materials Research Society 2000 Fall Meeting. Symposium on Low-Vacuum SEM/ESEM in Materials Science: Wet SEM-The liquid frontier of Microscopy. Boston, USA. November 2000.

Articles Published

- Romero-González, M. E., Williams, C. J. Gardiner, P. H. E. (2000) The application of dealginated seaweed as a cation exchanger for on-line preconcentration and chemical speciation of trace metals. Journal of Analytical Atomic Spectrometry. 15, 1009-1013.

- Romero-González, M. E. Williams, C. J. Gardiner, P. H. E. (2001) Study of the mechanism of cadmium biosorption by dealginated seaweed waste. Environmental Science and Technology. 35, 3025-3030.

References

1. Zouboulis, A. I. Matis, K. A. Hancock, I. C. (1997) Biosorption of metals from dilute aqueous solutions. Separation and Purification Methods. 26, 255-295.
2. Volesky, B. Holan, Z. R. (1995) Biosorption of Heavy metals. Biotechnology Progress. 11, 235-250.
3. Bailey, S. Olin, T. J. Bricka, M and Adrian, D. D. (1999) A review of potentially low-cost sorbents for heavy metals. Water Research. 33, 2469-2479.
4. Crist, R. H. Oberholser, K. Shank, N. Nguyen, M. (1981) Nature of bonding between metallic ions and algal cell walls. Environmental Science and Technology, 15, 10, 1212-1217.
5. Donmez, G. C. Aksu, Z. Ozturk, A. Kutsal, T. (1999) A comparative study on heavy metal biosorption characteristics of some algae. Process Biochemistry. 34, 885-892.
6. Drake, L. R. Rayson, G. D. (1996) Plant-derived materials for metal ion-selective binding and preconcentration. Analytical Chemistry. 22A-27A.
7. Gadd, G. M. Biosorption. Chemistry and Industry, July. 421-426.
8. Robles, L. C. Aller, A. J. (1996) immobilized bacterial cells as bio-sorbents for toxic elements. Quimica Analítica. 15, 21-31.
9. Madrid, Y. Cámara, C. (1997) Biological substrates for metal preconcentration and speciation. Trac-Trends in Analytical Chemistry. 16, 36-44.
10. Ren, D. (1997) Biothechnology and the red seaweed polysaccharide industry: status, needs and propects. TIBTECH. 15, 9-14.
11. Jang, L. K. Nguyen, D and Geesy, G. G. (1995) Effect of pH on the absorption of Cu(II) alginate gel. Water Research. 29, 315-321.
12. Dabrowski, A. (2001) Adsorption – from theory to practice. Advances in Colloid and Interfaces Sciences. 93, 135-224.
13. Adamson, A. W. (1990) Physical Chemistry of Surfaces. Wiley Interscience. New York. pp 345.
14. Stumm, W. Morgan, J. J. (1996) Aquatic chemistry. Chemical Equilibria and Rates in Natural Waters. 3rd edition. Wiley-Interscience. New York. pp 1022.
15. Webber W.J. Jr, McGinley, P. M. and Katz, L. E. (1991) Sorption phenomena in subsurface systems: concepts, models and effects on contaminant fate and transport. Water Research 25, 5, 499-528.
16. Israelachvilly J. (1992) Intermolecular and Surface Forces. Academic Press Limited. London. pp 450.
17. White, S. Wilkinson, S. C. Gadd, G. M. (1995) The role of microorganisms in biosorption of toxic metals and radionuclides. International Biodeterioration and Biodegradation 17-40.
18. Eccles, H. (1995) Removal of heavy metals from effluents streams – Why select a biological process? International Biodeterioration and Biodegradation, 5-16.
19. Brierley, J. A., Goyak, G. M. and Brierley, C. L. in: Immobilisation of Ions by Biosorption. (eds H. Eccles and S. Hunt), Chichester: Ellis Horwod, 1986, pp 105-117.
20. Kuyucak, N. Volesky, B. (1988) Biosorbents for recovery of metals from industrial solutions. Biotechnology Letters. 10, 2, 137-142.

21. Veglio, F. Beolchini, F. (1997) Removal of metals by biosorption: a review. Hydrometallurgy. 44, 301-316.

22. Muraleedharan, T. R. Iyengar, L. Venkobachar, C. (1991) Biosorption: an attractive alternative for metal removal and recovery. Current Science. 61, 6, 379-385.

23. Volesky, B. May, H. Holan, Z. R. (1993) Cadmium biosorption by *Saccharomyces cerevisiae*. Biotechnology and Bioengineering. 41, 826-829.

24. Luján, J. R. Darnall, D. W. Stark, P. C. Rayson, G. D. Gardea-Torresdey, J. L. (1994) Metal ion binding by algae and higher plant tissues: A phenomenological study of solution pH dependence. Solvent Extraction and Ion Exchange. 12, 4, 803-816.

25. Wilde, E. W. Benemann, J. R. (1993) Bioremoval of heavy metals by the use of microalgae. Biotechnology Advances. 11, 781-812.

26. Pearson, R. G. (1963) Hard and soft acids and bases. Journal of the American Chemical Society. 85, 3533-3539.

27. Cox, P. A. (1995) The Elements on Earth. Oxford University Press. Oxford. pp 227.

28. Bunce, N. J. (1993) Introduction to Environmental Chemistry. Wuerz Publishing Ltd. Winnipeg, Canada. Pp 559.

29. Spiro, T. G. Stigliani, W. M. (1996) Chemistry of the Environment. Prentice-Hall, Inc. New Jersey, USA. Pp 356.

30. Lin, S. Rayson, G. D. (1998) Impact of surface modification on binding affinity distributions of *Datura innoxia* biomass to metal ions. Environmental Science and Technology. 32, 1488-1493.

31. Figueira, M. M Volesky, B. Ciminelly, V. S. T and Roddick, F. A. (2000) Biosorption of metals in brown seaweed biomass. Water Research. 34, 1, 196-204.

32. Mahan, C. Majidi, V. Holcombe, J. A. (1989) Evaluation of the metal uptake of several algae strains in a multicomponent matrix using inductively coupled plasma emission spectrometry. Analytical Chemistry, 61, 624-627.

33. Majidi, V. Holcombe, J. A. (1989) Pre-concentration of cadmium from environmental samples by algae and analysis by graphite furnace atomic absorption spectrometry. Journal of Analytical Atomic Spectroscopy. 4, 439-442.

34. Shengjun, M. Holcombe, J. A. (1991) Preconcentration of nickel and cobalt on algae and determination by slurry graphite-furnace atomic absorption spectrometry. Talanta. 38, 5, 503-510.

35. Crist, R. H. Oberholser, K. Schwartz, D. Marzoff, J, Ryder, D. Crist, D. R. (1988) Interactions of metals and protons with algae. Environmental Science and Technology. 22, 755-760.

36. Darnall, D. W. Greene, B. Henzi, M. T. Hosea, J. M. McPherson, R. A. Sneddon, J. Alexander, M. D. (1986) Selective recovery of gold and other metal ions from an algal biomass. Environmental Science and Technology. 20, 2, 206-208.

37. Greene, B. Hosea, M. McPherson, R. Henzi, M. Alexander, M. D. Darnall, D. W. (1986) Interaction of Gold (I) and Gold (III) complexes with algal biomass. Environmental Science and Technology. 20, 6, 627-632.

38. Aderhold, D. Williams, C. J. Edyvean, R. G. J. (1996) The removal of heavy-metal ions by seaweeds and their derivatives. Bioresource Technology. 58, 1-6.

39. Williams, C. J. Edyvean, R. G. J. (1997) Ion exchange in nickel biosorption by seaweed materials. Biotechnology Progress. 13, 424-428.

40. Lin, S. Drake, L. R. Rayson, G. D. (1996) Applications of frontal affinity chromatography to the study of interactions between metal ions and a complex biomaterial. Analytical Chemistry. 68, 4087-4093.

41. Kuyucak, N. Volesky, B. (1989) Accumulation of gold by algal biosorbent. Biorecovery. 1, 189-204.

42. Kuyucak, N. Volesky, B. (1989) The elution of gold sequestered on a natural biosorbent. Biorecovery. 1, 205-218.

43. Xue, H. B. Sigg, L. (1990) Binding of Cu (II) to algae in a metal buffer. Water Research. 24, 1129-1136.

44. Holan, Z. R. Volesky, B. Prasetyo, I. (1993) Biosorption of cadmium by biomass of marine algae. Biotechnology and Bioengineering. 41, 819-825.

45. Holan, Z. R. Volesky, B. (1994) Biosorption of Lead and Nickel by biomass of marine algae. Biotechnology and Bioengineering. 43, 1001-1009.

46. Nourbakhsh, M. Sag, Y. Ozer, D. Aksu, Z. Kutsal, T. Caglar, A. (1994) A comparative study of various biosorbents for removal of chromium (VI) ions from industrial waste waters. Process Biochemistry. 29, 1-5.

47. Matheickal, J. T. Qiming, Y. (1996) Biosorption of lead from aqueous solutions by marine algae *Ecklonia radiata*. Water Science and Technology. 34, 9, 1-7.

48. da Costa, A. C. A. de Mesquita, L. M. S. Tornovsky, J. (1996) Batch and continuous heavy metal biosorption by a brown seaweed from a zinc-producing plant. Minerals Engineering. 9, 8, 811-824.

49. Kratochvil, D. Volesky, B. (1998) Biosorption of Cu from ferruginous wastewater by algal biomass. Water Research. 32, 9, 2760-2768.

50. Kratochvil, D. Pimentel, P. Volesky, B. (1998) Removal of trivalent and hexavalent chromium by seaweed biosorbent. Environmental Science and Technology. 32, 2693-2698.

51. Yang, J. Volesky, B. (1999) Biosorption of uranium on *Sargassum* biomass. Water Research. 33, 15, 3357-3363.

52. Yu, Q. Matheickal, J. T. Latten, J. (1998) Heavy metal adsorption properties of marine algae *Durvilliea potatorum*, *Ecklonia radiata* and *Laminaria japonica*. Chinese Journal of Chemical Engineering. 6, 1, 68-72.

53. Seki, H. Suzuki, A. Mitsueda, S-I. (1998) Biosorption of heavy metal ions on *Rhodobacter sphaeroides* and *Alcaligenes eutrophus* H16. Journal of Colloid and Interface Science. 197, 185-190.

54. Sag, Y. Acikel, U. Aksu, Z. Kutsal, T. (1998) A comparative study for the simultaneous bisorption of Cr (VI) and Fe (III) on C. *vulgaris* and R. *Arrhizus*: application of the competitive adsorption models. Process Biochemistry. 33, 3, 273-281.

55. Zhou, J. L. Huand, P. L. Lin, R. G. (1998) Sorption and desorption of Cu and Cd by macroalgae and microalgae. Environmental Pollution. 101, 67-75.

56. Matheickal J. T. Yu, Q. (1999) Biosorption of lead (II) and copper (II) from aqueous solutions by pre-treated biomass of Australian marine algae. Bioresource Technology. 69, 223-229.

57. Carrilho, E. N. V. M. Gilbert, T. R. (2000) Assessing metal sorption on the marine alga *Pilayella littoralis*. Journal of Environmental Monitoring. 2, 410-415.

58. Wong. J. P. K. Wong, Y. S. Tam, N. F. Y. (2000) Nickel biosorption by two Chlorella species, *C. vulgaris* (a commercial species) and *C. miniata* (a local isolate). Bioresource Technology. 73, 133-137.

59. Kratochvil, D. Volesky, B. (1998) Advances in the biosorption of heavy metals. Trends in Biotechnology, 16, 291-300.

60. Harris, P. O. Ramelow, G. J. (1990) Binding of metal ions by particulate biomass derived from *Chlorella vulgaris* and *Scenedesmus quadricauda*. Environmental Science and Technology. 24, 220-228.

61. Drake, L. R. Lin S. Rayson, G. D. Jackson, P. J. (1996) Chemical modification and metal binding studies of *Datura innoxia*. Environmental Science and Technology. 30, 110-114.

62. Majidi, V and Holcombe, J. A. (1988) Separation and preconcentration of cadmium by biological organisms and analysis by graphite furnace atomic absorption. Spectrochimica Acta. 43B, 12, 1423-1429.

63. Shengjun, M. Holcombe, J. A. (1990) Preconcentration of Copper on algae and determination by slurry graphite furnace atomic absorption spectrometry. Analytical Chemistry. 62, 1994-1997.

64. Kubiak, W. W. Wang, J. Darnall, D. (1989) Algae columns with anodic stripping voltametric detection. Analytical Chemistry. 61, 468-471.

65. Volesky, B. Prasetyo, I. (1994) Cadmium removal in a biosorption column. Biotechnology and Bioengineering. 43, 1010-1015.

66. Gardea-Torresdey, J. L. Tiemann, K. J. Gonzalez, J. H. Henning, J. A. Townsend, M. S. (1996) Ability of silica-immobilised *Medicago sativa* (alfalfa) to remove copper ions from solution. Journal of Hazardous Materials. 48, 181-190.

67. Kratochvil, D. Volesky, B. Demopoulos, G. (1997) Optimizing Cu removal/recovery in a biosorption column. Water Research. 31, 9, 2327-2339.

68. Bag, H. Mustafa, L. Turker, A. R. (1998) Determination of iron and nickel by flame atomic absorption spectrophometry after preconcentration on *Saccharomyces cerevisiae* immobilized sepiolite. Talanta. 41, 689-696.

69. Matheickal, J. T. Qiming, Y. Woodburn, G. M. (1999) Biosorption of cadmium (II) from aqueous solutions by pre-treated biomass of marine alga *Durvillaea potatorum*. Water Research. 33, 2, 335-342.

70. Gardea-Torresdey, J. L. Tiemann K. J. Gamez, G. Dokken, K. (1999) Effects of chemical competition for multi-metal binding by *Medicago sativa* (alfalfa). Journal of Hazardous Materials. B69, 41-51.

71. Figueira, M. M. Volesky, B. Azarian, K. Ciminelli, v. S. T. (2000) Biosorption column performance with a metal mixture. Environmental Science and Technology. 34, 20, 4320-4326.

72. Kratochvil, D. Volesky, B. (2000) Multicomponent biosorption in fixed beds. Water Research. 34, 12, 3186-3196.

73. Singh, R. Prasad, B. B. (2000) Trace metal analysis: selective sample (copper II) enrichment on an AlgaSORB column. Process Biochemistry. 35, 897-905.

74. Robles, L. C. García-Olalla, C. Aller, A. J. (1993) Determination of Gold by slurry electrothermal atomic absorption spectrometry after preconcentration by *Escherichia coli* and *Pseudomonas putida*. Journal of Analytical Atomic Spectrometry. 8, 1015-1022.

75. Bag, H. Turker, A. R. Lale, M. Tunceli, A. (2000) Separation and speciation of Cr (III) and Cr (VI) with *Saccharomyces cerevisiae* immobilized on sepiolite and determination of both species in water by FAAS. Talanta, 51, 895-902.

76. Bag, H. Turker, A. R. Lale, M. (2000) Determination of Cu, Zn, Fe, Ni and Cd by flame atomic absorption spectrophotometry after preconcentration by *Escherichia coli* immobilized on sepiolite. Talanta. 51, 1035-1043.

77. Gardea-Torresdey, J. L. Becker-Hapak, M. K. Hosea, J. M, Darnall, D. W. (1990) Effect of chemical modification of algal carboxyl groups on metal ion binding. Environmental Science and Technology. 24, 1372-1378.

78. Gardea-Torresdey, J. L. Tang, L. Salvador, J. M. (1996) Copper adsorption by esterified and unesterified fractions of Sphagnum peat moss and its different humic substances. Journal of Hazardous Materials. 48, 191-206.

79. Xia, H. Rayson, G. D. (1998) Investigation of aluminium binding to a *Datura Innoxia* material using ^{27}Al NMR. Environmental Science and Technology. 32, 2688-2692.

80. Tiemann, K. J. Gardea-Torresdey, J. L. Gamez, G. Dokken, K. Sias, S. Renner, M. W. Furenlid, L. R. (1999) Use of X-ray absorption spectroscopy and esterification to investigate Cr (III) and Ni (II) ligands in alfalfa biomass. Environmental Science and Technology. 33, 150-154.

81. Kantor, T. G. Schubert, M. (1957) A method for the desulfation of chondroitin sulfate. Journal of the American Chemical Society. 79, 152-153.

82. Fourest, E. Volesky, B. (1996) Contribution of sulfonate groups and alginate to heavy metal biosorption by the dry biomass of *Sargassum fluitans*. Environmental Science and Technology. 30, 277-282.

83. Xie, J. Z. Chang, H. L. Kilbane, J. J. (1996) Removal and recovery of metal ions from wastewater using biosorbents and chemically modified biosorbents. Bioresource Technology. 57, 127-136.

84. Kapoor, A. Viraraghavan, T. (1997) Heavy metal biosorption sites in *Aspergillus niger*. Bioresource Technology. 61, 221-227.

85. Mashitah, M. D. Zulfadhly, Z. Bhatia, S. (1999) Binding mechanism of heavy metal biosorption by *Pycnoporus Sanguineus*. Artificial Cells, Blood Substitutes, and Immobilization. Biotechnology. 27, (5&6), 441-445.

86. Crist, R. H. Martin, J. R. Guptill, P. W. Eslinger, J. M. Crist, D. R. (1990) Interaction of metals and protons with algae. 2. Ion Exchange in adsorption and metal displacement by protons. Environmental Science and Technology. 24, 3, 337-342.

87. Crist, R. H. Oberholser, K. Wong, B. Crist, D. L. (1992) Amine-algae interactions: cation exchange and possible hydrogen bonding. Environmental Science and Technology. 26, 8, 1523-1526.

88. Crist, R. H. Martin J. R. Chonko, J. Crist, D. R. (1996) Uptake of metals on peat moss: and ion-exchange process. Environmental Science and Technology. 30, 2456-2461.

89. Schiewer, S. Volesky, B. (1996) Modelling multi-metal ion exchange in biosorption. Environmental Science and Technology. 30, 2921-2927.

90. Schiewer, S. Volesky, B. (1997) Ionic strength and electrostatic effects in biosorption of dialent metal ions and protons. Environmental Science and Technology. 31, 2478-2485.

91. Schiewer, S. Wong, M. H. (1999) Metal binding stoichiometry and isotherm choice in biosorption. Environmental Science and Technology. 33, 3821-3828.

92. Schiewer, S. Wong, M. H. (2000) Ionic strength effects in biosorption of metals by marine algae. Chemosphere. 41, 271-282.

93. Yang, J. Volesky, B. (1999) Modelling uranium-proton ion exchange in biosorption. Environmental Science and Technology. 33, 4079-4085.

94. Tan, H. K. S. Spinner, I. H. (1994) Multicomponent ion exchange dynamics. Canadian Journal of Chemical Engineering. 72, 330-341.

95. Pagnanelli, F. Petrangeli Papini, M. Toro, L. Trifoni, M. Veglio, F. (2000) Biosorption of metal ions on *Arthrobacter sp.*: biomass characterisation and biosorption modelling. Environmental Science and Technology. 34, 2773-2778.

96. Benedetti, M. F. Milne, C. J. Kinniburgh, D. G. van Riemsdijk, W. H. Koopal, L. K. (1995) Metal-ion binding to humic substances: Application of the non-ideal competitive adsorption model. Environmental Science and Technology. 29, 446-457.

97. Benedetti, M. F. van Riemsdijk, W. H. Koopal, L. K. Kinniburgh, D. G. Gooddy, D. C. Milne, C. J. (1996) Metal ion binding by natural organic matter: From the model to the field. Geochimica e Cosmochimica Acta. 60, 2503-2513.

98. Knniburgh, D. G. Milne, C. J. Benedetti, M. F. Pinheiro, J. P. Filius, J. Koopal, L. K. van Riemsdijk, W. H. (1996) Metal ion binding by humic acid: application of the NICA-Donnan model. Environmental Science and Technology. 30, 1678-1698.

99. Koopal, L. K. van Riemsdijk, W. H. de Wit, J. C. M. Benedetti, M. F. (1994) Analytical isotherm equations for multicomponent adsorption to heterogeneous surfaces. Journal of Colloidal and Interface Science. 166, 51-60.

100. Plette, A. C. C. Benedetti, M. F. van Riemsdijk, W. H. (1996) Competitive binding of protons, calcium, cadmium, and zinc to isolated cell walls of a gram-positive soil bacterium. Environmental Science and Technology. 30, 1902-1910.

101. Aksu, Z. Acikel, U. (1999) A single-staged bioseparation process for simultaneous removal of copper (II) and chromium (VI) by using C. *vulgaris*. Process Biochemistry. 34, 589-599.

102. Ozer, A. Ekiz, H. I. Ozer, D. Kutsal, T. Caglar, A. (1997) A staged purification process to remove heavy metal ions from wastewater using *Rhizopus arrhizus*. Process Biochemistry. 32, 319-326.

103. Ozer, A. Ozer, D. Ekiz, H. I. (1999) Application of Freundlich and Langmuir models to multistage purification process to remove heavy metal ions by using *Schizomeris leibleinii*. Process Biochemistry. 34, 919-927.

104. Montaser, A. McLean, J. A. Liu, H. Merment, J. M. (1998) An introduction to ICP spectrometry for elemental analysis. In: Inductively Coupled Plasma Mass Spectrometry. A. Montaser (ed.). Wiley-VCH, Inc. New York. Pp 964.

105. Thompson, M. Walsh, J. N. (1989) Handbook of inductively Coupled Plasma. 2nd edition. Blackie and son Ltd. London. pp 315.

106. Skoog, D. A. Holler, F. J. Nieman, T. A. (1998) Principles of Instrumental Analysis. Fifth edition. Harcourt Brace College Publishers. Philadelphia.

107. McKelvy, M. L. Britt, T. R. Davies, B. L. Gillie, J. K. Lentz, L. A. Leugers, A. Nyquist, R. A. Putzig, C. L. (1996) Infrared Spectroscopy. Analytical Chemistry. 68, 93R-160R.

108. Kuyucak, N. Volesky, B. (1989) The mechanism of gold biosorption. Biorecovery. 1, 219-235.

109. Kiefer, E. Sigg, L. Schosseler, P. (1997) Chemical and spectroscopic characterization of algae surfaces. Environmental Science and Technology. 31, 759-764.

110. Danilatos, G. D. Postle, R. (1982) The environmental scanning electron microscope and its applications. Scanning Electron Microscopy. I, 1-16.

111. Danilatos, G. D. (1991) Review and outline of environmental SEM at present. Journal of Microscopy. 162, 391-402.

112. Amelinckx, S. van Dyck, D. van Landuyt, J. van Tendeloo, G. (1997) Electron Microscopy. Principles and Fundamentals. VCH Verlagsgesellschaft. Weinheim, Germany. Pp 307.

113. Danilatos, G. D. (1994) Environmental scanning electron microscopy and microanalysis. Mikrochimica Acta. 114/115, 143-255.

114. Danilatos, G. D. (1993) An introduction to ESEM instrument. Microscopic Research Techniques. 249,

115. Mahan, C. Holcombe, J. (1992) Immobilization of algae cells on silica gel and their characterization for trace metal preconcentration. Analytical Chemistry. 64, 1933-1939.

116. Gardea-Torresdey, J. L. Cano-Aguilera, I. Webb, R. Gutierrez-Corona, F. (1997) Enhanced copper adsorption and morphological alterations of cells of copper-stressed *Mucor rouxii*. Environmental Toxicology and Chemistry. 16, 435-441.

117. Yu, Q. Kaewsarn, P. Van Duong, L. (2000) Electron microscopy study of biosorbents from marine macro alga *Durvillaea potatorum*. Chemosphere. 41, 589-594.

118. Figueira, M. M. Volesky, B. Mathieu, H. J. (1999) Instrumental analysis study of iron species biosorption by *Sargassum* biomass. Environmental Science and Technology. 33, 1840-1846.

119. Adams, F. Janssens, K. Snigirev, A. (1998) Microscopic X-ray fluorescence analysis and related methods with laboratory and synchrotron radiation sources. Journal of Analytical Atomic Spectrometry. 13, 319-331.

120. Stern, E. A. (1988) Theory of EXAFS. In X-ray absorption. Principles, applications, techniques of EXAFS, SEXAFS and XANES. D. C. Koningseberger and R. Prins (eds) Wiley-Interscience. New York. Pp 673.

121. Polette, L. A. Gardea-Torresdey, J. L. Chianelli, R. R. George, G. N. Pickering, I. J. Arenas, J. (1998) XAS and microscopy studies of the uptake and bio-transformation of copper in *Larrea tridentata* (creosote bush). Microchemical Journal. 65, 227-236.

122. Tiemann, K. J. Gardea-Torresdey, J. L. Gamez, G. Dokken, K. Cano-Aguilera, I. Renner, M. W and Furenlid, L. R. (2000) Effects of oxidation state on metal ion binding by *Medicago Sativa* (alfalfa): Atomic and X-ray absorption spectroscopic studies with Fe (II) and Fe (III). Environmental Science and Technology. 34, 693-698.

123. Gardea-Torresdey, J. L. Tiemann, K. J. Armendariz, V. Bess-Oberto, L. Chianelli, R. R. Rios, J. Parsons, J. G. Gamez, G. (2000) Characterization of Cr (VI) binding and reduction to Cr (III) by the agricultural byproducts of *Avena monida* (Oat) biomass. Journal of Hazardous Materials. B80, 175-188.

124. Gardea-Torresdey, J. L. Tiemann, K. J. Gamez, G, Dokken, K. Cano-Aguilera, I. Furenlid, L. R. Renner, M. W. (2000) Reduction and accumulation of gold (III) by *Medicago sativa* alfalfa biomass: X-ray absorption spectroscopy, pH and temperature dependence. Environmental Science and Technology. 34, 4392-4396.

125. APHA-AWWA-WPCF. Standard Methods for the Examination of Water and Wastewater. American Public Health Association. Washington DC. 19th edition 1995.

126. Williams, C. J. Aderhold, D. Edyvean, R. G. J. (1998) Comparison between biosorbents for the removal of metal ions from aqueous solutions. Water Research. 32, 216-224.

127. Cotton, F. A. Wilkinson, G. Murillo, C. A. Bochmann, M. (1999) Advanced Inorganic Chemistry. 6th Edition. John Wiley and sons, Inc. New York, U. S. A. pp 1355.

128. Keating, C. D. Musick, M. D. Keefe, M. H. Natan, M. J. (1999) Kinetics and thermodynamics of Au colloid monolayer self-assembly. Journal of Chemical Education. 76, 949-955.

129. Schnitzer, M. and Skinner, S. I. M (1965) Organic-metallic interactions in soil. 4. Carboxyl and hydroxyl groups in organic matter and metal retention. Soil Science. 99, 278-248.

130. Gardea-Torresdey J L, Tiemann K J, Gonzalez J H, Cano-Aguilera I, Henning J A and Townsend M S. (1996) Removal of nickel ions from aqueous solution by biomass and silica-immobilized biomass of *Medicago sativa* (alfalfa). Journal of Hazardous Materials. 49, 205-216.

131. Crist, R. H. Martin, R. J. Crist, D. R. (1999) Interaction of metal ions with acid sites of biosorbents Peat Moss and *Vaucheria* and model substances alginic acid and humic acids. Environmental Science and Technology. 33, 2252-2256.

132. Kadlec, R. H. Keoleian, G. A. (1986) Metal Ion Exchange on Peat. In: Peat and Water. Aspects of water retention and dewatering in Peat. C. H. Fuchsman (ed). Elsevier Applied Science Publishers Ltd, London. pp 61-93.

133. Percival, E. McDowel, R. H. (1967) Chemistry and Enzymology of Marine Algal Polysaccarides, Academic Press. London, U. K. pp 99-124.

134. Yu, Q. Kaewsarn, P. (1999) A model for pH dependent equilibrium of heavy metal biosorption. Korean Journal of Chemical Engineering. 16, 753-757.

135. Deshkar, A. M. Bokada, S. S. Dara, S. S. (1990) Modified *Hardwickia binata* bark for adsorption of mercury (II) from water. Water Research. 24, 1011-1016.

136. Schneider, I. A. H. Rubio, J. Misra, M. Smith, R. W. (1995) *Eichlornia crassipes* as biosorbent for heavy metal ions. Minerals Engineering. 18, 979-988.

137. Grimshaw, R. W. Harland, C. E. (1975) Ion-exchange: Introduction to Theory and Practice. The Chemical Society. London. pp 91.

138. Lee, H.S. Volesky, B. (1999) Characteristics of Aluminium biosorption by *Sargassum fluitans* biomass. Marine Biotechnology. 1, 380-383.

139. Watkins, W. Elder, R. C. Greene, B. Darnall, D. W. (1987) Determination of gold binding in an algal biomass using EXAFS and XANES. Inorganic Chemistry. 26, 1147-1151.

140. Hosea, M. Greene, B. McPherson, R. Henzl, M. Dale, A. M. Darnall, D. W. (1986) Accumulation of elemental gold on the alga *Chlorella vulgaris*. Inorganic Chimica Acta. 123, 253-261.

141. Crist, R. H. Martin, R. J. Carr, D. Watson, J. R. Clarke, H. J. Crist, D. R. (1994) Interaction of metals and protons with algae 4. Ion exchange vs adsorption models and a reassessment of Scatchard plots; ion exchange rates and equilibria compared with calcium alginate. Environmental Science and Technology. 28, 1859-1866.

142. Schiewer, S. Volesky, B. (1995) Modelling of the proton-metal ion exchange in biosorption. Environmental Science and Technology. 29, 3049-3058.

143. Guibal, E. Roulph, C. Lecloirec, P. (1992) Uranium biosorption by a filamentous fungus *Muchor-miehei* pH effect on mechanisms and performances of uptake. Water Research. 26, 1139-1145.

144. Westall, J. C. Leuenberger, C. Schwarzenbach, R. P. (1985) Influence of pH and ionic strength on the aqueous nonaqueous distribution of chlorinated phenols. Environmental Science and Technology. 19, 193-198.

145. Parkhurst, D. L. Appelo, C. A. J. (1999) User's guide to PHREEQC (version 2). A computer program for speciation, batch reaction, one-dimensional transport, and inverse geochemical calculations. U.S. Geological Survey. Denver, U.S.A. pp 311.

146. Dzombak, D. A. Morel, F. M. M. (1990) Surface Complexation Modeling. Hydrous Ferric Oxide. John Wiley. New York. Pp. 393.

147. Appelo, C. A. J. Postma, D. (1996) Geochemistry, Groundwater and Pollution. Rotterda, AA. Balkema. Pp 536.

148. Schecher, W. D. McVoy, V. C. (1994) MINEQL+ User's manual. Environmental research software. Hallowel, M. E. U.S.A.

149. Fergusson, J. E.(1990) The Heavy Elements: Chemistry, Environmental Impact and Health Effects. Pergamon Press. Oxford. Pp 614.

150. Schweiger, R. G. (1962) Acetylation of alginic acid II. Reaction of algin acetates with calcium and other divalent ions. Journal of Organic Chemistry. 27, 1789-1791.

151. Ke, H.Y.D. Anderson, W. L. Moncrief, R. M. Rayson, G. D. (1994) Luminescence studies of metal ion-binding sites on *Datura innoxia* biomaterial. Environmental Science and Technology. 28, 586, 591.

152. Trujillo, E. M. Jeffers, T. H. Fergusson, C. Stevenson, H. Q. (1991) Mathematically modelling the removal of heavy metals from a wastewater using immobilised biomass. Environmental Science and Technology. 25, 1559-1565.

153. Cox, A. G. Cook, I. G. McLeod, C. W. (1985) Rapid sequential determination of chromium (III) chromium (VI) by flow injection analysis-ICP-AES. Analyst. 10, 331-333.

154. Gardea-Torresdey, J. L. Tiemman, K. J. Armendariz, V. Bess-Oberto, L. Chianelli, R. R. Rios, J. Parsons, J. G. Gamez, G. (2000) Characterisation of Cr (VI) binding and reduction to Cr (III) by the agricultural byproducts of *Avena monida* (oat) biomass. Journal of Hazardous Materials. B80, 175-188.

155. Dupuy B, Arien A, Perrot Minot, A. (1994) Artificial Cells, Blood substrates, and Immobilisation. Biotechnology. *22*, 71- 82.

156. Kohn R. (1975) Ion binding on polyuronates, alginate and pectin. Pure and Applied Chemistry. 42, 371-397.

157. Sartori C. Finch, D. Ralph, B. Gilding, K (1997) Determination of the cation content of alginate thin films by Fti.r. spectroscopy. Polymer. 38, 43-51.

158. Golab, Z. Smith, R. W. (1992) Accumulation of lead in two fresh water algae. Minerals Engineering. 5, 1003-1010.

159. Siegee, D. C. (1998) Environmental SEM and X-ray microanalysis of biological materials. Mikrochimica Acta. 15, 283-293.

160. Gurman, S. J. Binsted, N. Ross, I. (1984) A rapid, exact curved-waved theory for EXAFS calculations. Journal of Physics C: Solid state Physics. 17, 143-151.

161. Gurman, S. J. (1988) The small atom approximation in EXAFS and surface EXAFS. Journal of Physics C: Solid State Physics. 21, 3699-3717.

162. Roy, M. Gurman, S. J. (1999) Amplitud reduction in EXAFS. Journal of Synchrotron Radiation. 6, 228-230.

163. Joyner, R. W. Martin, K. J. Meehan, P. (1987) some applications of statistical tests in analysis of EXAFS and SEXAFS data. Journal of Physics C: Solid State Physics. 20, 4005-4012.

164. Viegele. J.W. (1973) Atomic Data Tables. 5, 51.

165. Harrison, W. Trotter, J. (1972) Crystal and molecular structure of cadmium diacetate dihydrate. Journal of Chemical Society Dalton Transactions. 956-960.

166. Kwestrov, W. Langereis, C. (1965) Basic lead acetates. Journal of Inorganic Nuclear Chemistry. 27, 2533-2536.

167. Downie, T. C. Harrison, W. Raper, E. S. (1971) A three-dimensional study of the crystal structure of nickel acetate tetrahydrate. Acta Crystallographica Part B. 27, 706-712.

168. Mehrotra, R. C. Bohra, R. (1983) Metal Carboxylates. Academic Press INC. London. pp 396.

169. Davey,G. Stephens, F. S. (1970) Crystal and molecular structure of mono-α-picolinecopper (II) chloro-acetate. Journal of Chemical Society Communications (A). 2803-2805

170. Prout, C. K. Armstrong, R. A. Carruthers, J. r. Forrest, J. G. Murray-Rust, P. Rossotti, F. J. C. (1968) Structure and stability of carboxylate complexes. Part I. The crystal and molecular structures of copper (II) glycollate, DL-lactate, 2-hydroxy-2-methylpropionate, methoxyacetate, and phenoxyacetate. Journal of Chemistry Society A. 2791- 2813.

171. Yawney, D.B.W. Doedens, R. J. (1970) The crystal and molecular structure of copper (II) formate monourea. Inorganic Chemistry. 9, 1626-1632.

172. Blackeslee, A. E. Hoard, J. L. (1956) The structure of silver perfluorobutyrate. Journal of American Chemical Society. 78, 3029-3033.

173. Coggon, P. McPhail, A. T. (1972) X-ray crystal structure of a dimeric silver (I) complex containing short metal-metal separations. Journal of American Chemical Society Communications. 91, 92.

174. Crist, R. H. Oberholser, K McGarrity, J. Crist, D. R. Johnson, J. K. Brittsan, J. M. (1992) Interaction of metals and protons with algae. 3. Marine algae, with emphasis on lead and aluminium. Environmental Science and Technology 26, 496-502.

1. Atomic concentrations from X-ray Absorption Edge Steps

Standard transmission measurements of EXAFS or XANES spectra can be used to measure the concentration of the atom of interest in the sample. This cannot be done using fluorescence or reflection spectra because of the presence of unknown functions of energy in the data collection method.

In a transmission experiment, measurement of the voltages produced by two ion chambers was performed, one in front and one behind the sample, usually denoted by I_o and I_t respectively. The X-ray flux at the front and back surfaces of the samples, i_o and i_t are then given by:

$$i_o = aI_o \quad i_t = bI_t$$

Where a and b are unknown, slowly-varying functions of energy arising from the gas pressure in the ion chambers, amplifier settings, air absorption, etc. The absorption coefficient of the sample is then given by:

$$\mu = \ln(i_o / i_t) = \ln(a/b) + \ln(I_o / I_t)$$

The routine EXCALIB calculates $\ln(I_o / I_t)$ for a single scan and saves it. This function is equal to μ plus an unknown, slowly-varying function of energy. Thus, an absolute value for the sample absorption simply can not be obtained.

The sample absorption coefficient μ is due to all the atoms in the sample. It may be written as:

$$\mu = \sum_i \sigma_i n_i t$$

Where the sum is over the different atom types. σ_i is the absorption cross-section of atom type i, whose concentration is n_i atoms, m^{-3} and t is the sample thickness.

If two measurements are to be considered, immediately above and below the adsorption edge of an atom of interest, σ_i, a and b are constant except for σ_1 where the edge appears.

Therefore, the edge step as given by EXCALIB is:

$$\Delta\mu = \Delta\sigma_1 n_1 t$$

The adsorption edge step $\Delta\sigma_1$ can be obtained from tables (1). It is important to ignore the white line in the measured $\Delta\mu$ if these tables are used. The sample thickness is known. Hence, n_1, the atomic concentration of the species of interest can be determined.

5.3. Mean square deviation in interatomic distance

The mean square deviation in interatomic distance, σ^2, is one of the structural parameters obtained from an EXAFS analysis. In the EXCURV program, the parameter An is equal to $2\sigma^2$Å^2. This parameter contains two contributions, which are usually assumed to be independent:

$$\sigma^2 = \sigma_{th}^2(T) + \sigma_{st}^2$$

The first term is the thermal contribution arising from atomic vibrations, and this is clearly a function of sample temperature. The second is the static contribution, arising from the presence of different, unresolved, interatomic distances grouped together. It is of particular significance for non-crystalline samples although it may also arise in more complex crystalline structures. The two contributions can be separated by obtaining data at different sample temperatures. They can also be calculated, within simplifying assumptions. Thus for the thermal

contribution the Debye or Einstein model could be used, or a simple one-dimensional oscillator model of a molecular bond. For these calculations the values of characteristic temperatures or a vibration frequency are needed.

Static disorder

Because of the limited data range of an EXAFS spectrum, closely spaced contributions may not be resolved. The programmes will then fit to an average distance. In this, the presence of two or more different distances will contribute σ_{th}^2 to σ^2. In the simplest case of two distances, the mean distance is:

$$\bar{R} = (n_1 R_1 + n_2 R_2)/(n_1 + n_2) = R_1 + [n_2/(n_1 + n_2 1]\Delta R$$

where n_j atoms line at R_j and ΔR and $\Delta R = R_2 - R_1$:

Therefore

$$\sigma_{st}^2 = n_1(R_1 - \bar{R})^2 + n_2(R_2 - \bar{R})^2$$

$$= \frac{n_1 n_2}{(n_1 n_2)^2}(\Delta R)^2$$

Unresolved contributions generally will occur it $\Delta R \leq 0.1$ Å. For $n_1 = n_2$, $\sigma_{st}^2 = (\Delta R)^2/4$ or 25 x 10^{-4} Å^2 or less. Since $n_1 + n_2$ is generally constant, σ_{st}^2 arising from this source has a characteristic quadratic dependence on n_1 (and $\bar{R}$ a linear dependence on n_1) and this may be used to resolve the two distances in favourable circumstances (2).

Thermal disorder – Debye Theory

The thermal disorder arising from thermal vibrations produces well-know effects in both X-ray diffraction and EXAFS theory. For simple crystal structures, it is very well described by the Debye theory.

Textbooks on X-ray diffraction theory (3) show that the Debye theory results for the mean square amplitude of thermal vibration is

$$\bar{u^2} = \frac{3h^2T}{4\pi^2 mk\theta_o^2} f(\theta_0/T)$$

Where m is an atomic mass, θ_0 the Debye characteristic temperature and f a standard function as $T \to \infty, f(\theta,T) \to 1.0. f(\theta/T)$ rises slowly as T falls taking the value 1-1 at $T = \theta_0/2$. Except at low temperatures and for a few materials with very high Debye such as diamond we may take $f(\theta/T) = 1$.

EXAFS measures the m.s.d. in interatomic distance. If the atomic motions are uncorrelated, then $\sigma^2 = 2\bar{u^2}$. However, they are correlated, lon wavelength vibrations contributing little to changes in interatomic distance. The correlation may be calculated in the Debye theory (4) and we find:

$$\sigma_{th}^2 = 2(1-\gamma)\bar{u^2} = \frac{6(1-\gamma)h^2T}{4\pi^2 mk\theta_0^2} f(\theta_0/T)$$

γ is a function of both temperature and interatomic distance. For nearest neighbour at reasonable temperatures $\gamma \approx 1/3$. Thus if θ_0 is known, σ_{th}^2 may be calculated. For most materials at room temperature we find $\sigma_{th}^2 \approx$ 1000 x 10-4 Å^2. An EXAFS analysis with values very different from this is not accurate.

Thermal disorder – One-dimensional oscillator

In molecular applications a model using a one-dimensional oscillator, oscillating at the bond stretch frequency, is perhaps more appropriate. It is also much simpler than the Debye theory (in physics it is known as the Einstein (1906) model) and gives reasonable results for crystals.

A one-dimensional harmonic oscillator has allowed energy levels (n+1/2)hν where ν is the oscillation frequency. The probability of an oscillator being in the state n is given by the Boltzmann factor exp[-h-(n1/2) hν/kT] and so the mean energy of such an oscillator is:

$$\bar{\varepsilon} = h\upsilon\left[\frac{1}{2} + \frac{e^{-h\upsilon/kT}}{1-e^{h\upsilon/kT}}\right]$$

As $T \to 0, \bar{\varepsilon} \to h\upsilon/2$, the zero point of energy. $\bar{\varepsilon}$ may also be written as:

$$\bar{\varepsilon} = \frac{1}{2} h\upsilon \infty th(h\upsilon/2kT)$$

Showing that $\varepsilon \to kT$ as $T \to \infty$, the classical limit.

The mean P. E. is $\frac{1}{2}k\sigma^2$ with k the constant, or $\frac{1}{2}4\pi^2\mu\upsilon^2\sigma^2$, since $\omega = 2\pi\upsilon = \sqrt{k/\mu}$. μ is the reduced mass of the oscillator. Combining this result with equation 7 we have:

$$\sigma_{th}^2 = \frac{h}{8\pi^2\mu\upsilon}\infty_{th}\left(\frac{h\upsilon}{2kT}\right)$$

As $T \to \infty, \infty_{th} \to 2kT/h\upsilon$, therefore $\sigma_{th}^2 \to kT4\pi^2\pi\upsilon^2$, the classical limit, independent of h.

An Einstein temperature may be defined analogous to the Debye temperature, by $h\upsilon = k\theta_\varepsilon$.

In terms of this we have:

$$\sigma_{th}^2 = \frac{h^2}{8\pi^2 \mu k \theta_\varepsilon} \infty_{th}\left(\frac{\theta_\varepsilon}{2T}\right) \rightarrow \frac{h^{2kT}}{4\pi^2 \mu k^2 \theta_\varepsilon^2} \text{ as } T \rightarrow \infty$$

At high temperature we can compare the Debye and Einstein forms easily. The correlation factor γ takes care of the difference between the three-dimensional Debye and one-dimension oscillator forms. If we take γ = 1/3 we find the two values of σ_{th}^2 are identical if:

$$(\theta_\varepsilon/\theta_0)^2 = m/4\mu \approx 1/2$$

If we assume that $\mu = m/2$, the case for a element oscillator. This ratio is fairly well abeyed by values of θ_ε and θ_0 derived from specific heat measurements. Thus either model may be used to calculate σ_{th}^2. θ_ε may also be calculated for a molecular system if the stretch frequency ν is known. Alternatively, EXAFS measurements of σ^2 will indicate which part of the IR spectrum ν is to be sought. One obvious problem is the estimation of the effective mass μ.

References

1. Viegele, J.W. (1973) Atomic Data Tables, 5, 51.
2. Gurman, S. J. Williams, B. T Amiss, J. C. (2000) Structure and properties of amorphous silicon-metal alloys: II. The Si_{1-x} Ti_x system. Journal of Physics and Condensed Matter, 12, 5981-5990.
3. Cullity, B. D. (1956) Elements of X-ray Diffraction. Addison-Wesley Publishers Company. New York. pp 514
4. Gurman, S. J.(2001) personal communication.

Study of the Mechanisms of Cadmium Biosorption by Dealginated Seaweed Waste

MARÍA E. ROMERO-GONZALEZ,† CERI J. WILLIAMS,*,‡ AND PHILIP H. E. GARDINER†

Division of Chemistry, School of Science and Mathematics, Sheffield Hallam University, Howard Street, Sheffield S1 1WB, U.K., and Department of Chemical and Process Engineering, The University of Sheffield, Mappin Street, Sheffield S1 3JD, U.K.

The ability of dealginated seaweed waste, a waste material derived from the commercial processing of seaweed for alginate production, to remove cadmium from solution was determined. Cadmium sorption was found to be rapid (91% removal within 5 min), achieving a residual concentration of 0.8 mg L^{-1} after 1-h contact time from an initial solution concentration of 10 mg L^{-1}. The binding of cadmium by dealginate was found to be pH dependent, optimal sorption occurring at around pH 6–8. The mechanism of cadmium ion binding by dealginate was investigated by a number of techniques. Potentiometric titration of the dealginate revealed two distinct pK_a values, the first having a value similar to carboxyl groups and the second comparable with that of saturated thiols and amines. Esterification of the dealginate resulted in the subsequent reduction in cadmium sorption (95% to 17%), indicating that carboxyl groups are largely responsible for sorption. Evidence from FT-IR spectra confirmed the presence of carboxyl groups in untreated dealginate, while the number of carboxyl groups was markedly reduced in the esterified sample. Furthermore, the FT-IR spectrum for dealginate was found to be similar to that previously reported for mannuronic acid-rich calcium alginate. Determination of a molar ratio in the displacement of calcium by cadmium on dealginate further supported the presence of an ion-exchange relationship. The ion-exchange constant was calculated to be 0.329×10^{-6}. The speciation of cadmium in solution both before and after sorption was determined by an ion-selective electrode (ISE) technique. The findings of this study suggest that the sorption of cadmium by dealginate is mainly due to an ion-exchange mechanism.

Introduction

The contamination of water by toxic heavy metals is a worldwide environmental problem. Concern over this problem has led to the development of alternative technologies for effecting the removal of these pollutants from aqueous effluents. The use of low-cost and waste materials as adsorbents of dissolved metal ions has been shown to provide economic solutions to this global problem.

The search for an effective treatment technology for the removal of heavy metal ions, such as cadmium, has included the use of microorganisms (*1*), fungi (*2*–*4*), seaweeds and seaweed derivatives (*5*), and waste materials (*6*). The use of dead cells offers the following advantages (*7*): (i) the metal removal system is not subjected to metal toxicity limitations, (ii) there is no requirement for growth media and nutrients, and (c) the sorbed metal ions can be easily desorbed and the biomass can be reused. Furthermore, in a dead biomass-based sorption system where there are no metabolic interactions, they can be subjected to conventional theories and mathematical models already in place for traditional adsorption systems.

Cadmium is regarded as being highly toxic and is included with mercury in the so-called "Red List" of priority pollutants published by the Department of the Environment in 1987 and in List I of the EEC Dangerous Substances Directive (*8*). While the use of mercury in industrial processes is declining due to the introduction of new technologies, the worldwide industrial use of cadmium is increasing. This represents a great potential hazard to humans and the environment.

The potential of nonviable brown seaweeds in the recovery of heavy metal ions from liquid effluents has been demonstrated (*9*). Other researchers have demonstrated that the alginates, which are extracted from seaweeds for the food processing industry, also perform well as biosorbents (*10*). In addition, research by Apel and Torma (*11*) demonstrated that metal recovery by alginate biopolymers could be more easily achieved than the separation of other metal-loaded biomasses from the treated solutions.

In order to progress the understanding and application of these biosorbent systems so that they may be commercially exploited, it is important that the mechanisms involved in metal ion binding are elucidated and optimized. When a metal ion in solution interacts with a solid surface, a limited number of outcomes are possible (*12*). It can be sorbed by physical adsorption, associated with the weak forces of attraction such as van der Waals's forces, or by chemical sorption, associated with the exchange of electrons and the formation of a chemical bond between the sorbate and the solid surface (biosorbent). Alternatively, ion exchange may take place between the incoming cation and either sorbed metal ions or hydrogen ions of the functional groups at the sorbent surface. It is well-recognized that seaweeds and seaweed derivatives contain an array of functional groups on their surface structure, including carboxyl and sulfate groups that may be responsible for metal ion sorption and exchange.

This study aims to begin to unravel the mechanisms of the binding of cadmium to dealginated seaweed waste material through a detailed understanding of the behavior of those ions and their interaction with the surrounding environment (pH, presence of the biosorbent, presence of other ions). The findings suggest that ion exchange by electrostatic interaction is the mechanism of metal ion uptake. It is recognized that the chemical speciation of an element, which is defined as the determination of the individual physicochemical form of that element which together determines its total concentration as a sample, is critical to its availability for adsorption (*13*). Moreover, variations in the distribution of the species of an element due to physical and chemical changes within the sample can drastically affect its form and oxidation state and thus its bioavailability.

* Corresponding author e-mail: c.j.williams@sheffield.ac.uk; telephone: +44-114-222 7510; fax: +44-114-222 7501.
† Sheffield Hallam University.
‡ The University of Sheffield.

10.1021/es991133r CCC: $20.00
Published on Web 06/07/2001

In this study, the ability of dealginated seaweed waste, a waste product from the alginate industry, to sorb cadmium ions from dilute solution is determined. Polysaccharides produced by marine macroalgae (seaweeds) form the basis of an economically important and expanding global industry, which produces significant tonages of alginate-free seaweed waste (*14*). The use of this waste material to remove and recover metal ions from aqueous effluents would be both environmentally and energetically satisfying.

Materials and Methods

Source and Pretreatment of Dealginate. The dealginated seaweed waste, referred to from hereon as dealginate, was supplied courtesy of FMC BioPolymer AS, Haugesund, Norway. This material is the residue remaining after the commercial extraction of alginates and carageenans for the food and pharmaceutical industries. The material has undergone a number of processing steps in the extraction of alginates before being finally dewatered by calcium precipitation prior to disposal. This material has a moisture content of 66%, and the fresh product was stored in the frozen state in order to prevent microbiological spoilage and possible alterations in the biosorption performance of the material. Before use, the material was washed several times with deionized water to remove any precipitated salt. Any cations bound to dealginate such as calcium, sodium, potassium, and magnesium were removed by washing with 1.0 M HCl. The mixture of acid and dealginate at a mass-to-volume ratio of 10 g L^{-1} was stirred with a magnetic stirrer for 2 h, and then the supernatant was decanted. This washing process was repeated five times, and finally the sample of dealginate was washed with deionized water. The water was carefully decanted, making sure that none of the dealginate was lost. The moist dealginate was air-dried before use.

Effect of pH on Cadmium Biosorption. All reagents used were of Aristar grade supplied by BDH, Poole, U.K. A total of 10 g of dealginate was weighed into individual 2-L beakers that had been acid-washed with 1% HNO_3 to remove metal contamination. One liter of 10 mg L^{-1} cadmium solution, prepared from a 1000 mg L^{-1} stock solution made by dissolving 2.7436 g of cadmium nitrate in deionized water, was transferred into each beaker. The mixture was agitated with a magnetic stirrer, and the pH was adjusted to a given value and kept constant with the addition of either 0.1 M NaOH or 0.1 M HCl. The pH was continuously monitored using an immersed pH electrode (Gelplas, BDH, Poole, Dorset, U.K.) connected to a pH meter (Orion, model 740A, Beverly, MA). The pH values investigated were 2.0, 3.0, 4.0, 5.0, 6.0, 7.0, 8.0, and 10.0, respectively.

After pH adjustment, 5-mL aliquots of the solution were taken at 5-, 10-, and 30-min and 1-, 2-, 3-, 4-, 5-, 6-, 7-, 8-, 12-, and 24-h intervals, making sure that the dealginate was not removed during the process. Each 5-mL aliquot was filtered through a Whatman No. 1 filter paper, and the cadmium concentration in the filtrate was determined by inductively coupled plasma atomic emission spectrometry (ICP-AES). All experiments were conducted in triplicate. Control experiments without dealginate were carried out in order to determine the degree of removal of cadmium from solution by the glassware and filter papers. Extraneous metal contamination was found to be negligible.

Calculation of Ion-Exchange Constant K_{ex}^{H}. Sorption experiments were conducted using a batch method, except that the initial solution pH was maintained at pH 6, and the solution and the dealginate were in contact for 1 h. The initial cadmium concentration was varied between 1 and 1000 mg L^{-1}. The concentrations of cadmium in these solutions were determined by ICP-AES.

Ion-exchange equilibrium constants were determined using the model proposed by Crist et al. (*15*). The following reaction was assumed, at pH 6:

$$Cd^{2+} + 2(HX) = 2H^{+} + (CdX_2) \quad (1)$$

$$K_{ex}^{H} = \frac{[H^{+}]^2(CdX_2)}{[Cd^{2+}](HX)^2} \quad (2)$$

where (HX) represents the number of acid sites on the solid phase, (CdX_2) is sorbed Cd^{2+}, and [H^+] was calculated from the solution pH.

The unreacted (HX) required for this calculation is given by

$$(HX) = (HX)_o - H^{+}off \quad (3)$$

where $(HX)_o$ is the initial number of acids sites present at pH 6.

Calcium Displacement Investigation. A total of 0.2 g of dried dealginate was weighed into each of five 25-mL flasks. Following the addition of 10 mL of deionized water to each flask, the pH was adjusted to 6 by the addition of 0.01 M calcium hydroxide. Aliquots of 0.1 M cadmium standard solution were added to each flask to give final cadmium concentrations of 0, 0.5, 1, 2, and 4 mM, respectively. The pH of the solutions was kept at 6 with the addition of 0.01 M lithium hydroxide as required. The solutions were stirred and left in contact with dealginate for a period of 2 h. The dealginate was removed by filtration (Whatman No. 1 filter paper), and the concentrations of cadmium, lithium, and calcium ions in the solutions were determined by ICP-AES. The dealginate samples remaining at the end of the experiment were analyzed for calcium content after suspension in 10 mL of concentrated HNO_3.

Titration of Dealginated Seaweed. Dealginated seaweed samples were titrated potentiometrically using an automatic titrator (Metrohm 678 EP/KF processor, Herisau, Switzerland) with a combined pH glass electrode (model 6.0202). A total of 2.0 g of the dry sample was suspended in a reaction vessel containing 50 mL of 0.1 M $NaClO_4$ used as an inert electrolyte to keep the ionic strength of the solution constant. The sample was stirred and continuously purged with nitrogen. Standardized 0.1 M HCl or 0.1 M NaOH was added to the sample, and the solution pH was recorded. The software package Microcal Origin 5.0 (Microcal Software Inc, Northhampton, USA) was used to calculate the first derivative of the titration curve.

Speciation of Cadmium Ions in the Sorption Process. To find out the form of cadmium in the supernatant after metal sorption on dealginate, the concentration of free metal ions in the solution was determined using a cadmium ion-selective electrode (Orion Sure Flow combination cadmium electrode model 9648, Beverly, MA). The electrode response and the calibration curve were determined using standard solutions of cadmium, prepared from cadmium nitrate at concentrations ranging from 0.01 to 1000 mg L^{-1}. The pH of all the solutions was adjusted to 7, and a 5 M $NaNO_3$ solution (Orion ISA 940011, Beverly, MA) was used in order to adjust the ionic strength of the samples and standards. The 10-mL aliquots of cadmium standard solution or sample were placed in a beaker, and 200 μL of ionic strength adjustor was added. The electrode was immersed in the solution until a stable reading was obtained. Calibration curves were constructed from the least concentrated to most concentrated standard. The minimum detectable concentration was 1 μg L^{-1} of cadmium, and the linear range of the calibration curve was found to be within the concentration range of 0.1−1000 mg L^{-1} of cadmium.

Esterification of Dealginated Seaweed. Modification of the carboxyl groups on the surface of the dealginate using

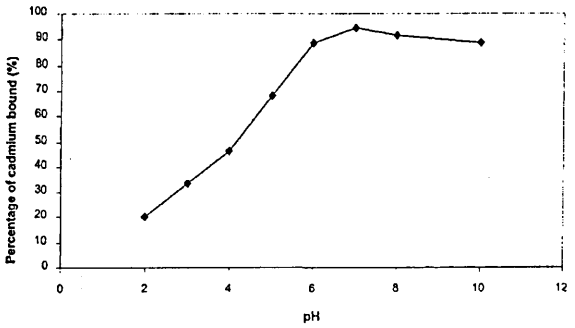

FIGURE 1. Effect of solution pH on cadmium sorption.

acidic methanol was performed as follows: 9 g of dry-washed dealginate was suspended in 633 mL of 99.9% methanol to which 5.4 mL of concentrated hydrochloric acid was added (0.1 M HCl final concentration). The solution was continuously stirred and heated to 60 °C for 48 h. The biomass was then washed three times with cold deionized water in order to quench the esterification reaction and was then centrifuged to remove excess water. The esterified sample was lyophilized and used in metal binding experiments (*16*).

FT-IR Spectroscopy. The spectra of dried, calcium-containing, cadmium-containing, and esterified dealginate were obtained using a Nicolet 860 ESP Magna infrared spectrometer (Nicolet, Wisconsin) employing a Nicolet Smart Golden Gate Single Reflection Diamond ATR accessory (Specac, Nicolet, Wisconsin) and featuring a type IIa diamond with up to 250 lb of pressure available to keep the sample in optical contact with the diamond. An aliquot of the dry sample was placed in the Golden Gate Single Reflection Diamond accessory in the infrared spectrometer, and the infrared spectra were obtained and averaged over 5 scans in transmission mode.

Results and Discussion

Rate of Cadmium Sorption. Results showed that at pH 6, where there was maximum cadmium retention (see below for pH effect), sorption was rapid, and about 91% of the cadmium in solution was removed in the first 5 min with a residual concentration of 0.8 mg L^{-1} achieved after the first hour. This fell to 0.4 mg L^{-1} after 24 h. As a result of these findings, 1-h contact time was used in all subsequent sorption experiments unless otherwise stated. The coefficient of variation of all data points was less than 6%. Although only data for cadmium sorption has been reported in this paper, the authors have found that a range of toxic metals (Pb, Cu, Ni, and Cr) can be removed from solution by this sorbent material (*17*).

Effect of pH on Cadmium Biosorption. Figure 1 shows the removal of cadmium from 10 mg L^{-1} solution after 1 h at solution pH values of 2, 3, 4, 6, 7, 8, and 10. The optimal cadmium removal occurred at a solution pH of 6. The least cadmium was removed when the solution pH was maintained at 2. Gardea-Torresdey et al. (*18*) noted that the ionization constants for different carboxyl groups were around 3–4. This means that when the pH is higher than 4 the carboxyl groups are deprotonated and therefore negatively charged and able to bind positively charged metal ions. At pH values less than 3, the carboxyl groups become protonated and thus are no longer available to attract metal ions from solution. The situation is likely to be different at high solution pH values. Stumm and Morgan (*19*) reported that hydroxyl species are formed above pH 8, with $Cd(OH)_2$ and $Cd(OH)_3^-$ formed at pH values of 9 and 11, respectively. Therefore at pH 6, cadmium precipitation as hydroxide is not a possible retention mechanism.

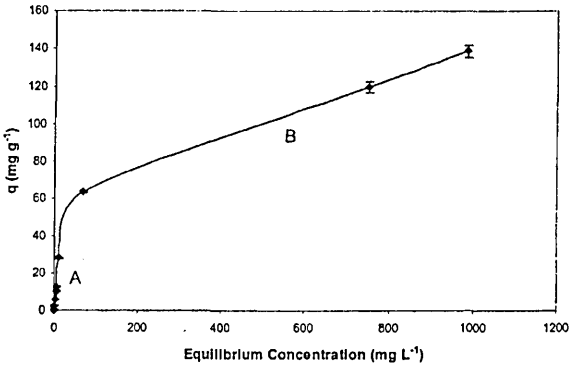

FIGURE 2. Isotherm for the adsorption of cadmium by dealginate.

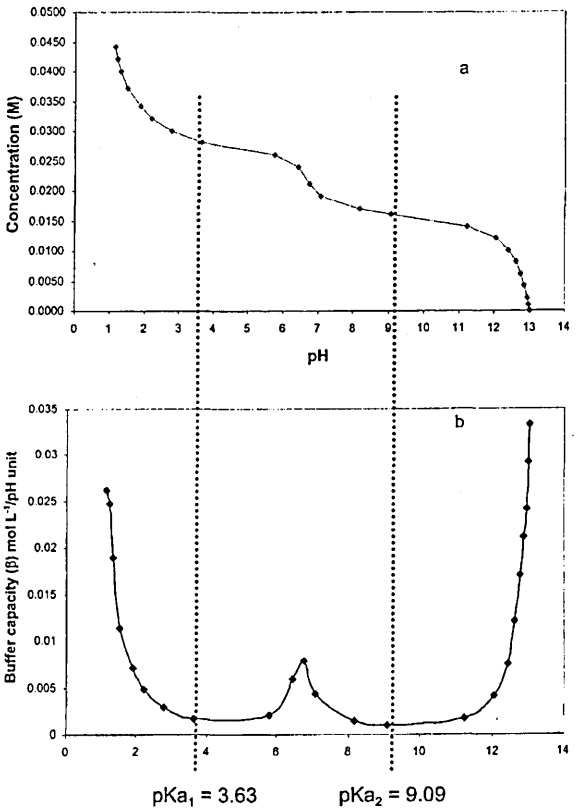

FIGURE 3. (a) Titration data for dealginate. (b) Plot of buffer capacity (β) against pH.

Sorption Isotherm. Figure 2 shows the representation of the cadmium sorption isotherm, the capacity (q) of dealginate (in mg g^{-1}) against the equilibrium concentration at pH 6. The shape of the curve can be divided into two regions, A and B. The shape of the curve would seem to indicate that there are two types of cadmium binding sites. As the readily available sites in region A become saturated, the excess cadmium is bound to another type of site with reduced affinity for the metal as shown by the slope of the graph in region B.

Titration of Dealginated Seaweed. A sample of dealginate was titrated with acid or alkali in order to identify possible metal binding sites. The titration data obtained are shown in Figure 3a. Two end points were clearly discernible in the plot of the cadmium concentration against pH. Figure 3b shows a plot of buffer capacity, defined as the inverse of the slope of the titration curve: $\beta = -\delta C/\delta pH$, against pH. This approach was used to calculate the acidity constants (pK_a)

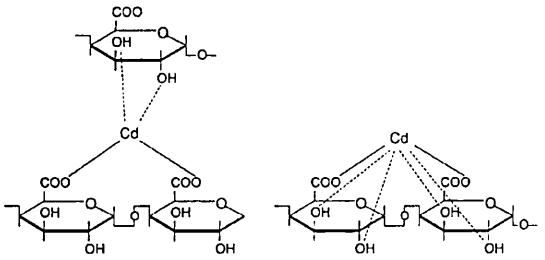

FIGURE 4. Possible cadmium binding sites on polyuronates (after Schweiger (*20*)).

since the maximum buffer capacity occurs where [HA] = [A^-] and, therefore, pH = pK. The two pK_a values found were pK_{a1} = 3.63 and pK_{a2} = 9.09, respectively. The pK_{a1} is comparable to the values reported for carboxylic acids (*18*). The pK_{a2} value is similar to those reported for saturated thiols or saturated amines (8.5−12.5) (*19*). These groups are likely to be responsible for metal ion sorption. The point of zero charge calculated from the relationship PZC = 0.5(pK_1 + pK_2) was 6.36. Thus, at low pH below 6.4, the biomass has a net positive charge resulting in low metal sorption. Maximum sorption is likely to occur at pH values greater than 6.4 when the biomass has a net negative charge.

Esterification of Dealginated Seaweed. In an attempt to identify the nature of the functional group responsible for cadmium adsorption, the carboxyl groups were esterified using the procedure described by Gardea-Torresday et al. (*16*). Results from the adsorption experiments showed that the amount of cadmium bound was reduced from 95% to 17%, suggesting that cadmium ions bind to carboxyl groups. However, the residual sorption after esterification is indicative of the presence of other cadmium binding sites. Although this material has been produced from a mixture of seaweeds that have been chemically treated, it could still contain residues of polyuronates (alginates). According to the manufacturers, the waste contains about 1% alginic acid. The decrease in the affinity for cadmium is analogous to that reported for calcium in which its affinity for polyuronates decreases with increasing esterification. Schweiger (*20*) has proposed two possible mechanisms by which divalent cations bind to polyuronates (see Figure 4). It is to be expected that in either case esterification of the carboxyl groups will result in diminished affinity for cations. However, some metal binding will still remain presumably due to the interaction with the vicinal hydroxyl groups.

FT-IR Spectra of Dealginate. To better understand the nature of the functional groups responsible for cadmium binding, FT-IR spectra of preparations of dealginate bound

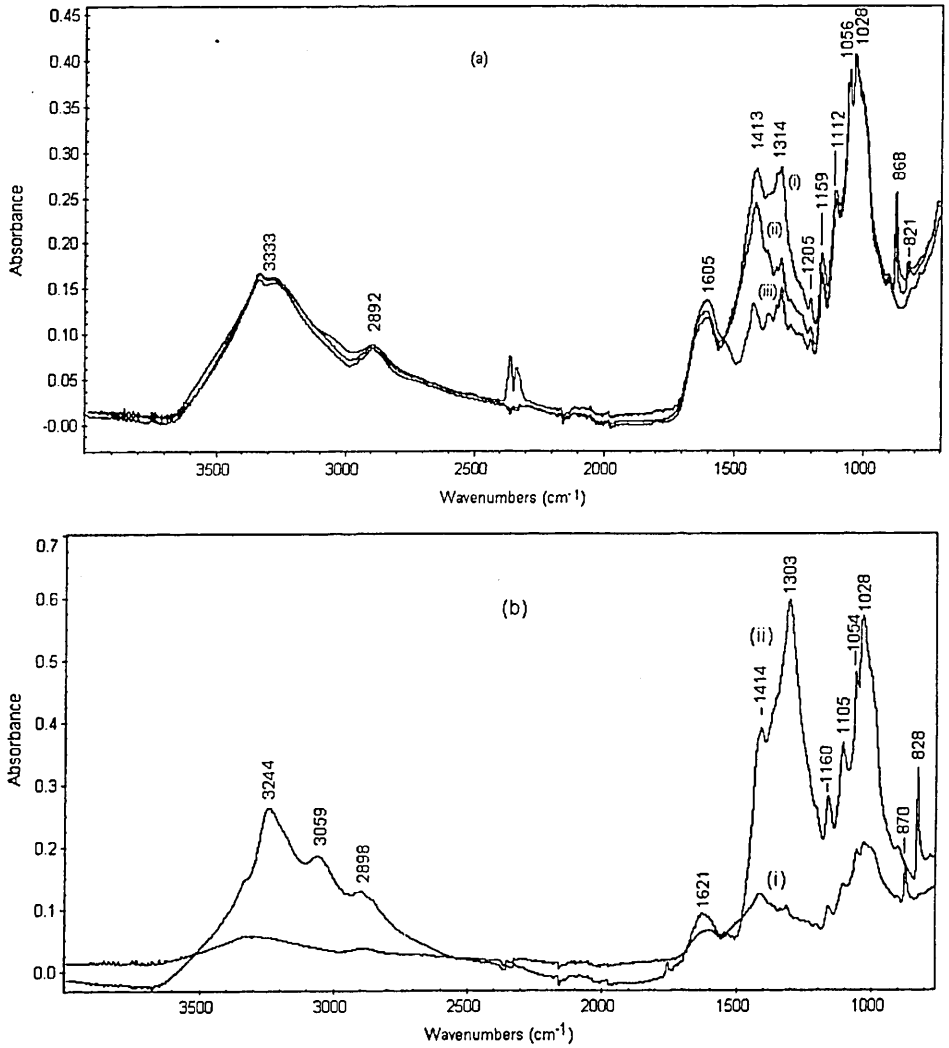

FIGURE 5. (a) FT-IT spectra of (i) cadmium-bound dealginate, (ii) calcium-bound dealginate, and (iii) dried HCl-washed dealginate. (b) FT-IR spectra of (i) esterified dealginate and (ii) cadmium-bound esterified dealginate.

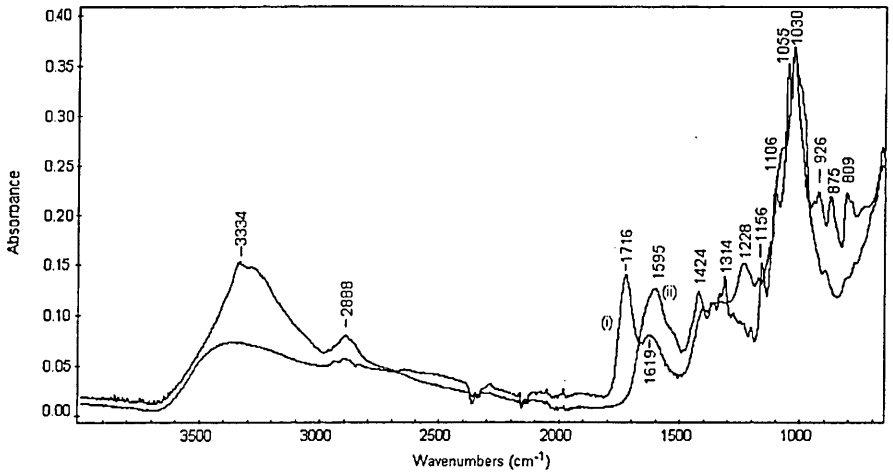

FIGURE 6. FT-IR spectra of (i) alginic acid and (ii) dried HCl-washed dealginate.

TABLE 1. Assignments of Infrared Absorption Bands for Cadmium Dealginate, Calcium Dealginate, and Hydrochloric Acid-Washed Dealginate[a]

wavenumber (cm^{-1})	intensity-shape	assignment
3500–3000	strong-broad	O–H stretching C–H stretching
2892 (2904)	medium-shoulder	C–H stretching O–H stretching
1605 (1609)	medium-shoulder	COO^- stretching (asymmetric)
1413 (1420)	(i) v strong-shoulder (ii) v strong-sharp (iii) medium-shoulder	COO^- stretching (symmetric)
1314 (1328)	(i) v strong-shoulder (ii) medium-shoulder (iii) medium-sharp	C–O stretching
1205 (1200)	medium-shoulder	C–C stretching
1159 (1155)	medium-sharp	C–C stretching C–O stretching C–C–C bending
1112 (1115)	strong-shoulder	C–C stretching C–O stretching
1056 (1047)	v strong-shoulder	O–H bending
1028 (1027)	v strong-sharp	C–C
868 (882)	strong-sharp	C–C–O C–O–C
821 (811)	medium-sharp	C–O

[a] Numbers in parentheses are those of mannuronic acid-rich calcium alginate.

samples were obtained. The FT-IR spectra of the dried HCl washed, calcium- and cadmium-containing dealginate are shown in Figure 5a. The bands assignments are shown in Table 1. In the fingerprint region (below 2000 cm^{-1}) bands at 1605, 1413, 1205, 1159, 1112, 1056, 1028, and 868 cm^{-1} overlap in all the three samples; the band at 1314 cm^{-1} is weak in the HCl and calcium spectra, whereas it is strong in the case of cadmium. The medium sharp band at 821 cm^{-1} is unique to the cadmium-bound sample. In a review of ion binding on polyuronates, Kohn (*21*) proposes that divalent cations are bound by ionic exchange through binding to carboxyl groups. The FT-IR results show that cadmium and calcium bind to the carboxyl groups. This is confirmed by the disappearance of the strong band and the appearance of a shoulder at 1414 cm^{-1}, when the cadmium esterified sample was examined (see Figure 5b).

The spectrum of the HCl-washed dealginate shows similar characteristics to that of mannuronic acid-rich calcium alginate as reported by Dupuy et al. (*22*) (see numbers in parentheses in Table 1). The wavenumber difference between the two bands assigned to the asymmetric and symmetric vibrations of the carboxyl group in both calcium alginate and dealginate are similar: 189 and 186 cm^{-1}, respectively. Although the dealginate sample has been acid-washed to remove metals bound to the material, there is no evidence of the presence of nonionized carboxyl groups as seen at 1716 cm^{-1} in the alginic acid spectrum (Figure 6). Evidence from the FT-IR spectrum of dealginate suggests that functional groups contributing to the dealginate spectrum may be similar to those in calcium alginate. Mannuronic and guluronic acid units make up alginate, and the dealginate spectrum is similar to that for the mannuronic acid-rich calcium alginate. According to Kohn (*21*), the affinity of the monomers of the two acids for calcium are identical, suggesting that the nature of the calcium interactions with both are similar. This is possible because all polyuronates have to some extent similar primary structures. Comparison of the spectra obtained from esterified dealginate with and without cadmium addition show prominent new bands at 3244, 3059, 1303, and 828 cm^{-1}, respectively, in the former. The bands at 1314 and 1304 cm^{-1} in the cadmium-containing nonesterified and esterified dealginate samples, respectively, point to the presence of another cadmium binding site in addition to the carboxyl groups (see Figure 5b).

TABLE 2. Effect of Calcium Displacement on Cadmium Sorption by Dealginate

parameter	value			
initial Cd concn (mM)	0.5	1	2	4
Ca displaced (μmol g^{-1})	225	225	450	675
Cd adsorbed (μmol g^{-1})	300	369	588	875
ratio of Ca:Cd	1:1.3	1:1.6	1:1.3	1:1.3

Calcium Displacement Investigation. To investigate the nature of the cadmium dealginate interaction, the dealginate was contacted with a solution containing calcium, and then solutions of cadmium at known concentrations were added to the samples. The amount of calcium displaced was then estimated. This allowed the relationship between calcium displacement and cadmium sorption to be determined. The data are shown in Table 2. The ratios of calcium displaced to cadmium sorbed showed that approximately 1 mol of calcium was displaced when 1 mol of cadmium was sorbed, regardless of the initial cadmium concentration. These results confirm that ion exchange may be one of the mechanisms for the binding of cadmium by dealginate.

Calculation of Ion-Exchange Constant K_{ex}^{II}. To assess the extent of cadmium binding by ion exchange, the ion-

TABLE 3. Cadmium Concentration before and after Addition of Dealginate as Determined by ICP-AES and ISE

initial Cd concn by ICP-AES (mg L^{-1})	initial Cd concn by ISE (mg L^{-1})	Cd concn by ICP (mg L^{-1}) after adsorption	Cd concn by ISE (mg L^{-1}) after adsorption
1.02	0.99	0.17	0.03
5.10	5.02	0.49	0.17
9.96	9.87	0.68	0.22
24.99	25.30	1.20	0.71
49.93	49.48	2.09	0.60
79.80	80.01	3.56	1.31
100.30	100.02	4.49	1.65

exchange constant K_{ex}^{H} was determined. The ion-exchange constant was calculated using a value of $(HX)_o$ of 2.90 mM g^{-1}. This value of $(HX)_o$ was derived using a minimization procedure in which the value of $(HX)_o$ was adjusted by several iterations until the values of K_{ex}^{H}, which was calculated for a series of solutions with different initial metal concentrations, gave a minimum error. This was considered to be the optimum value of $(HX)_o$. The value of the ion-exchange constant, K_{ex}^{H}, was found to be $0.329 \pm 0.049 \times 10^{-6}$ as compared with a value of K_{ex}^{H} of $9.3 \pm 0.85 \times 10^{-6}$ reported by Crist et al. (*15*) for cadmium adsorption by peat moss at pH 6.

Speciation of Cadmium Ions in the Adsorption Process. The speciation of cadmium ions in the solutions collected during the isotherm experiments was determined by comparative analysis of the samples by ICP-AES and by ion selective electrode (ISE). The results of these analyses are shown in Table 3. The ISE technique is the only analytical technique available that can measure the concentration of free metal species (*13*). The results from the ISE analysis provide a measure of the concentration of free Cd^{2+} ions in the dealginate supernatant solution. It should be noted that while the results of the determination of cadmium by the two techniques in the initial solution are similar, once dealginate is added only about 30% of the cadmium left in solution was in the free form. These results show that despite extensive washing before use, ligands that bound cadmium are introduced into the solution. Therefore, only a fraction of the cadmium in equilibrium with dealginate is available for exchange. The amount of cadmium in this fraction was less than 10% of the initial concentration. This could explain the residual cadmium concentration in solution even after 24 h of contact.

This study has demonstrated that cadmium binding to dealginate seaweed waste is similar in some aspects to that of calcium to polyuronates. Mannuronic and guluronic acid residues may be the major constituents responsible for cadmium sorption in dealginate. The evidence is of a predominantly ion-exchange mechanism involving carboxyl groups on the surface of the dealginate.

Acknowledgments

M.E.R.-G. is grateful for the financial support from CONICIT and LUZ, Venezuela. J. Meza is thanked for assistance with the potentiometric titration experiments.

Literature Cited

(1) Brierley, C. L. *Geomicrobiol. J.* **1990**, *8*, 201–223.
(2) Huang, C.; Huang, C. P. *Water Res.* **1996**, *30*, 1985–1990.
(3) Volesky, B.; Holan, Z. R. *Biotechnol. Prog.* **1995**, *11*, 235–250.
(4) Tobin, J. M.; Cooper, D. G.; Neufeld, R. J. *Appl. Environ. Microb.* **1984**, *47*, 821–824.
(5) Williams, C. J.; Edyvean, R. G. J. *Trans. Inst. Chem. Eng.* **1997**, *75B*, 19–26.
(6) Orhan, Y.; Buyukgungor, H. *Water Sci. Technol.* **1993**, *28*, 247–255.
(7) Gadd, G. M. In *Microbial Mineral Recovery*; Ehrlich, H. J., Brierley, C. L., Ed.; McGraw-Hill: New York, 1990; pp 249–276.
(8) *Dangerous Substances Directive*; 1976; 76/464/EEC.
(9) Wilson, M. W.; Edyvean, R. G. J. *Inst. Chem. Eng. Symp. Ser.* **1993**, *132*, 185–196.
(10) Jang, L. K.; Brand, W.; Resong, M.; Manieri, W.; Geesey, G. G. *Environ. Prog.* **1990**, *9*, 269–274.
(11) Apel, M. L.; Torma, A. E. *Can. J. Chem. Eng.* **1993**, *71*, 652–656.
(12) Delgado, A.; Anselmo, A. M.; Novais, J. M. *Water Environ. Res.* **1998**, *70*, 370–375.
(13) Florence, T. M. *Talanta* **1982**, *29*, 345–364.
(14) Renn, D. *Tibtech* **1997**, *5*, 10–14.
(15) Crist, R. H.; Martin, J. R.; Crist, D. R. *Environ. Sci. Technol.* **1999**, *33*, 2252–2256.
(16) Gardea-Torresdey, J. L.; Becker-Hapak, M. K.; Hosea, J. M.; Darnall, D. W. *Environ. Sci. Technol.* **1990**, *24*, 1372–1378.
(17) Romero-González, M. E.; Williams, C. J.; Gardiner, P. H. E. *J. Anal. At. Spectrom.* **2000**, *15*, 1009–1013.
(18) Gardea-Torresdey, J. L.; Tiemann, K. J.; Gonzalez, J. H.; Cano-Aguilera, I.; Henning, J. A.; Townsend, M. S. *J. Hazard Mater.* **1996**, *49*, 205–216.
(19) Stumm, W.; Morgan, J. J. *Aquatic Chemistry*; John Wiley and Sons: New York, 1996; p 1022.
(20) Schweiger, R. G. *J. Org. Chem.* **1962**, *27*, 1789–1791.
(21) Dupuy, B.; Arien, A.; Perrot Minot, A. *Artif. Cells, Blood Substitutes, Immobilization Biotechnol.* **1994**, *22*, 71–82.
(22) Kohn, R. *Pure Appl. Chem.* **1975**, *42*, 371–397.

Received for review October 4, 1999. Revised manuscript received April 11, 2001. Accepted April 17, 2001.

ES991133R

The application of dealginated seaweed as a cation exchanger for on-line preconcentration and chemical speciation of trace metals

JAAS
Interlaboratory Note

María Elena Romero-González,[a] Ceri J. Williams[b] and Philip H. E. Gardiner*[a]

[a]*Division of Chemistry, School of Science and Mathematics, Sheffield Hallam University, Howard Street, Sheffield S1 1WB, UK. E-mail: P.H.Gardiner@shu.ac.uk*
[b]*Department of Chemical and Process Engineering, University of Sheffield, Mappin Street, Sheffield S1 3JD, UK*

Received 6th April 2000, Accepted 12th June 2000
Published on the Web 11th July 2000

Methods for the on-line preconcentration of Cd^{2+}, Cr^{3+}, Cu^{2+} and Pb^{2+} and chemical speciation of Cr^{3+} and CrO_4^{2-} using a microcolumn (50 × 7 mm id) packed with about 0.34 g dealginated seaweed biomass are described. Preliminary batch experiments showed that metal sorption by the biomass is rapid, about 90% of the metals in solution is taken up in less than 5 min, and occurs in a wide pH range, 2–7. Maximum binding was obtained between pH 6 and 7 and the effective binding capacities at pH 6, determined from column breakthrough measurements using a flow rate of 0.8 mL min^{-1}, were 4.0, 8.7, 9.4 and 8.5 μmol g^{-1} for Cd, Cr Cu and Pb, respectively. Unretained CrO_4^{2-} was separated from Cr^{3+} thus making it possible to determine the levels of both species in solution. The analytical procedures developed for metal preconcentration and chromium speciation were validated by analyses of two Lake Ontario water reference materials, TMDA 51.2 and TMDA 54.2, and a synthetic seawater sample. Comparison of the results obtained by the proposed methods with the certified total values using the Student *t* test at 95% confidence limit showed that the differences were not statistically significant. Independent confirmation of the accuracy of the chromium speciation results was obtained using the measurement of absorbance of the 1,5-diphenylcarbohydrazide–chromium complex, before and after treatment with nitric acid, to determine the levels of CrO_4^{2-} and Cr^{3+} by difference. The results obtained with the proposed method for the analyses of TMDA 51.2 and TMDA 54.2 for Cr^{3+} and CrO_4^{2-} were 20±0.2 and 39±0.3 μg L^{-1}, and 162±1 and 299±1 μg L^{-1}, compared with 12±5 and 54±31, and 132±12 and 313±16 μg L^{-1}, respectively.

Introduction

Metal sorption by biomasses involves active uptake determined by metabolic processes such as ion transport, internal compartmentation and extracellular precipitation by excreted metabolites, as well as passive physico-chemical interactions with functional groups on cellular structural components.[1] The use of live microorganisms for active as opposed to passive retention and concentration of metals has been well documented.[2–7] In a number of applications, biomasses have been used to preconcentrate metals before determination by graphite furnace atomic absorption spectrometry,[8,9] inductively coupled plasma atomic emission spectrometry[10] and flame atomic absorption spectrometry.[11] Using this approach, enrichment factors of between 2- and 200-fold have been obtained after tedious and time-consuming sample pre-treatment steps. To improve the efficiency of this process, cells have been immobilised on suitable supports and used as column packing materials.[11–15]

In order to develop column materials that can withstand repeated use, non-living biomasses are preferred. Work in our laboratories has demonstrated that dealginated seaweed, a non-living biomass, can be used as a biosorbent to remove metals from aqueous solutions.[16,17] Dealginated seaweed is a seaweed derivative produced when commercially harvested seaweeds are subjected to alginate extraction by precipitation using calcium hydroxide or sodium hydroxide. This material, referred to as dealginate, is easy to handle and can be stored for long periods. It is physically stable and, therefore, there is no need to immobilise the material onto a support. In contrast to most commercially available ion exchangers, biosorbents possess an array of weakly acidic and basic functional groups, which enable them to bind metal ions.[18,19] All these attributes make dealginated seaweed a suitable material for use in the on-line preconcentration and subsequent determination of these metals by spectrometric techniques.

In this study the preconcentration and determination of copper, cadmium, chromium and lead in aqueous solutions using dealginated seaweed as a biosorbent in an on-line microcolumn configuration is described. These four elements were chosen because they are important environmental pollutants. The use of the column to study the distribution of Cr(III) and Cr(VI) species in aqueous solution is also reported.

Experimental

Reagents

A multielement stock solution containing 10 mg L^{-1} of Cd, Cr, Cu and Pb was prepared from individual 1000 mg L^{-1} Spectrosol solutions (BDH, Poole, Dorset, UK). Working standard solutions were prepared by dilution of the 10 mg L^{-1} stock solution. All reagents were Aristar grade and supplied by BDH. Concentrated HCl was diluted to give a 1.0 M solution. Deionized Millipore (Milli-Q RG) water was used throughout. The unbuffered standard solutions were kept in the pH range 5.5–6.5 by the addition of either 1.0 M solutions of HCl or NaOH. Buffered solutions were prepared in 0.05 M ammonium acetate except for copper which was prepared in 0.1 M potassium dihydrogen phosphate in order to avoid the formation of copper–ammine complexes.

Biosorbent

The biomass used was dealginated seaweed, a waste product from a mixture of commercially harvested brown seaweeds including *Ecklonia maxima* from which alginate has been

DOI: 10.1039/b002737p

removed by calcium hydroxide precipitation. The moisture content of the residue was about 66%. This material has currently no marketable value and was donated by Pronova Biopolymers Limited, Norway. Previous energy dispersive X-ray spectroscopy (EDAX) analysis[17] showed no significant quantity of metal ions except calcium, on the surface of the material prior to use.

Apparatus

Fig. 1 shows the schematic diagram of the on-line system. An ICP-AES (Spectro Instruments) or an ICP-MS (Hewlett Packard 4500) was used to determine the metal ion concentrations. The instrumental conditions are shown in Table 1. An orbital shaker (Gallenkamp) was used to agitate the samples during the batch uptake experiments. A pH electrode (Gelplas, BDH) connected to a pH meter (Orion model 740A) was used for pH measurements.

All glassware was cleaned and stored in a 1% v/v HNO_3 solution until required, and then thoroughly rinsed with deionised water before use.

Metal ion uptake efficiency

The time it took for equilibrium to be attained when solutions containing a single metal were added to dealginated seaweed was determined in batchwise experiments. A 50 mL aliquot of a 10 mg L^{-1} solution containing either Cd, Cr, Cu or Pb was added to 1.5 g of dealginated seaweed in a 150 mL conical flask at room temperature. The pH of the solution was taken and then the conical flask was agitated on an orbital shaker at 100 rpm for 5, 10, 30, 60, 120, 240, 300, 360 or 420 min. Following the period of agitation, the solution was filtered using a Whatman No 1 filter paper, and a sample of filtrate was taken for pH measurement. The concentrations of the metal in the initial and final solution were determined by ICP-AES and the amount of metal adsorbed was calculated from the results.

pH studies

1.5 g of dealginated seaweed was brought into contact batch wise with 50 mL of 10 mg L^{-1} single metal ion solutions of Cd, Cr, Cu or Pb. Both buffered and unbuffered solutions were used in this investigation. The buffered standard solutions were prepared in 0.05 M ammonium acetate, except for Cu which was prepared in a 0.01 M potassium dihydrogen phosphate. After pH adjustments with either hydrochloric acid, acetic acid, phosphoric acid, potassium hydroxide, sodium hydroxide or ammonium hydroxide, the solutions were left in contact with the biomass for 2 h. The solutions were filtered through a Whatman No 1 filter paper and the final pH values of the filtrates were recorded. The metal concentrations in the filtrates were determined by ICP-AES or ICP-MS.

Preparation and operation of the microcolumn

A sample of dealginate was oven dried at 105 °C overnight, allowed to cool and gently separated with a spatula. The sample was ground using a pestle and mortar and sieved. Particles retained in an 85-mesh screen (mean particle size approximately 120 μm) were used to pack the column. The column (50 mm × 7mm id MF-plus, Alltech Associates, Carnforth, Lancashire, UK) fitted with an acid resistant plastic PEEK frit was packed with a known weight of dry biomass (*ca.* 0.34 g) that had been slightly moistened to aid packing. The biomass was held in place by another frit fitted at the top of the column. The column was connected to the inductively coupled plasma atomic emission spectrometer. Deionised water followed by 1 M HCl was pumped through the column using the pump on the instrument at a flow rate of 0.8 mL min^{-1} for 10 min. In use, the column was connected on-line to either of the spectrometers using a 1.42 mm internal diameter tube (Altec Products Limited, Alton, Hampshire, UK) with the tube length (70 mm) kept short to minimise dead volume in operation. Deionised water was used as the carrier solution and pumped continuously through the column at a flow rate of 0.8 mL min^{-1}. For metal preconcentration, 1 mL of the multielement standard solutions at metal concentrations of 0.1, 0.25, 0.5 and 1.0 mg L^{-1} or samples were loaded into the injection valve using a syringe and then injected into the carrier stream and onto the column. The preconcentrated metals were stripped off by manually injecting 500 μL of 1.0 M HCl into the 1 mL sample loop on the column and detected by ICP-AES. Calibration graphs were constructed from the integrated area under each metal peak using the software package Microcal Origin 5.0 (Microcal Software Inc, Northampton, USA). Breakthrough experiments were carried out by pumping either individual or multielement standard solutions through the column at a flow rate of 0.8 mL min^{-1} until a constant signal intensity was obtained. When not in use, the column and contents were store at 4 °C in order to prevent bacterial and fungal growth.

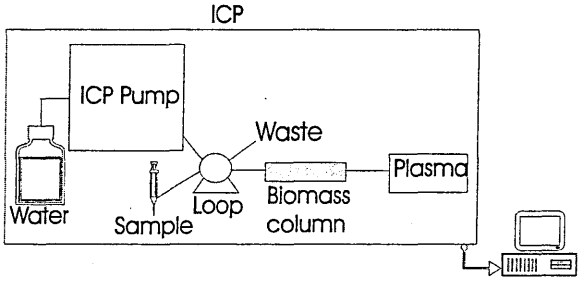

Fig. 1 Schematic diagram of the on line system for the preconcentration, speciation and determination of the metals.

Table 1 ICP operation conditions

ICP and sample introduction	ICP-MS	ICP-AES
Rf generator	1200 W	1200 W
Column to spray chamber distance	70 mm	70 mm
Torch	Fassel Torch	Three piece torch
Spray chamber	Cyclonic	Cyclonic
Nebulizer	Babington	Cross flow
Sample introduction	Peristaltic pump	Peristaltic pump
Solution uptake rate	0.8 ml min^{-1}	0.8 ml min^{-1}
Coolant gas flow rate	16 L min^{-1}	16 L min^{-1}
Nebulizer gas flow rate	1.28 L min^{-1}	1.0 L min^{-1}
Nebulizer gas pressure	590 kPa	234 kPa
No of sweeps per replicate	1	1
No of replicates	3	3
Masses/Wavelength/nm	^{111}Cd	Cd 226.502
	^{53}Cr	Cr 267.716
	^{63}Cu	Cu 324.754
	^{208}Pb	Pb 220.351
Measurement mode	Time resolved analysis	
Integration time	2 s	2 s
Detector mode	Dual mode	—

Distribution of Cr(III) and Cr(VI)

The same system configuration was used to study the distribution of chromium species, but here ICP-MS was used for Cr detection. As with metal preconcentration, 1 mL of a mixed chromium standard or sample was loaded onto the column *via* the injection valve. Unretained Cr(VI) was eluted almost immediately and detected. Adsorbed Cr(III) was stripped off using 500 μL of 1.0 M HCl as described for metal preconcentration. Calibration curves in the range 10–250 μg L^{-1} were prepared from mixed Cr(III) and Cr(VI) standards. Independent confirmation of the Cr(III):Cr(VI)

ratio was obtained by using the 1,5-diphenylcarbohydrazide method based on UV/Visible detection.[20]

Results and discussion

pH studies

Rate experiments in which metal solutions were in contact with the biomass for varying length of time have shown that 90% of the metals studied were taken up by the biomass in the first 5 min, with the equilibrium attained after 2 h (Fig. 2). The effects of pH on metal uptake as determined in batch experiments are shown in Fig. 3. The percentage of bound metal increases with pH from 2.0 to 6.0 with maximum binding occurring between pH 6.0 and 7.0. At pH 6, between 90 and 99% of Cd(II), Cu(II), Cr(III), Pb(II) and in solution was removed. Results obtained using both buffered and unbuffered solutions were similar. In the experiments with unbuffered solutions, the difference in pH before and after contact with the biomass was less than 0.1 pH units.

A net negative charge on the surface of dealginate at pH values greater than the isoelectric point would be expected to lower any electrostatic energy barrier for the cations to bind to the negatively charged material. This might explain the increased binding capacity at pH greater than 5. The functional groups responsible for binding these metals under different pH conditions are yet to be identified. Gardea Torresday *et al.*[21] found that this kind of behaviour suggests that carboxyl groups may play a major role in metal binding by biomass since the acid dissociation constants (pK_a) for various carboxyl groups are reported to be around 3–4. It is likely that the metal ions are bound to the biomass through the carboxyl groups in an ion-exchange type mechanism. At low pH values, the carboxyl groups are protonated thus reducing the available sites for metal binding.

Column capacity

The breakthrough curves for the four metals obtained separately are shown in Fig. 4. The eluted metals were detected by ICP-AES. A similar breakthrough volume of 6.4 mL was obtained for both Cd and Cr, and the values for Cu and Pb were 7.9 mL and 25.0 mL, respectively, using a 5 mg L^{-1} multielement solution buffered at pH 6. Based on the volumes at which saturation was obtained, the effective column capacities for each of the elements were: 4.0, 8.7, 9.4, 8.5 μmol g^{-1} for Cd, Cr, Cu and Pb, respectively. In similar experiments performed with single 5 mg L^{-1} element solutions, the column capacities were 8.0, 33.7, 26.0 and 12.0 μmol g^{-1} for Cd, Cr, Cu and Pb, respectively. The lower values obtained for the mixed standard indicate that the column capacity for each element is affected by the presence of the other elements. However, for preconcentration of trace metals, the available column capacity is more than adequate. It is important to note that the uptake of the metals by the column from the solution

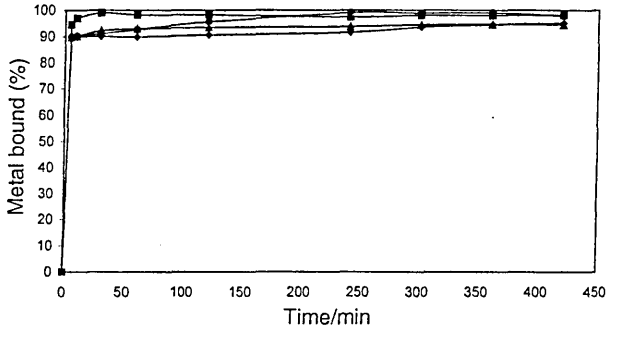

Fig. 2 The extent of Cd (▲), Cr (■), Cu (◆) and Pb (●) retention at pH 6 as a function of time ($n=3$).

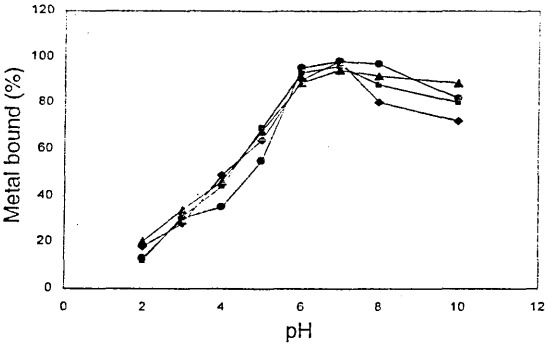

Fig. 3 The effect of the pH on the retention of Cd (▲), Cr (■), Cu (◆) and Pb (●) as determined in batch experiments at pH 6 ($n=3$).

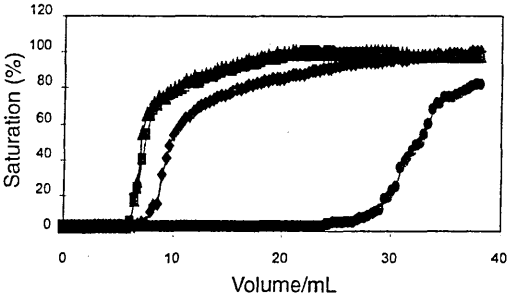

Fig. 4 Column breakthrough curves for Cd (▲), Cr (■), Cu (◆) and Pb (●) obtained using 1 mg L^{-1} of single metal ion solution at a flow rate of 0.8 mL min^{-1}, and pH 6.

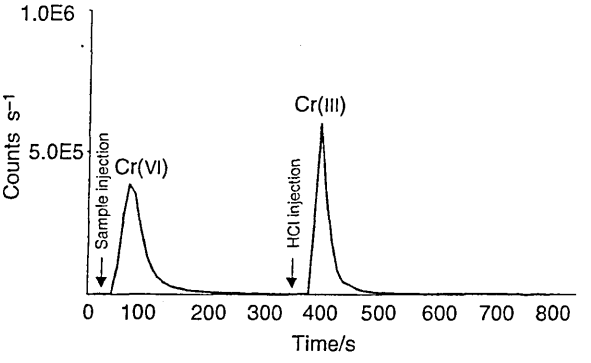

Fig. 5 Chromatogram of 25 μg L^{-1} of a mixed Cr(III) and Cr(VI) standard solution.

pumped in at 0.8 mL min^{-1} was complete until the breakthrough point, suggesting that the metal uptake by the biomass at that flow rate is not limited by kinetic factors.

The differences in breakthrough volumes suggest that the

Table 2 Results of the determination of Cd, Cr, Cu and Pb in two Lake Ontario water reference material and a simulated seawater sample

Sample	Element determined	Values found/ μg L^{-1} ($n=3$)	Certified values/ μg L^{-1} ($n=3$)
		$\bar{X}\pm1\,s$	$\bar{x}\pm1\,s$
TMDA 51.2	Cd	25±3	72±18.9
	Cr	60±8	62.5±6.6
	Cu	101±6	91±10.2
	Pb	67±13	72.9±10.6
TMDA 54.2	Cd	172±33	165±16.1
	Cr	450±34	432±32.1
	Cu	457±65	460±41.9
	Pb	498±66	531±54.4
Seawater	Cd	221±13	250±1
	Cr	243±6	251±2
	Cu	257±51	250±1
	Pb	249±17	252±4

Table 3 Comparison of the chromium speciation results obtained by the proposed and the 1,5-diphenylcarbohydrazide methods

		1,5-Diphenylcarbohydrazide method $\bar{x}\pm1\ s$ ($n=3$)		Proposed method $\bar{x}\pm1\ s$ ($n=3$)	
Sample	Reference value/μg L^{-1}	Cr(III)/μg L^{-1}	Cr(VI)/μg L^{-1}	Cr(III)/μg L^{-1}	Cr(VI)/μg L^{-1}
TMDA 51.2	62.5±6.6	12±5	54±31	20±0.2	39±0.3
TMDA 54.2	432±32.1	132±12	313±16	162±1	299±1

binding sites for Pb and Cu are different from those of Cd and Cr. Clearly, the sites for Pb are still available long after the sites for the other elements have become saturated. The aim of on going work is to characterise the different binding sites.

Development and validation of the analytical procedures

Sample volume and desorption experiments. Different volumes of a mixed standard solution at pH 6 containing 5 mg L^{-1} of each metal were preconcentrated and desorbed from the column using dilute HCl solutions. Up to 5 mL sample solutions could be injected, and about 90% of the metals was desorbed with 1.0 mL of 1.0 M HCl. The preconcentration and desorption cycles were repeated for a period of up to four months without adverse effects on the performance of the column. It is important to emphasis that no reconditioning of the column is necessary after the initial column preparation. For these series of measurements, a 1 mL sample loop was used and the metals were desorbed with 500 μL of 1.0 M HCl. With this set up, a two-fold increase in sensitivity, compared to when no column is used, was obtained for all four elements. This preconcentration factor is adequate for the analysis of the samples in this study. The calibration graphs in the range 0.1–1 mg L^{-1}, obtained from mixed metal standard solutions, were rectilinear with correlation coefficients (r^2) of 0.9982, 0.9984, 0.9995 and 0.9954 for Cd, Cu, Cr and Pb, respectively, and corresponding detection limits of 0.069 mg L^{-1}, 0.018 mg L^{-1}, 0.012 mg L^{-1} and 0.077 mg L^{-1} ($n=5$).

Analyses of water reference materials. Two Lake Ontario water reference materials (National Water Research Institute, Canada) TMDA 51.2 and TMDA 54.2 and a synthetic sea-water (Sea water corrosion test mixture to DEF 1053/B.S. 3900/B.S 2011, BDH, Poole, UK) were analysed in order to test the suitability of the procedure for the determination of the four elements in real samples. Up to 5 mL of the 5 mg L^{-1} mixed standard could be injected onto the column, and mean recoveries of 96, 93, 94 and 97% obtained for Cd, Cr, Cu and Pb, respectively, when 0.5 mL of 1.0 M HCl was used for desorption. For these determinations, the pH values of the Lake Ontario water reference materials were adjusted to 7.0 before metal preconcentration on the column. Comparisons of the results obtained with the certified values are given in Table 2. The differences between the two sets of results, except for Cd in TMDA 51.2, are not statistically significant at the 95% confidence limit. The reason for this disparity in the cadmium results is currently being investigated. The metal recoveries from the simulated sea-water sample were between 93–96% at pH 6.0 for the four elements studied, even though the ratio of Ca, Mg, Na and K ions to the elements were in most cases in excess of 100 : 1. In this configuration, the major cations Ca, Mg, Na and K in the sample were unretained by the column, and eluted well ahead of the preconcentrated metals.

Speciation studies. Fig. 5 shows that a broad chromium peak identified as Cr(VI) is eluted first and on subsequent injection of 500 μL of 1.0 M HCl a much sharper peak, corresponding to Cr(III), is observed. The point at which acid is injected could be chosen such that the sample throughput is increased. For these experiments the acid was injected after 350 s, but, as can be seen in the chromatogram, anytime between 250–350 s could have been chosen. The microcolumn was re-used immediately after the elution of Cr(III), in contrast to the system based on using activated alumina where three injections were required to completely strip the adsorbed Cr(VI) species.[22] A throughput of about fifty samples a day could be achieved using the system described here.

The results of the determination of the two chromium species were 39±0.3 μg L^{-1} and 20±0.2 μg L^{-1} for Cr(VI) and Cr(III), respectively, which gives a total chromium value of 59±0.4 μg L^{-1}, compared to a total certified value of 62.5±6.6 μg L^{-1}. A similar analysis of TMDA 54.2 ($n=3$) found 299±1 μg L^{-1} and 162±1 μg L^{-1} of Cr(VI) and Cr(III), respectively, and a total of 461±0.2 μg L^{-1}, compared to a certified total value of 432±32.1 μg L^{-1}. Detection limits, calculated as three times standard deviation of the background noise levels, were 0.97 μg L^{-1} and 0.28 μg L^{-1} ($n=10$) for Cr(VI) and Cr(III), respectively.

In order to demonstrate that chromium speciation was not altered when the sample was in contact with the column material, the Cr(VI) and total Cr levels were determined spectrophotometrically. The complexing agent 1,5-diphenylcarbohydrazide reacts with Cr(VI) to form a coloured complex, the absorbance of which is measured at 540 nm. Total Cr is determined after oxidation of Cr(III) to Cr(VI) with nitric acid. Comparison of the results obtained by both methods is presented in Table 3. The precision of the 1,5-diphenyl carbohydrazide method was poorer particularly at low concentrations. However, the comparison of the results shows that the differences in the values obtained by both methods are not statistically significant at the 95% confidence limit.

Conclusion

This study has demonstrated that dealginate, a waste product of the alginate extraction process, can be used as a column packing material for the preconcentration and determination of Cd, Cr, Cu and Pb at trace levels in aqueous solutions. Because dealginate is, in the main, a cation-exchanger, it can be used for separation and determination of levels of CrO_4^{2-} and Cr^{3+} in environmental samples. The binding capacities of the material for the elements studied are adequate for trace analysis and also the biomass is a much cheaper alternative to synthetic resins. In addition, a single 500 μL injection of 1 M HCl is adequate for stripping the adsorbed metals from the column. With this set-up, a preconcentration factor of two was adequate for the analysis of the reference materials, however, depending on the concentration on the metals in a sample and the method of detection, concentration factors of 10 and higher could easily be obtained when the column is used in an off-line configuration.

Acknowledgements

M. E. Romero-González is grateful for the financial support from CONICIT and LUZ, Venezuela.

References

1 G. M. Gaad, in *Biotechnology*, ed. H. J. Rehm and G. Reed, VCH, Winheim, 1998, vol. 613, p. 401.
2 A. Delgado, A. M. Anselmo and J. M. Novais, *Water Environ. Res.*, 1998, **70**(3), 370.
3 B. Volesky, H. May and Z. R. Holan, *Biotechnol. Bioeng.*, 1993, **41**, 826.
4 J. A. Scott and S. J. Palmer, *Appl. Microbiol. Biotechnol.*, 1990, **33**, 221.
5 N. Kuyucak and B. Volesky, *Biorecovery*, 1989, **1**, 219.
6 Y. Madrid, E. Barrio-Córdoba and C. Cámara, *Analyst*, 1998, **123**, 1593.
7 A. J. Aller and L. C. Robles, *J. Anal. At. Spectrom.*, 1998, **13**, 469.
8 V. Mahidi and J. A. Holcombe, *J. Anal. At. Spectrom.*, 1989, **4**, 439.
9 M. Shengjun and J. A. Holcombe, *Anal. Chem.*, 1990, **62**(18), 1994.
10 C. Mahan, V. Mahidi and J. A. Holcombe, *Anal. Chem.*, 1989, **61**, 624.
11 C. Mahan and J. A. Holcombe, *Spectrochim. Acta, Part B*, 1992, **47B**, 1483.
12 J. L. Gardea-Torresdey, K. J. Tiemann, D. H. Gonzalez, J. A. Henning and M. S. Towsend, *J. Hazard. Mater.*, 1996, **48**, 181.
13 D. Kratchovil, B. Volesky and G. Demapoulos, *Water Res.*, 1997, **31**(9), 2327.
14 C. Mahan and J. A. Holcombe, *Anal. Chem.*, 1992, **64**, 1933.
15 B. Volesky and I. Prasetyo, *Biotechnol. Bioeng.*, 1994, **43**, 1010.
16 C. J. Williams and R. G. J. Edyvean, *Trans. Inst. Chem. Eng.*, 1990, **75B**, 19.
17 C. J. Williams, D. Alderhold and R. G. J. Edyvean, *Water Res.*, 1998, **32**(1), 216.
18 S. Schiewer and B. Volesky, *Environ. Sci. Technol.*, 1995, **29**, 3049.
19 E. Fourest and B. Volesky, *Environ. Sci. Technol.*, 1996, **30**, 277.
20 APHA-AWWA-WPCF. *Standard Methods for the Examination of Water and Wastewater*, American Public Health Association, Washington DC, USA, 19th edn., 1995.
21 J. L. Gardea-Torresdey, M. K. Becker-Hapak, J. M. Hosea and D. W. Darnall, *Environ. Sci. Technol.*, 1990, **24**(9), 1372.
22 A. G. Cox, I. G. Cook and C. W. McLeod, *Analyst*, 1985, **10**, 331.